Validation and analysis of loading models for a multi-megawatt floating offshore two-bladed wind turbine

Ben Ralph

Technische Universiteit Delft

Validation and analysis of loading models for a multi-megawatt floating offshore two-bladed wind turbine

by

Ben Ralph

in partial fulfillment of the requirements for the degree of Master of Science in
Sustainable Energy Technology at Delft University of Technology,
to be defended publicly on Monday January 30, 2023 at 10:00 AM.

Student number:	5394635	
Project duration:	November 21, 2021 – November 14, 2022	
Thesis committee:	Dr. ir. AC. Viré,	TU Delft, Chairperson
	Dr. ir. W. Bierbooms,	TU Delft
	Dr. ir. A. Jarquin Laguna,	TU Delft
	G. Henderson,	Seawind Ocean Technology
	S. Caruso,	Seawind Ocean Technology

This thesis is confidential and cannot be made public until January 30, 2025.

Abstract

Offshore wind is a rapidly maturing renewable energy technology and is expected to play a central role in future energy systems. It has the potential to generate more than 420,000 TWh per year worldwide, an amount approximately equal to eighteen times the global electricity demand today [51]. While many of the most abundantly resourceful sites are at water depths too extreme for fixed-base solutions, current floating turbine technologies suffer with high-costs and inefficiencies. Seawind Ocean Technology B.V., a Netherlands based company, is a manufacturer of fully integrated floating wind turbine systems. They have designed an innovative set of low-cost, low-weight, upwind two-bladed wind turbines, with teetering hinge and yawed power control. This teetering hinge decouples the shaft from rotor, by adding an extra degree of motion, and protects the turbine from harmful aerodynamic and gyroscopic loads, as well as the rotor from hydrodynamic loads. The innovative active yaw control eliminates the need for complex pitching systems to regulate power output, in turn reducing turbine head weight and turbine costs.

There are multiple goals for this thesis project. First and foremost, was to investigate two-bladed and floating offshore turbine technology, both of which had not been covered in-depth in university courses. Innovative wind turbine technologies, specifically geared for the fast growing floating offshore market, are detailed in this report, with the findings hopefully making their way into the hands of change-makers who can promote the technology and consequently accelerate the green transition.

The second was to optimise the loading analysis models of the Seawind 6 turbine using DNV GL's wind turbine design software, Bladed. This is a 6 MW two-bladed floating offshore turbine and is intended for commercialisation by 2024. Seawind have extensive operational data from the Gamma 60's deployment (the world's first variable speed, two-bladed, wind turbine with a teetering hinge) in the 1990s. The aim was to model the Gamma 60 and compare it to this operational data. This, in turn, will be used to calibrate and optimise the current offshore Seawind 6 simulation models, which are based on those of the Gamma 60. The key calibrations suggested from this work involved minor adjustments to the torque and speed control loops of the external controller, as well as modifying the tower and blade's structural properties.

Once achieved, the third goal was to carry out a thorough ultimate and fatigue load analysis of the optimised Seawind 6 model for various design load cases at extreme water depths. This required extensive research during the literary review stage into two bladed turbine physics, teeter and yaw dynamics, and floating structure hydrodynamics to make sense of the Seawind 6's performance. Countless hours were spent setting up simulations with Bladed and visualising the results in the most appealing manner. This investigation proved that the various investigated turbine components have been adequately sized and that suitable construction materials have been selected considering the ultimate and fatigue loads they are expected to withstand.

The fourth goal of this thesis was to delve deeper into the fundamental areas of the Seawind 6 operating envelope in steady, uniform winds to gain a better appreciation of the turbine's operation. In particular, the Seawind engineers were keen to investigate the effect of aerodynamic damping on the turbine's teeter motion as a consequence of yawing. This misalignment between the rotor and oncoming wind caused the angles of attack to differ between the two blades when in a vertical orientation. It was found that a favourable teeter moment was generated that opposed the effect of wind shear.

The fifth and final goal of this thesis work was to pull everything together and compare the floating offshore two-bladed Seawind 6 to a conventional floating three-bladed state-of-the-art turbine competitor. This was in terms of ultimate and fatigue loads experienced, capital and operational expenses (CAPEX and OPEX), lifetime carbon abatement, levelised cost of energy (LCOE), ease of manufacture and deployment, and operational performance. The key findings were a 30% to 40% reduction in structural loads, a 40% lifetime cost reduction, a 20% lower installation time, and a 25.4% higher availability for the Seawind 6, all while producing the same energy output.

Acknowledgements

First, I would just like to say how grateful I am for the opportunity to study in TU Delft and follow my passion for renewable technologies through MSc SET. Although it has been unfortunate that I have not spent as much time as I would have liked in Delft, due to Covid, I have still learned an immeasurable amount from the experience. In particular, I would like to thank Dr. Axelle Viré for her support, kind words, and helpful feedback that shaped this thesis. I would also like to thank Dr. Wim Bierbooms for overseeing my progress, and Dr. Antonio Jarquin Laguna for sitting on my thesis committee and posing such thought provoking questions.

My utmost gratitude goes to all those in Seawind Ocean Technologies B.V., especially Geoff Henderson and Maarten Van Aller, who were extremely generous with their time and guidance on a day-to-day basis. Geoff, you are my two-bladed turbine sensei and I cannot express how appreciative of your expertise I am. I am also hugely grateful for the technical know-how of the Gamma 60 imparted by Silvestro Caruso, and for all the Bladed models support generously provided by Sesto Avolio (I literally jumped for joy when we got the Gamma 60 model finally running!). I really could not have completed this thesis work without all of your help.

A special mention also goes to all my former teachers and UCD lecturers, in particular Enda O'Rourke, for teaching me to think outside the box and not be too much of a perfectionist (okay, he may have failed at that!). Also, to the DNV Bladed support team who were always on hand to answer any questions and to help setting up Bladed licenses.

Finally, and most importantly, I would like to thank all my friends for keeping my spirits high and my family for feeding me and ensuring I was calm and collected throughout. I know everyone thought it was a bit mad taking the summer off to travel Australia and Asia, but this was the spark I needed to get stuck into my work. Lastly, Mum, you can eventually stop nagging me to finish this thesis now!

Ben Ralph
Wicklow, 14 November 2022

Contents

List of Figures

List of Tables

Nomenclature

Abbreviations

AEP	Annual Energy Production
API	Application Programming Interface
BEM	Blade Element Momentum
CAPEX	Capital Expenses
COD	Co-Directional
DEL	Damage Equivalent Load
DLC	Design Load Case
DLL	Dynamic-Linked Library
ECM	Extreme Current Model
ESS	Extreme Sea State
ETM	Extreme Turbulence Model
EWM	Extreme Wind Model
GFRP	Glass Fiber Reinforced Plastic
GL	Germanische Lloyd
HSS	High Speed Shaft
IEC	International Electrotechnical Commission
IGCT	Integrated Gate-Commutated Thyristor
LCOE	Levelised Cost of Energy
LIDAR	Light Detection and Ranging
LSS	Low Speed Shaft
MBL	Minimum Breaking Load
MIS	Misaligned
ML	Mooring Line
MUL	Multi-Directional
NCM	Normal Current Model
NREL	National Renewable Energy Laboratory
NSS	Normal Sea State
NTM	Normal Turbulence Model
OMS	Operations, Maintenance, and Service
OPEX	Operational Expenses
PMG	Permanent Magnet Generator
RNA	Rotor Nacelle Assembly

TLP	Tension Leg Platform
UNI	Uni-Directional
UPS	Uninterruptible Power Supply
WEG	Wind Energy Group

Symbols

α	Platform pitch angle
δ_3	Delta-3 angle
ω	Angular velocity
ϕ	Yaw angle
Ψ	Rotor axis direction
σ	Standard deviation of turbulence
σ_{max}	Maximum bending stress
$\sigma_{ultimate}$	Ultimate bending stress
ζ	Teeter angle
C_p	Coefficient of performance
C_a	Aerodynamic damping coefficient
C_h	Hub teeter restraint damping coefficient
d_{inner}	Inner diameter
d_{outer}	Outer diameter
$F_{buoyant}$	Buoyant force
H_s	Significant wave height
I	Turbulence intensity
J	Mass moment of inertia
k_a	pitch-teeter coupling stiffness coefficient
k_{cf}	Centrifugal stiffness coefficient
k_h	Hub teeter restraint stiffness coefficient
L_i	Load range bin
m	S-N curve slope
M_y	Yaw moment
M_{EI}	Teeter restraint moment
$M_{h\Delta\alpha}$	Teeter restraining moment
M_{hy}	Hinge moment
N	Number of cycles
n_i	Number of rain flow cycles
P	Power
T	Torque
t	thickness
T_p	Peak spectral period

V_{hub}	Hub wind velocity
W	Incident wind vector
W	Weight
W_C	Wind cross component
W_N	Wind normal component
y	Distance from the neutral axis

1 Introduction

1.1. Motivation

Current projections indicate that the world will face a 50% increase in energy demand by 2050. Today, 85% of the global energy is still supplied by fossil fuels. Without large scale intervention this will lead to catastrophically high CO_2 emission levels [20]. Offshore wind is a rapidly maturing renewable energy technology and is expected to play a central role in future energy systems. Political commitment to net zero has already put offshore wind in a vital position, with the current energy crisis and the Russian invasion of Ukraine prompting governments to further increase their offshore wind targets as they look to secure their energy supplies [45]. Momentum is gathering, with roughly 22% of the total wind capacity growth of 94 GW being delivered by offshore technology in 2021, the highest in history and three times the average of the previous five years [52]. It has the potential to generate more than 420,000 TWh per year worldwide, an amount approximately equal to eighteen times the global electricity demand today [51]. The most abundantly resourceful sites, however, are at water depths too extreme for fixed-base solutions, with 330,000 TWh of this potential existing at depths in excess of 50 m. There is huge scope here with floating wind still in its infancy, having just moved from the demonstration phase to pre-commercial, with only 57 MW of new installations globally in 2021 [45]. DNV predicts that the installed capacity of floating wind will grow from 100 MW today to 250 GW by 2050, while the levelised cost of energy would fall to a global average of 40 €/MWh, in line with nuclear and fossil fuels [36]. Furthermore, the floating turbine technologies that have already been deployed are less than optimal, suffering with high-costs and inefficiencies.

Seawind are hoping to take advantage of this perfect storm and become forerunners of this industry that has an expected valuation of $1 trillion over the next two decades [51]. They hope to achieve this through their innovative two-bladed, teetering turbine, which is vastly simplified compared to conventional three-bladed competitors currently in the market. The Seawind technology including the integrated floating structure has been patented, proven at 1.5 MW, and achieved technological certification with DNV [20]. Their 6 MW Seawind 6 turbine will be their initial demonstrator project, with an expected 25% to 35% LCOE advantage and a 60% lower lifecycle energy footprint compared to the offshore industry standard when commercialised. This will make offshore wind energy accessible at a significantly lower cost for all seas, including cyclonic regions and ultra-deep waters [20]. The motivation for this thesis is to learn about this exciting new technological innovation, spread awareness for it, and attempt to improve turbine performance wherever possible. The Seawind technology has incredible potential, and could well be the catalyst for the necessary gargantuan rise in floating offshore development in the near future.

1.2. Aims and Objectives

There are a number of aims and objectives for this thesis project. The first, and most fundamental, was to investigate two-bladed and floating offshore turbine technologies. These are the two fundamental aspects that differentiate the Seawind design from conventional three-bladed fixed offshore turbines and have convinced the team that they will revolutionise the wind industry, yet they are not widely covered in university courses or in industry. These findings will be shared with the hope that they make their way into the hands of change-makers who can promote the technology and consequently accelerate the green transition. The second was to optimise the loading analysis models of the Seawind 6 turbine using DNV GL's wind turbine design software, Bladed, through a calibration process. The Seawind 6 is a 6 MW two-bladed floating offshore turbine and is intended for commercialisation by 2024. It is principally based on the Gamma 60 (the world's first variable speed, two-bladed, wind turbine with a teetering hinge), for which Seawind have extensive operational data from its deployment in the 1990s. The Gamma 60 was modelled and compared to this operational data, with the calibrations in turn applied to the Seawind 6 models to improve its accuracy. Once achieved, the third aim was to carry out a thorough ultimate and fatigue load analysis of the optimised Seawind 6 model for various design load cases at extreme water depths. This investigation should prove whether or not the turbine components have been adequately sized and that suitable construction materials have been selected considering the loads they are expected to withstand. Following this large body of work, the fourth objective was to verify the theory that teeter motion is aerodynamically damped when the blades of a two-bladed, teetered turbine, are vertically oriented due to differences in angles of attack of the oncoming and retreating blades when yawed out of the wind. The fifth and final objective of this thesis work was to pull everything together and compare the floating offshore two-bladed Seawind 6 to a conventional floating three-bladed state-of-the-art turbine competitor. This should be done in terms of ultimate and fatigue loads experienced, capital and operational expenses (CAPEX and OPEX), lifetime carbon abatement, levelised cost of energy (LCOE), ease of manufacture and deployment, and operational performance.

1.3. Research Questions

These aims and objectives were formulated into six key research questions:

- **Research Question 1:** What design and control features of two-bladed turbine technology makes it ideal for floating offshore installations? In particular, with respect to the Gamma 60 and Seawind 6.
- **Research Question 2:** To what extent does the Gamma 60 Bladed simulation results match those of the operational data, and how can this model be calibration to improve the real-world accuracy of its performance?
- **Research Question 3:** What improvements to the accuracy of the Seawind 6 models can be achieved as a result of these calibrations?
- **Research Question 4:** What are the key ultimate and fatigue loads of the Seawind 6 with its updated model and controller?
- **Research Question 5:** Can the theory that yaw misalignment of the rotor to the prevailing wind will aerodynamically damp the two-bladed turbine's teeter motion be validated?
- **Research Question 6:** How will the Seawind 6's predicted performance compare to that of a state-of-the-art three-bladed competitor turbine?

Based on the findings of this thesis work, these research questions will be answered in the conclusions and recommendations section in Chapter 8.

1.4. Methodology

To address these research questions, the following methodologies will be followed:

- **Methodology 1:** Carry out an extensive literary review examining the underlying principles of two-bladed technologies, teeter motion, active yaw control, and floating offshore technologies. Following this, an in-depth review of the Gamma 60 and Seawind 6 turbines will be completed, focusing on structural design, electrical systems, and control algorithms.
- **Methodology 2:** Use Bladed 4.5 to model onshore Gamma 60 behaviours using input data from Seawind and compare results to collected operational data from prototype testing at Alta Nurra in the 90's. Do this by replicating Gamma 60 graphs and tables which have been shared by Seawind engineers personally involved with the Gamma project.
- **Methodology 3:** The Seawind 6 model and controller is based on that of the Gamma 60. From the operational comparison of the Gamma 60 model, suggest calibrations that can be brought through to the Seawind 6 model to improve its accuracy.
- **Methodology 4:** Based on international wind turbine design standards, IEC 61400, use Bladed 4.12 to simulate various design driving design load cases (DLCs) for the Seawind 6 and carry out an ultimate and fatigue loads analyses. DLCs 1.2, 1.3, 6.1, and I.1 were selected, with the analyses being focused on the Seawind 6's blade roots, hub, yaw bearing, various tower sections, floating platform arm, mooring lines, and anchors.
- **Methodology 5:** Run power production simulations with the Seawind 6 subjected to uniform wind speeds between cut-in and cut-out. These will be short, lasting less than 100 s. Export data to Microsoft Excel, including blade tip height, rotor azimuth, yaw misalignment, angles of attack along the blade, and blade root moments. Tabulate results and calculate the net aerodynamic moment acting on the teeter hinge to determine if its motion is damped.
- **Methodology 6:** Time permitting, model and run an offshore version of the NREL 5-MW reference wind turbine in Bladed 4.12 and compare key ultimate and fatigue loads to those of the offshore Seawind 6. If there is not enough time, compare the loads from the standard onshore models to each other to see how the two-bladed turbine compares to the conventional three-bladed. Following this, go through Seawind data to compare it in terms of developmental costs and logistics, timelines, abated carbon, and operational performance against the turbines used in the world's first operational floating offshore wind farm, Hywind Scotland.

1.5. Report Organisation

This report is structured around systematically addressing each of the aforementioned research questions. Chapter 1 provides a brief introduction to this thesis project and Seawind, the motivation for completing this work, and the methodology formulated to achieve the desired aims and objectives. Chapter 2 details an in-depth review of relevant literature, including an overview of the Gamma 60 and Seawind 6, two-bladed turbine technology, teetering hinges, active yaw control, floating offshore technology, and an introduction to Bladed. Chapter 3 examines the structural design, electrical systems, and control algorithms of the Gamma 60 and Seawind 6. Chapter 4 aims to validate the Gamma 60 model against its operational data, acquired during prototype testing, and suggests calibration improvements to implement to both turbine models. Chapter 5 presents the ultimate and fatigue loads analyses of the Seawind 6 for four design driving DLCs. The blades vertical teeter motion aerodynamic damping investigation is covered in Chapter 6. Following this, Chapter 7 compares the Seawind 6 to the two conventional three-bladed turbines in terms of ultimate and fatigue loads, and turbine development and operation. Finally, Chapter 8 concludes the findings of the report by referring back to the initial research questions, and outlines multiple recommendations for future work on the topic.

1.6. About Seawind Ocean Technology B.V.

Seawind Ocean Technology B.V., headquartered in the Netherlands, was established in 2014 by Martin Jakubowski and Silvestro Caruso, with the ambition to design, develop, and demonstrate fully integrated floating offshore wind turbines. With their innovative set of low-cost, low-weight, upwind two-bladed wind turbines, with teetering hinge and active yaw power control, they hope to take advantage of the enormous potential for floating offshore wind as detailed in Section 1.1. Their patented technology has already been proven during the successful testing of the 1.5 MW Gamma 60 during the 90's, and their 6 and 12 MW designs have recently been awarded Type D technical certification by DNV. It is an incredibly exciting time for the company at the moment as they move quickly to deliver the important demonstrator projects of the Seawind 6 technology in multiple locations across Europe. Over fifty experienced and driven innovators are working as part of Seawind, all with the joint ambition of providing low cost, simplified, floating turbine solutions for the offshore market. Seawind is confident that they can be forerunners of this floating offshore wind boom by achieving a 25% to 35% LCOE advantage compared to state-of-the-art three-bladed floating offshore wind energy technologies.

2

Fundamentals

This chapter introduces the fundamental theoretical components of this thesis project which form the foundations for further development in subsequent chapters. Section 2.1 provides a brief overview of the two primary turbines of interest for this research; the Gamma 60, the predecessor of the Seawind turbines, and the Seawind 6, the first turbine Seawind intends to manufacture and demonstrate. Following this, Section 2.2 investigates the relatively novel concept of two-bladed wind turbines. In order for two-bladed turbines to function efficiently, an extra degree of freedom must be introduced for the running rotor. This is achieved using a teetering hinge, an elastic and damped joint between the hub and the shaft with its axis perpendicular to the shaft axis, which is examined in Section 2.3. Section 2.4 details active yaw control, the method of power regulation for both the Gamma 60 and Seawind 6, only made possible by the aforementioned teetering hinge. This is where the rotor is misaligned with the prevailing wind to reduce its swept area, and therefore power output, rather than pitching its blades as is typical for most modern turbines. Section 2.5 introduces various floating concepts for offshore turbines in deep waters, with particular attention paid to detailing how the Seawind 6 platform conceptually works. Finally, Section 2.6 considers the wind turbine design tool used for all simulations in this project, Bladed, as well as on overview of the external controllers developed to enable desired operation of the turbine models.

2.1. Turbine Concepts in Focus

This section covers the two most important turbines of the Seawind story so far, the Gamma 60 and the Seawind 6. Subsection 2.1.1 provides an overview of the design, manufacture, and testing of the Gamma 60 during the 90's on the Italian island of Sardinia, while Subsection 2.1.2 discusses the development and ambitions for its successor, the Seawind 6. This serves only as an introduction to the turbines, with both thoroughly examined in terms of design and performance in later chapters.

2.1.1. Gamma 60

The Gamma 60, displayed in Figure 2.1a below, was a revolutionary two-bladed, fixed-pitch, upwind horizontal axis wind turbine with a rotor diameter of 60 m, hub height of 66 m, and rated power of 1.5 MW. Based on original research by NASA and Hamilton Standard (see Section 2.2), it incorporated a teetering hub to decouple the rotor from the shaft (see Section 2.3), active yaw power regulation (see Section 2.4), and variable rotor speed range to increase the energy generation and fatigue life [29]. The Gamma 60's teetering hinge drastically reduced fatigue loads and allowed for a lighter drive train, while the active yaw power control meant the industry-standard blade pitch mechanisms could be removed. The turbine was installed by Wind Energy Systems Taranto S.p.A. (WEST) at Alta Nurra, Sardinia, Italy in April 1992, and was successfully tested until 1997. An overview of the project's milestones is presented in Table 2.1 below. The WEST Gamma 60 team was comprised of Hamilton Standard, ENEL (the Italian National Electricity Board), Aeritalia, Finmeccanica (now Leonardo S.p.A.), ENEA (the Italian National Committee for Research and Development of Nuclear and Alternative Energies), and Sulzer

[25]. The turbine was designed to meet the requirements of the electricity utilities, namely high power output combined with long life time and low capital and maintenance costs [47]. The prototype was a success, actively inputting electricity to the grid for 4390 hours over the course of its operational lifetime and producing a total of 1319 MWh of energy [29]. Commercialisation of the Gamma 60 was intended, with a conditional investment for ten units by a US utility, however contractual disputes between WEST and ENEL, ENEL's privatisation, and the end of the oil crisis meant the programme was terminated [26]. Following this, the rights to the Gamma 60 technology were acquired by engineers, Glidden Doman and Silvestro Caruso, who founded Gamma Ventures, Inc, which subsequently passed the rights to Seawind Ocean Technology BV, founded by Martin Jakubowski and Silvestro Caruso.

Table 2.1: Gamma 60 milestones [29]

Description	Date
Design started	April 1987
Installation	April 1992
First grid connection	June 1992
Commissioning starts	April 6, 1993
Continuous operation with limited power (750 kW)	April 6 – Nov. 15, 1993
Continuous operation with limited power (1100 kW)	Nov. 15, 1993 – Feb. 2, 1994
Continuous operation with limited power (1200 kW)	Feb. 2, 1994 – Aug. 26, 1994
New brake pads of sintered material installed	July 1994
Continuous operation with limited power (1500 kW)	Aug. 26, 1994 – Jan. 23, 1995
End of contractual commissioning obligation with ENEL	Dec. 23, 1995
Fire in the nacelle	May 12, 1995
Wind turbine repair and design review	May 12, 1995 – Oct. 30, 1996
Tests on site without grid connection	Oct. 30, 1996 – Jan. 1, 1997
First grid connection	Jan. 21, 1997
Tests on site with rotation. Commissioning test	Jan. 21 – April 24, 1997
Contractual recommissioning with ENEL	April 24 – June 30, 1997

2.1.2. Seawind 6

The Seawind 6 is based on the Gamma 60, uprated to 6.2 MW, with a rotor diameter of 126 m, and hub height of 95 m. It builds on the successful testing of the variable speed, teetering hinge, and active yaw control elements [21]. Integrated atop a concrete semi-submersible floating platform, as shown in Figure 2.1b, the Seawind 6 has been designed for offshore operation in ultra-deep waters greater than 50 m. The patented integrated floating structure and elastomeric teetering hinge (see Subsection 3.2.2), means the turbine system on a whole is simpler, more flexible, and more robust compared to the current state-of-the-art three-bladed technology. The fully integrated and optimised design, lack of pitching mechanisms, lighter drive-train, and one less blade means the Seawind 6 can achieve a 25% to 35% Levelised Cost of Energy (LCOE) advantage compared to their competitors [20]. The Seawind turbine also has a 60% lower life-cycle energy footprint compared with offshore industry standard. This positions Seawind perfectly to take full advantage of the huge potential for the offshore wind market, with over 1500 GW projected to be installed offshore worldwide by 2050, 80% of which is floating [20]. A demonstrator of the Seawind 6 is planned for launch in the next few years, following a design certification by DNV GL to level D (TRL 5 equivalent) based on rigorous Bladed calculations [56].

(a) Gamma 60 prototype

(b) Seawind 6 visualisation

Figure 2.1: Turbine concepts in focus

2.2. Two-Bladed Wind Turbines

2.2.1. Technological Overview

There is no doubt that the current design standard for the wind industry is the three-bladed turbine. However, this was not always the case, with initial strong interest in two-bladed turbines during the end of the last century, as will be detailed in Subsection 2.2.2. As the name suggests, these turbines have just two blades and typically make use of a teetering hinge that decouples the rotor from the shaft in order to reduce the increased effect of dynamic loads on the turbine's drive-train. This is a flexible structure with limited pivoting capability that is connected to the end of the drive shaft and coupled to the rotor blades [35]. This teeter technology is only suitable for two-bladed rotors and has the potential to reduce the loads below those of any comparative three-bladed turbine [46]. Without a teetering hinge, fluctuating dynamic loads would be a major problem for two-bladed wind turbines. The effect of wind shear is shown in Figure 2.2 below, with a substantial nacelle nodding moment while the rotor is vertical and no effect when horizontal. This would cause dynamic loads twice per rotor revolution [63]. The second challenge relates to the yaw system and originates from gyroscopic effects, where the mass of inertia of the two blades is dependent on the rotor position. The third problem comes from yaw misalignment, leading to unequal loads on blades and therefore a higher dynamic impact [63]. Additionally, floating offshore platform pitching effects would be troublesome [16]. Furthermore, research by Dr. Andrew Garrad in the early 1980's found that this teeter motion was fundamentally resonant, with the natural frequency of an undamped teetering rotor and the driving frequency of periodic teeter excitation from wind shear and tower shadow both being 1/rev. Many early two-bladed models were stall-regulated and experienced damaging under-damped resonance in strong winds without sufficient aerodynamic damping. The addition of a pitch-teeter coupling or delta-3 (δ_3) hinge takes the system away from resonance and remedies this instability [3]. These topics will be covered in more detail in Section 2.3. No ideal state-of-the-art turbine design currently exists, with many questions particularly surrounding the optimum load reduction systems [65]. As a result, this thesis work will be particularly interesting.

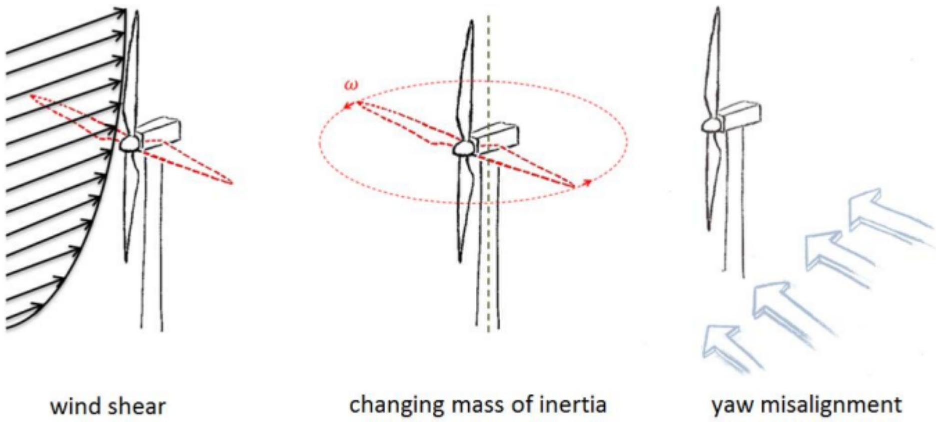

Figure 2.2: Loads on a two-bladed turbine [63]

Development of these early two-bladed turbines slowed, however, primarily as a result of their infamous premature design failures due to rapid wear of pivoting mechanism and resulting vibrations [35]. Additionally, they were simply not as well suited for the onshore market. In order to maximise its power coefficient, the two-bladed turbines have to be operated at higher tip speed ratios which has a greater acoustic impact than three-bladed and was not fully compliant with EU regulations regarding noise emissions onshore [19]. The three-bladed turbines also have a more favourable optical impression as their rotation appears less irregular due to their circular design [63]. However, the competitiveness of wind energy depends strongly on decreasing the cost of energy and two-bladed turbines offer an approximate 10% cost reduction compared to the industry standard [68]. This results mainly from a reduced number of components, less complexity, lighter drive train and nacelle, and easier installation, operation, and maintenance [63]. Three-bladed turbines need to be assembled mid-air, while two-bladed can be assembled on the ground and transported fully pre-assembled and pre-tested to the offshore installation site [3]. As turbines are now increasingly being designed to take advantage of offshore winds, it makes sense for the two-bladed turbine to make its comeback.

Removing one of the blades from the rotor means the missing blade must be compensated by either increasing the two remaining blade's chord widths by a third or by increasing the rotational speed of the turbine by a third [23]. The first option obviously increases tip speed and aerodynamic sound level, whereas the latter would make the two blades heavier and therefore more expensive [56]. An increase in rotor speed will increase the cost of structural components like the hub and shaft that will need to withstand higher loads. However, the cost of drive-train components will be reduced as transmitted torque drops with increasing rotational speed as per Equation 2.1 below [23].

$$P = T * \omega \tag{2.1}$$

This trade-off between increased tip speed or chord length is visualised in Figure 2.3 below, where the coefficient of performance (C_p) is plotted against the tip speed ratio for two- and three- bladed turbines with similar rotor diameters. Both two-bladed configurations result in marginally lower values of C_p than the three-bladed counterpart, but this can be easily compensated by slightly increasing the blade lengths [19].

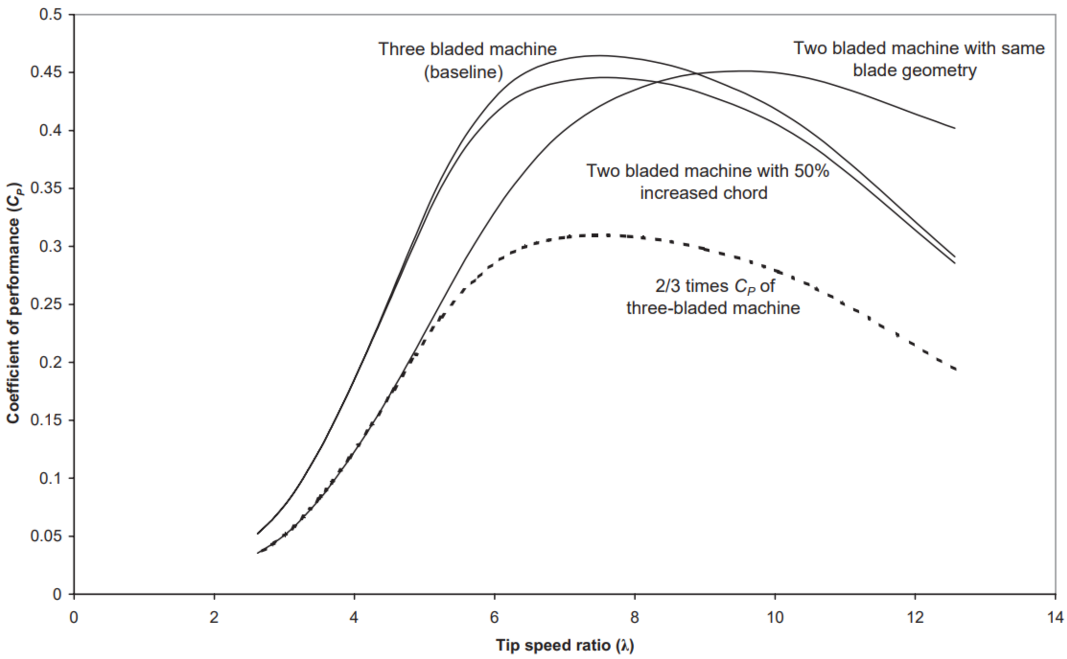

Figure 2.3: C_p curve for two- and three- bladed rotors [23]

2.2.2. Concepts

The evolution of two-bladed wind turbine technology can be traced back to World War II when the American engineer, Glidden S. Doman, was hired by Sikorsky to investigate helicopter structural and dynamic issues [34]. Doman, along with the German-born aerospace engineer Kurt Hohenemser, were convinced that a flexible two-bladed helicopter type wind turbine rotor design that is compliant with the forces of nature was more suitable for producing electricity than the rigid industry standard three-bladed airplane type wind turbine rotors that, by design, can only be constructed to resist the forces of nature [34]. As a result of the oil crisis in the 1970s, NASA was tasked with managing a programme to develop utility-scale wind turbines to combat increasing oil prices by the US Department of Energy and Department of Interior. In 1978, Doman was hired by Hamilton Standard to design and test his two-bladed wind turbines, including the WTS-3, and was provided funding by NASA to explore broad range variable speed on the WTS-4 [34]. This kick-started a plethora of development, with the majority of former multi-megawatt research turbines during this time being two-bladed [65]. However, few of these have been commercially proven due to the failure of economically delivering sufficiently stable operation throughout a full range of wind conditions [3]. Figure 2.4 below provides a timeline of all former teetered two-bladed turbines, in excess of 500 kW, and includes information on their pitch teeter coupling (see Subsection 2.3.1). Only turbines with at least one prototype are present meaning conceptual studies, like the Seawind 6, are not considered [64]. It is of interest to note that there was also a Dutch interest in two-bladed turbines at this early period, with Lagerwey developing smaller scale turbines primarily for agricultural use.

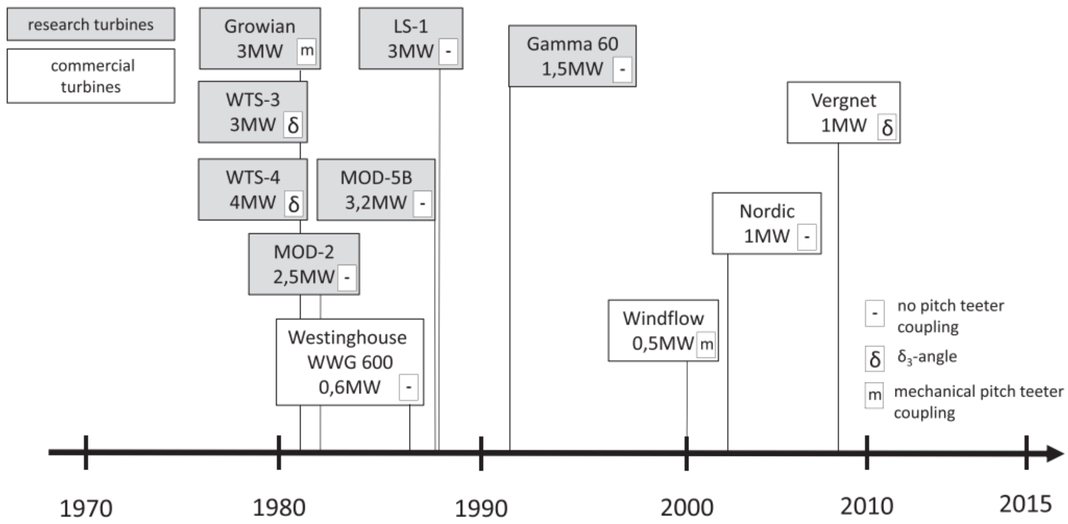

Figure 2.4: Timeline of former two-bladed teetered turbines with a capacity in excess of 500 kW [64]

The two-bladed Smith Putnam turbine, with a power of 1.25 MW, was the world's first megawatt-size wind turbine when it was connected to the grid in 1941. It operated for 1100 hours before blade failure, and remained the largest ever built until 1979 [25]. Figure 2.4 starts with the German research turbine, the Growian 3 MW. This was a full-span pitch-regulated turbine with mechanical pitch-teeter coupling [64]. The WTS-3 and WTS-4 were essentially the same turbine, with filament winded blades, full-span mechanical-hydraulic pitch mechanism system, δ_3 hinge, and soft tower, but with different running speeds. The 4.2 MW WTS-4, as shown in Figure 2.5a below, was installed by Hamilton Standard in Medicine Bow, Wyoming in 1982 and was the most powerful wind turbine to have operated onshore in the US, holding the world record for power output for over 20 years [24]. The 3MW WTS-3 was installed by Karlskronavarvet in the town of Maglarp, Sweden in 1983. It was decommissioned in 1993 after generating 37 GWh over its 11 years of operation which, at the time, was a world record for wind turbines [58]. Several 2.5 MW MOD-2 turbines were designed and constructed by Boeing during the early 1980s. These were partial-span (tip only) pitch-regulated turbine with no pitch-teeter coupling [64]. The MOD-5B wind turbine, built by Boeing in 1987, was the largest operating wind turbine in the world in the 1990s. It was an uprated version of the MOD-2 with a rated capacity of 3.2 MW [70]. The first commercial two-bladed teetered turbine was the 600 kW Westinghouse WWG 600, with several units installed at Kahuku wind farm in Hawaii. This was based on the MOD-0 technology [64]. The 3 MW LS-1 was designed by the Wind Energy Group (WEG) and operated in Orkney between 1988 and 1997. It was partial-span (tip only) pitch-regulated and was the UK's largest turbine at the time [72]. The 1.5 MW Gamma 60 is the predecessor of the Seawind turbines and was a full-span, fixed-pitch, active yaw-regulated turbine with no pitch-teeter coupling. The Windflow 500 kW turbines were commercially produced and 96 units were installed in the 46 MW Te Rere Hau wind farm in New Zealand, shown below in Figure 2.5b. These are full-span pitch-regulated turbines with a mechanical pitch-teeter coupling and have been successfully operating for the last 15 years [16]. The current Seawind Chief Technological Officer (and my thesis supervisor), Geoff Henderson, was the CEO and founder of Windflow, responsible for developing these turbines. The Nordic 1 MW turbine reverts to an active stall principle to regulate its power output, with no pitch-teeter coupling [3]. The most recently commercially available two-bladed turbines have been produced by Vergnet. Their GEV HP 1 MW is a full-span pitch-regulated turbine with δ_3 pitch-teeter coupling [64]. As illustrated by Figure 2.4, no state-of-the-art two-bladed teeter design has thus far been achieved.

(a) WTS-4

(b) Windflow 500

Figure 2.5: Two-bladed turbine examples

The Seawind technology is the next logical leap forward, based on a number of key learning's from these past projects. First, the WTS-3 and WTS-4 demonstrated that impressive performance could be achieved by a two-bladed, pitch controlled, rigid rotor. Second, that the implementation of a teetering hinge between the nacelle and rotor dramatically reduces the torque necessary to yaw the nacelle, as well as reducing loads acting on the blades and drive train. Third, it was observed that an upwind rotor configuration has superior stability when compared to a downwind rotor, with a zero δ_3 angle further improving this [26]. Motivated by the discovery that a two-bladed teetering hinge rotor results in a small yaw torque, the Gamma 60 project was commissioned to assess the feasibility and performance of power regulation through yaw control, rather than the industry-standard blade pitch control. This procedure allowed for the blade pitch system to be eliminated, reducing the overall cost and weight of the machine. In addition, the Gamma 60 also was designed to operate in broad range variable speed mode, 15 to 44 rpm, increasing energy capture and fatigue lifetime [47]. These were both highly advanced and innovative systems at this time, and the engineers working on this project were at the cutting-edge of the industry. The testing was a success with only the teeter angle found to be higher than the expected at times [26]. The Seawind turbines builds on this legacy and will be the largest two-bladed turbines produced in history and the first to be deployed offshore.

2.3. Teetered Hub

2.3.1. Principle

As described in Section 2.2, the teetering hinge is an elastic and damped joint between the hub and the shaft with its axis perpendicular to the shaft axis. It introduces an additional degree of freedom to the running rotor. This degree of freedom, decoupling the rotor from the drivetrain, greatly reduces not only the aerodynamic cyclic loads transferred from the rotor to the drivetrain, but also the gyroscopic forces and therefore the torque needed to yaw the nacelle, as well as hydrodynamic loading from the floating platform. These cyclic loads are transformed into teetering motion of the rotor, similar to that of a see-saw. The first complete equation of this teeter movement was defined by Garrad in 1982 and defines the teeter motion relative to the axis rotating with the main shaft [42]. This was expanded on by Anderson et al. in 1984 to predict teeter excursions of a two-bladed turbine in a turbulent velocity field [2]. Garrad found that the teetering motion of an two-bladed rotor is fundamentally resonant, with its undamped natural frequency of 1/rev matching the driving frequency of periodic teeter excitation caused by wind shear and tower shadow. This instability can be remedied by either shifting its natural frequency substantially away from 1/rev or by maintaining adequate damping in all wind conditions [3]. This can be achieved through pitch-teeter coupling in the form of a delta-3 (δ_3) angle or mechanical pitch-teeter coupling (by gears), as described by Henderson et al. [49]. In recent times, this coupling may also be implemented by individual pitch control of the turbine's blades [64]. The δ_3 hinge originated in the helicopter industry with extensive work was carried out on its behaviour during the 1980s and 1990s by Kurt Hohenemser. As shown in Figure 2.6 below, the δ_3 angle is the angle between the teeter axis and the axis perpendicular to the rotor pitch axis. This induces a component of feathering rotation about the blade's pitch axis as they flap due to teeter motion [50].

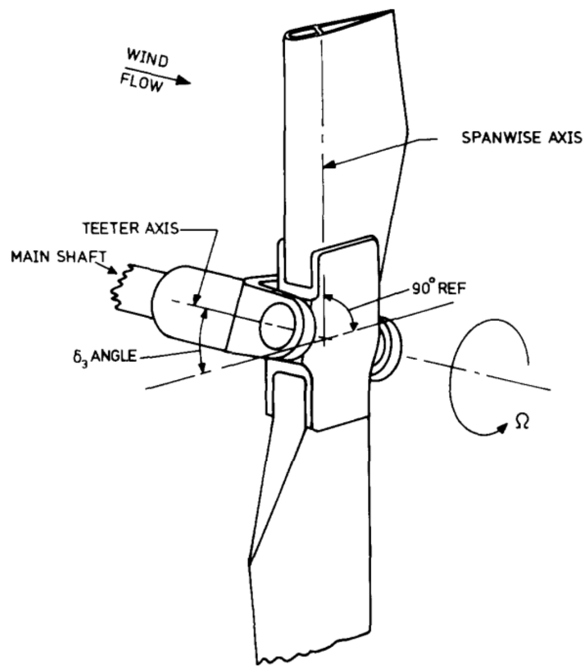

Figure 2.6: A teeter hinge with δ_3 angle [42]

With pitch teeter coupling included, the complete equation for teeter motion may be written as follows:

$$J\ddot{\zeta} + (C_a + C_h)\dot{\zeta} + (k_{cf} + k_a + k_h)\zeta = M(t) \tag{2.2}$$

Equation 2.2 is visualised in Figure 2.7 below with all the parameters that influence the teeter movement shown. M(t) is a disturbing moment (from turbulence fluctuation, wind shear, or yaw misalignment) that leads to a teeter excursion. On the left side of Equation 2.2 is the mass moment of inertia J, as well as the teeter resisting and restoring moments caused by spring (k) and damping (C) coefficients. Table 2.2 provides an overview of these parameters. The spring constants are the centrifugal stiffness k_{cf}, pitch teeter coupling stiffness k_a, and the spring constant of the teeter restraint in the hub k_h. Resisting moments are caused by aerodynamic damping C_a and by the damping constant of the teeter restraint in the hub C_h. The two hub components are design parameters of the turbine. If the free teeter angle ζ_{free} is exceeded, the teeter restraint moment M_{EI} is applied by a spring and/or damper in the hub. The teeter restraint must ensure that a certain maximum teeter angle ζ_{max} is not exceeded to prevent the rotor from hitting the nacelle or tower. This is referred to as a teeter-end impact and destroys the load reducing advantage of the teeter mechanism [62]. The teeter amplitude depends on rotor running speed (the higher the rotor speed the lower is the teetering angle), yaw rate (the higher the yaw rate the higher the teetering angle), rotor azimuth angle (maximum when blades are horizontal), and the rotor's Lock number (ratio aerodynamic forces and inertia forces) [22]. As such, teetering should be restrained during start-up and shut-down when centrifugal stiffening, aerodynamic stiffening, and aerodynamic damping are reduced due to low rotational speeds [49].

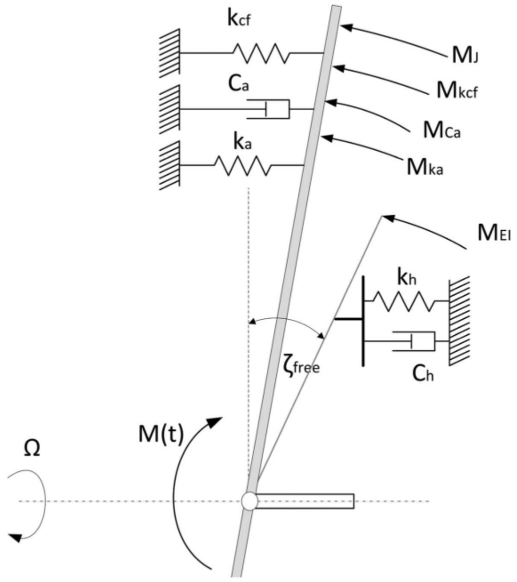

Figure 2.7: Spring and damping constants, angles, and moments of the teeter movement [64]

Table 2.2: Restoring and resisting moments of the teeter movement [64]

Moment	Description	Spring/Damping Constant
M_{ka}	Restoring moment of pitch teeter coupling	$k_a = \frac{1}{2}\rho\Omega^2 C_{l\alpha} C_{pt} \int_{-R}^{R} c(r)\lvert r\rvert r^2 dr$
M_{cf}	Restoring moment caused by centrifugal force	$k_{cf} = J\Omega^2$
M_{kh}	Restoring moment of teeter spring	k_h, design parameter of turbine
M_{Ch}	Resisting moment of teeter damper	C_h, design parameter of turbine
M_{Ca}	Resisting moment of aerodynamic damping	$C_a = \frac{1}{2}\rho\Omega C_{l\alpha} \int_{-R}^{R} c(r)\lvert r\rvert r^2 dr$

2.3.2. Benefits

Teetering allows for three key benefits for a two-bladed turbine in comparison to a conventional fixed-hub three-blader. First, relative to the fixed-hub three-bladers, teetering allows for lower turbine weights by reducing the fatigue bending moment on the blades, the shaft, the drive-train and all tower head structural members. These are caused by aerodynamic asymmetries that causes imbalanced blade root flap moments for a fixed hub three-blader, but is converted to harmless teeter motion for a teetered two-blader [21]. Second, teetering allows for yaw-regulation of two-bladed turbines, a control strategy that is not feasible for three-bladers. As a turbine yaws, inertial and gyroscopic effects (covered in Subsection 2.4.2) increase the shaft bending on fixed-hub 3-bladers, putting a limit on the rate of yawing. Teetering prevents this shaft bending from being imposed and reduces yaw drive duty [22]. Third, floating offshore platform pitching effects, including yaw torques and shaft bending, are also greatly reduced by the teetering hinge. This reduces the incremental cost of floating offshore turbines [21]. Overall, the lower fatigue loads, lighter drive-train, and simpler components means that teetered two-bladers can achieve notably reduced fabrication, installation and maintenance costs which is the key driver for a turbine's commercial success.

2.4. Active Yaw Power Control

2.4.1. Principle

The nacelles of conventional wind turbines are typically rotated about their tower's central axis in order to capture as much energy as possible by following the changing wind direction. This process is referred to as yawing [54]. Unique to the Gamma 60 and Seawind technology, yawing is expanded upon and used to regulate the turbine's power output. This control strategy removes the need for blade pitching requirements which is the industry standard for regulating the power output of three-bladed turbines. This is only possible due to the teetering hinge gives the rotor an additional degree of freedom, allowing the turbine to overcome gyroscopic forces, and to modulate the yaw angle sufficiently quickly to control the rotor speed of the turbine, as detailed shortly in Subsection 2.4.2 [27]. Below rated wind speed the rotor faces directly into the oncoming wind, maximising the power output. At higher wind speeds, the active hydraulic yaw system gradually turns the rotor out of the wind, reducing its swept area [35]. Power regulation of a two-bladed turbine through active yaw control is visualised in Figure 2.8 below.

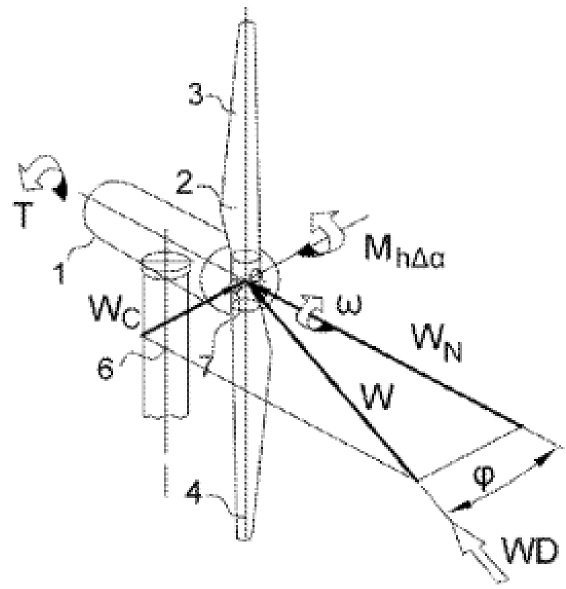

Figure 2.8: Active yaw power control - Visualisation [27]

Figure 2.8 shows the wind speed vectors and angles associated with a vertically oriented rotor (2), two-bladed turbine, spinning clockwise with an angular velocity ω, when the nacelle (1) has been yawed counter-clockwise out of the wind by an angle ϕ [27]. The incident wind vector W is divided into a normal component W_N that gives the active power, and a cross component W_C that causes flapping moments in higher wind speed ranges [35]. In yaw controlled turbines, the yaw control system is used to adjust the angle ϕ to keep the rotor shaft speed at rated value, while the retaining torque T is kept at its rated value by the electrical generator converter. As the wind speed increases or decreases, ϕ is adjusted to keep the wind normal W_N constant, ranging from 0° below rated to roughly 60° near cut-out. For shut down, ϕ is increased to 90°, resulting in minimal aerodynamic torque being generated by the wind, allowing the rotor to slow to a stop [27]. For the clockwise running rotor in Figure 2.8, the cross component W_C results in a different angle of attack for the top blade (3), moving with W_C, than for the bottom blade (4), moving against W_C. This, in turn, generates a restraining moment $M_{h\Delta\alpha}$ around the teetering hinge (7) [27]. This has the positive effect of counteracting wind shear, by forcing the upper blade away from the tower, and is the topic of investigation in Chapter 6.

Active yaw control as a principle works for both upwind and downwind rotor configurations. However, the Gamma 60 testing proved that an upwind rotor is aerodynamically more stable. An upwind rotor is also not affected by tower shadowing impact when blades are passing the tower, which greatly reduces fatigue loading [56]. Additionally, no stall effects occur [35]. The Seawind turbines use soft hydraulic yaw drives to further damp the yaw motion and reduce fatigue loads [54]. A yaw system for rapid power regulation requires high yawing rates as the decrease in power production in relation to the yaw misalignment is small. The yaw torque also has to overcome high yaw moments due to the large moment of inertia of the nacelle and rotor [23]. The teetering hinge reduces these yawing moments and gyroscopic loads, allowing yaw rates of 10°/s for the Seawind turbines in contrast to the industry standard 0.5°/s [54]. The required yawing torque increases in relation to the yaw misalignment, so is greatest for higher wind speeds. The highest yaw rates are also required for shutdown procedures [27]. Additionally, when installed in wind parks, the yawing of upwind turbines at high wind speeds will cause a deflection of their wakes out of the path of downwind turbines, resulting in higher possible energy yields and an overall increase in energy production of the wind park [73].

2.4.2. Gyroscopic Effect

As a running turbine yaws around its vertical axis, the combination of the spinning and yawing rotations attempts to originate a third rotation perpendicular to the previous two in an effect called gyroscopic precession [22]. This is shown in Figure 2.9 below, where the gyroscopic effect of the rotor, with yaw torque M_y and rotor running speed ω, generates a hinge moment M_{hy}. The direction of M_{hy} depends on the direction of the yaw moment M_y and on the direction of the rotor rotation. The greater the yaw torque, the greater the hinge moment [27]. This effect is proportional to the yaw rate meaning yaw-regulation, which requires high yaw rates, will cause significant gyroscopic forcing [27]. For a fixed-hub turbine with blades rigidly attached to the shaft, as is the case for all three-bladed turbines, this overturning moment is reacted structurally and subjects considerable stresses on the shaft and drive-train [48]. For a two-bladed rotor with a teetering hinge, such as the Gamma 60 and Seawind turbines, the rotor is free to tilt around its hinge meaning limited loading is transferred [48]. As such, these gyroscopic forces caused by fast yawing rates, which are prohibitive for fixed-hub turbines, are made insignificant by the teetering hinge [21]. In a frictionless gyroscopic system this teeter motion would grow at the same rate as the change of yaw angle. However, the relative motion causes an aerodynamic response which resists it, as mentioned in the previous section, and prevents the teeter motion from growing in amplitude to the point where mechanical interference between components could occur [48]. For a two-bladed rotor, the gyroscopic forcing is shown to not be reacted when blades are vertical and reduces to a very small value when the blades are horizontal. The latter is actually reacted as a moment around the blades' pitch-axis, regardless if it is pitchable or not [48].

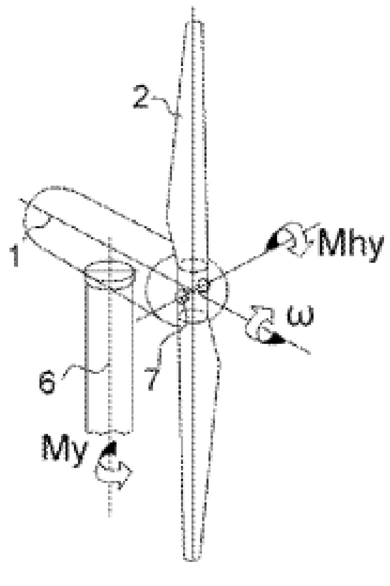

Figure 2.9: Active yaw control - Gyroscopic effect [27]

2.5. Floating Offshore Wind Turbines

2.5.1. Technological Overview

Offshore wind has the potential to generate more than 420,000 TWh per year worldwide, roughly eighteen times the global electricity demand today. Approximately 330,000 TWh of this is found in deep waters, greater than 50 m, only accessible by floating technologies [51]. DNV predicts that the installed capacity of floating wind will grow from 100 MW today to 250 GW by 2050, while the levelised cost of energy will fall to a global average of 40 €/MWh in line with nuclear, solar, and fossil fuels [36]. Located further offshore, floating turbines have access to stronger and more consistent winds, result in less visual pollution, and provide better accommodation for fishing and shipping lanes. Floating wind farms could unlock the vast potential of ocean areas with water depths too great for fixed turbines and be a vital energy transition tool for countries such as Japan, Korea, Portugal, France, and the west coast of the United States [52]. The technical feasibility and survivability of deep-water floating wind turbines has already been proven, with many decades of successful demonstrations by the marine and offshore oil industries. The four main floating platform concepts, each using a different approach to achieve hydrostatic stability, are visualised in Figure 2.10 and detailed as follows:

- **Semi-submersible type:** Comprised of multiple large hollow columns connected together by tubular arm members. The turbine may sit on one of the columns or at the platform's geometric centre. The columns are partially filled with water to provide ballast, with their water-plane area providing buoyancy stabilisation. The semi-submersible floating platform is kept in position by mooring lines. The heave plates on the base of the platform reduce heave and pitch motion without increasing size. The turbine is assembled onshore and towed to its offshore installation site [74].

- **Spar buoy type:** A steel or concrete cylinder is filled with a ballast of water and gravels to keep the centre of gravity below the centre of buoyancy. This ensures the turbine floats while remaining upright. The draft of the platform is at least equal to the turbine's hub height above water for stability and to minimise heave motion. The spar floating platform is kept in position by a taut or a catenary spread mooring system. During installation the floater is towed in a horizontal position to deep waters before being upended, stabilised, mounted with the turbine [74].

- **Barge (pontoon) type:** A large pontoon structure is used to support either a single or group of wind turbines. Stability is achieved through distributed buoyancy and by taking advantage of the large weighted water-plane area. The barge floating platform may be moored by conventional catenary anchor chains. The primary drawback of this concept is its susceptibility to roll and pitch motions in waves and may only be sited in calm seas or harbours [74].

- **Tension leg platform (TLP) type:** The conventional TLP platform comprises a square pontoon with a central column on which the turbine sits. It is held in position and stabilised by pre-tensioned vertical mooring lines, called tethers, which are anchored by suction or pile driven anchors. The TLP is dynamically less responsive to hydrodynamic loading when compared to the other three concepts. Like the semi-submersible, the fully assembled TLP is towed to the deployment site, removing the need for expensive offshore lifting vessels [74].

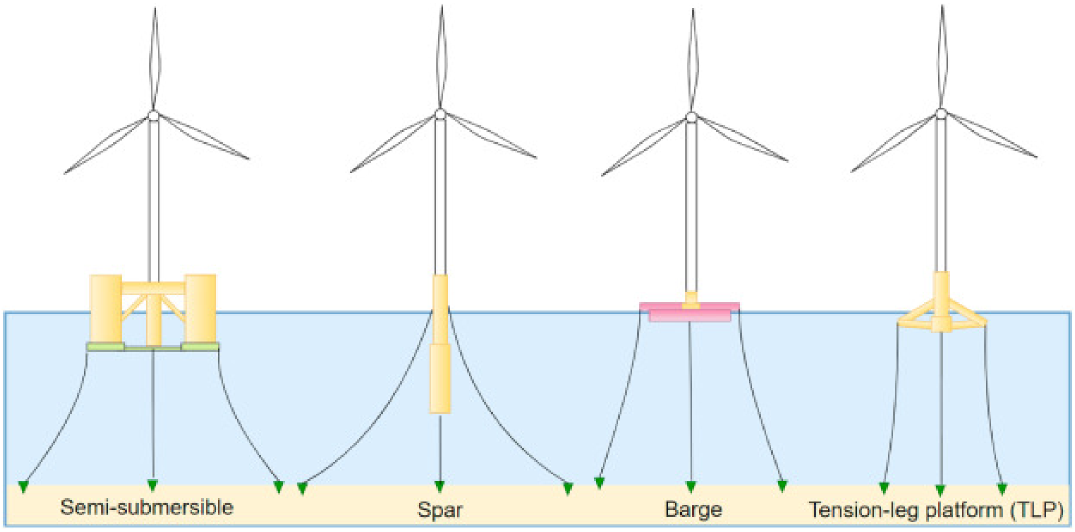

Figure 2.10: Floating wind turbine platforms [33]

The world's first floating wind turbine was deployed by Blue H Technologies, established by the founders of Seawind, off the coast of Italy in 2007. This was an 80 kW prototype utilising a tension-leg platform (TLP) design supporting a two-bladed turbine and was installed in water depths of 113 metres [38]. The first large-capacity floating wind turbine was the 2.3 MW Hywind, which became operational in the North Sea near Norway in 2009. The turbine was constructed by Siemens Wind Power and mounted atop a spar-buoy floating tower with a 100 m deep draft [75]. Commercial floating wind turbines are mostly at the early phase of development, with only three operational floating wind farms as of 2021. The world's first commercial floating offshore wind farm was the 30 MW Hywind Scotland with five 6 MW Siemens Gamesa turbines sitting atop spar-buoy floating platforms. This was developed by Equinor ASA and commissioned in 2017 off the coast of Peterhead, Scotland [39]. The second is WindFloat Atlantic, commissioned in 2020 off the coast of Portugal, with a total capacity of 25 MW. Three 8.4 MW Vestas turbines are supported by semi-submersible floating platforms. The most recent operational wind farm is the 48 MW Kincardine Offshore Wind Farm commissioned off the coast of Scotland in 2021, and hosting five 9.5 MW Vestas turbines atop WindFloat semi-submersible floating platforms [75]. In terms of wind farms under construction, the most noteworthy is the 88 MW Hywind Tampen project off the coast of Norway set to be commissioned fully by 2023. This will be the world's largest floating wind farm and the first to supply electricity to oil and gas platforms. Eleven 8 MW Siemens Gamesa turbines will be supported by spar-buoy floating platforms. Looking ahead, Crown Estate Scotland awarded a total of 14.5 GW of floating wind farm capacity split between ten leases in January 2022 as part of the ScotWind project [66].

2.5.2. Seawind 6 Platform

All the floating platform concepts introduced rely on Archimedes's principle of buoyancy which states that the buoyant force ($F_{buoyant}$) on an object is equal to the weight of the fluid (W_f) displaced by the object [1]. This is provided in Equation 2.3 below:

$$F_{buoyant} = W_f \tag{2.3}$$

Seawind have developed and patented an integrated semi-submersible floating platform, constructed from reinforced concrete. This design is thoroughly detailed and visualised in Subsection 3.2.2. It is composed of a central vertical body, which supports the two-bladed turbine and houses the bulk of the electrical system, and is linked to three vertical peripheral floaters through hollow rectangular arms. These have internal reinforcing transverse walls and, during operation, they are flooded with water to prevent structural buckling from external sea pressure. The primary role of the floating platform is to sustain the weight of the turbine head (W_1), tower (W_2), and platform (W_3). This is achieved through the buoyancy of the submersed central body (B_c) and three peripheral floaters (B_p) as per Archimedes principle, where:

$$W_1 + W_2 + W_3 \simeq 3B_p + B_c \tag{2.4}$$

These forces are visualised in Figure 2.11a for the turbine in static equilibrium. These forces exert bending moments and shear forces on the arms, with the maximum values experienced at the joint between the central body. Figure 2.11b shows how the Seawind floating platform conceptually works during operation. It is important to note that this figure omits the inertial forces that play an important role in the dynamic equilibrium of the floating turbine. The change in global pitch angle (α) of the floating turbine is calculated from Equation 2.5 and Equation 2.6 below:

$$\Delta B_p \equiv F_v * H_1 + F_w * H_2 \tag{2.5}$$

$$\alpha \equiv \Delta B_p \tag{2.6}$$

where F_v is the wind loading force on the rotor, F_w is the wave loading force on the platform, H_1 is the distance from the hub to the top of the rear floater, H_2 is the distance from the top of the rear floater to the platform's tilting center, and ΔB_p is the change in floater buoyancy [22]. Of particular importance for the yaw-regulated Seawind turbine, the pitch motion of the platform will stimulate the rotor's yaw direction gyroscopic moment. In the same way, the yaw motion of the platform or rotor will excite the gyroscopic moment of the overall system in the pitch direction. Therefore, during violent motion of the platform or yawing of the nacelle, it is recommended to reduce the rotor or yaw speed to restrain induced gyroscopic forcing [28]. Furthermore, during operation the central body is predominantly subjected to bending moments from wind loading, through the tower, with the maximum value experienced at its base. The floaters are also subjected to bending moments due to the action of the waves and mooring lines. The peripheral floaters, with their distance from the platform axis, create a straightening moment that balances the overturning moment caused by wind, waves, and currents. Additionally, large concrete heave disks are fitted to the bases of these floaters to damp the tilting motion of the system in rough seas [15].

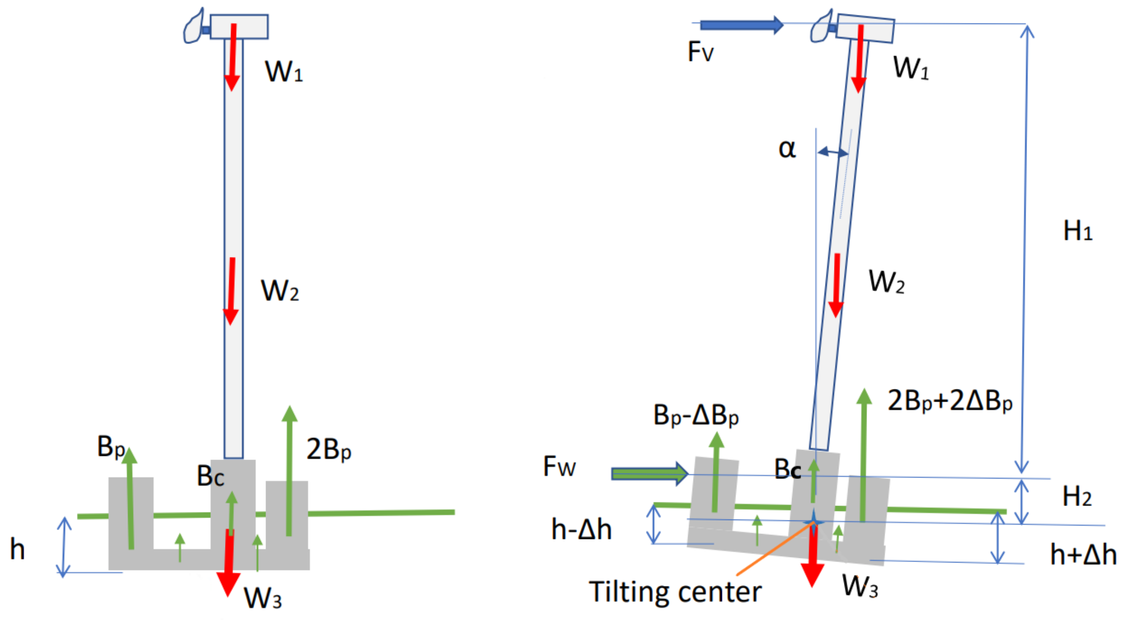

(a) Steady state (b) Operational

Figure 2.11: How the Seawind platform conceptually works [22]

2.6. Simulation Tool

2.6.1. Bladed

Bladed, developed by DNV GL, has been the industry standard aero-elastic wind turbine design software for the past twenty years, providing critical insight into wind turbine dynamics and optimisation. It is a computer-aided engineering tool that builds wind turbine models, runs calculations, and processes the results. To this end, it is also used for the certification of both onshore and offshore wind turbines [43]. Luckily, for the purposes of this project and Seawind's work, Bladed can model dynamics of two bladed teetering turbines, as well as floating substructure hydrodynamics. The software builds sophisticated numerical models of wind turbines and their operational environment, and are constantly updated and validated against real-world turbine measurements. The turbine model is described in terms of the following [43]:

- **Structural dynamics:** a completely self-consistent and thorough multi-body formulation is utilised.
- **Aerodynamics:** a modern and rigorous blade element momentum (BEM) implementation is used which includes best practice aerodynamic models. The fundamental BEM theory is extended to deal with complex unsteady flow conditions.
- **Environmental models:** Bladed's wind models include various steady and dynamic models necessary to cover all the required load cases. Wind shear can be user-defined, with wind speed and direction transients following the standard IEC profiles, and turbulent wind files follow either Kaimal, von Karman, or Mann spectral formulations. Bladed also includes models for regular and irregular wave states and sea currents.
- **Offshore modelling:** floating wind turbines can be modelled using a variety of mooring line configurations and hydrodynamic models.
- **Electrical modelling:** simple generator torque models are typically sufficient to determine most component turbine loads. Bladed also provides more detailed models to analyse electrical component and grid interaction.
- **Control systems:** Bladed provides an in-built controller with basic PI generator torque, blade pitch control, and drive-train damping feedback for simple initial calculations. For more advanced control features for turbine design, Bladed allows for user-defined external controllers as discussed in Subsection 2.6.2.

Seawind has already completed some in-house functional analyses using Bladed for the Seawind 6. From their findings, DLCs 1.2, 1.3, and 6.1 were deemed as being the most important design driving cases. However, these simulations from 2016 are now outdated, using an old version of the external controller and a less optimised floating substructure. As such, these three cases, plus an additional tropical cyclone DLC I.1, were selected for investigation in this project with the most up-to-date model and controller. For each DLC, the main input data are the spatially and temporally varying; wind speed, direction and turbulence, water depth, wave height, direction and period, and current speeds and direction [21]. Bladed version 4.5 was used for the Gamma 60 simulations in Chapter 4, while the most recent version, 4.12, was used for the Seawind 6 simulations in Chapter 5 and Chapter 6.

2.6.2. External Controller

When turbine manufacturers want to use their own, more advanced, control logic, in excess of the in-built power production and supervisory controllers, Bladed enables the use of user-defined external controllers. For the case of the Gamma 60 and Seawind 6, this includes the control of the generator torque, yaw actuation, and shaft braking. The initial Gamma 60 and Seawind 6 controllers were both developed by a company called Coelme following detailed instructions by Seawind. In recent months, the German company Sowento has written a new version of the Seawind 6 controller in Simulink with the goal of improving reliability and management. It is important to note that all aforementioned controllers are the intellectual property of Seawind. The control logic followed for both external controllers is covered in Section 3.4. These operate on a discrete time-step, like controllers in an actual turbine, communicating with Bladed at fixed time intervals. The external controller may be written in any language as a 32-bit DLL file (Dynamic-Linked Library) [37]. In many cases, the same code may be used to control the actual turbine. Robust and extendable communication is facilitated between Bladed and the external controller DLL via a modern, function based controller API (Application Programming Interface) [43].

3

Turbine Design and Control

In this chapter the structural design, electrical, and control systems for both the Gamma 60 and Seawind 6 will be examined. In each of these sections, when relevant, there will also be a description of how these elements were implemented in Bladed. Section 3.1 provides an overview and comparison of the most important design specifications for both turbines. Section 3.2 then examines the structural design of the two turbines, with the focus of Subsection 3.2.1 on the Gamma 60 and the focus of Subsection 3.2.2 on the Seawind 6 machine. An overview of all the key structural components will be provided, including the blades, teetering hinge, nacelle, and tower, as well as the floating platform and moorings when applicable. Following this, Section 3.3 examines both turbine's electrical control systems, from the drive train and yaw drives to the converters. Again, the Gamma 60 is the focus of Subsection 3.3.1, while the Seawind 6 is covered in Subsection 3.3.2. Lastly, in Section 3.4, the control procedures and implemented algorithms that ensure these machines operate as intended are investigated. Unfortunately, with the passing of time, many of the details and technical drawings regarding the Gamma 60 have been archived and were not readily available for inclusion in this report. As such, more emphasis is placed on the Seawind 6 details, particularly when describing the structural designs and electrical systems. This also works out nicely as there is less repetition of information. All CAD renders of the Seawind 6 were produced by Seawind affiliated designers.

3.1. Overview

As mentioned before, the Seawind 6 is based on the proven Gamma 60 concept, uprated from 1.5 MW to 6.2 MW and designed for floating offshore deployment in ultra-deep ocean waters. The two tables below display the principle design specifications for both turbines, Table 3.1 for the Gamma 60 and Table 3.2 for the Seawind 6. It is interesting to look through both tables and compare the corresponding values to see what elements have been altered when up-rating to the floating offshore version of the Seawind 6 and considering improvements from testing of the Gamma 60 prototype. With the increasing rated power output, from 1.5 MW to 6.2 MW, the rotor diameter needed to be increased to capture more wind flow which meant the hub height was also increased to ensure suitable blade-surface clearance. The cut-in, both rated, and cut-out wind speeds were all decreased slightly for the Seawind 6 when compared to the Gamma 60. This is a result of the Seawind 6 being certified as an IEC 1B class turbine for lower wind speed sites. Both turbines operate over a variable speed range so rotor performance can be optimised and greater power can be generated without increasing torque or generator current [29]. The range is shown to decrease from 12 to 44 rpm for the Gamma 60 to 8 to 28 rpm for the Seawind 6. This is a result of the rotor diameter increasing, leading to larger distances for the tip blades to travel per rotation. It is interesting to note that the rotor speed at rated power is at the top of its range for the Gamma 60 (44 rpm) but is decreased for the Seawind 6 (20.8 rpm). With the larger rotor speeds and smaller blade tip path, the Gamma 60's tip speed is shown to be comparable to that of the Seawind 6, 138 and 137 m/s respectively. Both turbines regulate their power output through active yaw control, with their primary braking achieved by the same action. Differences are present with the safety braking system, however, with the Gamma 60 making use of single disk brake on both the low speed shaft (LSS) and high speed shaft (HSS), compared to the Seawind 6 with a double disk brake on only the LSS. The teeter motion has also been allowed to increase with the Seawind 6, increasing to 11° from 6°. This was modified after the Gamma 60 experienced multiple teeter bumper impacts, which are extremely undesirable, during testing. The Gamma 60 was land based, whereas the Seawind 6 is mounted on a floating platform for deployment at sea in depths in excess of 50 m. At smaller depths, a fixed base version of the turbine would be more economically sensible. Both turbines should have similar design lifetimes of 20 and 25 plus years. Unfortunately, this this could not be verified for the Gamma 60 as it was decommissioned following the five year testing period.

Table 3.1: Gamma 60 - Design specifications [29]

Parameter	**Value**
Rated power	1.5 MW
Rotor diameter	60 m
Hub height	66 m
Cut-in wind speed	4 m/s
Wind speed at rated power	14.6 m/s
Wind speed at rated torque	12.3 m/s
Cut-out wind speed	27 m/s
Survival wind speed	54 m/s (lasting 2 s)
Rotor speed range	12 to 44 rpm (variable)
Rotor speed at rated power	44 rpm
Maximum tip speed	138 m/s
Power control	Active yawing
Primary braking system	Active yawing
Safety braking system	LSS and HSS disk brakes
Maximum allowable teeter angle	6°
Design life	20 years
Operational period	1992 - 1997
Location	Alta Nurra, Sardinia, Italy

Table 3.2: Seawind 6 - Design specifications [8]

Parameter	**Value**
Rated power	6.2 MW
Rotor diameter	126 m
Hub height	95 m (from sea level)
Cut-in wind speed	3.5 m/s
Wind speed at rated power	12.42 m/s
Wind speed at rated torque	11.06 m/s
Cut-out wind speed	25 m/s (peak 30 m/s)
Survival wind speed	70 m/s (peak 90 m/s)
Rotor speed range	8 to 28 rpm (variable)
Rotor speed at rated power	20.8 rpm
Tip speed	137 m/s
Power control	Active yawing
Primary braking system	Active yawing
Safety braking system	LSS double disk brake
Maximum allowable teeter angle	11°
Water depth	>50 m
Design life	25+ years
Certified wind class	IEC 1B

3.2. Structural Design

3.2.1. Gamma 60

Overview

The Gamma 60 has a hub height of 66 m, a rotor diameter of 60 m, and was tested in Alta Nurra, Sardinia, between 1992 and 1997. The turbine was manufactured by WEST s.p.a, with the blades and various electrical components produced by external suppliers. Below, Figure 3.1 displays both an aerial image of the Gamma 60 at its test site and the Bladed model. This model was initially designed by Seawind engineers in Bladed 4.5 as a basis to design the Seawind 6 models. This model was based on technical drawings and specifications used in the design and construction of the Gamma 60 prototype. This ensured a high level of detail and accuracy for the model to ensure high simulation accuracy. Modifications to the tower structure and external controllers were made for this thesis investigation as detailed in Chapter 4. In this section, each of the main Gamma 60 structural components will be examined.

(a) Operational turbine [26]　　(b) Bladed model

Figure 3.1: Gamma 60 - Full body view

Blades

The two 28.73 m blades of the Gamma 60 combined to produce a rotor diameter of 60 m and a swept area of 2827 m^2. The blades were based on those used by the WTS-4 turbine, with a rotor diameter of 79.2 m, and were manufactured using a filament winding method by the American aircraft propeller company, Hamilton Standard. Minor modifications were made, including shortening the cylindrical blade root section and installing an internal bulkhead (compression) rib to reduce centrifugal loads at high speeds [25]. Using the same moulds and processing techniques meant that they could be produced faster and more cost effectively, however it also meant the aerodynamic design could not be optimised. The blades were composed of various airfoils from the NACA 230XX series, developed by the National Advisory Committee for Aeronautics (the predecessor of NASA), as shown in Table 3.3. This shows a chord length of 3.82 m at the blade's root, decreasing to 1.06 m at the tip [47]. The thickness refers to the width of the blade and is provided as a percentage of the chord's length.

Table 3.3: Gamma 60 - Blade configuration

Radius	Chord	Thickness	Twist
(m)	(m)	(%)	(°)
0	3.82	0.34	0
2.3	4.36	0.29	6.2
6.2	3.96	0.26	3.2
10.2	3.48	0.24	1.2
14.2	2.93	0.22	0.0
18.1	2.38	0.19	-0.6
22.1	1.82	0.17	-0.9
26.0	1.35	0.14	-1.1
38.73	1.06	0.12	-1.3

The blades were constructed from a glass fiber reinforced plastic (GFRP) composite material, resulting in a total blade weight of 6.3 t each [26]. A few original images of this manufacturing process were made available for inclusion in this report [29]. Figure 3.2 shows the winding of glass fibres around the blade structure to produce the shell, while Figure 3.3 shows the curing of the filament and resin composite blade in a large custom-built oven.

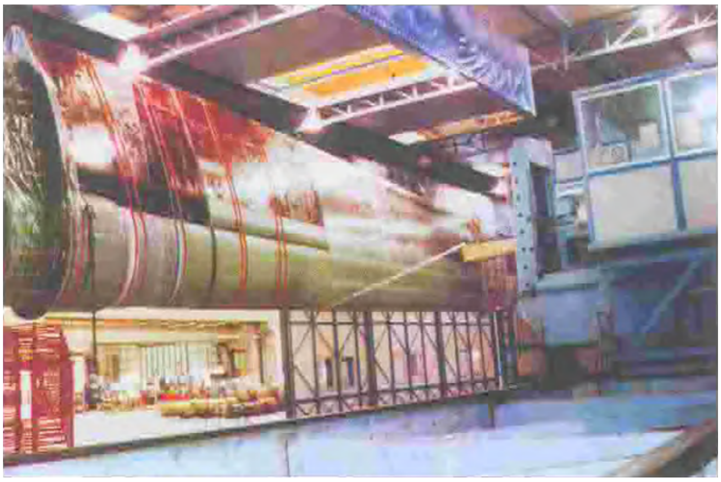

Figure 3.2: Gamma 60 - Shell winding of the blade [29]

Figure 3.3: Gamma 60 - Oven curing the blade [29]

Hub and Teetering Hinge

As described in Section 2.3, the teetering hinge decouples the rotor from the drivetrain by introducing an additional degree of freedom, which ensures major reductions of both aerodynamic cyclic loads and gyroscopic forces without a loss of energy capture [8]. The hub had a cast steel structure, with a diameter of 2.54 m, a cone angle of 3°, and a tilt angle of 6° [47]. Including the rotor, the total hub weight was 21 t. At the extremities of the hub structure, flanges have been included to allow connection with the two blades as shown in Figure 3.4. The teetering hinge was produced by forging a steel shaft with a T-shaped head, displayed in Figure 3.5, which was interfaced to the hub body via elastomeric bearings. These bearings allowed the hub to oscillation in the plane perpendicular to the shaft axis, enabling the teeter motion. Bumpers were fitted either side of the shaft opening in the hub to reduce the effect of teeter end impacts if they were to occur [29].

Figure 3.4: Gamma 60 - Hub flange for blade connection [29]

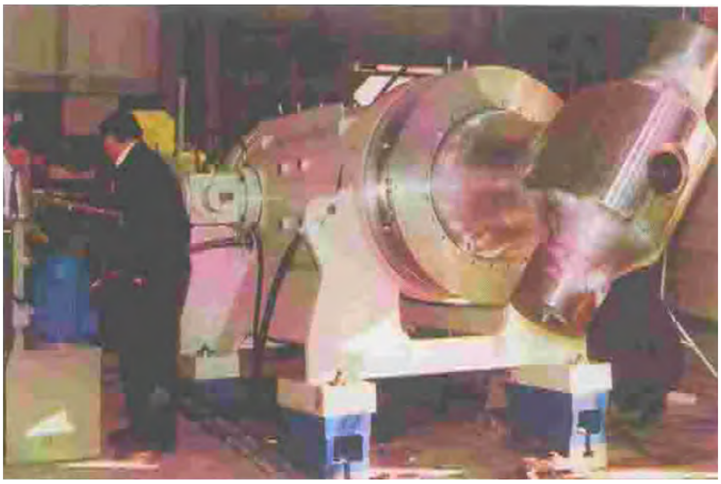

Figure 3.5: Gamma 60 - LSS with T-shaped head for teetering [29]

The Gamma 60 had a maximum allowable teeter angle of 6° before the hard-stop bumpers were impacted. During normal start-up the maximum teeter angle experienced was 3.87°, during normal operation this increased to 4.34°, and during normal shutdown a maximum of 5.11° was reached. These maximum angles were all reached while the blades were in their horizontal position, so impacts with the tower were not an issue. In the case of emergency shutdowns the maximum teeter angle flirted with 6°, resulting in the highly undesirable teeter end impacts as discussed in Subsection 2.3.1 [26].

Nacelle and Drivetrain

The main function of the nacelle was to support the rotor and house the drive train, composed of its shaft, gearbox, generator, and actuation components. It was connected to the tower via the yaw housing and was composed of a welded steel bed plate, as shown in Figure 3.6, enclosed by a welded steel and sandwich panelled cover. The total tower head weight, including the rotor, nacelle frame, drive train, and electrical equipment, was 110 t [29]. The main LSS shaft was forged from a single block of steel, hollowed out to allow signal wires to pass through. The shaft was supported by two roller bearings and enclosed within a stiff container housing as shown at the rear of Figure 3.5. The front one primarily handled radial loads while the rear one, a combination of one straight and two tapered roller bearings, primarily withstood axial loads. The function of this enclosing structure was to relieve the shaft of the bending stresses caused by the compliance of the bearings [29]. During erection of the Gamma 60 at Alta Nurra, the tower head was hoisted to the top of the tower with the blades locked in a horizontal orientation as shown in Figure 3.7.

Figure 3.6: Gamma 60 - Nacelle bed plate and internal components [29]

Figure 3.7: Gamma 60 - Erection of the Gamma 60 at Alta Nurra [29]

Yaw Housing

The yaw housing of the Gamma 60 was located between the nacelle and tower top, with the function of storing the yaw system components. It was split into an upper and lower section, that could rotate around each other thanks to a 3 m diameter slewing bearing. Like the tower structure, the yaw housing was also constructed from calendered steel. At a high level, the yaw system was composed of the slewing bearing, two hydraulic yaw drives, and a yaw lock. The yaw system is responsible for controlling the rotational yaw movement of the nacelle that is required for active power control [29]. This system and its operation is discussed in more detail in Subsection 3.3.1.

Tower

The 61.6 m high tower was constructed from tubular steel with a uniform external diameter of 3 m. It was made up of eight sections, each roughly 7.8 m tall, which were processed by calendering to obtain their tubular form and joint welded together [29]. The sections varied in thickness from 16 mm at the top to 32 mm at the base. The tower was used to house power and signal cables, with a lift included to provide access to the nacelle. The equipment in the tower weighed 9 t, combining with the steel structure to result in a total tower weight of 121 t [29].

3.2.2. Seawind 6

Overview

The Seawind 6 has a hub height of 95 m, a rotor diameter of 126 m, and sits on a floating concrete platform. Below, Figure 3.8 displays both the CAD generated render of the Seawind 6 and the Bladed model. Both have been meticulously designed by Seawind engineers in order to visualise and test the turbine's performance, respectively. Unlike the Gamma 60 model, the Seawind 6 model was designed and tested in the latest release of Bladed, version 4.12. In this section, each of the main Seawind 6 structural components will be examined.

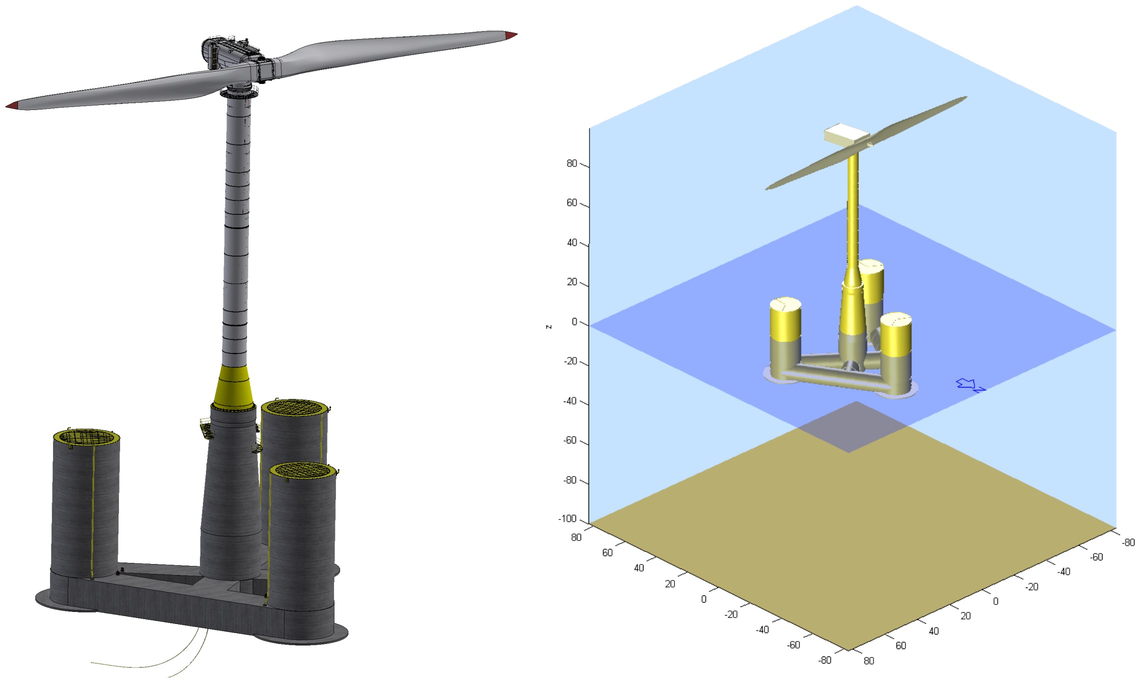

(a) CAD render

(b) Bladed model

Figure 3.8: Seawind 6 - Full body view

Blades

The full Seawind 6 rotor is displayed in Figure 3.9, with a zoomed in version of the hub-root assembly shown in Figure 3.10a. Each blade is 61.25 m in length, with a total rotor diameter of 126 m and swept area of 12462.66 m^2. The blades are rigidly mounted onto the hub with zero coning angle and zero δ_3 angle. The blade root has a crown of metal studs which connect to the inserts which are arranged internally in the hub's flange, as shown in Figure 3.10b. Both the hub and Blade root have a quasi-square shaped geometry [9].

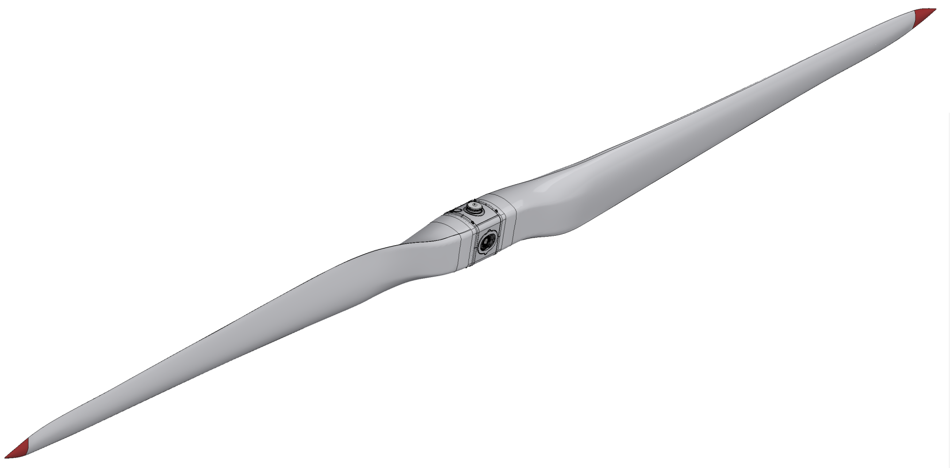

Figure 3.9: Seawind 6 - Rotor

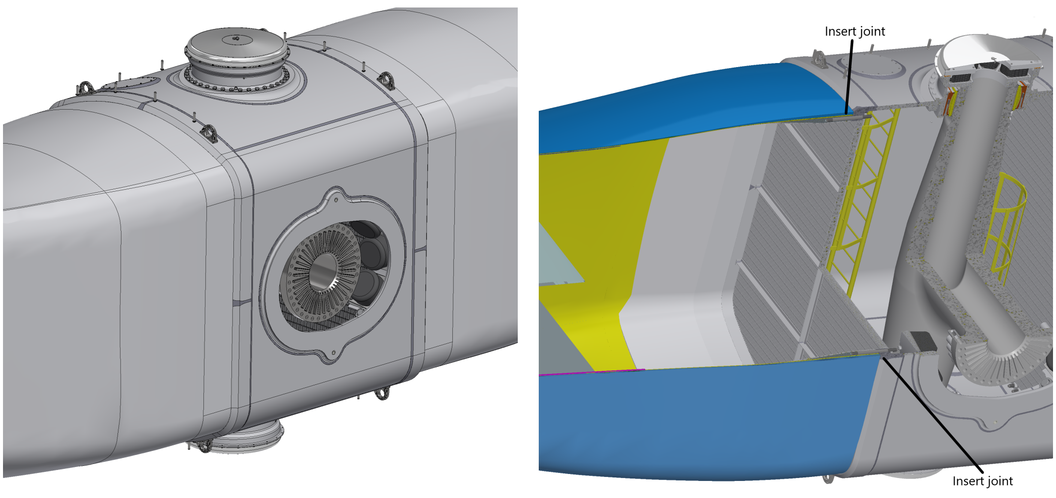

(a) Rotor close-up

(b) Cut-through of the insert joint

Figure 3.10: Seawind 6 - Hub-root assembly

The main blade characteristics are provided in Table 3.4 below. The maximum design values for chord and thickness are 5.58 m and 3.69 m, respectively, where thickness refers to the width of the blade and is provided as a percentage of the chord length. The same geometry and mass distribution is ensured for both blades by using the same moulds for the two blades [9]. This results in a well balanced rotor from both an aerodynamic and mechanical stand point. The blade body is characterized by a high bending and torsional stiffness, with the global bending stiffness subsequently reduced by the teetering hinge [9]. The blade is composed of the following airfoils; section 1 (Cylinder 1), section 2 (DU40_A17), section 3 (X818 and DU40_A17), section 4 (X830 and X818), section 5 (X831 and X830), section 6 (X832 and X831), and section 7 (X832). [6].

Table 3.4: Seawind 6 - Blade configuration

Radius (m)	Chord (m)	Thickness (%)	Twist (°)	Airfoil	Mass dist. (kg/m)
0	4.56	80.84	0	1	4652.98
1.25	4.56	80.84	0	1	963.46
4.25	4.60	71.14	22.51	1	611.43
7.25	4.98	59.28	20.71	2	428.60
10.25	5.48	47.48	17.54	2	412.55
13.25	5.58	40.62	12.28	3	394.32
16.28	5.57	35.64	8.80	3	395.74
19.31	5.34	32.21	7.09	3	343.45
23.36	4.95	29.89	6.22	3	305.56
26.51	4.66	28.07	5.68	3	287.28
29.67	4.36	26.08	5.20	3	250.52
32.83	4.10	24.20	4.82	3	216.76
33.30	4.06	24.00	4.78	4	216.76
35.99	3.86	22.79	4.55	4	197.76
39.15	3.63	21.87	4.38	4	182.97
42.30	3.40	21.35	4.28	4	157.67
45.46	3.18	21.00	4.22	5	139.70
48.62	2.97	20.58	4.25	5	113.79
51.78	2.80	19.36	4.39	5	90.76
54.93	2.51	18.00	4.33	6	73.93
55.72	2.39	17.34	4.17	6	64.36
56.51	2.25	16.59	4.03	6	56.25
58.09	1.84	15.00	3.61	6	47.01
59.67	1.11	15.00	4.80	7	27.09
61.25	0.06	15.00	6.01	7	2.66

Table 3.5 outlines the materials used to construct the blades [9]. The various parts of the blade referred to in this table are displayed in the blade cross-section in Figure 3.11. The spar caps are made of carbon fiber, fabricated using a pultrusion process, with the remaining parts made of glass fibers via infusion [8]. Using these materials, each blade is expected to weigh roughly 20 tonnes. A specialty Polyurethane type erosion protection coating will be applied to the blades of the Seawind 6 to avoid damage which is particularly prevalent above tip speeds of 100 m/s (Seawind 6 has rated tip speed of 137 m/s). This has been developed for application of military helicopter blades working in desert areas [8].

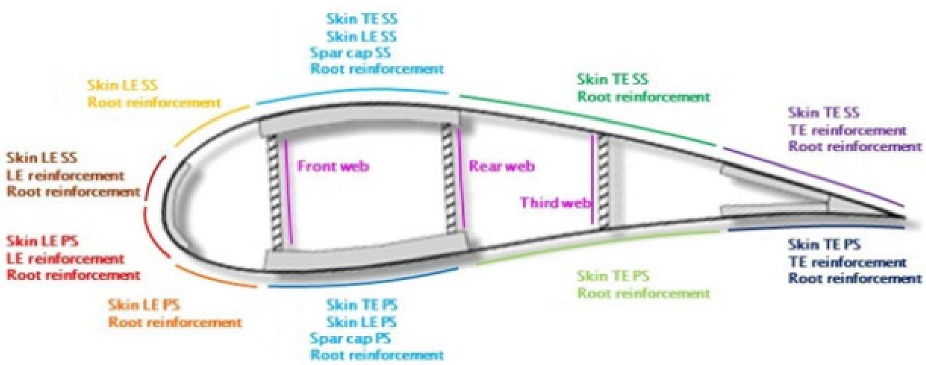

Figure 3.11: Seawind 6 - Airfoil cross-section

Table 3.5: Seawind 6 - Blade construction

Component	Material	Process
Shell	%Glass 3AX 0/-45/+45	Infusion
Spar caps	%Carbon UD 600	Pultrusion
Spar webs	%Glass 2AX -45/+45	Infusion
Root additional material	%Glass 3AX 0/-45/+45	Infusion
TE, LE	%Glass UD 1200, reinforced	Infusion
Third web	%Glass 2AX -45/+45	Infusion

Hub and Teetering Hinge

The hub body is a quasi-squared shaped structure, constructed from welded steel (S355 J2+N) plates and various forged parts. Looking at Figure 3.12, the two co-axial opposite housings of the hybrid teeter bearings are shown on the left and right of the hub, as well as the two connection flanges to the blades roots on the top and bottom, and the oval opening for the shaft at the rear. The hub weight, excluding the T-shaft, is estimated to be approximately 25 tonnes [11]. The T-shaft head is a hollow forged steel piece (ASTM A668 class D) with horns machined to fit neatly within the two sliding bearings [11].

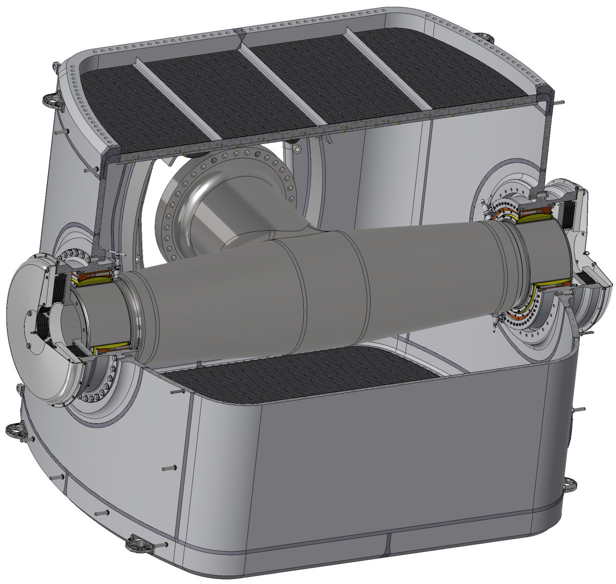

Figure 3.12: Seawind 6 - Hybrid teeter hub cross-section

Seawind has two patented teeter hinges, a hybrid and an elastomeric variant, with the choice depending on the size of the turbine. The hybrid teetering hinge is made of two hybrid ”sleeve and elastomeric” bearings, as displayed in Figure 3.12. The elastomeric teetering hinge is displayed in Figure 3.13, with its associated loading forces indicated. The bearings of both hinges are located between their housings (which are bolted to the hub body) and the horns of the T-shaped head of the shaft [10]. The metal-elastomeric bricks provide the desired torsional stiffness, of 165 nkNm/°, to the hinge through the shear strain of the elastomeric material. They also bear the compressive axial force of the weight of the rotor, as demonstrated in Figure 3.13. Spherical and cylindrical, self- and grease lubricated, bronze bushes (sleeves) are incorporated to handle radial loads due to aerodynamic torque and thrust. The radial force acting on the bushes (coming from the rotor thrust and the torque) acts within a limited angle. The wear will therefore be limited to within this angle, meaning they can simply be rotated after some years of operation to prolong their lifetime [10].

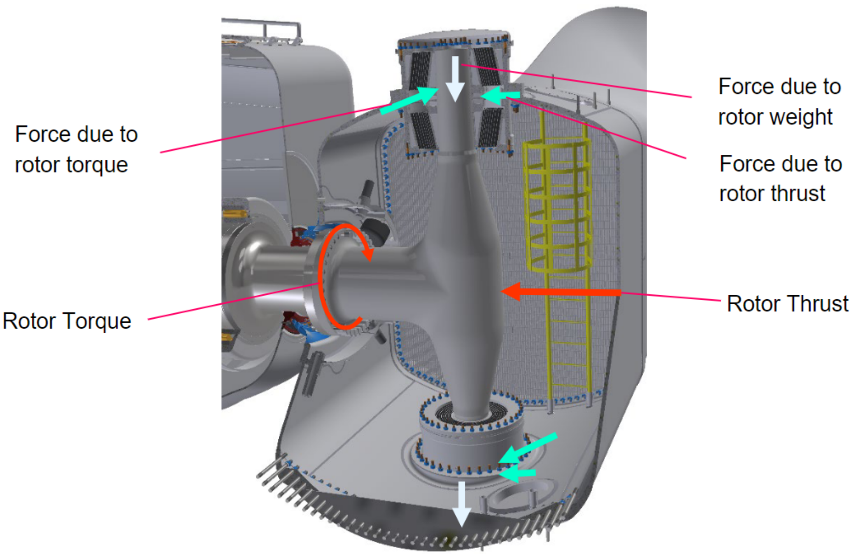

Figure 3.13: Seawind 6 - Elastomeric teeter hinge

As shown in Figure 3.14, the inner edges of the shaft opening are equipped with a full stop bumper if teeter angles were ever to become excessively large. These are made of material that is less flexible than the torsional stiffness provided by the teetering hinge. Luckily, all the in-house simulations to date show that the bumper is never impacted [8].

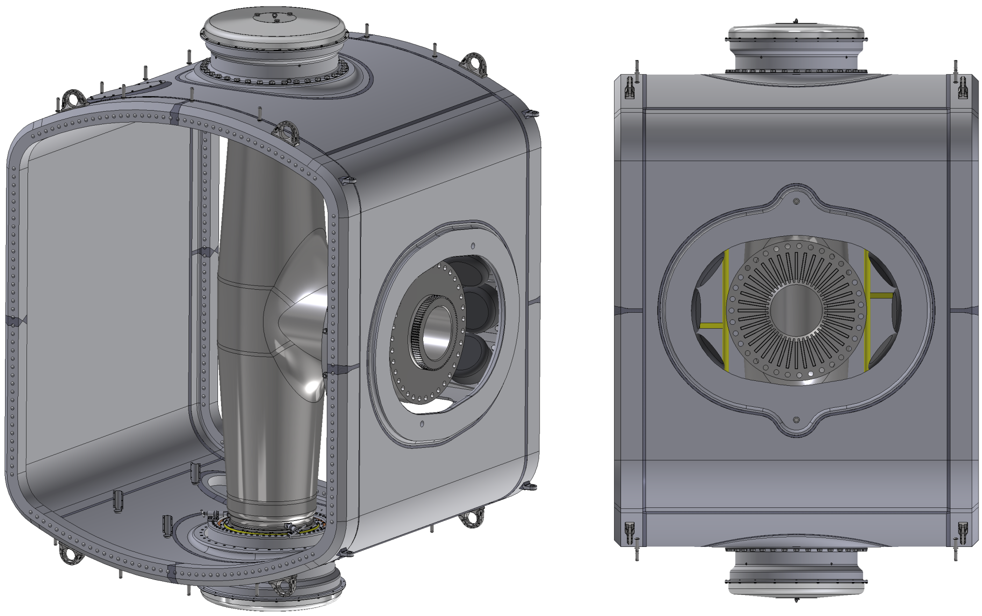

(a) Hub and teeter hinge assembly

(b) Side view of teeter bumpers

Figure 3.14: Seawind 6 - Hub view rotations

Nacelle and Drive train

The Seawind 6 nacelle is a tubular steel structure designed to house the components of the drive train and support the helideck (when included). The longitudinal steel (S355J2+N) frame of the nacelle is about 14m long, 6 m wide, and 5 m high, as displayed in Figure 3.15. This sits above the vertical steel (S355J2+N) cylindrical extension which is roughly 5 m in diameter and flanged to the yaw housing [8]. A 16 m diameter helideck may also be included atop the nacelle to allow easy access for maintenance personnel. When connected to the rotor and put in operation, an overhang of 6 m, 7° shaft tilt angle, 0° coning angle, and 0° delta-three angle results in a blade tip-tower clearance of 6.5 m during normal operation and 3.8 m during extreme conditions [8]. Both of these are more than acceptable.

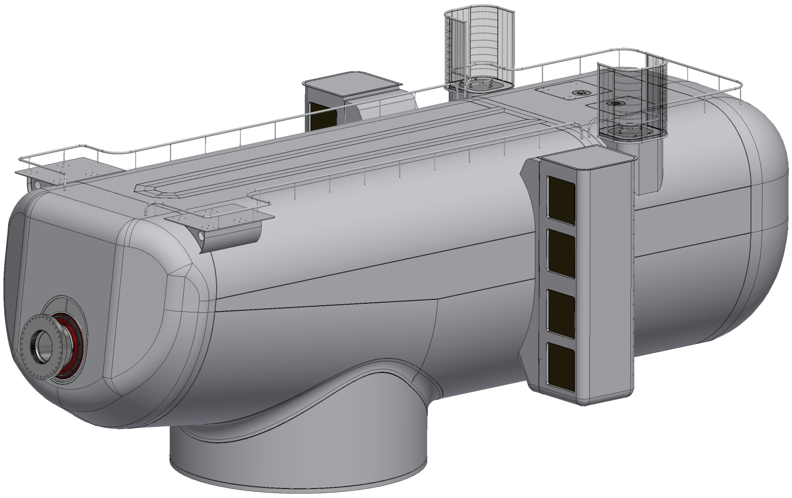

Figure 3.15: Seawind 6 - Nacelle structure

The Seawind 6 drivetrain is displayed in Figure 3.16. The main structural elements are the hollow forged turbine steel shaft (ASTM 688 Class D like the T-shaft head), the front radial toroidal roller CARB bearing, the rear radial and axial spherical roller bearing, the double disk brakes (GGG50) on the LSS, the gearbox, and the generator [8]. The weight of the nacelle, including all associated structural pieces mounted onto it, is estimated to be 75 t [12].

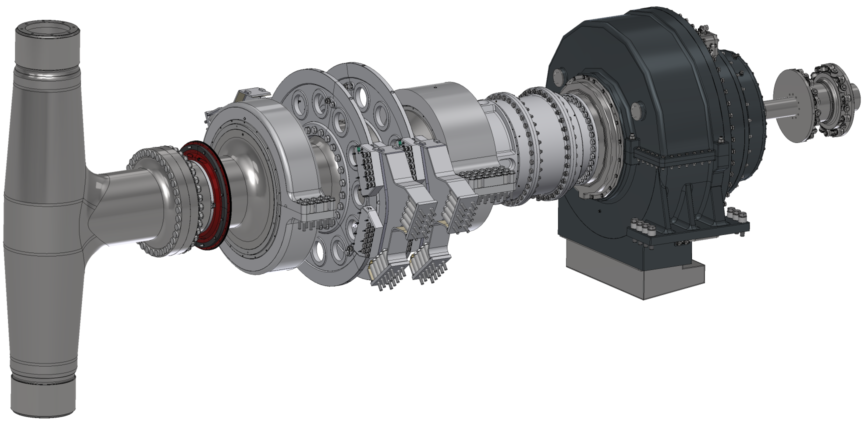

Figure 3.16: Seawind 6 - Drive-train

Yaw Housing

The yaw housing is the transition structure between the nacelle and the tower. It is split into two parts, as shown in Figure 3.17, and constructed from S355J2+N steel [8]. The upper part is a cylindrical structure with a top flange coupled to the nacelle and a bottom flange coupled to the slewing bearing and crown gear package. This part also houses the four yaw drives, the slewing bearing and associated yaw gear, yaw lock, electrical equipment, and sensors. The bottom part has a similar shape with an upper flange coupled to the slewing bearing and the crown gear package, and the bottom flange coupled to the tower flange. The combined weight of both pieces is roughly 22 t [13]. The yaw bearing rings, gear, and pinions are all to be constructed from steel as well (42CrMo4V, 42CrMo4, and 16MnCr5, respectively) [8].

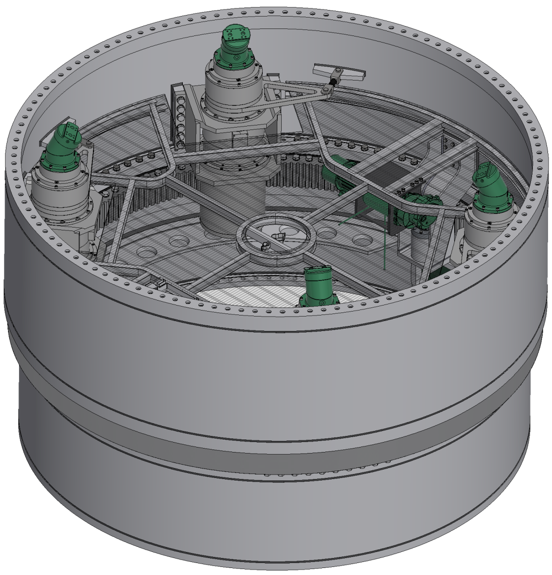

Figure 3.17: Seawind 6 - Yaw housing

Tower and Floating Platform

The Seawind 6 sub-structure is composed of a 5 m diameter steel (S355J2+N) tower mounted onto a reinforced and post-tensioned concrete floating semi-submersible platform, as shown in Figure 3.18. The tower is composed of three sections, with a total height of 69 m. The thickness of the tower increases towards the base to counteract the bending moments. It is equipped with a ladder and elevator to allow access to the nacelle if maintenance personnel were to arrive by sea [8]. The concrete floating platform is made of a central vertical shaft which is linked to three vertical floaters through rectangular arms. The top of the central vertical body will be reinforced and bolted to the steel turbine tower. The hollow arms are rectangular in cross-section with internal reinforcing transverse walls which can be seen in Subsection 3.3.2 in Figure 3.26. During operation, the volume of the arms will be flooded with water in order to counteract the structural instability of the walls under sea pressure [15]. Examining Figure 3.18, large concrete heave plates are shown at the base of the floaters. These play an important role in damping the tilting motion of the system in rough waters. Internally, the central vertical body hosts much of the electrical system and will be covered in Subsection 3.3.2. It is the intention that these concrete platforms will be constructed on a floating or dry dock close to the offshore installation site [15].

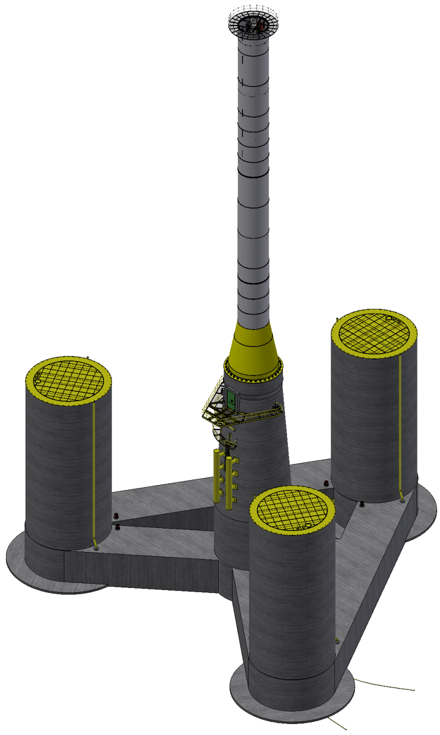

Figure 3.18: Seawind 6 - Tower and floating platform

It is worth noting the direction convention used for Bladed simulations in later stages of this report. As visualised in Figure 3.19, α is the direction of the wind, waves, and current, while Ψ is the direction of the rotor axis (while parked or operating). The platform is initially installed with the x-axis parallel to the long-term prevailing wind direction.

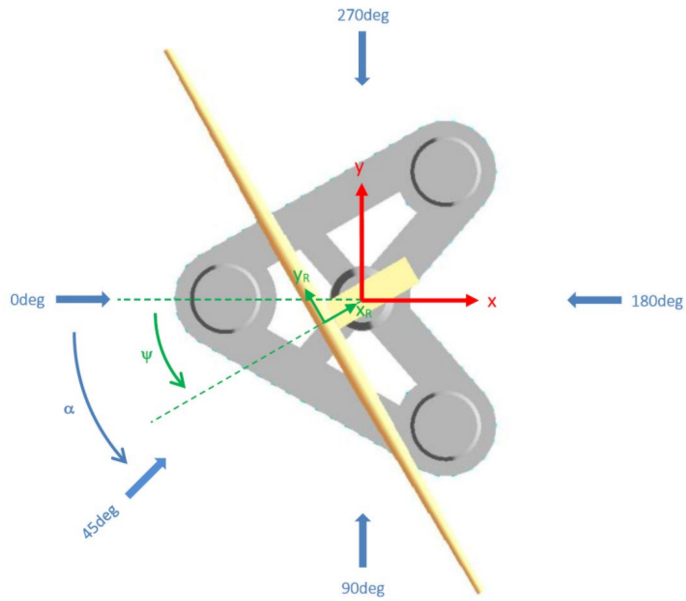

Figure 3.19: Seawind 6 - Platform direction convention

Mooring Lines and Anchors

The mooring configuration for the Seawind 6 is displayed in Figure 3.20. Here, six identical 114mm R4S (marine application) stud-link chain mooring lines are connected to three gravity anchors [61]. Two mooring lines are connected to the same anchor, with the naming convention for the anchors consisting of the two line's numbers. For instance, Mooring Lines 2 and 4 (ML2 and ML4, respectively), are fixed to Anchor 24 (A24). Each of the mooring lines have a length of 415 m and radius (distance between fairlead and anchor) of 335 m. This is the basic configuration, with modifications made depending on the sea depth and turbine size, including using dynamic mooring technologies and suction bucket anchors.

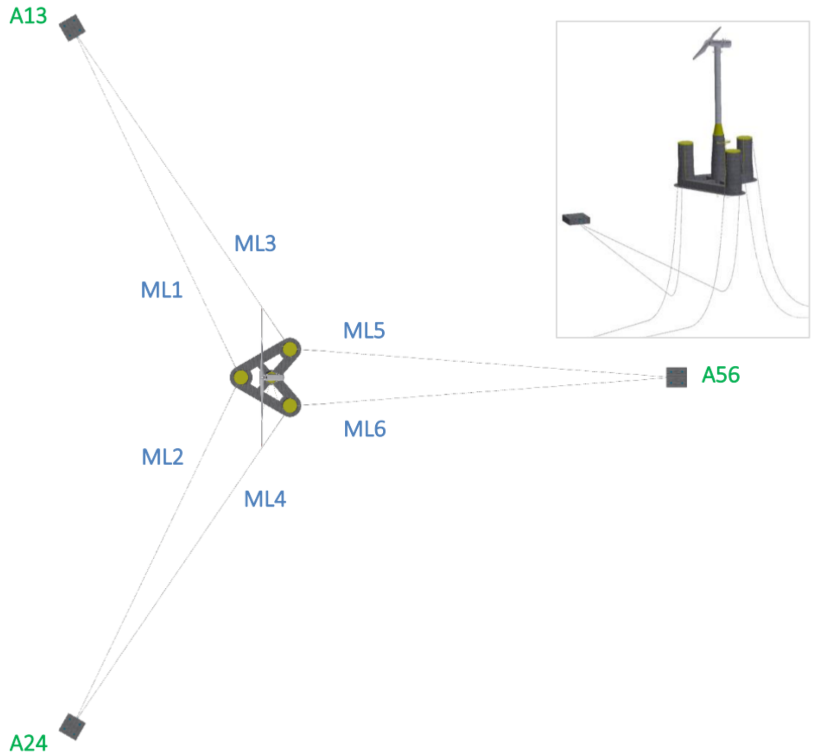

Figure 3.20: Seawind 6 - Mooring line configurations

The mooring lines are connected to the platform at the tops of the three floaters, as shown in Figure 3.21a below, with two fairleads for each floater. The anchors are also attached to two chains each, as shown in Figure 3.21b. The chain Minimum Breaking Load (MBL) is 13780 kN while the anchor horizontal holding capacity is 14000 kN [61].

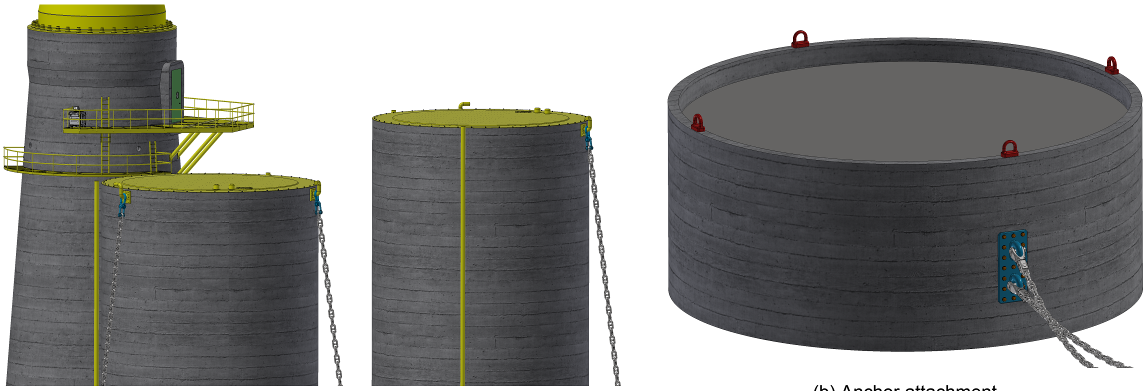

(a) Platform floater attachment

(b) Anchor attachment

Figure 3.21: Seawind 6 - Mooring line attachments

3.3. Electrical System

3.3.1. Gamma 60

Nacelle and Drivetrain

The Gamma 60 drivetrain is composed of a main shaft coupled to a generator via a gearbox. As shown in Figure 3.22, the majority of the electrical components are housed in the nacelle [29]:

- The monolithic main shaft with T-shaped head, supported by bearings and enclosed within the stiff steel housing.
- Two hydraulic disk brakes, one on the main shaft (LSS) and one on the HSS. The LSS brake was manufactured by the British company Twiflex and had a rated torque of 900 kNm, while the HSS brake was manufactured by the Danish company Svendborg and had a rated torque of 16.8 kNm [29]. The LSS disk brake was 1.5 m in diameter and was designed to be capable of stopping the machine from excessive speed or from some other emergency entirely on its own. The HSS disk brake was only engaged when parking the turbine [25].
- The two-stage epicyclical gearbox was manufactured by the German company Desch and had a ratio of 1:33 and rated torque of 380 kNm [29].
- The induction generator was manufactured by the Italian company Ansaldo S.p.A. and had a rated power of 2000 kW and nominal voltage of 1450 V [29].
- The static frequency, line commutated converter, with six-phase reaction and rated power of 2000 kW, allowed connection to the AC grid. The converter was also capable of driving the generator as a motor. Accordingly, the gearbox was constructed to transmit torque in both directions [25].
- The yaw actuation oil tank, the yaw nacelle hydraulic components and piping, and coolers.
- The command and monitoring system was manufactured by Ansaldo S.p.A. and ensured that control was maintained both in normal and emergency operating modes [29].
- The nacelle electrical cabling and monitoring devices.
- The fire and lightening protection system.

The nacelle was then connected to the yaw housing, as shown at the bottom of Figure 3.22, where the yaw drive system was located.

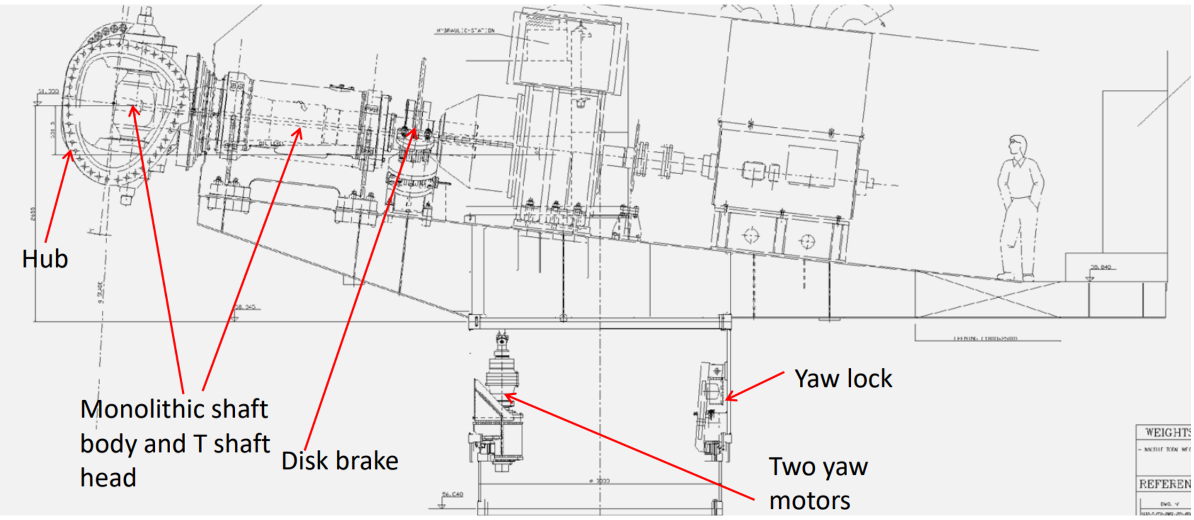

Figure 3.22: Gamma 60 - Nacelle technical drawing [26]

Yaw Drive

The yaw drives were powered by two separate hydraulic supply and actuation systems, one driven by the main shaft (LSS) and the other by the gearbox [29]. Each yaw drive consisted of a hydraulic motor, gearbox, clutch, and pinion. The pinions engaged the teeth of the slewing bearing, as shown in Figure 3.23, and allowed the yaw rotation of the nacelle. The two yaw drives combined to produce a total yaw torque capacity of 400 kNm [26]. This meant they could yaw variably with a rate between 2°/s and 8°/s [47]. Peaks of 10 °/s were experienced during testing at Alta Nurra, when extreme wind conditions caused rotor speeds of up to 55 rpm and resulted in an emergency shutdown of the turbine [29].

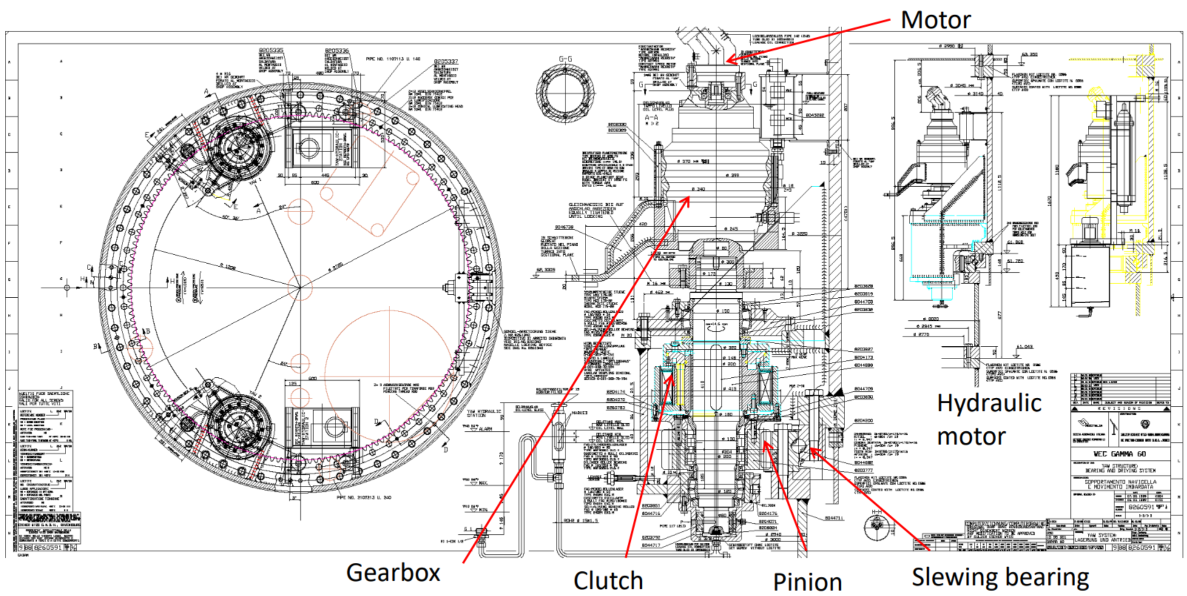

Figure 3.23: Gamma 60 - Yaw system and drive technical drawing [26]

3.3.2. Seawind 6

Nacelle and Drivetrain

Like the Gamma 60, the Seawind 6 drivetrain is also composed of a shaft and gearbox coupled to a generator. These, along with the other electrical components that are housed in the nacelle, are displayed in Figure 3.24 and detailed below [12]:

- The the main shaft, with an over-speed of 28 rpm, and bearings.
- Two large disk brakes, 2.5 m in diameter, each with four hydraulic calipers producing a total brake torque capacity 4800 kNm. These are both mounted on the LSS and are normally just used to completely stop the rotor at the end of a shutdown procedure. However, to increase turbine safety, they are also sized so that they are capable of braking the rotor from full load at any operating wind speed [8].
- The two stages planetary gearbox, with ratio of 1:34.8, rated inlet torque of 3000 kN, and coolers included.
- A flexible sliding component is mounted between the gearbox and the generator, to protect the gearbox in the case of a generator short circuit.
- The asynchronous squirrel cage generator, which is the simplest and most reliable industrial electrical generator. It has four pole couples, a rated power output of 6.6 MW, and coolers included. This is coupled with the full power frequency converter, which is housed in the platform, through a disconnector for mechanical isolation in case of service and for pre-charging a unit to turn the rotor below cut-in speeds [8].
- The yaw actuation oil tank, the yaw nacelle hydraulic components and piping, and coolers.
- The electrical cabinet fed by the auxiliary transformer. This powers the nacelle and yaw housing electrical equipment.
- The controller board and its UPS (Uninterruptible Power Supply) [8].
- The nacelle electrical cabling and monitoring devices.
- The aerosol based fire protection system.
- The two lines of lighting protection system. One that runs from the blade tip to the tower, and a second that protects the wind sensors.
- The functional and structural sensors.

Externally, the nacelle supports, by bolting, the oil-air coolers of the gearbox, gearbox lubrication oil and the yaw actuation oil, and the glycol water-air coolers of the generator. The rest of the electrical sub-system equipment is housed at the base of the turbine in the floating platform [8].

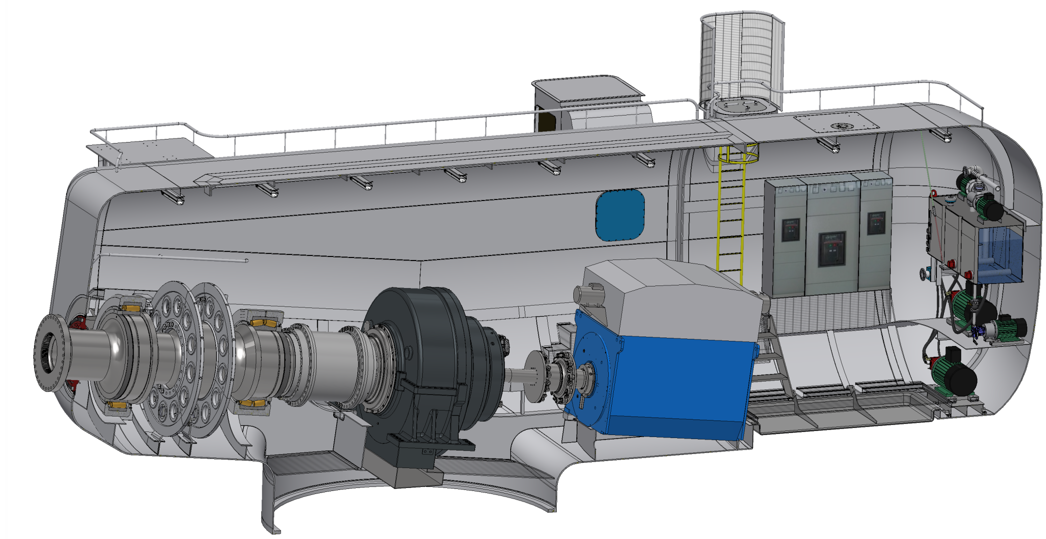

Figure 3.24: Seawind 6 - Open nacelle view of electrical components

Yaw Drive

As described earlier, the Seawind 6 regulates its power output by yawing in and out of the wind at a rate of up to 10 °/s. Indeed, for power control, a lower yawing rate of approximately 4°/s is sufficiently quick. Only in emergency shut down the yawing rate is set at its maximum capacity [8]. Yaw drives are responsible for generating this yawing motion by rotating the nacelle about a 5 m diameter slewing bearing at the top of the turbine's tower. The rated yaw torque capacity is 4340 kNm (four motors at 350 bar) with a peak of 5580 kNm (four motors at 430 bar) [8]. Figure 3.25 shows a cross section of the yaw housing, with two of the four yaw drives, the yaw lock, hoisting crane, and slewing bearing included. The hydraulic yaw system is composed of four parallel independent main closed circuits and four parallel auxiliary closed circuits. Each main circuit is fed by a main pump mechanically driven by the turbine gearbox, while each auxiliary circuit is fed by an auxiliary electrical pump [14]. Each yaw drive can be fed by either its main or auxiliary circuit. The auxiliary circuit is used during start-up, as well as when the turbine is parked and the controller demands to yaw the nacelle in order to keep the blades aligned with the wind. The auxiliary electrical motors are powered by the grid through the auxiliary transformer or, in case of lack of grid, by a reserve battery bank [14]. Looking at the yaw drives in Figure 3.25 and working from the top down, each drive has a hydraulic motor, gearbox, hydraulic clutch, pinion, and a support that is bolted to the yaw housing wall. Three out of the four yaw drives are sufficient to overcome the yaw torque (rotor wind loads and yaw bearing friction) and yaw the nacelle. It is, however, best to keep all four drives in operation at reduced torque. There are no yaw brakes included in the Seawind 6 design, with the yaw lock only used when the machine is parked [14].

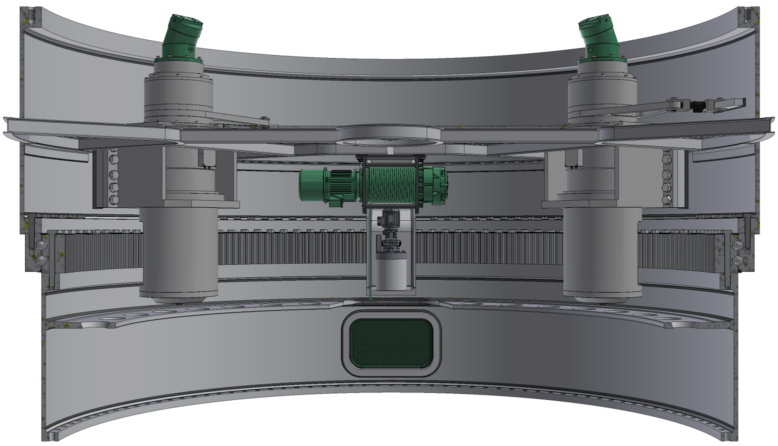

Figure 3.25: Seawind 6 - Yaw system cross-section

Platform

The remaining electrical components are housed internally in the central concrete shaft of the platform, above which the steel tower is mounted. They are all are arranged at the bottom of the shaft, with the exception of the converter which is located at the elevation of the main door, as shown in Figure 3.26 [15]. An IGCT (Integrated Gate-Commutated Thyristor) bidirectional full power converter is employed with a rated voltage 3.3 kV. This enables the shaft torque of the turbine, and therefore the running speed, to be controlled while also meeting the grid requirements in terms of voltage, frequency, and quality of the electricity [8]. The main transformer, used to step up the output voltage from 3.3 kV to 66 kV is shown at the bottom of Figure 3.26. Between the converter and transformer is a harmonic filter to stabilise the DC power and remove any remaining AC harmonics [8]. The auxiliary transformer, and both the Low Voltage (LV) and Medium Voltage (MV) boards are also placed here. A reserve battery bank with inverter for a peak of 250 kW and a capacity of 600 to 1000 kWh is arranged in an isolated box of the support structure ventilated from the outside. As for the converter and transformer, their primary mean of cooling is by using demineralised sea water [8]. This is a great design in both an environmental and economical sense.

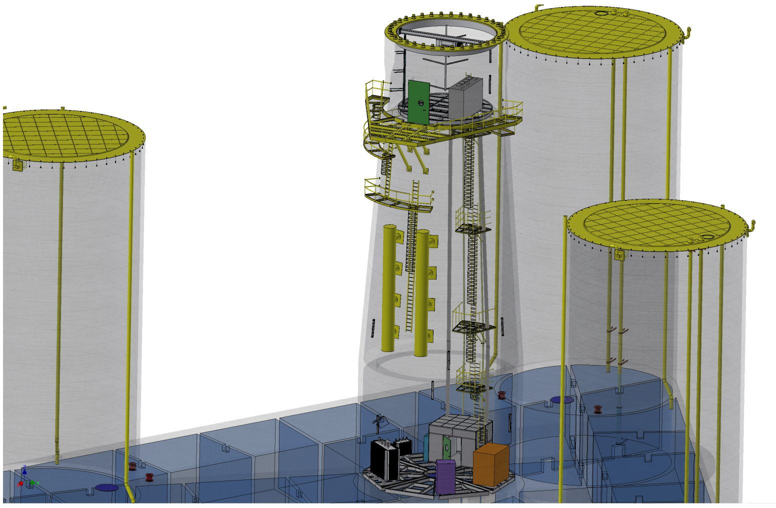

Figure 3.26: Seawind 6 - Electrical components housed in the Platform

Single Line Diagram

The single line diagram in Figure 3.27 below is the simplest symbolic representation of the Seawind 6's electrical power system. There are two main broken line boxes, one at the top and one at the bottom of the image, that contain the subsystems found in the tower and the nacelle, respectively. Located in the tower section is the medium voltage board, auxiliary transformer, low AC voltage board, main transformer, low DC voltage board, and converter. In the nacelle and yaw housing section, the nacelle electrical cabinet and generator are found [8].

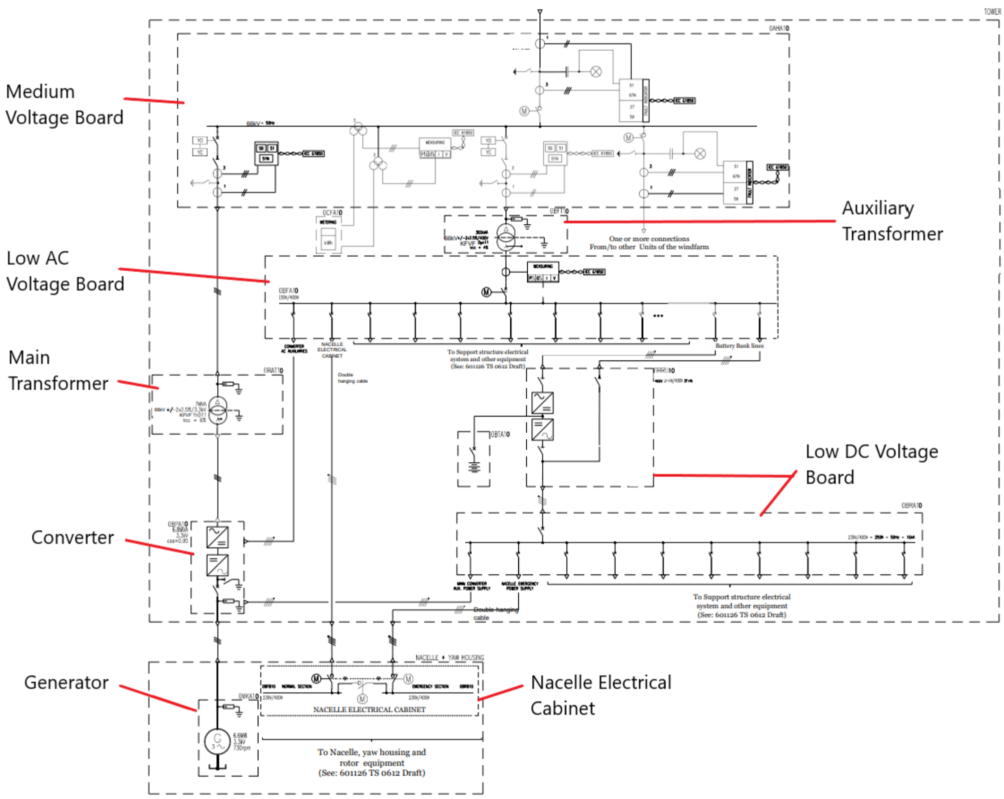

Figure 3.27: Seawind 6 - Single line diagram [8]

3.4. Control

The Seawind 6's control strategy was based, almost entirely, on that of the Gamma 60. The Gamma 60's external controller was initially developed by Coelme for Bladed 4.2. Over time it had become corrupted, and remedying it involved extensive investigation, trial and error, downloading legacy versions of Bladed, and discussions with both Seawind engineers and DNV technical support. Frustratingly, however, the accuracy of results was far from perfect and it was not compatible with Bladed Batch runner. Therefore, it was decided that the best approach was to take the old Seawind 6 external controller, also developed by Coelme, and modify it for the Gamma 60. This controller read in a list of prescribed input variables in Bladed and ran the control algorithms based on these. For example, there were rotor running speed schedules, generator torque schedules, yaw pump hydraulic details, threshold, and ramping constants. By looking through Gamma 60 documentation and input lists for the Coelme controller, it was possible to replace all the Seawind 6 inputs with suitable Gamma 60 substitutes. This ensured that the Gamma 60 model ran as desired. The Seawind 6 simulations were then carried out using a new, optimised version of the external controller developed by Sowento. This was still based entirely on the old Coelme controller, meaning any calibration improvements suggested from the Gamma 60 work can, and should, be applied to the Seawind 6 controller to further improve its real-world accuracy. The following control algorithms were used to operate the physical turbines and have been coded in to all the above controllers for use in Bladed. For this report, the control procedures will be examined rather than the coding implementation. As both turbines use similar control procedures, the focus of this section will be on the Seawind 6 with comparisons made to the Gamma 60. This is due to a larger reserve of in-depth information being available for the Seawind 6.

3.4.1. Controller Overview

The controller of Seawind 6, like that of the Gamma 60, covers three principle functions:

- To control the power output, the torque, and the running speed of the turbine for each operation mode.
- To set and clear flags which determine the desired operation mode of the turbine.
- To monitor turbine operation, components, sensors, and environmental conditions.

The controller operates with two parallel control loops, both of which are described in more detail in Subsection 3.4.2. The generator "torque control loop" which controls the shaft restraining electrical torque through the full power converter and the "speed control loop" which controls the nacelle's yaw angle relative to the wind direction [8]. The two loops operate in a coordinated way. For example, during operation at wind speeds below rated, the torque control loop adjusts the torque to yield the maximum efficiency while the speed control loop ensures zero yaw misalignment. Above rated wind speeds, the the torque control loop maintains the torque at the rated value while the speed control loop adjusts the yaw misalignment to keep the rated running speed. The same loops control the maneuvers of start and shutdown [4]. These primary operation modes are expanded on in Subsection 3.4.3. The high-level control and monitoring system architecture is examined in Subsection 3.4.4. This controller was compiled as a .dll file and interfaced with Bladed to run simulations.

3.4.2. Control Loops

Torque Control Loop

Note: Following consultation with the Seawind management team, this section of the report has had to be modified slightly to maintain confidentiality of some of the company's proprietary information. Detailed images of the two control loops have been removed and replaced with a simplified conceptual version, as shown in Figure 3.28 below. Paired with the original written description, it is the intention that this still provides the reader with an adequate understanding of the turbine's control procedures.

Focusing on the torque control loop first, the measured generator speed (SGD) is first passed through a band-pass filter and then a notch filter to remove any high frequency content which is not used in the controller and would lead to high frequency control actions. The generator speed (SGD_NOTCH) is then compared to the map, as shown in Figure 3.29, which outputs the computed generator torque (HSS_TQ). During start-up Flag AA is set (FLAGAA = 1), meaning HSS_TQ is read from the map. In shutdown Flag AA is cleared (Flag A = 0), meaning no torque is demanded [4]. The difference between computed (HSS_TQ) and actual generator (QGEN) torque is then calculated. Following this, a Proportional–Integral–Derivative (PID) controller is used to determine the demanded generator torque (QEREF), cleaned from the electric disturbance. A PID controller reads sensor data and then computes the desired actuator output by summing the calculated proportional, integral, and derivative response components. Finally, the supervisory control checks if the grid is present, clearing flag LL (FLAGLL = 0) and outputting QEREF if present, and setting it to zero if Flag LL (FLAGLL = 1) is set for loss of grid [4].

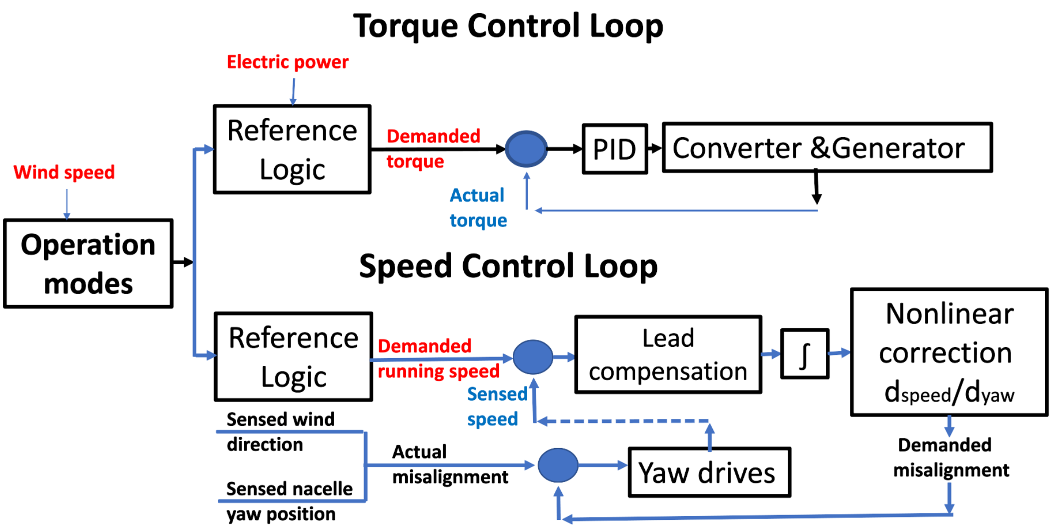

Figure 3.28: Seawind 6 - Simplified torque and speed control loops [8]

The map displayed in Figure 3.29 relates to the control of the Seawind 6. The same phases were used for the Gamma 60, but slight improvements have been made to the curves following testing. Phase 1 shows motoring of the turbine until 212 rpm (6 rpm on the LSS with gearbox ratio of 1:34.8), with a motoring limit of -15250 Nm [25]. In Phase 2, below rated wind speed, the control system attempts to maximise the power coefficient by increasing the generator torque and holding a constant tip-speed ratio, maintaining the rotor speed proportional to the wind speed. Following this, from 530 to 725 rpm, there is a short Phase 3 where the drivetrain torque limit has been reached and it is held constant at 80300 Nm until the generator power limit is reached. Phase 4 lasts until 1450 rpm when the rated power of the turbine has been reached. Here, the power is held constant through a combination of gradual generator torque reduction to 40166 Nm and yawing [25].

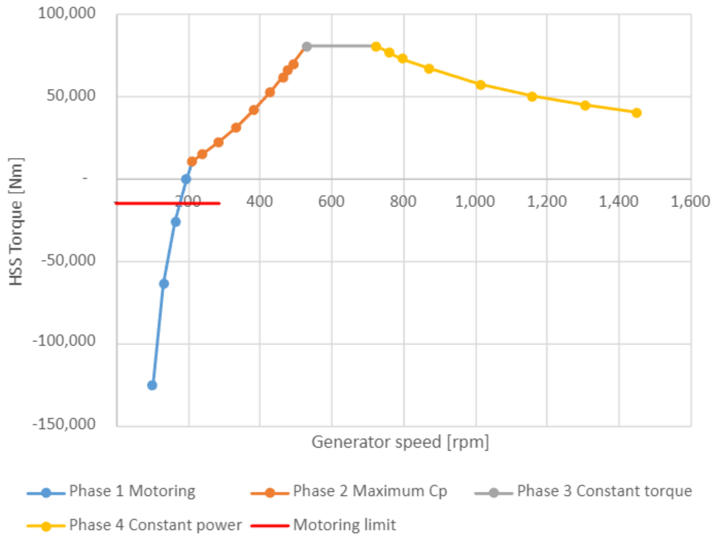

Figure 3.29: Seawind 6 - HSS torque versus rotor speed map [8]

Speed Control Loop

Figure 3.28 also displays the controller's speed control loop. Both the Seawind 6 and Gamma 60 used the exact same loop. The measured wind direction (WDSENDF2) and rotor running speed (SHD1) are first inputted to the controller. The rotor running speed error (SER1) is then calculated from the difference between the measured and filtered rotor running speed (SHD) and the required rotor running speed (SREF1) when in operation. Lead compensation is then applied to SER1 for both turbine rotor lag and yaw actuation lag [4]. The relative nacelle position reference (WDREF) is obtained from the integrated speed error (ISE). The measured wind direction (WDSEND) and nacelle direction (YPSEND) are then inputted and treated to obtain the filtered estimated wind direction (WAF). The WDREF is then subtracted from the WAF to obtain the absolute nacelle position reference (YPREF), which is in turn subtracted from the YPSEND to determine the yaw misalignment (YE). Based on this yaw misalignment, a particular voltage signal (VCC) is sent to the yawing actuation system to achieve the correct yaw motion for active power control [4].

3.4.3. Operating Procedures

Start-up and Operation

The start-up and operation yaw orientations have been visualised in Figure 3.30 below. During start-up, the controller demands the electric pumps to move, at low yaw rate, the nacelle to -90° misalignment. The controller then stops the yaw system, opens the shaft brake, and starts motoring the turbine using the generator in reverse. When the rotor speed reaches 6 rpm (for the Seawind 6), the controller switches from the electric pumps to the main pumps in order to yaw the nacelle towards zero misalignment. Power generation now begins, with the yaw angle and torque controlled according to the logic described in Subsection 3.4.2 [4]. A more detailed flowchart of the controller logic for start-up and operational procedures are presented in Figure 3.31 below, with the contributions from both controller loops and brake calipers specified. Here, Flag A is the speed control loop reference logic flag and Flag AA is the torque control loop integrator limiter flag [4].

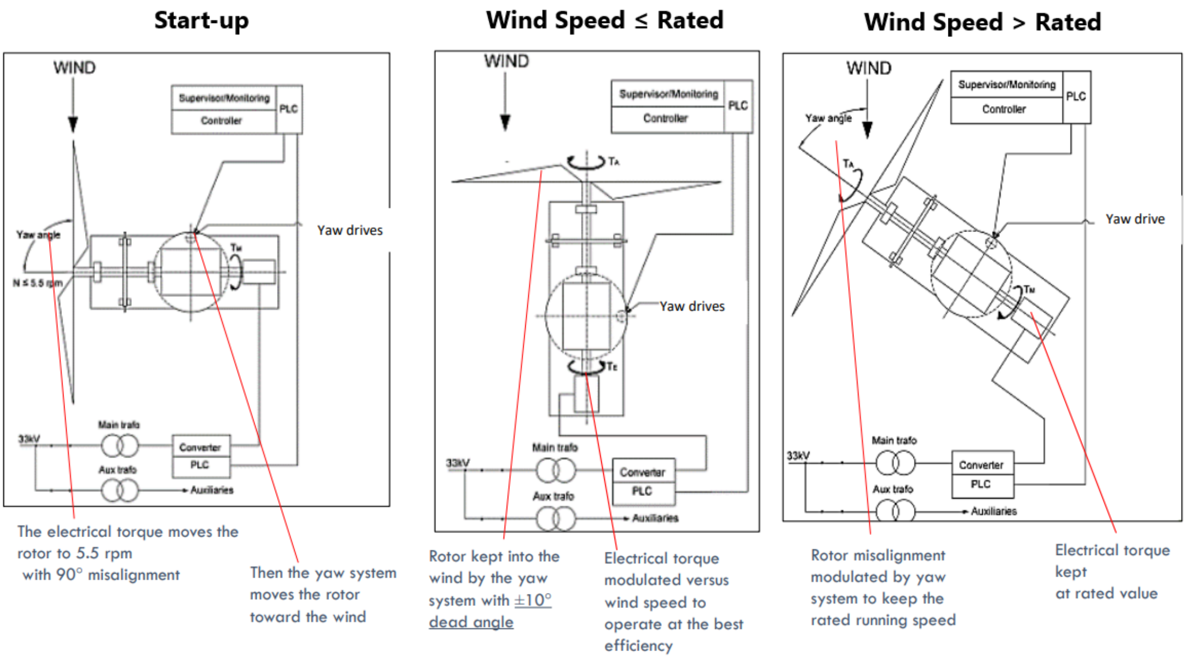

Figure 3.30: Seawind 6 - Start-up and operation procedure [8]

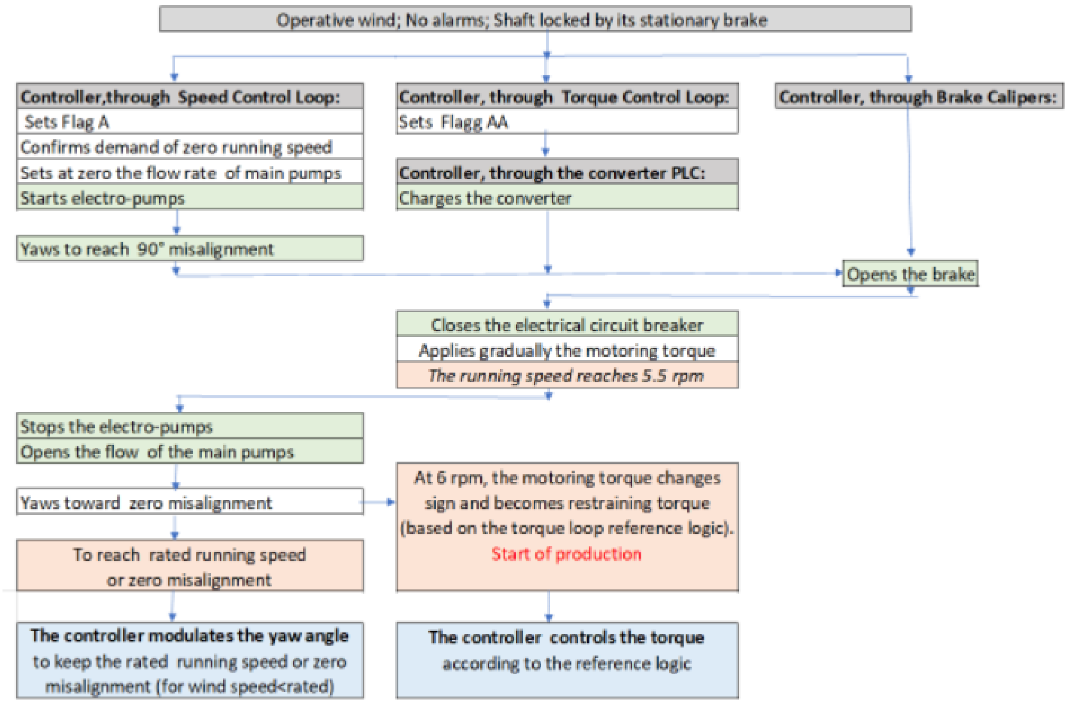

Figure 3.31: Seawind 6 - Logic of start-up and operation [8]

Normal Shutdown

The normal shut-down procedure has been visualised in Figure 3.32 below. This would be initiated for the case of insufficient wind, for non-critical alarms, or for loss of grid [4]. Here, the main pumps gradually yaw the nacelle back to -90° misalignment at a rate of 3°/s in order to aerodynamically reduce the rotor speed while the electrical torque follows the curve of Figure 3.29. The controller stops yawing once the parked position of -90° misalignment has been reached and, once the rotor running speed reduces below 6 rpm, the LSS disk brakes are applied to bring the shaft to a complete stop [4]. Like before, a flowchart of the controller logic for the shut-down procedure is presented in Figure 3.33 below with the contributions from both controller loops and brake calipers specified.

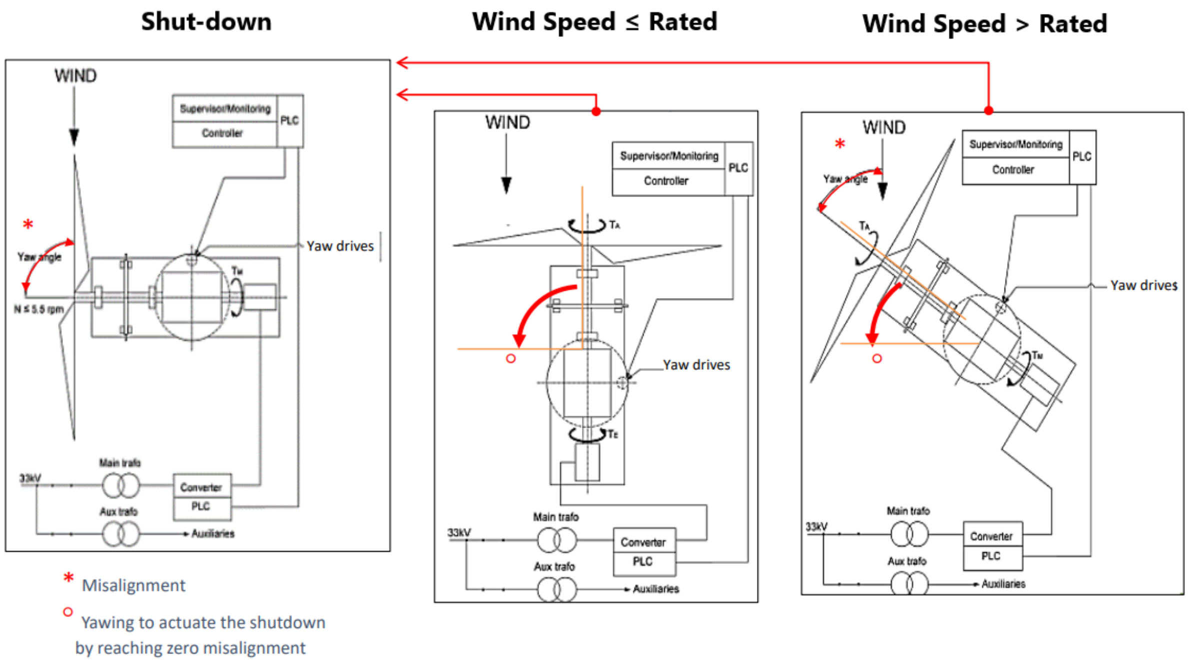

Figure 3.32: Seawind 6 - Shut-down procedure [8]

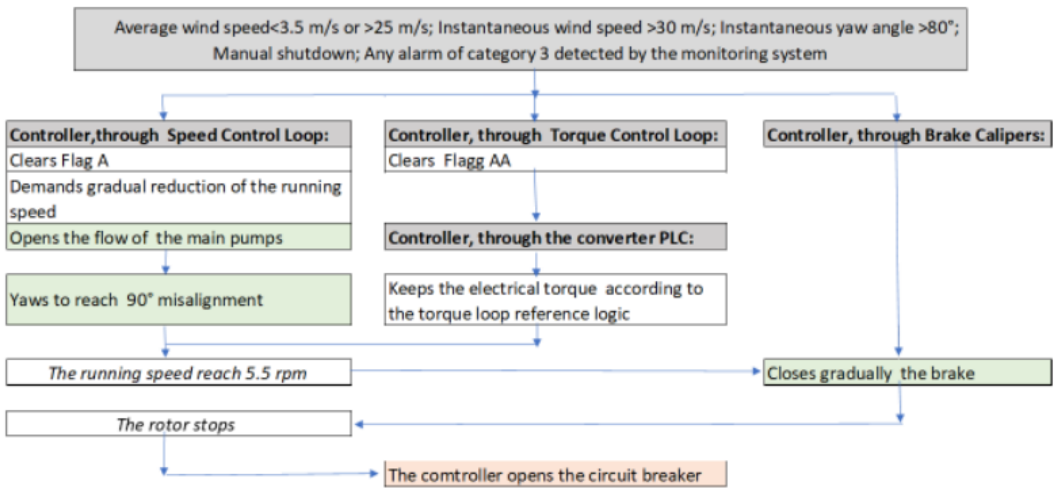

Figure 3.33: Seawind 6 - Logic of normal shutdown [8]

Emergency Shut-down

An emergency shut-down is initiated to bring the turbine to rest for critical alarms regarding the braking system or the rotor, for over-speed or over-thrust, for failure of the electrical system, or in the case that the safety button is triggered in the turbine [4]. An emergency shut-down is achieved in much the same manner as a normal shut-down, but with increased yaw rates of 10°/s. This is achieved by the controller clearing Flag C (=0) in order to actuate the yawing at maximum speed. An emergency shut-down would also be initiated if an extreme gust was detected incoming towards the turbine. The Seawind 6 is equipped with two LIDAR laser sensors installed on the turbine roof that can sense extreme coherent gusts up to 500 m ahead of the turbine within a large horizontal and vertical angle [8].

Parked

For exceptional wind speeds the turbines will be put in their parked positions. Here, an emergency shutdown is first initiated before fully applying and holding the LSS disk brakes. The electric pumps are activated in order to orient the blades in a horizontal position, parallel to the wind direction (the result of -90° misalignment). The teeter hinge is unlocked and, in case of coming hurricane, the yaw system is mechanically locked. Again, this procedure would be triggered by the Lidar system. This would be particularly important for ensuring the safety of Seawind 6 turbines deployed in cyclonic regions [4].

3.4.4. System Architecture

Figure 3.34 displays the control and monitoring system for the Seawind 6. The Gamma 60 has a very similar architecture. The controller PLC has the double function of control and monitoring of the turbine. It communicates with the converter PLC which, in turn, interacts with the electrical system. Roughly 500 turbine parameters are constantly monitored, including wind speed and direction, LIDAR, yaw angle and misalignment, electric power, generator speed, teeter angle, blade strains, and mooring line tensions [14]. This monitored data is recorded and sent to the operator station consoles in real time. For safety reasons, the turbine has a backup controller which has the sole function of supervising an emergency shutdown. This is activated by a watchdog signal in the controller PLC. The control architecture shows two methods of braking; the primary aerodynamic brake achieved by turning the rotor out of the wind, as well as hydraulic double disk brake used to complete the shut-down when the rotor is at -90° misalignment and below 6 rpm [4]. This double disk brake has been sized to make possible the braking of the rotor from full load, at any operating wind speed, in combination with the restrain electrical torque [8]. In the bottom right of Figure 3.34, the four yaw drives with hydraulic motors are shown. As mentioned in Subsection 3.3.2 these are typically powered by the main pumps, driven by the turbine gearbox, but can also be fed through the same manifold by auxiliary electric pumps powered by the grid or battery bank. If the monitoring system detects the failure of any one of the four independent circuits of the yaw system, the failed circuit is detached without preventing the operation of the remaining three circuits [8].

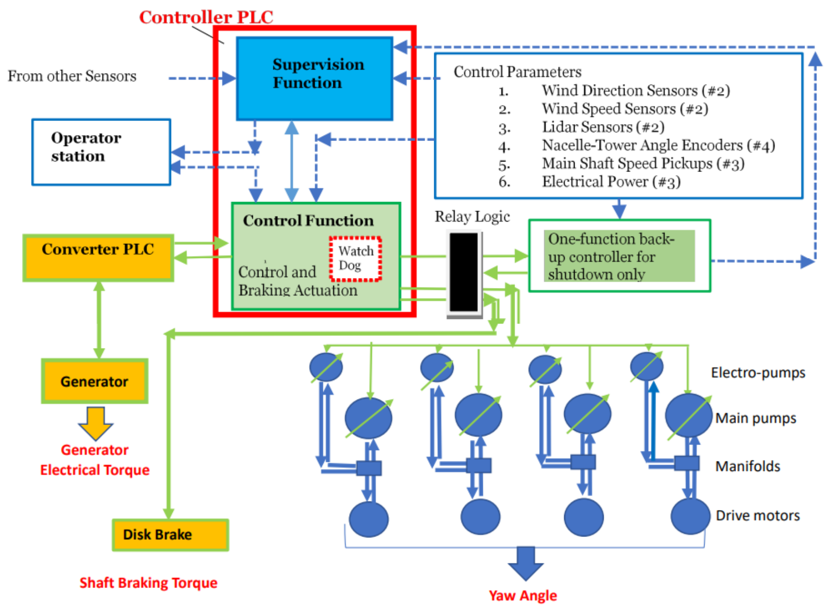

Figure 3.34: Seawind 6 - Control and monitoring architecture [8]

4 Gamma 60 - Model Validation and Calibration

This chapter focuses on the validation and calibration of the Gamma 60 model. It begins with Section 4.1 with a general model validation, where data from various Gamma 60 operational runs at different wind speeds were first verified against the design specifications of the turbine provided in Section 3.1, followed by a thorough comparison against various uniform wind runs of the Gamma 60 model in Bladed 4.5. An in-depth validation of the model follows this in Section 4.2, where a recommissioning field test is recreated in Bladed 4.5 (simulating start-up, normal operation, and shut-down procedures) and the accuracy of each investigated signal is examined. Lastly, any discrepancies between the test data and simulation data are outlined in Section 4.3 and calibration adjustments are suggested to improve the accuracy of the Bladed model against real world operational performance. As the model and external controller of the Seawind 6 are based on those of the Gamma 60, any calibration improvements suggested here should also be carried through to these. The work covered in this chapter marks the first time the Gamma 60 field testing results have been used for Bladed model calibration purposes, and will be an extremely useful for comparing the operation of the model when considering real world phenomena. This will hopefully instill an extra level of confidence for the Seawind engineering team that the models are accurate, and may also highlight areas that require improvement.

As mentioned previously in Chapter 3, a low level model of the Gamma 60 did exist prior to this thesis work which was initially used to model the current Seawind 6 models. However, the Coelme external controller was not operational and the source code was not available. As such, upon discussion with the Seawind engineers, the best option was to complete the model and take the previous version of the Seawind 6 controller and replace all the parameter inputs with the Gamma 60 counterparts. This was an extremely tedious, time consuming task, trying to locate and calculate the hundreds of different inputs. However, the hard work paid off and the model runs now successfully. Ideally, the exact wind file recorded during field testing of the Gamma 60 would have been loaded into Bladed for the simulations to ensure the least variability during model validation. Unfortunately, it was only discovered after completing all the runs that a “single point history” option was available that supplies a time history of wind speed and direction. Instead, the ”3D turbulent wind” option was used which models the 3-dimensional turbulent winds based on defined spectral and spatial coherence characteristics. To achieve this, the wind speed and direction signals were each separately examined in Excel, determining their means and standard deviations, and calculating the turbulence intensities (mean divided by standard deviation). With this model, the two previously calculated means were inputted for the wind speed and direction. The wind speed turbulence intensity modelled the longitudinal turbulence intensity, while the wind direction value modelled the lateral wind turbulence intensity. The field testing involved a start-up procedure, followed by a period of power production, ending with a normal shut-down. It was not possible to run both of these procedures in the same simulation, so separate start-up and shut-down simulations were carried out. The data outputs from these were then merged together during post-processing in Excel to create a single file that could be visualised in Matlab.

4.1. General Validation

Operational Data

Based on data obtained during field testing of the Gamma 60 at Alta Nurra, graphs were compiled for multiple variables of particular interest against wind speed [26]. These graphs have been meticulously recreated using a web-based plot digitiser and included in Figure 4.1 below for comparison against Bladed model outputs [60]. The generator power, rotor speed, and yaw misalignment graphs were constructed by initially plotting the raw data experienced across operational wind speeds, and adding a ”bins” trend line to show the average values. To ensure legibility of graphs, the average, minimum, maximum, and standard deviation values were provided for the final three variables; low speed shaft torque, and both flatwise and edgewise bending moments.

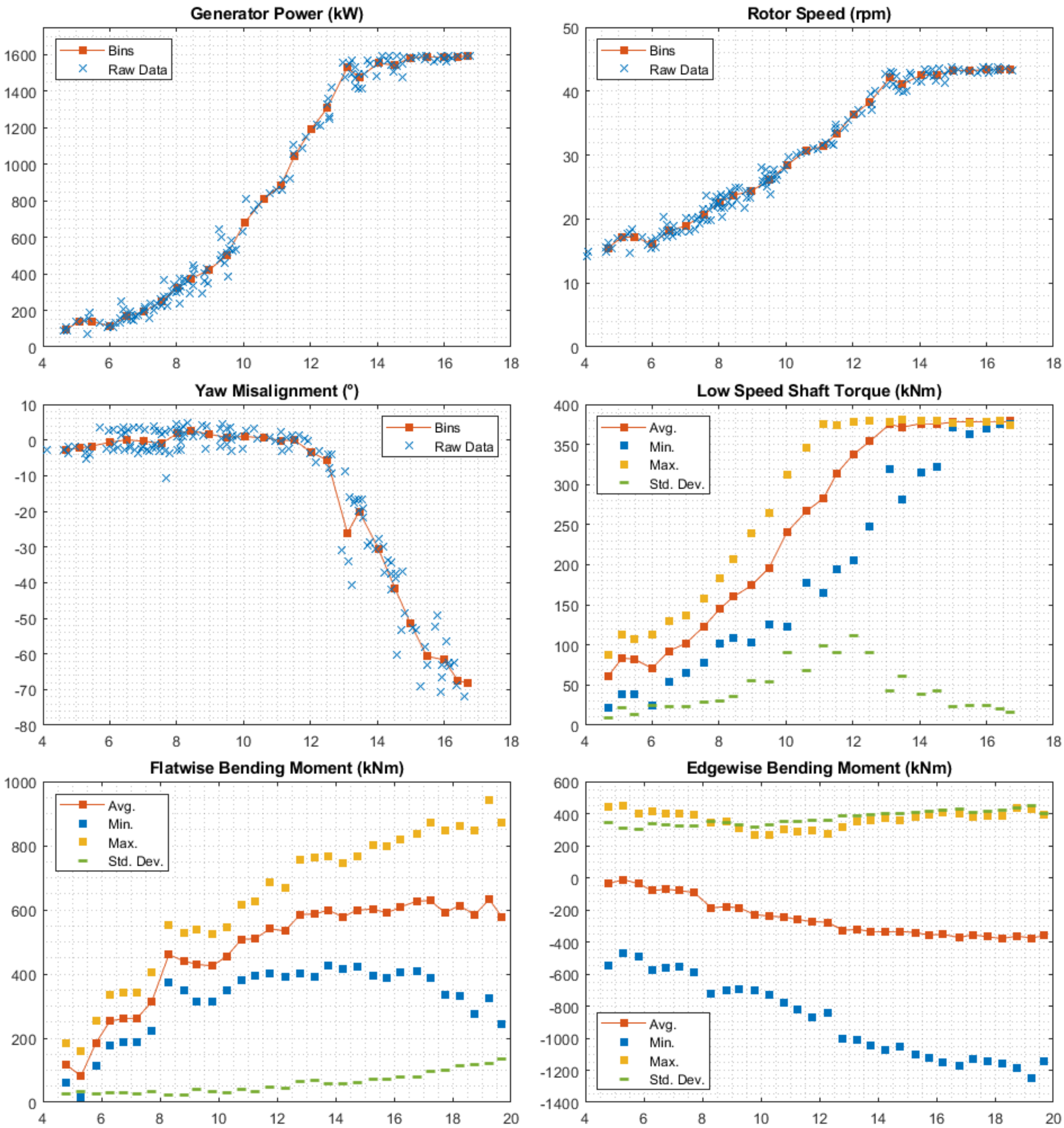

Figure 4.1: Gamma 60 Experience PDF operational data plots

Bladed Data

Then, using Bladed, 10 m/s, 12 m/s, 14 m/s, 16 m/s, 18 m/s, and 20 m/s uniform wind simulations were run, each lasting 200 seconds and having a wind direction of 0° from North, to compare against the operational data above. This particular selection of wind speeds was chosen to give the best overview of the turbine's operation. Table 4.1 was generated based on the simulation data in Figure 4.2 to simplify the validation process.

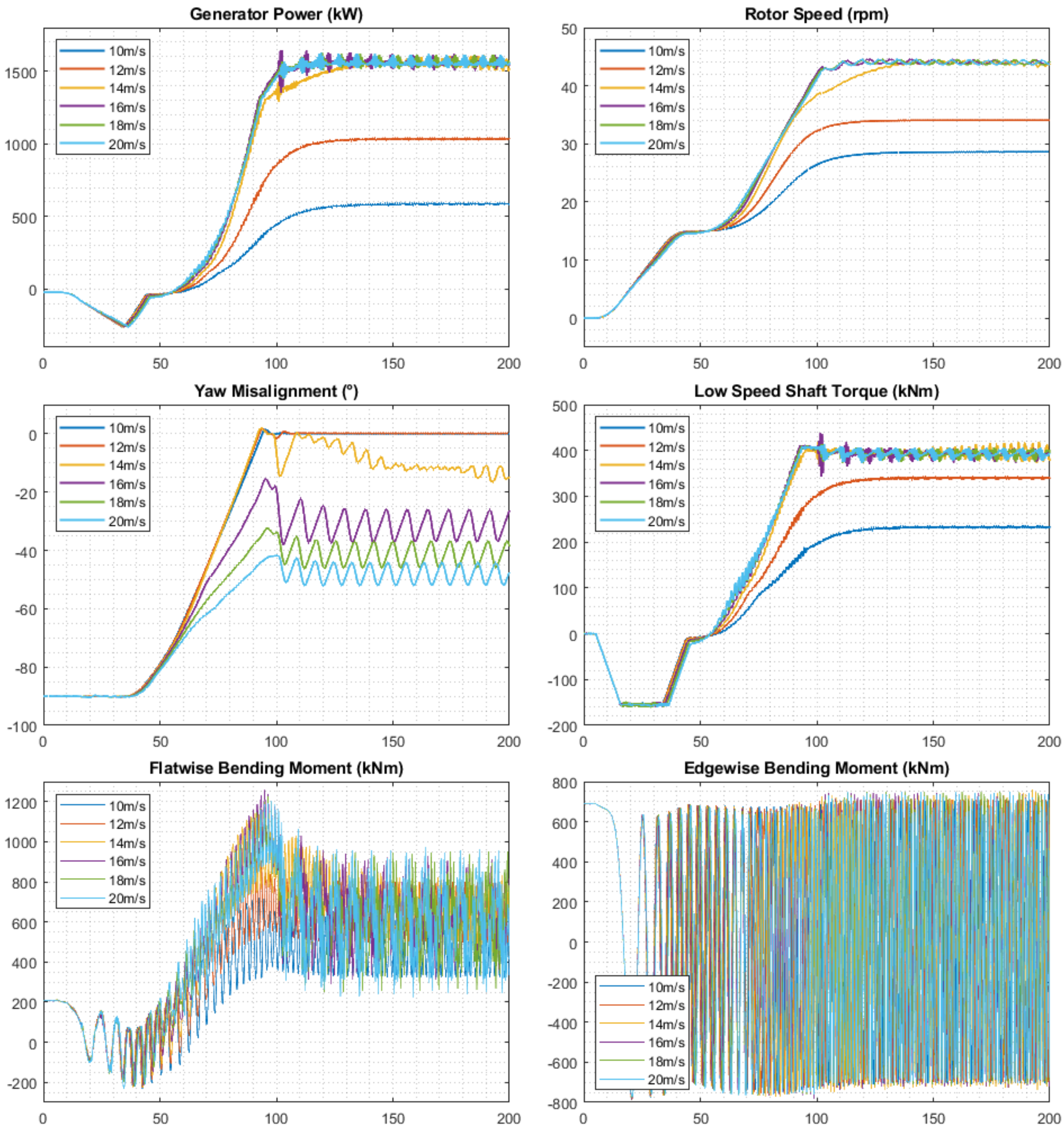

Figure 4.2: Gamma 60 Bladed uniform wind plots

Table 4.1 provides the average, minimum, maximum, and standard deviation from the Bladed runs for each of the examined variables in Figure 4.2. Comparing these values to those presented in Figure 4.1 allows for a general validation of the turbine model.

Table 4.1: Gamma 60 Bladed uniform wind statistics

Variable	Unit	Wind Speed (m/s)	Average	Minimum	Maximum	Standard Deviation
Generator Power	kW	10	586.06	580.16	590.34	2.84
		12	1034.18	1027.31	1039.51	3.93
		14	1555.07	1502.04	1604.79	23.09
		16	1554.66	1508.89	1615.58	16.09
		18	1554.90	1515.38	1613.43	16.10
		20	1554.82	1521.37	1615.61	16.98
Rotor Speed	rpm	10	28.60	28.57	28.62	0.01
		12	34.06	34.04	34.06	0.01
		14	43.93	43.27	44.29	0.23
		16	44.00	43.70	44.46	0.24
		18	44.00	43.66	44.45	0.26
		20	44.01	43.65	44.46	0.26
Yaw Misalignment	°	10	0.08	0.04	0.11	0.02
		12	0.15	0.12	0.18	0.02
		14	-12.37	-16.44	-10.20	1.47
		16	-31.55	-37.16	-25.96	3.63
		18	-41.27	-45.96	-36.83	3.07
		20	-48.22	-52.02	-44.21	2.64
Low Speed Shaft Torque	kNm	10	233.03	230.39	235.17	1.54
		12	340.15	337.35	342.58	1.75
		14	393.70	374.22	417.37	11.04
		16	392.99	373.97	404.20	5.31
		18	393.26	376.02	404.43	5.65
		20	392.86	376.33	405.74	5.98
Flatwise Bending Moment	kNm	10	467.06	325.91	619.28	100.71
		12	639.91	500.26	798.98	99.95
		14	644.91	436.31	839.00	97.87
		16	631.14	300.15	926.92	143.21
		18	623.55	256.88	948.25	159.21
		20	596.50	225.22	970.10	169.40
Edgewise Bending Moment	kNm	10	3.47	-706.18	704.53	497.75
		12	3.40	-696.37	710.78	499.26
		14	12.19	-740.32	758.43	509.26
		16	7.75	-725.80	744.71	502.31
		18	10.42	-712.55	749.43	498.64
		20	17.28	-704.51	747.88	497.12

Results Validation

First, the operational data displayed in Figure 4.1 was compared to the Gamma 60's design specifications provided in Section 3.1. Looking more closely at the individual plots in Figure 4.1, it was shown that the generator power increases from approximately 100 kW at speeds just above cut-in, to a steady 1.6 MW above the rated wind speed of 14 m/s. This makes sense, with electrical losses in the converter and cabling reducing the outputted power to 1.5 MW at rated conditions. The rotor speed was shown to increase from approximately 14 rpm, which is slightly greater than the 12 rpm provided in Subsection 2.5.1, to the rated rotor speed of 44 rpm. This increase in rotational speeds at cut-in is most likely a result of environmental transients and is not a major problem. The yaw misalignment behaved accurately below rated speeds, operating at 0° misalignment, but larger-than-anticipated yaw misalignments were experienced above rated speeds. Looking at the control algorithms in Chapter 3, the actual yaw misalignment comes from the convergence between the aerodynamic model and the requested rated power, resulting in smaller demanded yaw misalignments. According to the Seawind engineers, this difference in experimental values was due to the effect of the rotor turning out the wind field and was rectified by introducing an offset on measured values, which was estimated based on the position of the wind vane on the nacelle. These experimental results must have been acquired before this modification was made. The yawing should also not have started until rated speeds were reached. Although expected values for the remaining variables, low speed shaft torque and both flatwise and edgewise bending moments, were not included in the design specifications for the Gamma 60, they seem to behave as expected, and it will be interesting to see how they compare to their Bladed counterparts.

The Bladed results in Figure 4.2 and Table 4.1 were then validated against the operational data in Figure 4.1 which had been previously verified. Here, the accuracy of each variable is examined individually, with calibration improvements suggested in Section 4.3.

- **Generator power:** The Bladed model was shown to closely match the operational data, with an average of 586.06 kW compared to approximately 650 kW at 10 m/s, 1034.18 kW compared to 1200 kW at 12 m/s, and 1555 kW compared to 1550 kW above 14 m/s. The values were consistent, with a maximum standard deviation of just 23.09 kW at 14 m/s as the turbine reached rated power.
- **Rotor speed:** The operational and Bladed data matches exceptionally well, with the rotor rotating at approximately 28 rpm at 10 m/s, 34 rpm at 12 m/s, and 44 rpm above 14 m/s for both data-sets.
- **Yaw misalignment:** Below rated wind speed, both data sets output a yaw misalignment of 0° to the prevailing wind direction. However, at 14 m/s the turbine yawed to -30° during field field testing compared to just -12.37° in the Bladed simulation. This pattern continued for the remaining wind speeds tested too, with the Bladed yaw misalignment being considerably smaller than its operational counterpart. At the strongest wind speed investigated here, 16 m/s, the field testing reported a yaw misalignment of -70° whereas the Bladed simulations outputted a much less extreme -31.55°. Clearly, the operational results are incorrect as a yaw misalignment of -60° is expected at cut-out speeds of 25 m/s. Above rated, these discrepancies are most likely a result of the wind vane issues described earlier and, as the Bladed model more closely matches the desired yaw control schedule as detailed in Subsection 3.3.1, the values given by Bladed can be considered correct.
- **LSS torque:** At 10 m/s the operational data shows an average torque of 240 kNm, a minimum of 120 kNm, a maximum of 310 kNm, and a standard deviation of 90 kNm. This is in comparison to the Bladed data which outputs an average of 233.03 kNm, a minimum of 230.39 kNm, a maximum of 235.17 kNm, and a standard deviation of 1.54 kNm. At 14 m/s the average torque from the field testing and Bladed simulation were 380 kNm and 393.70 kNm respectively, the minimum was 315 kNm and 374.22 kNm, the maximum was 385 kNm and 417.37 kNm, and the standard deviation was 40 kNm and 11.04 kNm. The remaining wind speeds continued this trend of accurate average LSS torques, but much smaller minimum, maximum, and standard deviation values.
- **Flatwise bending moment:** At 10 m/s the average bending moment from the field testing and Bladed simulation were 450 kNm and 467.06 kNm respectively, the minimum was 350 kNm and 325.91 kNm, the maximum was 550 kNm and 619.28 kNm, and the standard deviation was 40 kNm and 100.71 kNm. At 16 m/s the average bending moment from the field testing and Bladed simulation were 600 kNm and 631.14 kNm respectively, the minimum was 400 kNm and 300.15 kNm, the maximum was 825 kNm and 926.92 kNm, and the standard deviation was 80 kNm and 143.21 kNm. Again, the average values for flatwise bending moment were shown to be very similar for both data sets, with the minimum, maximum, and standard deviation also matching to a high degree.
- **Edgewise bending moment:** At 10 m/s the average bending moment from the field testing and Bladed simulation were -250 kNm and 3.47 kNm respectively, the minimum was -700 kNm and -706.18 kNm, the maximum was 300 kNm and 704.53 kNm, and the standard deviation was 350 kNm and 497.75 kNm. At 16 m/s the average bending moment from the field testing and Bladed simulation were -350 kNm and 7.75 kNm respectively, the minimum was -1150 kNm and -725.80 kNm, the maximum was 400 kNm and 744.71 kNm, and the standard deviation was 400 kNm and 502.31 kNm. The Bladed values barely change across the various wind speeds and, all things considered, this signal has the worst similarity of those investigated.

4.2. In-Depth Validation

Operational Data

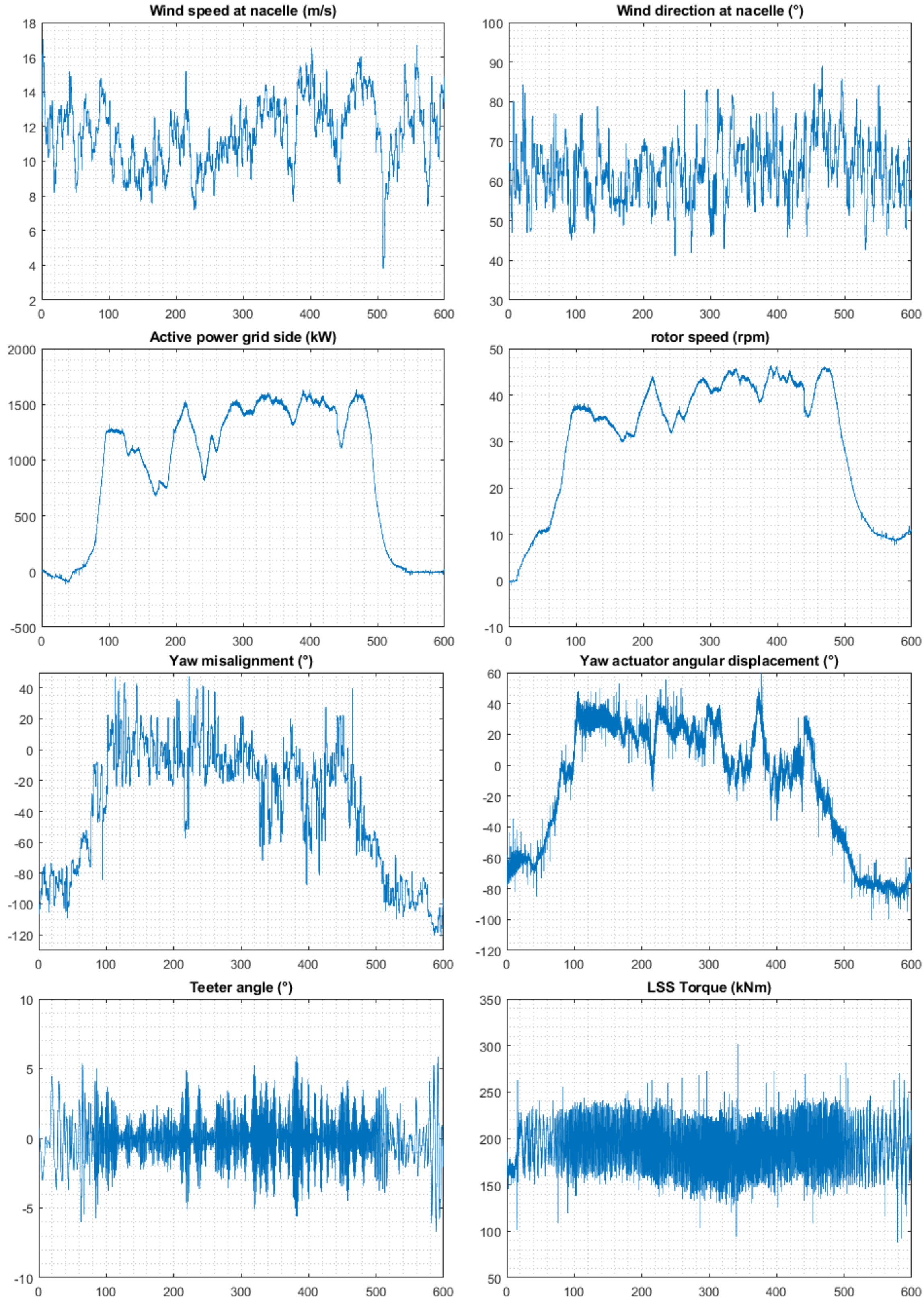

Figure 4.3: Part 1 - Gamma 60 field testing data plots

Figure 4.4: Part 2 - Gamma 60 field testing data plots

Bladed Data

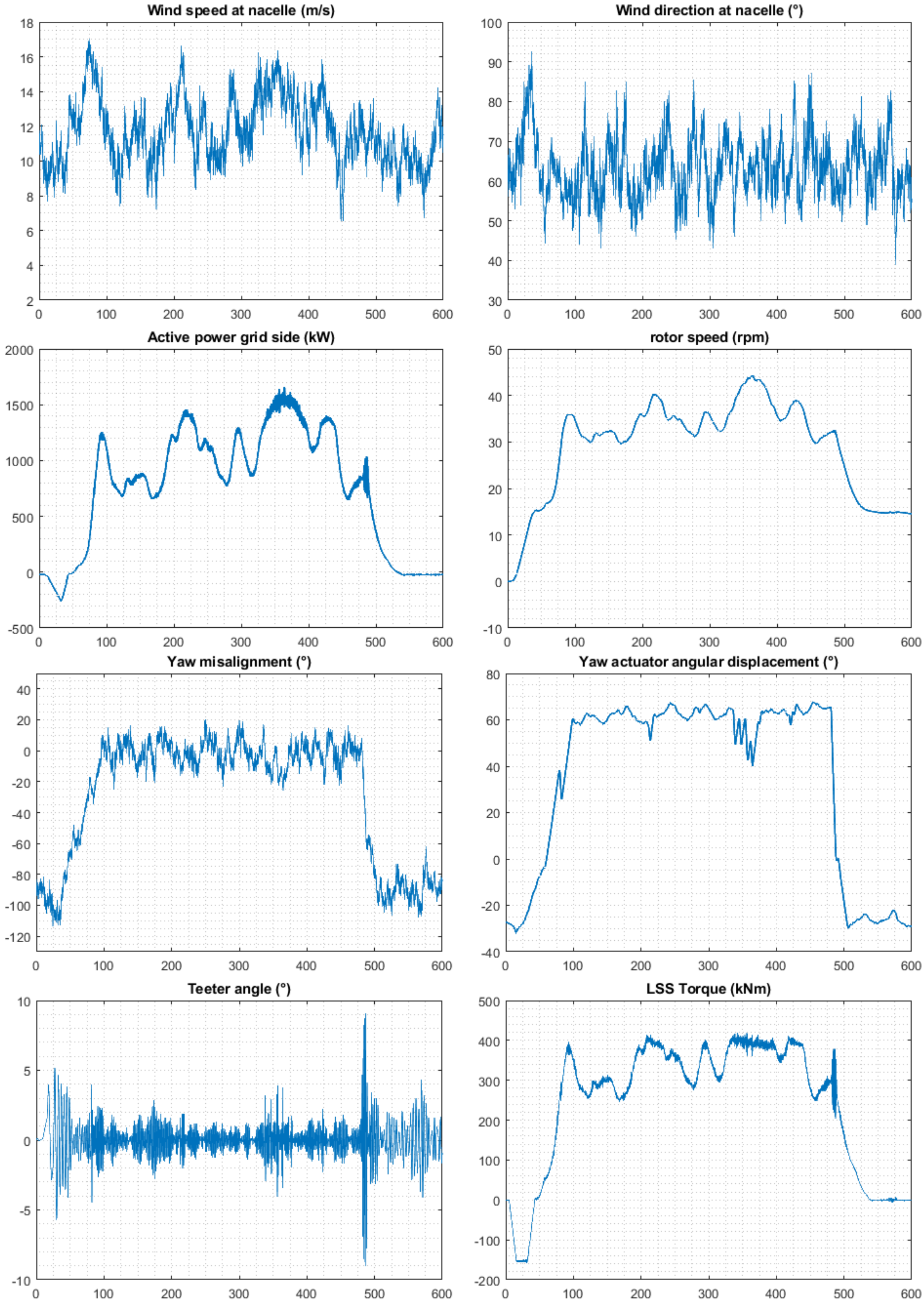

Figure 4.5: Part 1 - Gamma 60 Bladed plots

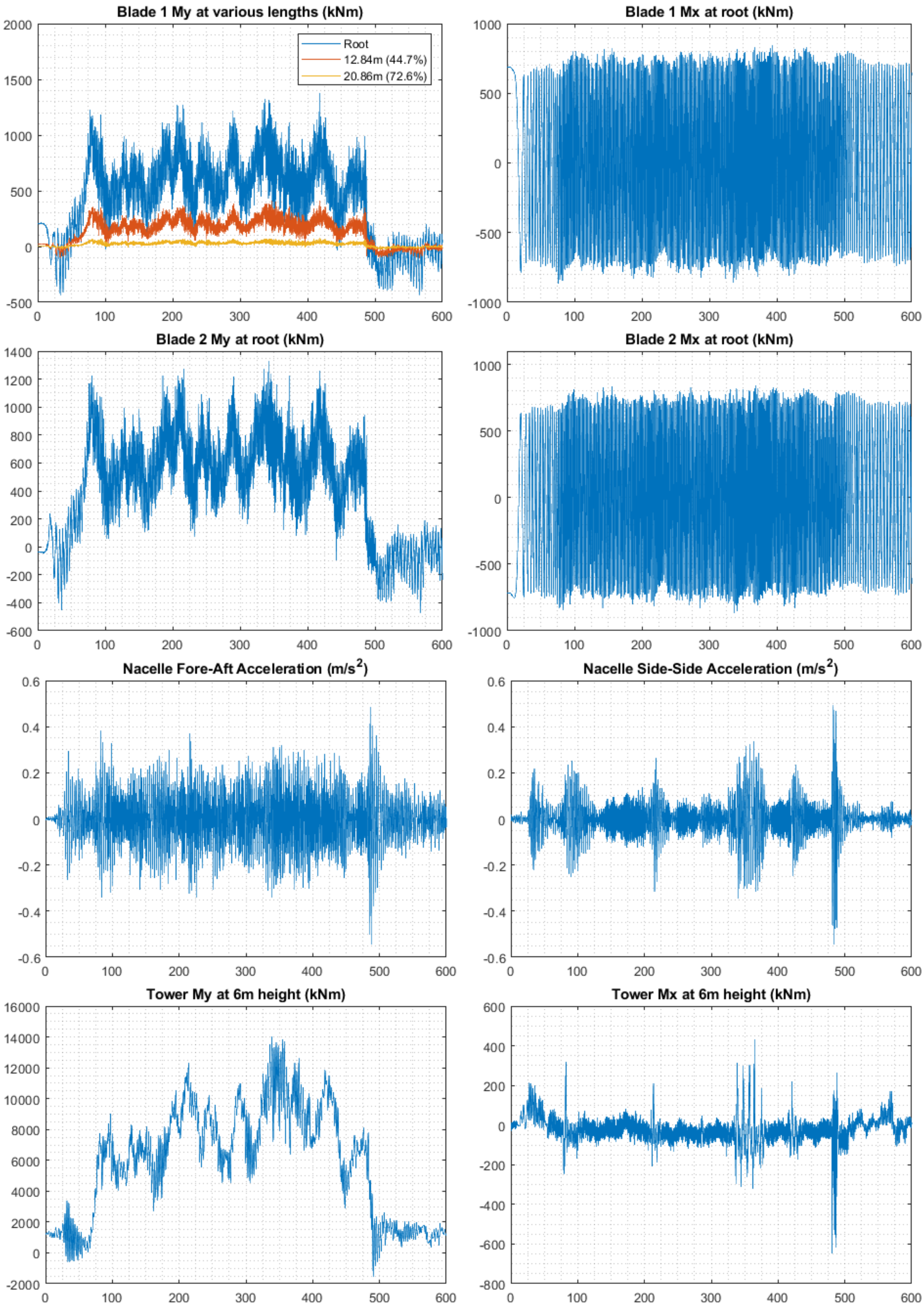

Figure 4.6: Part 2 - Gamma 60 Bladed plots

Results Validation

Following the Gamma 60 nacelle fire in 1995, recommissioning testing was carried out during March 1997 at Alta Nurra to evaluate the turbine's updated performance and ensure its safe operation. The tests were run by West S.p.A. and Enel S.p.A. technicians, with the results provided by Seawind for this thesis investigation. Although many tests were run, the most interesting for this investigation was an operational start-up and shut-down carried out on the 11th March 1997. Again, each signal will be investigated individually, with a comparison between the operational data in Figure 4.3 and Figure 4.4 and Bladed data in Figure 4.5 and Figure 4.6 being made in order to validate the model further. Any improvements that should be made to calibrate the model and improve its accuracy will be suggested in Section 4.3.

- **Wind speed:** Due to the Bladed wind having the same statistical characteristics as the operational wind file, both time series are broadly similar with the same prescribed mean (11.59 m/s) and turbulence intensity (17.32%). There are clearly inherent differences between both, including the large dip to 4 m/s after 500 s in the operational data not replicated in the Bladed series, but they are generally in agreement.
- **Wind direction:** Both data sets match even more closely here, sharing the same mean (62.81°) and turbulence intensity (12.85%), with the only obvious indifference occurring after 40 s in the Bladed time series with an unmatched spike up to 90° from North.
- **Active power:** The Bladed series matches the operational series and reaches 1.25 MW after 100 s. There was, however, a more apparent dip during the start-up procedure in the Bladed series at 30 s. As rated wind speed of 14 m/s was not reached while the turbine was operational until just after 200s, both series are shown to hover around 700 kW. Both Bladed model then acts as expected, reaching 1.5 MW when sustained speeds above rated occur. Unfortunately, the Bladed series was below rated speed when the shut-down procedure was initiated, which explains why it shuts-down from 1 MW at 480 s rather than 1.5 MW during field testing. The power levels drop at the same rate as the turbine yaws out of the wind, however there are unwanted large amplitude transients at the start of the shut-down procedure in Bladed.
- **Rotor speed:** There is a very close match between both time series, reaching 45 rpm at rated wind speeds. It is shown that the disk brakes are not engaged in either run at the end of the shut-down procedure, with a final rotor speed of 12 rpm when facing out of the wind.
- **Yaw misalignment:** Both series start in their parked positions at -90° and, as the mean wind speed experienced was less than rated, yaws to face directly into oncoming wind (0°) in 100 s. The Bladed model actually shows a preferable operation, with less extreme yaw rates and misalignment angles than those shown during field testing while controlling power output about rated.
- **Yaw actuator angular displacement:** During field testing the Gamma 60 yawed from -60° to 30° from North to face into the prevailing wind direction. This doesn't make a whole lot of sense, as the wind was coming from approximately 60° from North. The Bladed results appear more accurate, yawing from -30° to 60° to face straight into the oncoming wind. Again, this is a result of the wind vane issue and the Bladed model should not be calibrated as it is more correct.
- **Teeter angle:** Both series are relatively similar, remaining below 5° of teetering. The one exception is seen in the Bladed output at 480 s when the shut-down procedure causes a major fluctuation to 9°, which should have caused a teeter-end impact. With stronger winds, this could very easily prove disastrous.
- **LSS torque:** The test data shows a steady fluctuation of ±40 kNm about about 190 kNm, with a few larger exceptions. This is rather unexpected, with the Bladed series increasing from 0 kNm to 400 kNm and back to 0 kNm making more sense. This reason for this obscurity is uncovered when examining the Blade 1 root edgewise (Mx) bending moments below.
- **Blade 1 My:** The operational data provided flatwise moments for three locations along Blade 1, at its root, 50% length, and 75% length. The configuration of the blades in Bladed meant these exact positions could not be selected, so the root, 44.7%, and 72.6% were selected instead.

The Bladed series again provides a more believable output, with the moments increasing from less than 100 kNm towards the blade tip to 1.3 MNm at the root. The test series, on the other hand, deems the moments at 75% length to be grater than those at 50% length and comparable in magnitude to the root moments. There is also pre-loading of the blade at the root and 50% length, but not at 75%. Perhaps this is a result of a misbehaving strain gauge as explained below.

- **Blade 1 Mx:** For the operational test data, the strain gauge appears to have been misbehaving and recording vastly diminished, exclusively negative, edgewise moments. As this would be a component of calculating the LSS torque, this is a plausible explanation for why the LSS torque was misbehaving before. The Bladed series appears to behave normally, with steady fluctuations of ±800 kNm about about 0 kNm.
- **Blade 2 My:** Both signals closely match each other, starting and ending at 0 kNm, fluctuating about 600 kNm, and reaching a maximum of 1.3 MNm.
- **Blade 2 Mx:** A nice resemblance exists again between both signals, starting at -700 kNm, with steady fluctuations of ±700 kNm about about 0 kNm. The operational series is slightly less uniform in its fluctuation, with some larger moments experienced.
- **Nacelle fore-aft acceleration:** The operational signal shows accelerations with a maximum amplitude of 0.2 m/s^2 about -0.1 m/s^2. The Bladed signal shows larger amplitudes of 0.3 m/s^2 on average about 0 m/s^2, with the key difference being the much larger fore-aft acceleration of 0.5 m/s^2 when the shut-down was commenced.
- **Nacelle side-side acceleration:** The signals are similar, fluctuating to ±0.2 m/s^2 about about 0 m/s^2, with the only significant difference occurring in the Bladed series at shut-down again with a large 0.5 m/s^2 spike.
- **Tower My:** The operational series has clear variations about 1500 kNm, which is a factor of ten smaller than those experienced in the Bladed simulations. Doing the math, above rated, the moment at the tower base should be on average 280 kN (thrust) multiplied by 60 m (hub height at 6 m above the ground) which results in 16800 kNm. A few of the other operational signals required factors to be applied to them, so perhaps this is the case here also. In any case, the Bladed series also shows an increase and decrease either side of rated which is not present in the operational data.
- **Tower Mx:** The operational series starts at 350 kNm and decreases to -400 kNm during rated operation, before increasing back to 350 kNm after shut-down. The Bladed series remains fluctuating about 0 kNm, with a sizeable spike to -600 kNm when the shut-down was initiated. On average, however, both series remain between similar maximum and minimum values.

4.3. Calibration Improvements

From going through both of these validation processes, a number of key discrepancies were identified. In this section, suggestions are made for calibrations that could be made for improving the accuracy of the Gamma 60 model. As this Gamma 60 model uses a variation of the Seawind 6 external controller, any calibrations to the control algorithms suggested here should also be applied to the Seawind 6 to improve its accuracy. This is the principle motivation of this validation and calibration exercise, and will be the first time such an activity has been carried out by Seawind using the existing Gamma 60 operational data. The following possible calibrations were suggested from discrepancies uncovered during the general validation:

- The LSS torque readings from Bladed were shown to have high accuracy for the average reading, but with less spread compared to operational data. These increased fluctuations could be a result of turbulence in the operational data or variations in the shaft restraining torque from the full power converter. The latter would have to be verified before enforcing any calibration changes that would negatively effect the turbine's simulated performance.
- The edgewise bending moment has by far the worst accuracy out of all the signals investigated. This may have been explained by the lack of turbulence for the Bladed runs, but then the flatwise

bending moments would also have been more inaccurate. As such, it must be an affect of the design of the blades, potentially the pitch angle or mass distribution, causing a decrease in edgewise moments. A calibration improvement would be to modify the blade structural implementation.

From the in-depth validation, the following calibrations were suggested:

- The active power shows an unusually steep decrease just before power production occurs for the Bladed simulation, meaning too much power is being used to motor the turbine to 6 rpm. This could be remedied by adjusting the torque schedule of the controller. Additionally, a series of rapid fluctuations are experienced when the shut down procedure is commenced. Again, this is a generator torque issue (as yaw profile is accurate) and can be remedied by appropriate control calibrations.
- The Bladed run is shown to have a smoother yaw misalignment control at above rated speeds. Although this is preferable, it may be calibrated by modifying the speed control loop of the controller.
- The unexpectedly large teeter displacement after 480 s in the Bladed run could be prevented by programming a more gradual change between the power production and shut-down procedures. This would involve a calibration to the controller's operating algorithms.
- Unfortunately, the misbehaving sensor has distorted the test results for the LSS torque and both Blade 1 bending moments. As such, no calibrations can be suggested for these components.
- The fore-aft nacelle acceleration should generally be reduced for the Bladed model, with an emphasis on the large fluctuation at shut-down. This may be achieved by changing the stiffness of the tower and gradually changing to the shut-down procedure.
- The side-side nacelle accelerations only require the shut-down damping of the controller.
- Considering the multiplication factor discussed in Section 4.2 for the My moment, the tower moments generally share the same statistical descriptors for both data-sets. The only calibrations that could be made are for the structural implementation of the tower.

A high level of accuracy for the Bladed model and controller has been shown to already exist. Applying the aforementioned calibrations to the Gamma 60 and Seawind 6 turbine models will ensure that their ”real-world” simulation performance is further improved.

In hindsight, it would also have been of great interest to investigate the modal response of the Gamma 60 to see if resonant behaviour was occurring. However, at the time of running these simulations this exercise was outside the scope of works set. Nevertheless, it is a worthwhile thought exercise to investigate how the experienced onshore Gamma 60 eigenfrequency (natural frequency) values compare to those of the simulated offshore Seawind 6, and what calibrations may be suggested. Below, Table 4.2, provides an overview of the eigenfrequencies experienced by the Gamma 60 during its operation (at rated rotor speed of 45 rpm).

Table 4.2: Gamma 60 Eigenfrequencies (rated 45 rpm)

Component	**Mode**	**Frequency (Hz)**
Blade	1st Flapwise	5.41
	2nd Flapwise	20.47
	1st Edgewise	5.55
	2nd Edgewise	24.57
	Torsional	17.17
Tower	1st Lateral	0.34
	2nd Lateral	3.45
	1st Longitudinal	0.34
	2nd Longitudinal	3.23
	Torsional	3.36
	Yaw + Lateral	0.26

Below, in Figure 4.7, is the Campbell diagram of the offshore Seawind 6. It is also noted that the blade torsional mode is 18.814 Hz and the yaw mode is 0.1 Hz. A Campbell diagram is used to determine if a structure is subjected to resonance or not. It shows both the excitation frequencies (1P, 2P, and 4P) and the natural frequencies of the system as a function of the rotor speed. For a two-blade wind turbine, only the multiples of the 2P harmonic remain. Considering that the operational range of this turbine is from 8 rpm to 28 rpm, the intersecting points on the graph highlighted with circles are the areas that should be avoided to decrease the chance of dangerous resonant behaviour. A margin of safety is considered around these excitation frequencies to allow for the dynamic amplification factor not having a sharp peak. The intersection between 4P and the tower modes (F) at 5 rpm can be disregarded as the time spent speeding up to the operational regional would be insufficient to cause resonance.

For the blades, the main modes of deformation are the first flap-wise motion and the first edge-wise motion (lead-lag motion). As shown from Figure 4.7, the natural frequencies increase slightly with the rotor speed as a result of centrifugal stiffening. In this case it would be a good idea to stiffen the blade in rotor in the flatwise mode, increasing the flatwise natural frequency, and moving its intersection with the 4P line out of the operational range. Considering now the tower modes, we are reminded that both the Seawind 6 and Gamma 60 have soft-stiff towers, meaning the first and second natural frequency modes of the tower are found between 1P and 2P. This is already a much narrower operational window compared to that of a three-bladed turbine, and posed a great challenge when designing the tower of the offshore Seawind 6. Its large rotor meant smaller rotational speeds were required to maintain a constant tip speed ratio, therefore narrowing the soft-stiff region even further, and undesirably moving towards the wave excitation frequencies. This is one of the key reasons why the tower design for an offshore wind turbine with a large rotor (particularly a two-blader) is so challenging.

Without knowing the excitation frequencies of the Gamma 60 it is difficult to judge how it would have interacted with the natural frequencies presented in Table 4.2. Although it was expected that the higher rated rotor speed of the Gamma 60 would mean that these blade related eigenfrequencies are increased, it appears that there must have also been additional stiffening included in both blade modes to increase their frequencies further. Considering that the Gamma 60's blades did not suffer from resonance issues, it may be worthwhile investigating if the Seawind 6's blades may require further operational mode analysis. The tower modes of the two turbines are similar, which makes sense considering the move to offshore and the larger rotor as discussed previously.

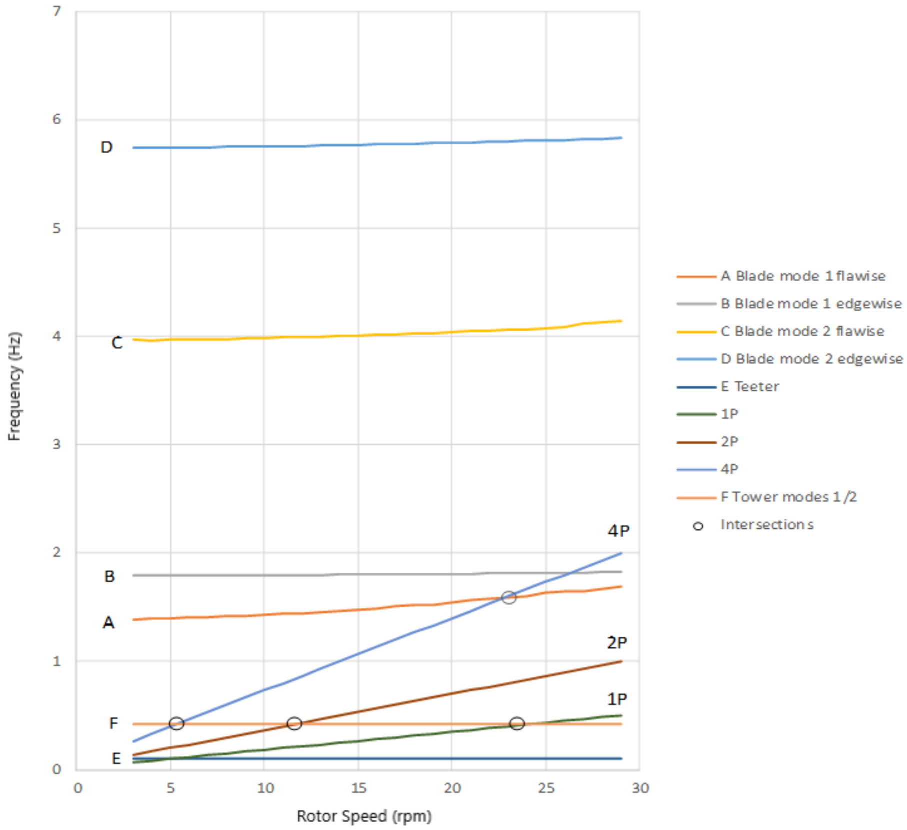

Figure 4.7: Seawind 6 Campbell diagram

5

Seawind 6 - Ultimate and Fatigue Loads Analyses

The aim of this chapter is to provide an analysis of ultimate and fatigue loads experienced by the Seawind 6 turbine. This will not only be of interest to the reader and provide deeper understanding of the turbine's operation, but will also be useful for verifying Seawind simulations previously run in-house. This is the first time that the current Seawind 6 model, with improved platform dynamics and mooring line configuration, in combination with new Sowento controller has undergone a thorough loading analysis. These are based on design loads cases (DLCs) from the international wind turbine standards IEC 61400-3-1, design requirements for fixed offshore wind turbines [31]. IEC 61400-3-2, design requirements for floating offshore wind turbines, includes all the DLCs in IEC 61400-3-1 plus some extra ones that are not included in this investigation [32]. Section 5.1 presents the inputs required for setting up the various simulations for this analysis. The DLC configurations of interest from Chapter 7 and Annex I of IEC 61400-3-1 were compiled into Table 5.1. For each of these selected DLCs, tables were then created displaying all the inputs required for configuring simulations of the Seawind 6 in bladed 4.12. Section 5.2 then displays and reviews time series plots for outputs of interest from the simulations. The same outputs are displayed for each DLC, allowing for an interesting comparison of turbine behaviour in different operating conditions. Furthermore, only one run is selected for each DLC so as to not overburden the reader. Section 5.3 addresses the ultimate loading analysis of the Seawind 6. Here, the maximum loads experienced during simulations for multiple turbine components are tabulated, converted to stresses, and compared to the maximum allowable design stresses to verify turbine integrity. Following this, in Section 5.4, Damage Equivalent Loads (DELs) for each of these turbine components are calculated from a rainflow counting analysis based on a 25-year lifetime for a Seawind 6 turbine.

5.1. Simulation Setups

IEC DLC Overview

Along with the Seawind engineers, it was decided that one fatigue and three ultimate load cases would be investigated. This would allow for the greatest possible depth of analysis of the turbine's behaviour given the time constraints of this thesis project. These DLCs were carefully selected from IEC 61400-3-1 and reproduced in Table 5.1. The table gives the initial turbine state, the case name, the environmental conditions (wind, wave, and currents), the type of analysis, and the associated safety factor to be applied when carrying out load analyses in later sections. DLC 1.2 was the fatigue load case used for the fatigue analysis in Section 5.4. This was a power production simulation, using a Normal Turbulence Model (NTM) with wind speeds between cut-in and cut-out, a Normal Sea State (NSS) with significant wave heights (H_s) corresponding to each wind speed, wind and wave directions misaligned (MIS) and multi-directional (MUL), no sea currents, and a safety factor of 1.00 applied. The first ultimate load case simulated was DLC 1.3, selected as it is the most typical of daily turbine operation. Again, this was a power production simulation, with an Extreme Turbulence Model (ETM) between cut-in and cut-out wind speeds and a NSS, with changes to co- and uni-directional (COD and UNI) wind and waves, a Normal Current Model (NCM), and a safety factor of 1.35. Following this, it was of interest to see how the Seawind 6 would fare when parked in extreme wind conditions with the rotor yawed -90° out of the wind, so DLC 6.1 was selected. For this, the turbulent variation of the Extreme Wind Speed Model (EWM) was applied with the 50 years extreme wind speed, an Extreme Sea State (ESS), MIS and MUL wind and waves, an Extreme Current Model (ECM), and a safety factor of 1.35. Lastly, the limits of the Seawind 6 were to be assessed and testing if it could withstand a tropical cyclone by running DLC I.1. This is a very similar, but shorter, simulation to DLC 6.1, using the steady EWM with wind speeds of 80 m/s and wind direction changes of ±15°, even more extreme wave conditions, and a lower safety factor of 1.00.

Table 5.1: Selected IEC 61400-3-1 DLCs overview

Design situation	DLC	Wind condition	Waves	Wind and wave directionality	Sea currents	Water level	Type of analysis	Safety factor
Power production	1.2	NTM $V_{in} < V_{hub} < V_{out}$	NSS Joint prob. distribution of H_s, T_p, V_{hub}	MIS, MUL	No currents	NWLR or ≥ MSL	F	1.00
Power production	1.3	ETM $V_{in} < V_{hub} < V_{out}$	NSS $H_s = E[H_s \mid V_{hub}]$	COD, UNI	NCM	MSL	U	1.35
Parked (standing still or idling)	6.1	EWM $V_{hub} = V_{ref}$	ESS $H_s = H_{s50}$	MIS, MUL	ECM $U = U_{50}$	EWLR	U	1.35
Parked (standing still or idling)	I.1	EWM $V_{hub} = V_{10min,500}$	ESS $H_s = H_{s500}$	MIS, MUL	ECM	EWLR	U	1.00

DLC 1.2

The specific inputs for configuring each of the eleven runs (a to k) simulated for DLC 1.2 are displayed in Table 5.2. Each run was 660 s in length, with the first 60 s disregarded to eliminate any unwanted transients during start-up. As this is a fatigue analysis, the number of hours per year that each wind speed was experienced were also included for determining turbine availability and calculating damage equivalent loads in Section 5.4. Wind speeds between cut-in and cut-out (4 m/s and 25 m/s, respectively) were selected, starting at 4.5 m/s and reaching 24 m/s with a 2 m/s step size. The wind, waves, and currents all share the same heading direction of 0° from North, towards the apex of the Seawind 6's floating platform. As per IEC 61400-1, Design requirements for wind turbines, the standard deviation of longitudinal turbulence (σ_1) for the NTM is calculated as shown in Equation 5.1 where V_{hub} is the wind speed at hub height and I_{ref} is the reference turbulence intensity (0.14) [30].

$$\sigma_1 = I_{ref}(0.75V_{hub} + b); \quad b = 5.6m/s \tag{5.1}$$

The lateral (σ_2) and vertical (σ_3) components of turbulence standard deviation may be computed by:

$$\sigma_2 = 0.7\sigma_1 \quad \text{and} \quad \sigma_3 = 0.5\sigma_1 \tag{5.2}$$

Bladed requires values for turbulence intensity when modelling wind profiles. These three components are then calculated according to Equation 5.3, by inputting the corresponding values for σ.

$$I = \frac{\sigma}{V_{hub}} \tag{5.3}$$

The significant wave height (H_s) and peak spectral period (T_p) for each individual sea state was conditioned on the corresponding mean wind speed, based on the long-term joint probability distribution of metocean parameters provided by Seawind. H_s evolved from a minimum value of 0.82 m at 4.5 m/s wind to 4.93 m at 24 m/s. T_p also increased as the waves became more substantial. As these were power production simulations, the initial yaw angles were set according to those in the control algorithms that produced the desired power output at each wind speed.

Table 5.2: Fatigue DLC Overview - DLC 1.2

Run	DLC	Wind speed (m/s)	Wind dir. (°)	Long. turb. int. (%)	Lat. turb. int. (%)	Vert. turb. int. (%)	Wave dir. (°)	H_s (m)	T_p (s)	Curr. dir. (°)	Curr. surf. vel. (m/s)	Curr. ref. depth (m)	Initial yaw angle (°)	Hours per year	Run time (s)
a	1.2	4.5	0	27.92	19.55	13.96	0	0.82	7.49	0	0	0	0	527.58	600
b	1.2	6	0	23.57	16.50	11.78	0	0.92	7.62	0	0	0	0	1237.50	600
c	1.2	8	0	20.30	14.21	10.15	0	1.13	7.89	0	0	0	0	1325.79	600
d	1.2	10	0	18.34	12.84	9.17	0	1.42	8.23	0	0	0	0	1250.91	600
e	1.2	12	0	17.03	11.92	8.52	0	1.78	8.64	0	0	0	0	1064.43	600
f	1.2	14	0	16.10	11.27	8.05	0	2.21	9.07	0	0	0	-27.5	827.22	600
g	1.2	16	0	15.40	10.78	7.70	0	2.69	9.51	0	0	0	-39	591.60	600
h	1.2	18	0	14.86	10.40	7.43	0	3.21	9.94	0	0	0	-46	391.23	600
i	1.2	20	0	14.42	10.09	7.21	0	3.77	10.35	0	0	0	-52	240.06	600
j	1.2	22	0	14.06	9.84	7.03	0	4.36	10.73	0	0	0	-56	136.98	600
k	1.2	24	0	13.77	9.64	6.88	0	4.93	11.08	0	0	0	-59	72.84	600

DLC 1.3

The first eleven runs (a to k in Table 5.3) for DLC 1.3 were quite similar to those for DLC 1.2. The two differences being the increased turbulence intensities due to the ETM and the inclusion of 0.5 m/s near-surface currents (extending to a depth of 50 m below water level). These are typical of currents during comparable wind speeds at offshore sites suitable for the Seawind 6 [44]. From IEC 61400-1, the longitudinal turbulence standard deviation (σ_1) for the ETM is calculated as:

$$\sigma_1 = c \cdot I_{ref} \cdot \left(0.072\left(\frac{V_{ave}}{c} + 3\right)\left(\frac{V_{hub}}{c} - 4\right) + 10\right); \quad c = 2m/s \quad \text{and} \quad V_{ave} = 0.2V_{ref} \tag{5.4}$$

where I_{ref} is again the reference turbulence intensity (0.14), V_{ref} is the reference wind speed (50 m/s), and V_{hub} is the wind speed at hub height. As for all DLCs, the lateral and vertical components are calculated in the same manner as described for DLC 1.2. The final three runs (l to n) represent interesting variations to the 24 m/s simulation, with increased wave behaviour and direction changes of 0°, 45°, and -45° to incoming wind, waves, and currents. This was just a further test of the Seawind 6's ability to withstand misaligned, uni-directional environmental conditions.

Table 5.3: Ultimate DLC Overview - DLC 1.3

Run	DLC	Wind speed (m/s)	Wind dir. (°)	Long. turb. int. (%)	Lat. turb. int. (%)	Vert. turb. int. (%)	Wave dir. (°)	H_s (m)	T_p (s)	Curr. dir. (°)	Curr. surf. vel. (m/s)	Curr. ref. depth (m)	Parked	Initial yaw angle (°)	Run time (s)
a	1.3	4.5	0	55.95	39.17	27.98	0	0.82	7.49	0	0.5	50	0	0	600
b	1.3	6	0	43.98	30.79	21.99	0	0.92	7.62	0	0.5	50	0	0	600
c	1.3	8	0	35.00	24.50	17.50	0	1.13	7.89	0	0.5	50	0	0	600
d	1.3	10	0	29.61	20.73	14.81	0	1.42	8.23	0	0.5	50	0	0	600
e	1.3	12	0	26.02	18.21	13.01	0	1.78	8.64	0	0.5	50	0	0	600
f	1.3	14	0	23.46	16.42	11.73	0	2.21	9.07	0	0.5	50	0	-27.5	600
g	1.3	16	0	21.53	15.07	10.77	0	2.69	9.51	0	0.5	50	0	-39	600
h	1.3	18	0	20.04	14.03	10.02	0	3.21	9.94	0	0.5	50	0	-46	600
i	1.3	20	0	18.84	13.19	9.42	0	3.77	10.35	0	0.5	50	0	-52	600
j	1.3	22	0	17.86	12.50	8.93	0	4.36	10.73	0	0.5	50	0	-56	600
k	1.3	24	0	17.04	11.93	8.52	0	4.93	11.08	0	0.5	50	0	-59	600
l	1.3	24	0	17.04	11.93	8.52	0	7.00	12.11	0	0.5	50	0	-59	600
m	1.3	24	45	17.04	11.93	8.52	45	7.00	12.11	45	0.5	50	0	-14	600
n	1.3	24	-45	17.04	11.93	8.52	-45	7.00	12.11	-45	0.5	50	0	-104	600

DLC 6.1

The thirteen runs (a to m) for DLC 6.1 investigate how the Seawind 6 would withstand under extreme environmental conditions. Here, the turbine is yawed -90° out of the wind into its parked position, disk brakes are applied to the turbine shaft, the teeter hinge is unlocked, the rotor is kept parallel to the wind direction, electric pumps are activated to orient the blades into the horizontal position, and the yaw system is mechanically locked (if LIDAR sensors observe an oncoming hurricane). For the turbulent EWM, this 10 min average wind speed (with recurrence period of 50 years) of 50 m/s was calculated as a function of z as follows:

$$V_{50}(z) = V_{ref}\left(\frac{z}{z_{hub}}\right)^{0.11} \tag{5.5}$$

where V_{ref} was the reference wind speed (50 m/s), and z equals z_{hub}. The longitudinal turbulence standard deviation was found according to:

$$\sigma_1 = 0.11V_{hub} \tag{5.6}$$

where V_{hub} equaled V_{50} which was 50 m/s. Clearly, by inputting this into Equation 5.3, the two V_{hub} cancelled resulting in a longitudinal turbulence intensity of 0.11. Heading directions from -90° to 90° were simulated for the co-directional wind, waves, and currents to investigate which direction would generate the largest loads on the turbine structure and moorings. Constant H_s and T_p values, of 13.06 m and 18.00 s respectively, were inputted based on maximum values prescribed by Seawind engineers possible during expected extreme weather conditions. The near-surface current velocity was also increased to 1 m/s, to reflect the heightened oceanic activity during the extreme weather.

Table 5.4: Ultimate DLC Overview - DLC 6.1

Run	DLC	Wind speed (m/s)	Wind dir. (°)	Long. turb. int. (%)	Lat. turb. int. (%)	Vert. turb. int. (%)	Wave dir. (°)	H_s (m)	T_p (s)	Curr. dir. (°)	Curr. surf. vel. (m/s)	Curr. ref. depth (m)	Parked	Initial yaw angle (°)	Run time (s)
a	6.1	50	0	11.00	7.70	5.50	0	13.06	18.00	0	1	50	1	-90	600
b	6.1	50	-15	11.00	7.70	5.50	-15	13.06	18.00	-15	1	50	1	-105	600
c	6.1	50	15	11.00	7.70	5.50	15	13.06	18.00	15	1	50	1	-75	600
d	6.1	50	-30	11.00	7.70	5.50	-30	13.06	18.00	-30	1	50	1	-120	600
e	6.1	50	30	11.00	7.70	5.50	30	13.06	18.00	30	1	50	1	-60	600
f	6.1	50	-45	11.00	7.70	5.50	-45	13.06	18.00	-45	1	50	1	-135	600
g	6.1	50	45	11.00	7.70	5.50	45	13.06	18.00	45	1	50	1	-45	600
h	6.1	50	-60	11.00	7.70	5.50	-60	13.06	18.00	-60	1	50	1	-150	600
i	6.1	50	60	11.00	7.70	5.50	60	13.06	18.00	60	1	50	1	-30	600
j	6.1	50	-75	11.00	7.70	5.50	-75	13.06	18.00	-75	1	50	1	-165	600
k	6.1	50	75	11.00	7.70	5.50	75	13.06	18.00	75	1	50	1	-15	600
l	6.1	50	-90	11.00	7.70	5.50	-90	13.06	18.00	-90	1	50	1	-180	600
m	6.1	50	90	11.00	7.70	5.50	90	13.06	18.00	90	1	50	1	0	600

DLC I.1

DLC I.1 models a tropical cyclonic event using the steady EWM, with allowance for short-term deviations from the mean wind direction made by assuming yaw misalignment of ±15º. To maintain co-directionality, the wave and current directions were also changed. The IEC tropical cyclone wind class must withstand sustained (10 min) wind speeds of up to 57 m/s and gusts (3 s) of 80 m/s [31]. An 80 m/s steady wind was run for just 60 s as it would be extremely unlikely that sustained gusts would last longer than this even during extreme cyclonic events offshore. This provides much more assurance of turbine safety than the required 3 s gust. Constant H_s and T_p values, of 15.00 m and 20.00 s respectively, were inputted based on maximum values experienced during tropical cyclones [67]. The same 1 m/s near-surface current speeds were simulated as for DLC 6.1.

Table 5.5: Ultimate DLC Overview - DLC I.1

Run	DLC	Wind speed (m/s)	Wind dir. (°)	Long. turb. int. (%)	Lat. turb. int. (%)	Vert. turb. int. (%)	Wave dir. (°)	H_s (m)	T_p (s)	Curr. dir. (°)	Curr. surf. vel. (m/s)	Curr. ref. depth (m)	Parked	Initial yaw angle (°)	Run time (s)
a	I.1	80	-45	0	0	0	-45	15.00	20.00	-45	1	50	1	-135	60
b	I.1	80	-30	0	0	0	-30	15.00	20.00	-30	1	50	1	-135	60
c	I.1	80	-60	0	0	0	-60	15.00	20.00	-60	1	50	1	-135	60

5.2. Time Series

In this section, time series of the sixteen most insightful variables are displayed and analysed for each of the four DLCs. Selecting the variables was not a trivial process, with much time and scrutiny expended to select those that would provide the best overview of the turbine's behaviour. Upon completion of the simulations and an examination of the ultimate loads results, the run from each DLC with the highest number of design driving loads was selected for inclusion here. Run f was selected from DLC 1.2, run m for DLC 1.3, and run a for both DLC 6.1 and DLC I.1. A direct comparison between these variables is then presented before moving onto the ultimate load analysis in Section 5.3. DLC 1.2f is displayed in Figure 5.1 and Figure 5.2, DLC 1.3m in Figure 5.3 and Figure 5.4, DLC 6.1a in Figure 5.5 and Figure 5.6, and DLC I.1a in Figure 5.7 and Figure 5.8.

Note: It was discovered after completing all the runs that the Sowento controller had not been fully configured, with its yaw velocity parameter set too high (maximum of 30°/s rather than 10°/s) and no supervisory control added to shutdown the turbine during emergency conditions (for example, at wind speeds in excess of 25 m/s and rotor speeds of 28 rpm). Unfortunately, the correct parameters were only applied after the expiration date of the Bladed license and so the results of the following exercises are at times frustratingly inaccurate. This was out of the control of the author as there was only a small time-frame available to complete all the required simulations. When analysing the results in the following sections, please be mindful of these inaccuracies and try to predict how the turbine should have behaved. This will be discussed further in the relevant conclusion sections of this report.

DLC 1.2f

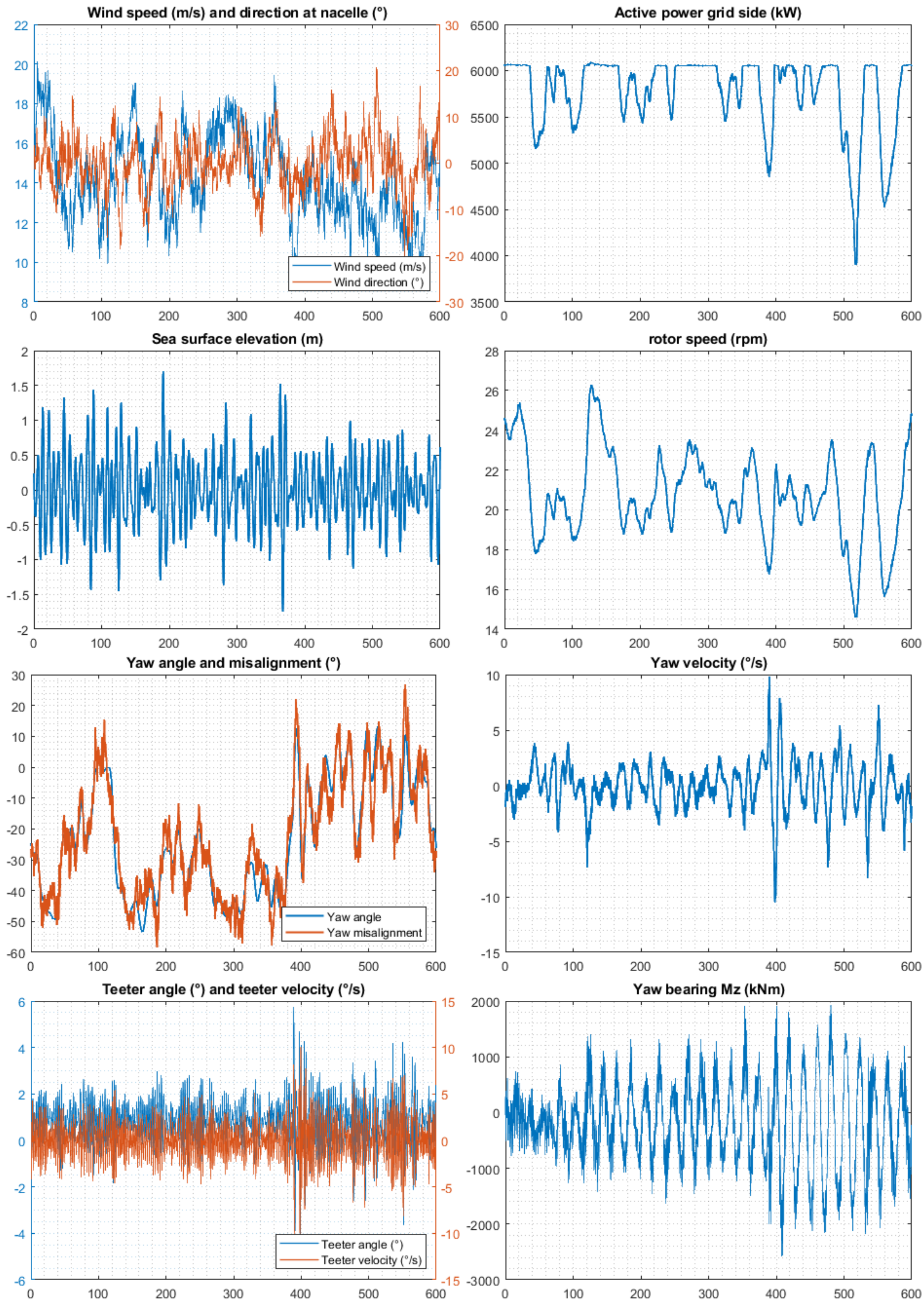

Figure 5.1: Part 1 - Seawind 6 DLC 1.2f time series plots

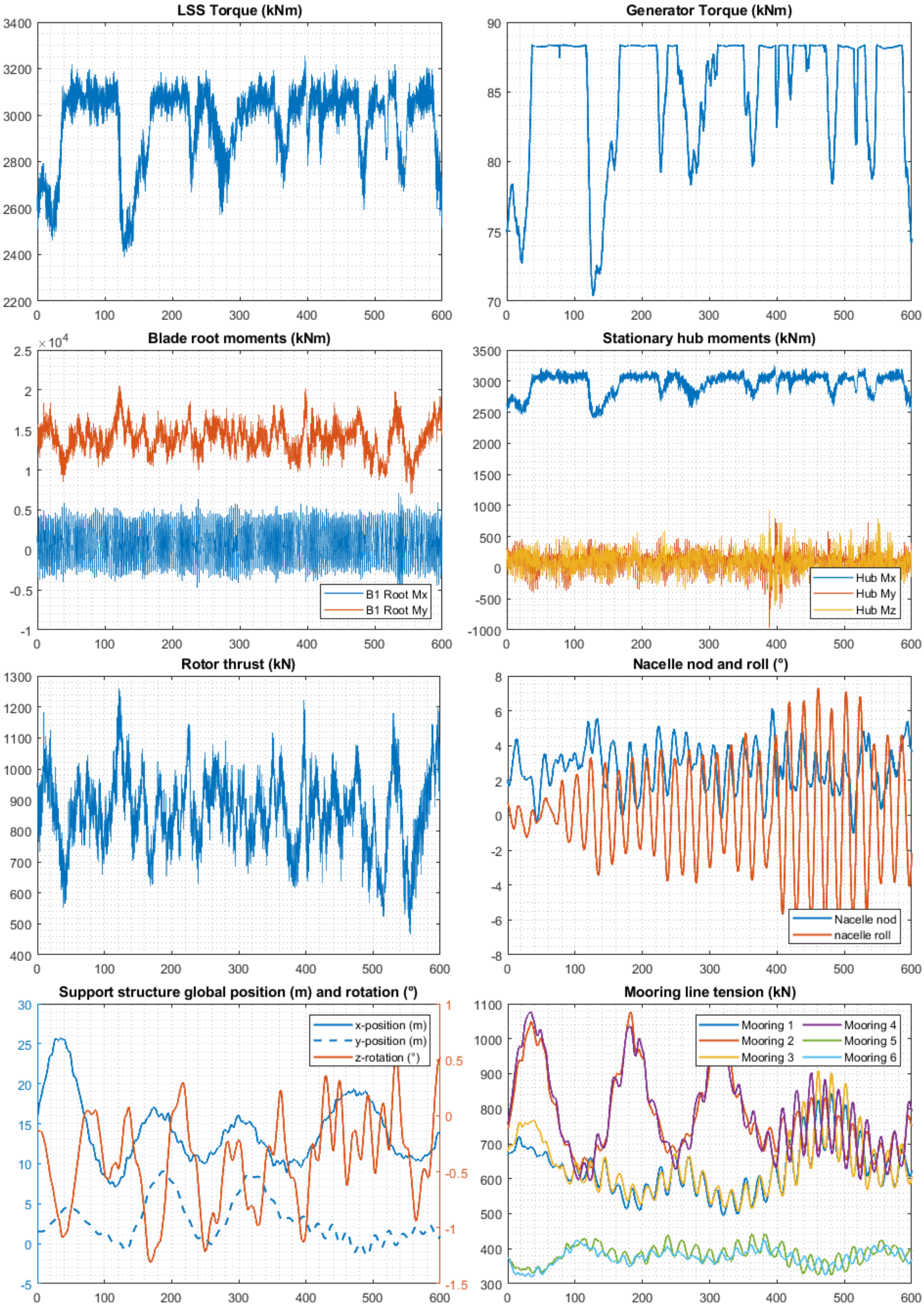

Figure 5.2: Part 2 - Seawind 6 DLC 1.2f time series plots

DLC 1.3m

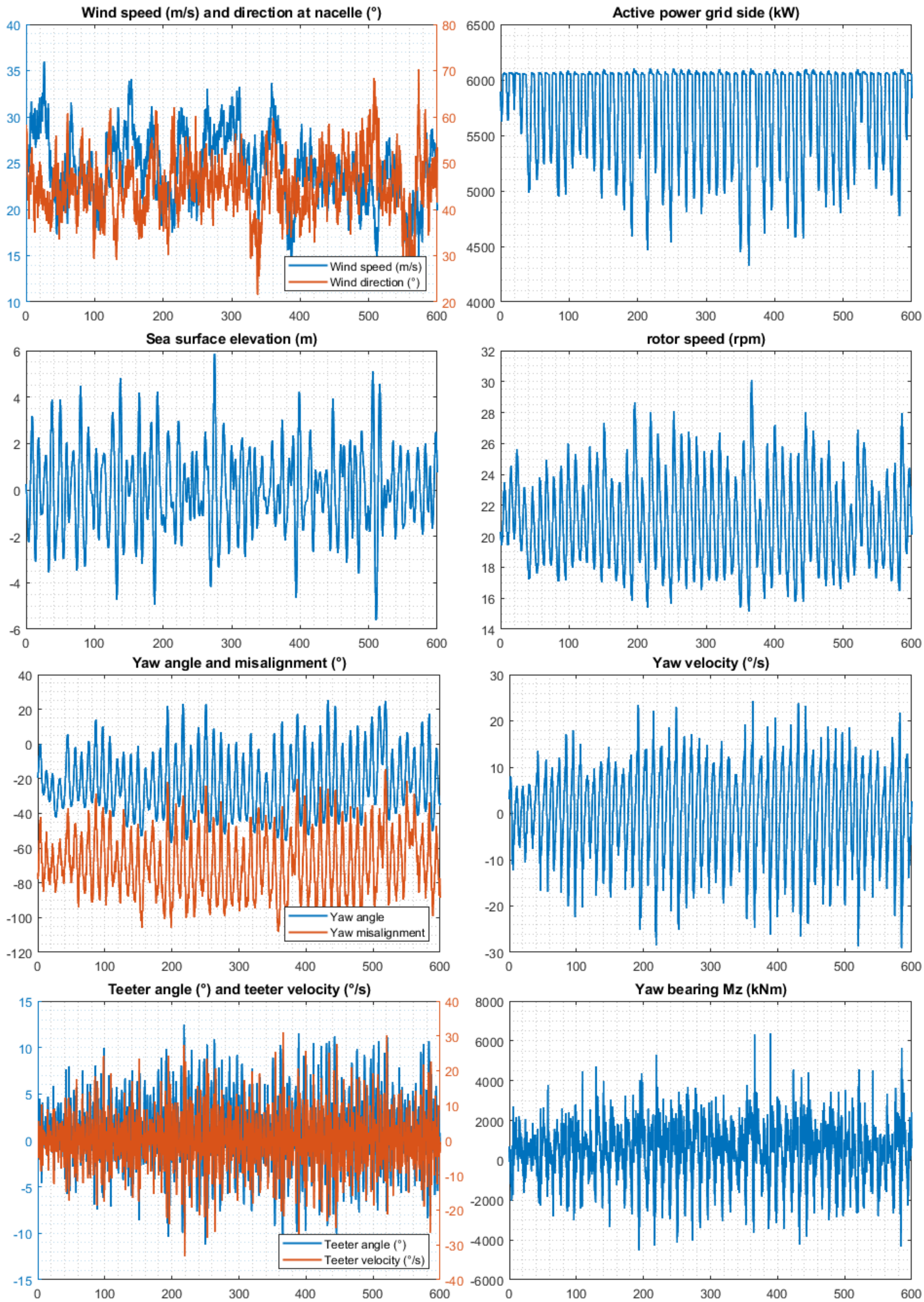

Figure 5.3: Part 1 - Seawind 6 DLC 1.3m time series plots

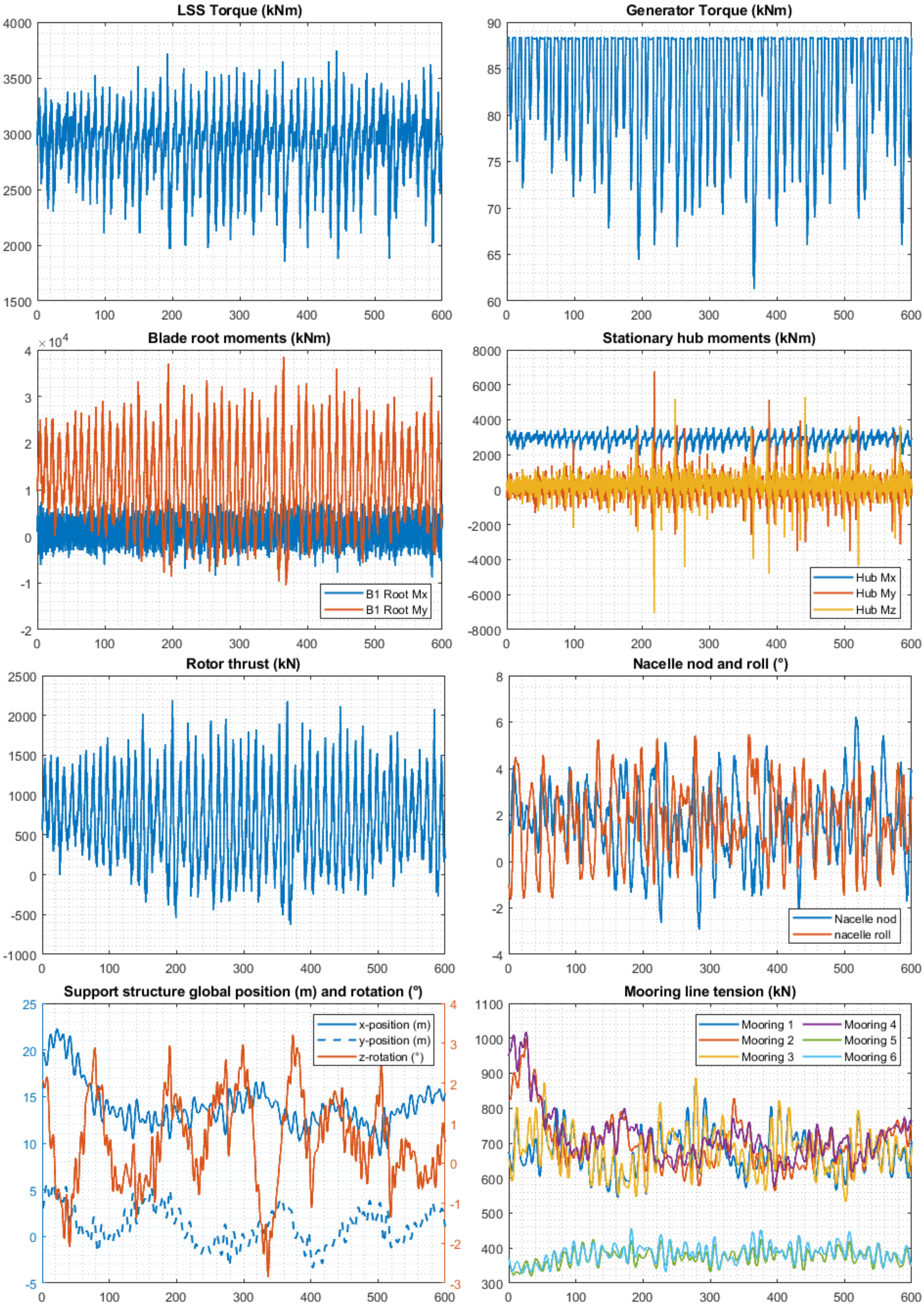

Figure 5.4: Part 2 - Seawind 6 DLC 1.3m time series plots

DLC 6.1a

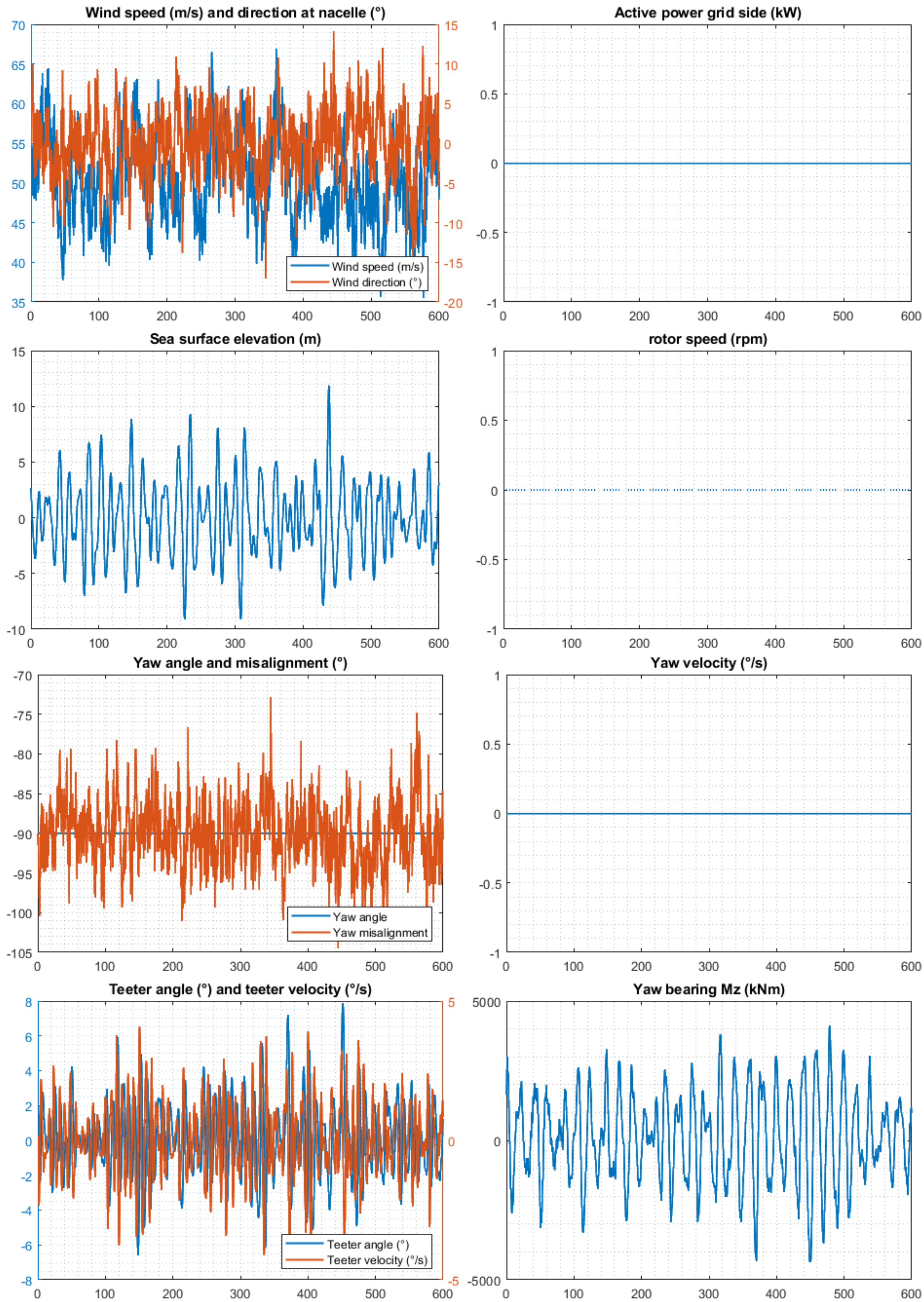

Figure 5.5: Part 1 - Seawind 6 DLC 6.1a time series plots

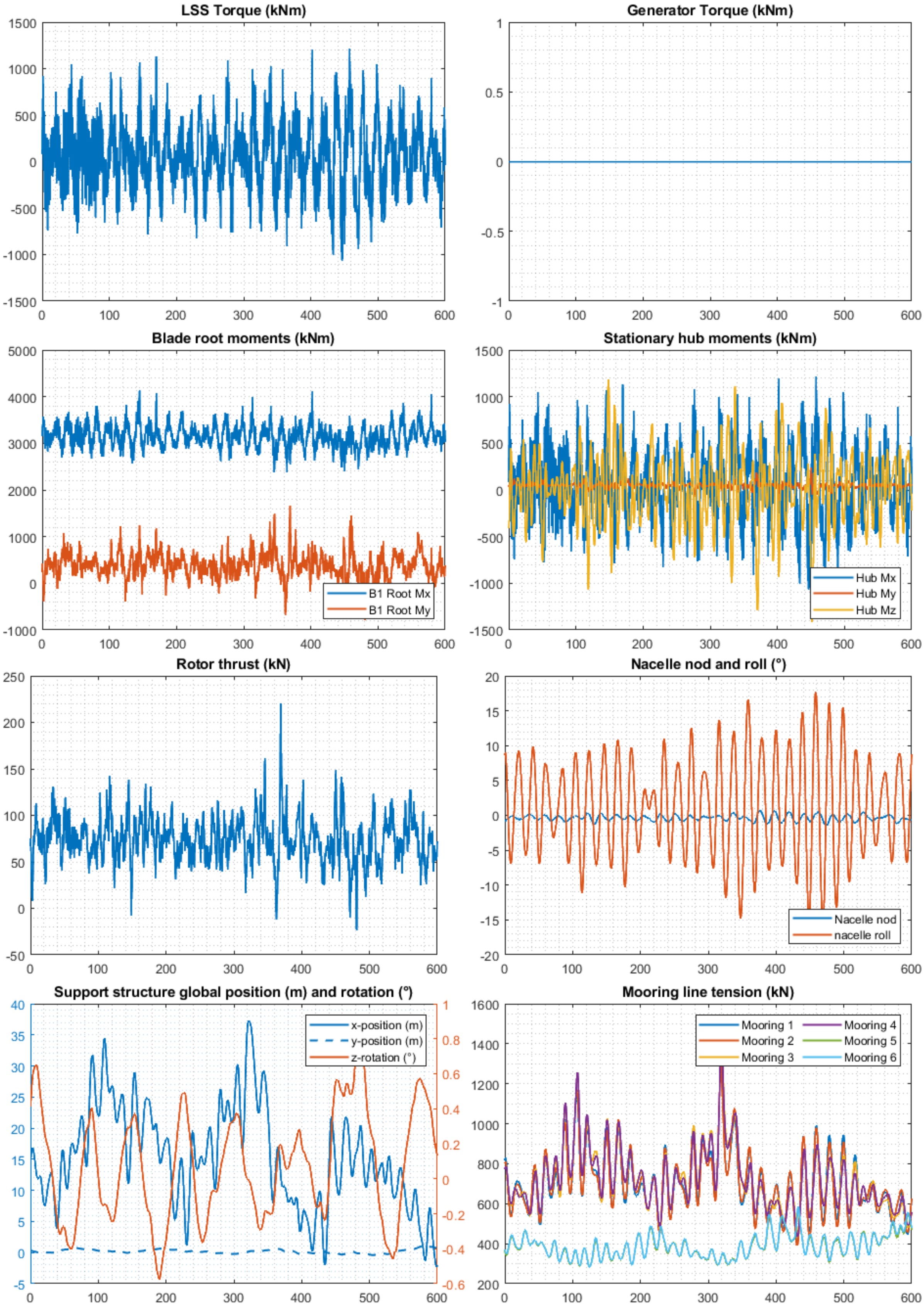

Figure 5.6: Part 2 - Seawind 6 DLC 6.1a time series plots

DLC I.1a

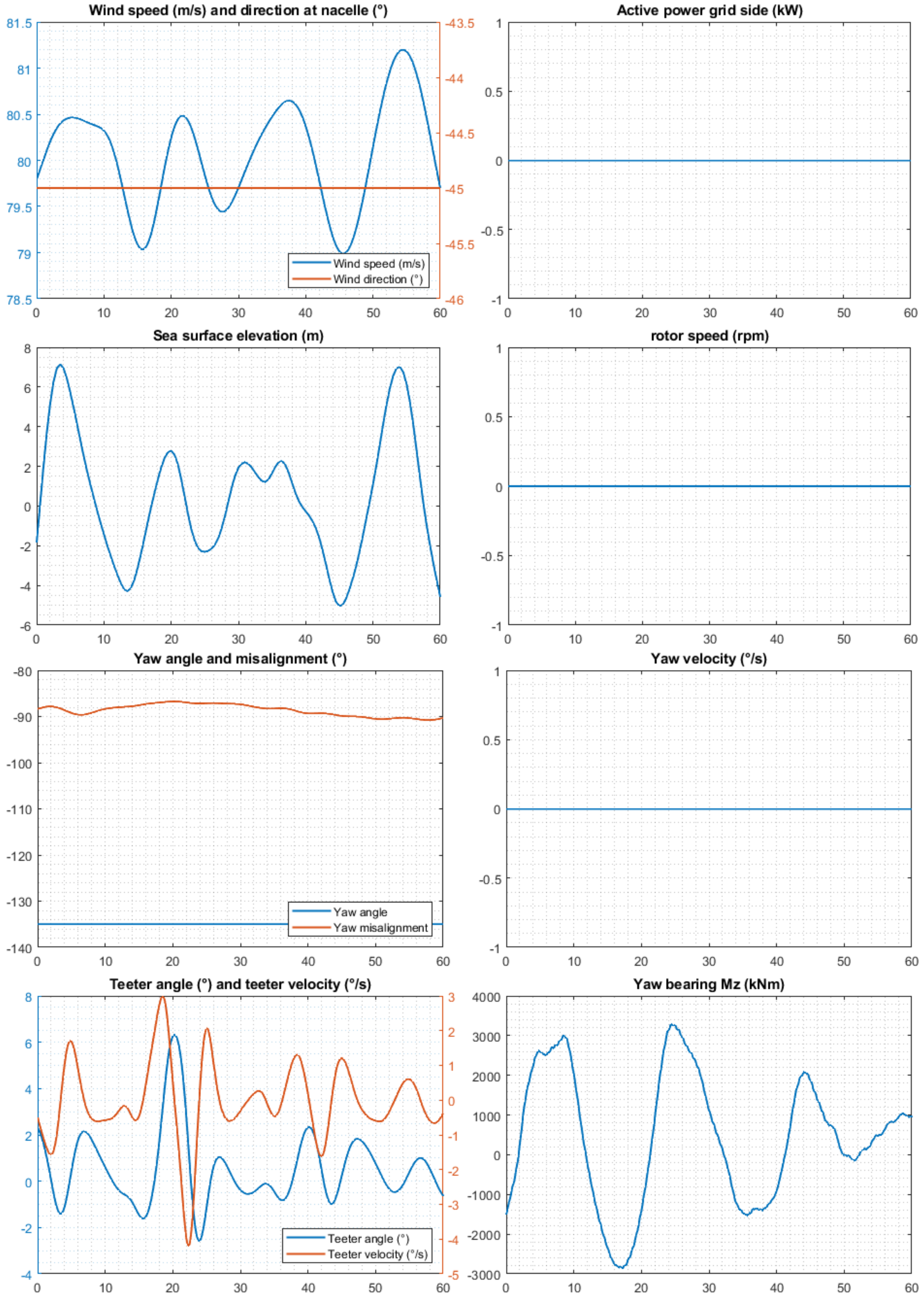

Figure 5.7: Part 1 - Seawind 6 DLC I.1a time series plots

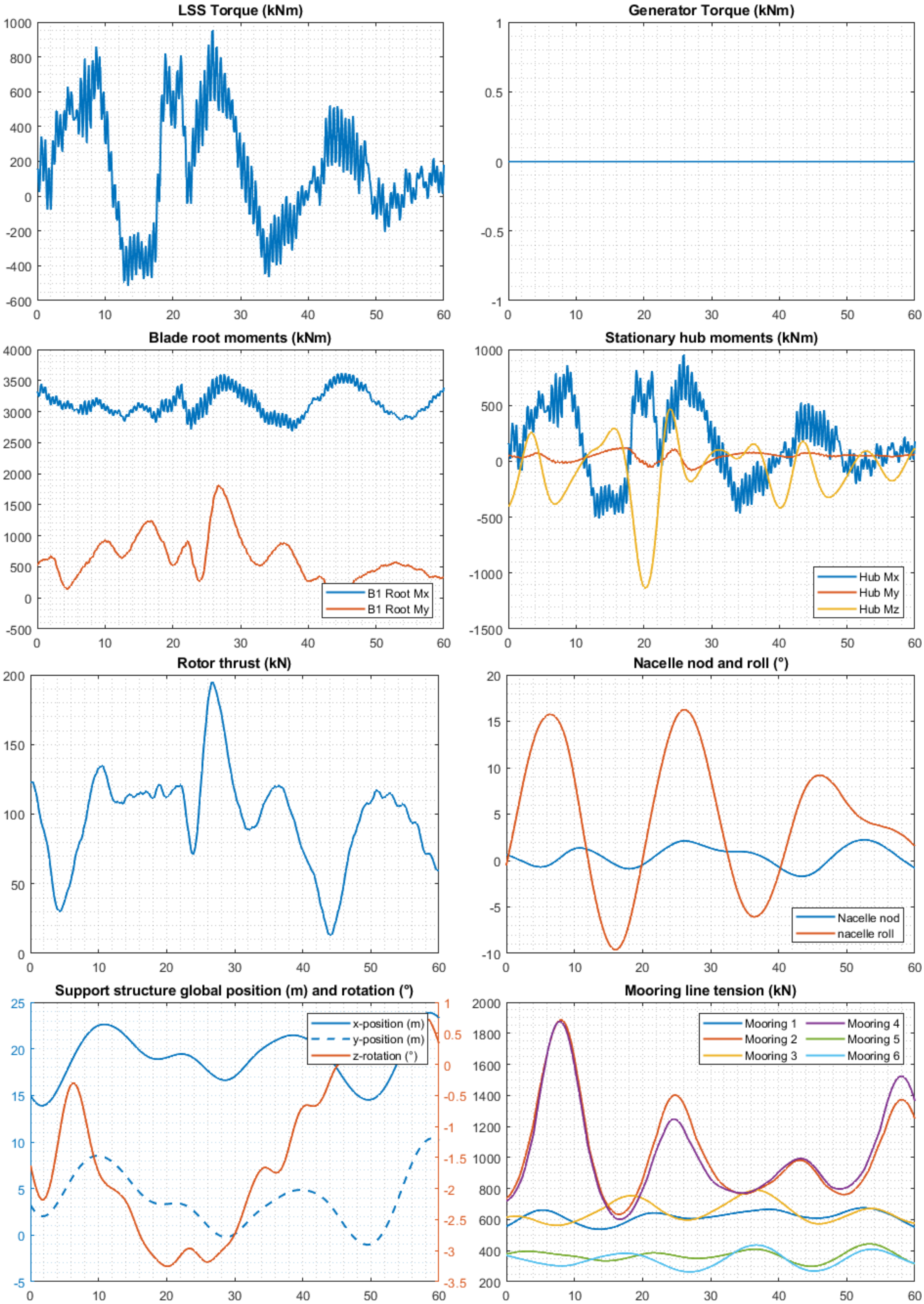

Figure 5.8: Part 2 - Seawind 6 DLC I.1a time series plots

Time Series Analysis

After all the simulations outlined in Section 5.1 were completed, the time series data was opened in the Bladed Results Viewer and exported to Excel. The data was then read into Matlab and the graphs presented in this section were meticulously configured to plot the results in the most visually appealing manner. Much like Chapter 4, a bullet point system will be used here again to analyse each of the variables across the four chosen DLCs as efficiently as possible. The maximum absolute values from these time series plots, as well as other signals not included here, will be used later in both the ultimate and fatigue loads analyses. It is a fun exercise to try and spot the maximum values presented in the ultimate loads tables in Subsection 5.3.1 in these time series plots (when applicable). Again, the first three DLCs all have outputs of 600 s recorded here, while DLC I.1 is just 60 s long.

- **Wind speed and direction:** All follow the specifications from simulation setup tables in Section 5.1. There is a clear lack of turbulence for DLC I.1a.
- **Active power:** Wind speeds remain below cut-out and sometimes dip below rated in DLC 1.2f, meaning the active power also dips below rated 6.2 MW. With a mean wind speed of 24 m/s, DLC 1.3m shows rapid fluctuations from rated power as the turbine is yawed out of wind. As wind speeds exceed cut-out and the turbine is parked for DLCs 6.1a and I.1a, both time series show 0 MW output.
- **Sea surface elevation:** Greatest wave heights observed for DLC 6.1a, with 12 m. If DLC I.1a was simulated for longer, even greater heights would have been experienced due to the simulation setup.
- **Rotor speed:** The Seawind 6 has a variable rotor speed of 8 to 28 rpm, running at 20.8 rpm at rated power. Both DLC 1.2f and 1.3m can be seen to regulate about this rated running speed, with larger fluctuations in the latter (maximum of 26 rpm and 30 rpm, respectively). Clearly, if the supervisory control of the Seawind 6 model was enforced the turbine would have been forced to shut down when the shaft over-speed of 28 rpm was exceeded. This would have prevented the subsequent, unrealistically, large loading experienced by the turbine. For both the parked DLCs the rotor speed is shown to be 0 rpm as the blades are held horizontally in alignment with the wind direction.
- **Yaw angle and misalignment:** Yaw misalignment fluctuations about -27.5° to regulate power output with changing wind speed and direction about 0° for DLC 1.2f. For DLC 1.3m, wind is incoming from 45°, meaning the rotor must be yawed to -14° to achieve the -59° yaw misalignment for power control. Fluctuations about these values again are from wind speed and direction changes. For DLC 6.1a, the rotor is parked and held at -90°. The wind heading is 0°, but lateral turbulence causes the yaw misalignment changes. For DLC I.1 the wind is approaching at -45° from North meaning the turbine has to be yawed to -135° to maintain its parked configuration.
- **Yaw velocity:** Greater yaw velocity magnitudes and fluctuation frequencies were experienced in DLC 1.3m than 1.2f (maximum of 29°/s versus 10.5°/s) as the turbine attempted to actively control power in winds with increased turbulence intensities (associated with the ETM). The yaw lock was engaged for both the parked simulations so yaw velocities remain at 0°/s. The Seawind 6 turbine has a yawing rate of up to 10°/s, which is sufficiently rapid to control the power output by yawing. Indeed, for power control, a yawing rate around 4°/s is sufficient with maximum yawing rate only required during emergency shut down. These unusually large yaw velocities occurred as a result of the Sowento controller having a parameter error at the time of these simulation runs. Unfortunately, the correct parameters were only applied after the expiration date of the Bladed license. This is rather unfortunate and falsifies the corresponding results somewhat.
- **Teeter angle and velocity:** Greatest teeter angle of 12.5° experienced in DLC 1.3m, followed by 8° in DLC 6.1a. The teeter stop must have been hit during DLC 1.3m which is not ideal, and again is an unrealistic result of the excessive yaw velocities. The lack of turbulence means the teeter angle is not as large for DLC I.1a even though greater wind speeds were experienced. Again, by far the largest teeter velocities were experienced in DLC 1.3m, reaching 35°/s.
- **Yaw bearing Mz:** The Seawind 6 has a yaw torque capacity of 4340 kNm (4 motors at 350 bar) with peak of 5580 kNm (4 motors at 430bar). The largest yaw torque was experienced in

DLC 1.3m, reaching 6400 kNm. The yaw torque can be seen to vary in DLCs 1.2f and 1.3m in an attempt to regulate the rotor running speed. Hence, there is a need for a soft yaw hydraulic system. For 6.1 and I.1, the yaw lock is applied to keep the turbine parked, but the yaw bearing moments are still shown to reach 2000 kNm due to the strong winds even though they pass parallel to the rotor. The wind loading is what increases the yaw torque in DLC 1.3m above peak yaw torque capacity.

- **LSS torque:** The Seawind 6 has a two stage planetary gearbox with rated inlet torque of 3000 kNm and peak inlet torque of 3700 kNm, which is controlled through the converter-generator system. DLCs 1.2f and 1.3m are shown to share this rated value and remain below the peak. For the two parked DLCs the double disk brakes have been applied to the LSS (with total brake torque capacity of 4800 kNm), with the displayed LSS torque fluctuations up to 1000 kNm an effect of wind loading.

- **Generator torque:** Torque and speed are inversely proportional to each other, meaning the gearbox ratio of 34.8:1 would reduce the rated generator torque (HSS torque) of roughly 86.2 kNm. This matches very closely to the outputs of DLCs 1.2f and 1.3m. As the LSS shaft was braked for the parked simulations, the generator torque was 0 kNm.

- **Blade root moments:** DLC 1.2f and 1.3m both have very similar edgewise moments fluctuating ±5 MNm about a mean of 0 kNm. They both also share the same mean flatwise moment of 15 MNm, with much larger fluctuations of ±24 MNm present in DLC 1.3m. For DLC 6.1a and I.1a this is reversed, with the edgewise moments being the largest. As the blades are held horizontally and parallel to the wind, the wind loading creates a positive edgewise moment of approximately 3250 kNm on the blade roots. A much smaller component of the wind is seen by the rotor face (the whole point of active yaw power control), so the flatwise moments are vastly reduced.

- **Stationary hub moments:** DLCs 1.2f and 1.3m both shared the same general behaviour, with the hub Mx moments (mean of 3000 kNm) shown to be larger than both the My and Mz moments (mean of 0 kNm). This makes sense as the rotor rotates about the x-axis and so the Mx hub moment should be the same as the rated LSS torque of 3000 kNm. The My and Mz moments should also intuitively be comparable as the rotor has a balanced rotation and wind shear only has a small effect. For DLCs 6.1a and I.1a, the My moments are negligible as the rotor faces out of the wind, while minimal forcing is experienced about the y- and z- axes.

- **Rotor thrust:** The Seawind 6 has a rated average rotor thrust of 900 kN, which is verified in DLCs 1.2f and 1.3m. again, larger fluctuations up to 2200 kN are present in the latter. Minimal rotor thrust is evidently present on the two parked rotors. The rotor thrust shares the same behaviour as flatwise (My) blade root moments for each of the DLCs.

- **Nacelle nod and roll:** DLC 1.3m has more extreme nacelle motion than its DLC 1.2f counterpart. A positive nod angle is in the downwind direction, with both DLCs showing maximum angles of around 6°. DLC 1.2f displays increasing roll motion as the simulation progressed due to a rapid yaw movement after 400 s. The nod motions are quite minimal for both parked runs, with the wind impacting the side of the nacelle and causing huge roll angles of up to 17° instead.

- **Support structure position and rotation:** The greatest displacement is shown in the x-direction for all runs. When producing power the rotor is facing into the wind and is pushed downwind, while the side of the nacelle is impacted by oncoming wind when parked. If the wind speeds were the same, larger y-displacements would have been expected in the power production simulations than DLC I.1 as the yaw misalignment of the rotor should have caused greater displacements in the y-direction. Rotation about the z-axis is comparable for all runs. Again, at similar wind speeds, greater rotations would have been expected for power production runs as the surface area of the rotor is larger than that of the parked rotor-nacelle assembly (RNA).

- **Mooring line tension:** As per the mooring line (ML) configuration displayed in Figure 3.20, ML 1 and 3 are attached to an anchor North-East of the Seawind 6's platform, ML 2 and 4 are to North-West, and ML 5 and 6 are to South. As the wind direction is 0° and yaw angle is -27.5° from North for DLC 1.2f, ML 2 and 4 correctly exhibit larger tensions than ML 1 and 3. As the turbine is being pushed downwind, tensions in ML 5 and 6 are minimal. For DLC 1.3m, the wind direction is 45° and yaw angle is -14° from North (to achieve -59° yaw misalignment), and so the tensions are similar for ML 1, 2, 3, and 4. The North facing mooring line tensions are almost all identical in DLC 6.1a as a result of the parked turbine which generates minimal y-displacements. The wind direction is -45° in DLC I.1a, with the rotor a further -90° misaligned to this, meaning ML 2 and 4 are subjected to almost all the wind loading.

5.3. Ultimate Loads

In this section, Bladed has been used to compute the ultimate loads experienced for a number of select turbine components during the ultimate DLC runs (DLCs 1.3, 6.1, and I.1) outlined in Section 5.1. The components investigated were; Blade 1 and 2 roots, the rotating and stationary variations of the hub, the yaw bearing, various sections of the steel tower and concrete shaft (expanded on in Subsection 5.3.2), the mooring lines, and the gravity anchors. The maximum and minimum values of each load component (three forces, three moments, one combined force in the section, and one combined moment) has been extracted from these runs and tabulated, along with their accompanying loads, in Subsection 5.3.1. The maximum and minimum value for the load component under consideration in each row is signaled by bold face text. The loads are presented in base metric units (N and Nm), with associated safety factors having been applied. It is important to note that these loads include contributions from aerodynamic, hydrodynamic, self-weight, rotational inertial, and dynamic inertial effects (from yawing, drive train, and control system modes amongst others) [37]. Following every ultimate load table, a histogram presents the maximum absolute load for each load case. These are colour-coded according to DLC, with the corresponding run identifier labelled above the bar. A synopsis of each turbine component's results is then provided in Subsection 5.3.2, followed by a comparison of the maximum absolute loads versus design loads. Again, these results should be taken with ”a pinch of salt” considering the yaw velocity inaccuracies and lack of supervisory control with the incomplete version of the controller. Intuitively, with a fully operational and accurate controller, these loads would likely be reduced.

The co-ordinate systems used for calculation of extreme and fatigue loads is given in Figure 5.9 to Figure 5.12 below [37]. The axis system is based on GL (Germanische Lloyd) regulations [55]. Obviously a two-bladed turbine is investigated in this report rather than the three-bladed machine displayed. The co-ordinate system for yaw bearing is the same as the tower's displayed in Figure 5.11, but with the origin specified at the intersection of the tower and shaft axes. Referring to Figure 5.12, only the line tension is provided for mooring line loads, while the horizontal anchor loads are the resultant of outputted x- and y-axis loads (neglecting vertical z-axis loads).

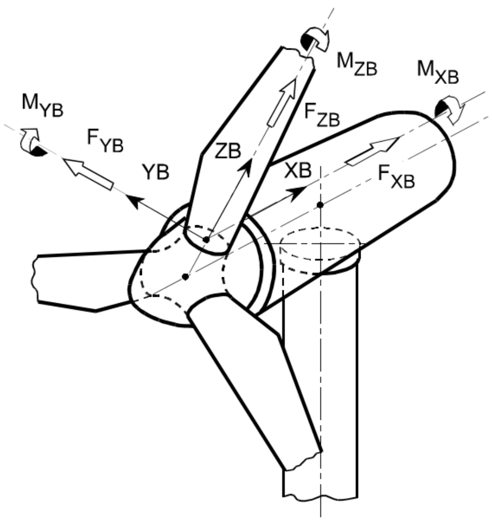

ZB	Radially along blade axis.
XB	Perpendicular to ZB, and pointing towards the tower for an upwind turbine, or away from the tower for a downwind turbine (the picture shows an upwind turbine).
YB	Perpendicular to blade axis and shaft axis, to give a right-handed co-ordinate system independent of direction of rotation and rotor location upwind or downwind of the tower.
Origin	At each blade station.

Figure 5.9: Co-ordinate system for blade loads and deflections [37]

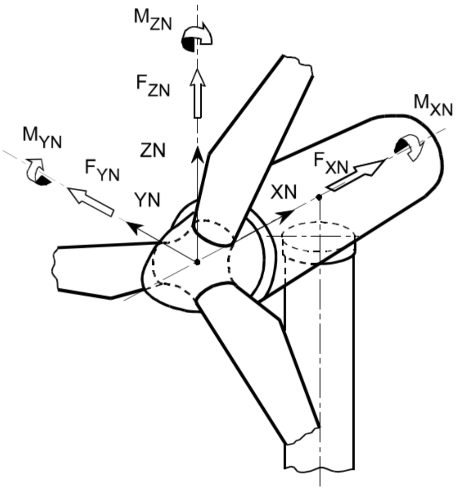

Hub loads in fixed frame of reference:

XN	Along shaft axis, and pointing towards the tower for an upwind turbine, or away from the tower for a downwind turbine (the picture shows an upwind turbine).
ZN	Perpendicular to XN, such that ZN would be vertically upwards if the tilt angle were zero.
YN	Horizontal, to give a right-handed co-ordinate system independent of direction of rotation and rotor location upwind or downwind of the tower.

Hub loads in rotating frame of reference:

XN	Along shaft axis, and pointing towards the tower for an upwind turbine, or away from the tower for a downwind turbine (the picture shows an upwind turbine).
ZN	Perpendicular to XN, such that ZN would be aligned with blade 1 axis if the cone angle were zero.
YN	Perpendicular to XN and ZN, to give a right-handed co-ordinate system independent of direction of rotation and rotor location upwind or downwind of the tower.
Origin	At hub centre (intersection of blade and shaft axes).

Figure 5.10: Co-ordinate system for hub loads [37]

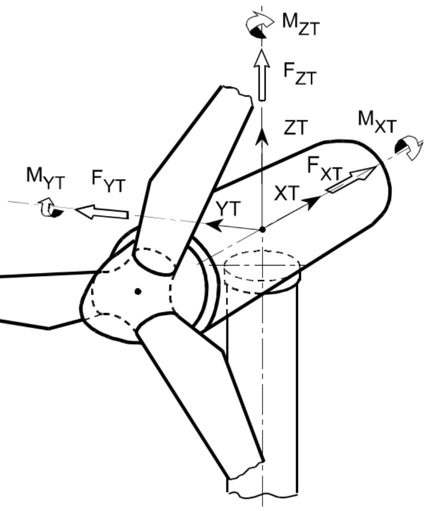

XT	Pointing South.
ZT	Vertically upwards.
YT	Pointing East.
Origin	At each tower station.

Figure 5.11: Co-ordinate system for tower loads and deflections [37]

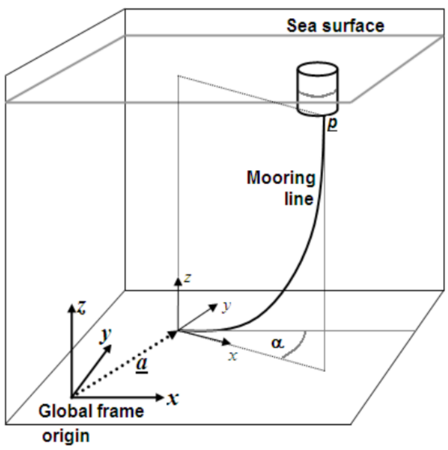

Figure 5.12: Co-ordinate system for mooring lines, with origin at line anchor point [37]

5.3.1. Ultimate Load Data

Blade 1 Root

Table 5.6: Ultimate load table - Blade root 1

		Load	Mx	My	Mxy	Mz	Fx	Fy	Fxy	Fz	Safety
		case	Nm	Nm	Nm	Nm	N	N	N	N	factor
Mx	**Max**	**1.3f**	**1.27E+07**	1.98E+07	2.35E+07	-5.40E+05	5.20E+05	-4.49E+05	6.87E+05	2.45E+06	1.35
Mx	**Min**	**1.3m**	**-1.20E+07**	2.90E+07	3.14E+07	-1.17E+06	1.12E+06	4.33E+05	1.20E+06	3.92E+06	1.35
My	**Max**	**1.3m**	4.60E+06	**5.20E+07**	5.22E+07	1.07E+05	1.36E+06	8.21E+04	1.36E+06	3.40E+06	1.35
My	**Min**	**1.3m**	-2.70E+05	**-1.42E+07**	1.42E+07	-7.61E+05	-4.36E+05	1.25E+05	4.54E+05	3.81E+06	1.35
Mxy	**Max**	**1.3m**	4.60E+06	5.20E+07	**5.22E+07**	1.07E+05	1.36E+06	8.21E+04	1.36E+06	3.40E+06	1.35
Mxy	**Min**	**1.3m**	-4.90E+04	-2.10E+05	**2.16E+05**	-6.33E+05	-7.76E+04	1.03E+05	1.29E+05	2.28E+06	1.35
Mz	**Max**	**1.3m**	1.13E+07	2.78E+07	3.00E+07	**3.94E+05**	4.80E+05	-3.15E+05	5.75E+05	3.97E+06	1.35
Mz	**Min**	**1.3m**	3.47E+05	2.01E+07	2.01E+07	**-1.69E+06**	7.75E+05	5.14E+04	7.77E+05	4.79E+06	1.35
Fx	**Max**	**1.3m**	1.83E+06	4.39E+07	4.39E+07	-8.07E+05	**1.53E+06**	-1.13E+05	1.54E+06	3.31E+06	1.35
Fx	**Min**	**1.3m**	2.91E+06	-1.35E+07	1.38E+07	-8.70E+05	**-4.61E+05**	3.48E+04	4.62E+05	3.87E+06	1.35
Fy	**Max**	**1.3m**	-1.13E+07	1.91E+07	2.22E+07	-1.19E+06	7.48E+05	**4.93E+05**	8.95E+05	3.71E+06	1.35
Fy	**Min**	**1.3f**	1.27E+07	1.98E+07	2.35E+07	-5.40E+05	5.20E+05	**-4.49E+05**	6.87E+05	2.45E+06	1.35
Fxy	**Max**	**1.3m**	1.83E+06	4.39E+07	4.39E+07	-8.07E+05	1.53E+06	-1.13E+05	**1.54E+06**	3.31E+06	1.35
Fxy	**Min**	**1.3m**	3.69E+06	4.94E+05	3.73E+06	-4.09E+05	-1.35E+04	-6.21E+03	**1.49E+04**	3.04E+06	1.35
Fz	**Max**	**1.3m**	3.47E+05	2.01E+07	2.01E+07	-1.69E+06	7.75E+05	5.14E+04	7.77E+05	**4.79E+06**	1.35
Fz	**Min**	**6.1h**	3.60E+06	7.37E+05	3.67E+06	-2.16E+04	3.77E+04	-2.39E+05	2.42E+05	**-1.77E+05**	1.35

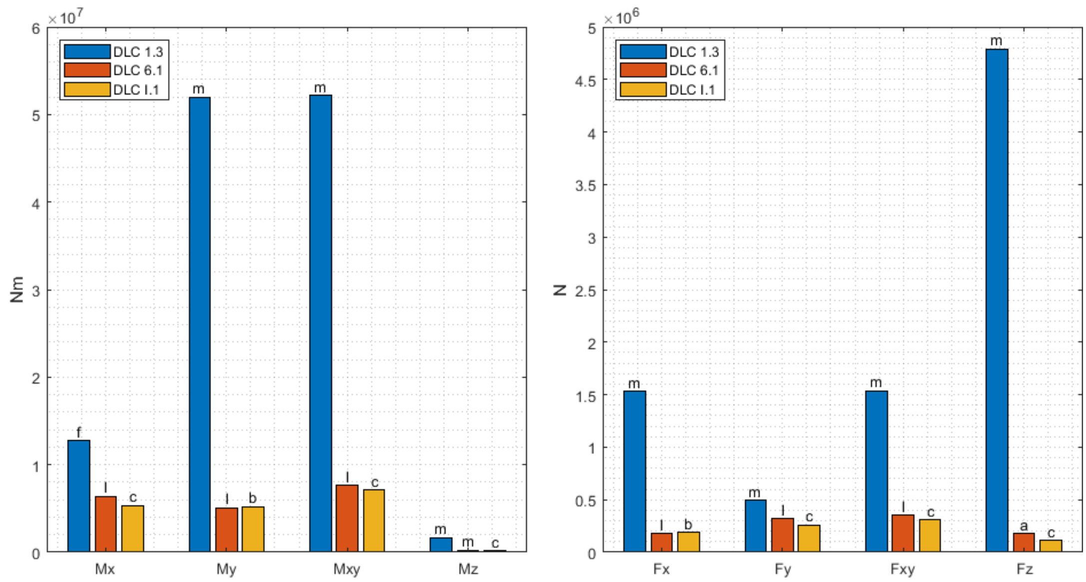

Figure 5.13: Ultimate load histogram - Blade root 1

Blade 2 Root

Table 5.7: Ultimate load table - Blade root 2

		Load	Mx	My	Mxy	Mz	Fx	Fy	Fxy	Fz	Safety
		case	Nm	Nm	Nm	Nm	N	N	N	N	factor
Mx	**Max**	**1.3m**	**1.39E+07**	3.19E+07	3.48E+07	2.56E+05	6.87E+05	-2.95E+05	7.48E+05	3.06E+06	1.35
Mx	**Min**	**1.3m**	**-1.07E+07**	3.28E+07	3.45E+07	-1.50E+06	1.26E+06	4.59E+05	1.34E+06	4.60E+06	1.35
My	**Max**	**1.3m**	-1.77E+06	**4.93E+07**	4.93E+07	1.35E+05	1.41E+06	2.06E+05	1.43E+06	2.49E+06	1.35
My	**Min**	**1.3m**	4.03E+06	**-1.37E+07**	1.42E+07	-2.58E+05	-4.55E+05	-1.37E+05	4.75E+05	3.47E+06	1.35
Mxy	**Max**	**1.3m**	-1.77E+06	4.93E+07	**4.93E+07**	1.35E+05	1.41E+06	2.06E+05	1.43E+06	2.49E+06	1.35
Mxy	**Min**	**1.3m**	1.45E+05	-9.81E+04	**1.75E+05**	-1.01E+06	1.01E+05	8.21E+04	1.31E+05	3.83E+06	1.35
Mz	**Max**	**1.3m**	3.03E+06	2.45E+07	2.47E+07	**4.30E+05**	4.29E+05	-3.59E+04	4.31E+05	3.15E+06	1.35
Mz	**Min**	**1.3m**	-1.87E+05	3.72E+06	3.72E+06	**-1.51E+06**	1.87E+05	3.24E+04	1.90E+05	4.46E+06	1.35
Fx	**Max**	**1.3m**	-2.47E+06	4.52E+07	4.53E+07	-8.56E+05	**1.62E+06**	3.74E+04	1.62E+06	3.80E+06	1.35
Fx	**Min**	**1.3m**	1.59E+06	-1.18E+07	1.19E+07	-8.64E+05	**-5.44E+05**	-1.55E+04	5.44E+05	3.55E+06	1.35
Fy	**Max**	**1.3m**	-9.28E+06	2.54E+07	2.71E+07	-1.49E+06	9.53E+05	**5.20E+05**	1.09E+06	4.54E+06	1.35
Fy	**Min**	**1.3m**	1.37E+07	2.03E+07	2.45E+07	-1.63E+05	4.28E+05	**-4.60E+05**	6.29E+05	3.32E+06	1.35
Fxy	**Max**	**1.3m**	-2.47E+06	4.52E+07	4.53E+07	-8.56E+05	1.62E+06	3.74E+04	**1.62E+06**	3.80E+06	1.35
Fxy	**Min**	**1.3m**	3.18E+06	1.96E+06	3.74E+06	-1.82E+05	3.81E+03	-4.39E+03	**5.81E+03**	2.70E+06	1.35
Fz	**Max**	**1.3m**	-1.07E+07	3.28E+07	3.45E+07	-1.50E+06	1.26E+06	4.59E+05	1.34E+06	**4.60E+06**	1.35
Fz	**Min**	**6.1a**	-3.70E+06	2.10E+05	3.70E+06	1.99E+04	1.79E+04	2.28E+05	2.28E+05	**-1.76E+05**	1.35

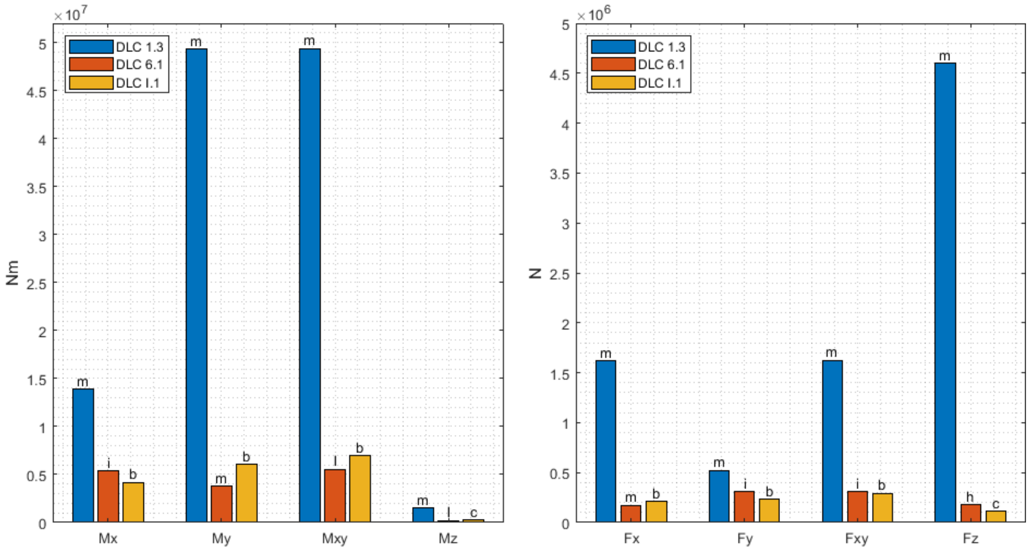

Figure 5.14: Ultimate load histogram - Blade root 2

Rotating Hub

Table 5.8: Ultimate load table - Rotating hub

		Load case	Mx Nm	My Nm	Mz Nm	Myz Nm	Fx N	Fy N	Fz N	Fyz N	Safety factor
Mx	**Max**	**1.3m**	**5.06E+06**	-8.50E+05	-5.98E+04	8.52E+05	2.40E+06	-3.91E+05	-4.22E+05	5.76E+05	1.35
Mx	**Min**	**6.1i**	**-1.81E+06**	2.71E+05	-1.13E+05	2.93E+05	-6.13E+04	-8.33E+05	-5.65E+05	1.01E+06	1.35
My	**Max**	**1.3m**	4.29E+06	**7.51E+06**	-9.77E+05	7.58E+06	1.58E+06	-1.07E+06	-4.09E+04	1.07E+06	1.35
My	**Min**	**1.3m**	3.63E+06	**-1.03E+07**	2.19E+05	1.03E+07	1.89E+06	-3.95E+05	1.07E+06	1.14E+06	1.35
Mz	**Max**	**1.3m**	3.00E+06	1.01E+06	**1.69E+06**	1.97E+06	1.34E+06	-1.11E+06	-8.85E+05	1.42E+06	1.35
Mz	**Min**	**1.3m**	2.75E+06	-1.45E+06	**-1.51E+06**	2.09E+06	7.41E+05	1.88E+05	1.02E+06	1.04E+06	1.35
Myz	**Max**	**1.3m**	3.63E+06	-1.03E+07	2.19E+05	**1.03E+07**	1.89E+06	-3.95E+05	1.07E+06	1.14E+06	1.35
Myz	**Min**	**6.1h**	9.78E+05	-4.60E+02	-3.30E+02	**5.70E+02**	1.96E+05	-8.31E+05	3.71E+05	9.10E+05	1.35
Fx	**Max**	**1.3m**	4.27E+06	1.56E+06	-2.57E+05	1.58E+06	**2.96E+06**	4.91E+05	4.35E+04	4.93E+05	1.35
Fx	**Min**	**1.3m**	3.35E+06	1.06E+05	8.05E+05	8.12E+05	**-8.55E+05**	1.34E+05	-9.01E+05	9.11E+05	1.35
Fy	**Max**	**1.3m**	3.30E+06	3.48E+05	-3.22E+05	4.74E+05	1.65E+06	**1.28E+06**	1.90E+05	1.29E+06	1.35
Fy	**Min**	**1.3m**	2.79E+06	2.96E+05	1.67E+06	1.70E+06	1.25E+06	**-1.32E+06**	-5.98E+05	1.45E+06	1.35
Fz	**Max**	**1.3m**	3.18E+06	-1.61E+06	-1.07E+06	1.93E+06	1.71E+06	7.00E+05	**1.52E+06**	1.67E+06	1.35
Fz	**Min**	**1.3m**	2.73E+06	1.63E+06	1.58E+06	2.28E+06	1.79E+06	-8.67E+05	**-1.45E+06**	1.69E+06	1.35
Fyz	**Max**	**1.3m**	2.73E+06	1.63E+06	1.58E+06	2.28E+06	1.79E+06	-8.67E+05	-1.45E+06	**1.69E+06**	1.35
Fyz	**Min**	**1.3f**	3.87E+06	-3.88E+05	-1.40E+04	3.89E+05	1.18E+06	-3.86E+05	8.83E+04	**3.96E+05**	1.35

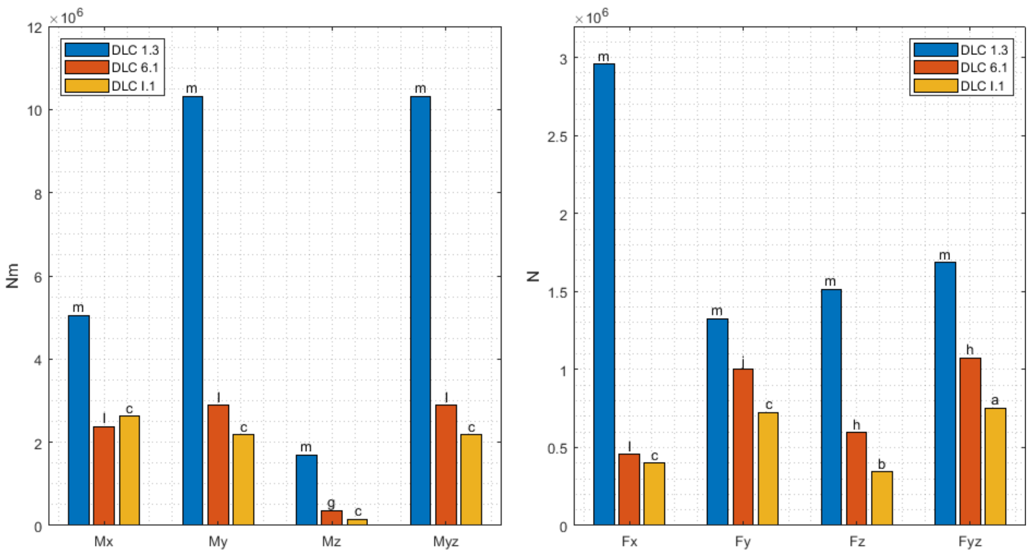

Figure 5.15: Ultimate load histogram - Rotating Hub

Stationary Hub

Table 5.9: Ultimate load table - Stationary hub

		Load case	Mx Nm	My Nm	Mz Nm	Myz Nm	Fx N	Fy N	Fz N	Fyz N	Safety factor
Mx	**Max**	**1.3m**	**5.06E+06**	-3.92E+05	-7.57E+05	8.52E+05	2.40E+06	1.57E+05	-5.54E+05	5.76E+05	1.35
Mx	**Min**	**6.1i**	**-1.81E+06**	1.13E+05	2.71E+05	2.93E+05	-6.13E+04	5.65E+05	-8.33E+05	1.01E+06	1.35
My	**Max**	**1.3m**	3.73E+06	**9.09E+06**	-4.84E+06	1.03E+07	1.69E+06	-3.90E+05	-1.28E+06	1.34E+06	1.35
My	**Min**	**1.3m**	4.18E+06	**-4.77E+06**	3.02E+06	5.65E+06	1.57E+06	2.92E+05	-5.07E+05	5.85E+05	1.35
Mz	**Max**	**1.3m**	4.54E+06	-2.20E+06	**7.13E+06**	7.47E+06	1.66E+06	7.04E+05	-7.90E+05	1.06E+06	1.35
Mz	**Min**	**1.3m**	3.63E+06	4.13E+06	**-9.45E+06**	1.03E+07	1.89E+06	-8.08E+05	-8.09E+05	1.14E+06	1.35
Myz	**Max**	**1.3m**	3.63E+06	4.13E+06	-9.45E+06	**1.03E+07**	1.89E+06	-8.08E+05	-8.09E+05	1.14E+06	1.35
Myz	**Min**	**6.1h**	9.78E+05	3.30E+02	-4.60E+02	**5.70E+02**	1.96E+05	-3.71E+05	-8.31E+05	9.10E+05	1.35
Fx	**Max**	**1.3m**	4.27E+06	-4.29E+05	-1.52E+06	1.58E+06	**2.96E+06**	-1.15E+04	-4.93E+05	4.93E+05	1.35
Fx	**Min**	**1.3m**	3.35E+06	3.27E+05	7.43E+05	8.12E+05	**-8.55E+05**	-1.23E+06	-9.03E+05	9.11E+05	1.35
Fy	**Max**	**1.3m**	4.89E+06	-2.81E+05	2.68E+06	2.70E+06	2.43E+06	**7.44E+05**	-8.74E+05	1.15E+06	1.35
Fy	**Min**	**1.3m**	3.15E+06	1.65E+06	-5.27E+06	5.52E+06	1.56E+06	**-9.00E+05**	-9.32E+05	1.30E+06	1.35
Fz	**Max**	**1.3m**	4.44E+06	-1.97E+06	-2.11E+05	1.99E+06	2.54E+06	3.31E+05	**-2.18E+05**	3.96E+05	1.35
Fz	**Min**	**1.3m**	2.73E+06	1.46E+06	1.74E+06	2.28E+06	1.79E+06	-7.13E+05	**-1.53E+06**	1.69E+06	1.35
Fyz	**Max**	**1.3m**	2.73E+06	1.46E+06	1.74E+06	2.28E+06	1.79E+06	-7.13E+05	-1.53E+06	**1.69E+06**	1.35
Fyz	**Min**	**1.3f**	3.87E+06	1.05E+05	-3.74E+05	3.89E+05	1.18E+06	4.69E+03	-3.96E+05	**3.96E+05**	1.35

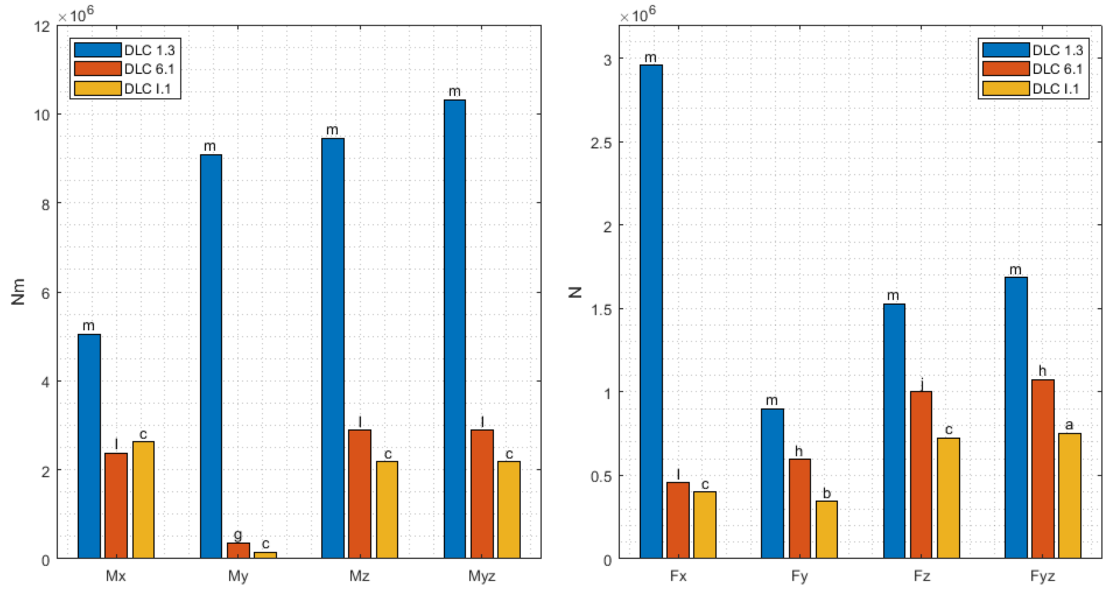

Figure 5.16: Ultimate load histogram - Stationary Hub

Yaw Bearing

Table 5.10: Ultimate load table - Yaw Bearing

		Load case	Mx Nm	My Nm	Mxy Nm	Mz Nm	Fx N	Fy N	Fxy N	Fz N	Safety factor
Mx	**Max**	**6.1h**	**1.65E+07**	-8.17E+06	1.84E+07	5.65E+06	-6.47E+04	-3.07E+06	3.07E+06	-4.13E+06	1.35
Mx	**Min**	**6.1h**	**-1.50E+07**	-9.31E+06	1.76E+07	-5.28E+06	-1.63E+05	2.89E+06	2.89E+06	-4.59E+06	1.35
My	**Max**	**1.3m**	5.16E+06	**7.82E+06**	9.37E+06	-3.69E+06	3.30E+06	-3.30E+05	3.31E+06	-4.63E+06	1.35
My	**Min**	**1.3m**	3.46E+06	**-1.50E+07**	1.54E+07	4.37E+06	-1.35E+06	-6.35E+04	1.35E+06	-4.55E+06	1.35
Mxy	**Max**	**6.1h**	1.65E+07	-8.17E+06	**1.84E+07**	5.65E+06	-6.47E+04	-3.07E+06	3.07E+06	-4.13E+06	1.35
Mxy	**Min**	**1.3f**	1.39E+05	-9.78E+04	**1.70E+05**	-1.28E+06	1.52E+06	7.73E+05	1.71E+06	-4.46E+06	1.35
Mz	**Max**	**1.3m**	1.04E+07	-2.61E+06	1.07E+07	**8.64E+06**	1.39E+06	-1.49E+06	2.04E+06	-4.39E+06	1.35
Mz	**Min**	**6.1g**	-1.27E+07	-9.51E+06	1.58E+07	**-7.06E+06**	-2.48E+05	2.67E+06	2.68E+06	-4.69E+06	1.35
Fx	**Max**	**1.3m**	5.16E+06	7.82E+06	9.37E+06	-3.69E+06	**3.30E+06**	-3.30E+05	3.31E+06	-4.63E+06	1.35
Fx	**Min**	**1.3m**	3.46E+06	-1.50E+07	1.54E+07	4.37E+06	**-1.35E+06**	-6.35E+04	1.35E+06	-4.55E+06	1.35
Fy	**Max**	**6.1h**	-1.50E+07	-9.31E+06	1.76E+07	-5.28E+06	-1.63E+05	**2.89E+06**	2.89E+06	-4.59E+06	1.35
Fy	**Min**	**6.1a**	1.63E+07	-8.23E+06	1.82E+07	5.48E+06	-7.29E+04	**-3.23E+06**	3.23E+06	-4.22E+06	1.35
Fxy	**Max**	**1.3m**	5.16E+06	7.82E+06	9.37E+06	-3.69E+06	3.30E+06	-3.30E+05	**3.31E+06**	-4.63E+06	1.35
Fxy	**Min**	**6.1j**	1.17E+05	-8.56E+06	8.56E+06	9.51E+04	-1.70E+02	-9.10E+02	**9.30E+02**	-4.63E+06	1.35
Fz	**Max**	**I.1b**	8.75E+06	-9.51E+06	1.29E+07	2.62E+06	-8.32E+05	-2.05E+06	2.21E+06	**-2.84E+06**	1
Fz	**Min**	**1.3m**	8.21E+06	-3.83E+06	9.06E+06	5.36E+06	1.94E+06	-1.07E+06	2.22E+06	**-5.46E+06**	1.35

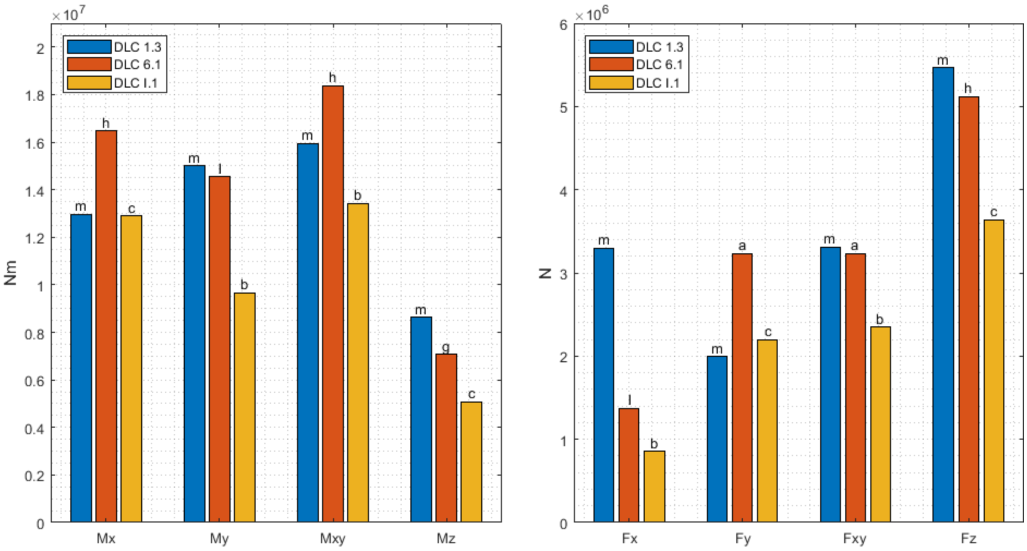

Figure 5.17: Ultimate load histogram - Yaw Bearing

Tower 1 - Member 16 End 1 - Steel

Table 5.11: Ultimate load table - Tower 1

		Load case	Mx Nm	My Nm	Mz Nm	Myz Nm	Fx N	Fy N	Fz N	Fyz N	Safety factor
Mx	**Max**	**1.3m**	**8.64E+06**	-7.14E+07	1.25E+08	1.44E+08	-7.24E+06	-2.22E+06	-1.07E+06	2.47E+06	1.35
Mx	**Min**	**6.1g**	**-7.05E+06**	1.23E+08	-1.66E+08	2.07E+08	-7.90E+06	3.02E+06	2.39E+06	3.85E+06	1.35
My	**Max**	**6.1l**	4.82E+06	**2.41E+08**	-3.30E+07	2.43E+08	-6.29E+06	7.42E+05	4.62E+06	4.68E+06	1.35
My	**Min**	**6.1k**	4.09E+06	**-2.36E+08**	3.92E+06	2.36E+08	-6.39E+06	-2.15E+05	-4.52E+06	4.52E+06	1.35
Mz	**Max**	**6.1a**	5.45E+06	-1.34E+07	**2.62E+08**	2.62E+08	-7.19E+06	-5.03E+06	-1.06E+05	5.03E+06	1.35
Mz	**Min**	**6.1e**	-6.30E+06	5.73E+07	**-2.14E+08**	2.21E+08	-7.86E+06	3.89E+06	1.18E+06	4.07E+06	1.35
Myz	**Max**	**6.1a**	5.45E+06	-1.34E+07	2.62E+08	**2.62E+08**	-7.19E+06	-5.03E+06	-1.06E+05	5.03E+06	1.35
Myz	**Min**	**1.3b**	-1.22E+05	-9.20E+04	-5.69E+04	**1.08E+05**	-7.55E+06	-1.27E+05	4.91E+04	1.36E+05	1.35
Fx	**Max**	**I.1b**	2.29E+06	6.76E+07	1.63E+08	1.76E+08	**-4.90E+06**	-3.11E+06	1.49E+06	3.44E+06	1
Fx	**Min**	**1.3m**	5.34E+06	-4.18E+07	1.46E+08	1.52E+08	**-8.75E+06**	-2.64E+06	-5.43E+05	2.70E+06	1.35
Fy	**Max**	**6.1c**	-5.63E+06	1.25E+07	-2.12E+08	2.12E+08	-7.87E+06	**3.89E+06**	3.72E+05	3.91E+06	1.35
Fy	**Min**	**6.1a**	5.45E+06	-1.34E+07	2.62E+08	2.62E+08	-7.19E+06	**-5.03E+06**	-1.06E+05	5.03E+06	1.35
Fz	**Max**	**6.1l**	5.07E+06	2.39E+08	2.49E+07	2.40E+08	-6.46E+06	-3.36E+05	**4.63E+06**	4.65E+06	1.35
Fz	**Min**	**6.1m**	4.94E+06	-2.36E+08	-9.68E+06	2.36E+08	-6.55E+06	5.93E+04	**-4.56E+06**	4.56E+06	1.35
Fyz	**Max**	**6.1a**	5.45E+06	-1.34E+07	2.62E+08	2.62E+08	-7.19E+06	-5.03E+06	-1.06E+05	**5.03E+06**	1.35
Fyz	**Min**	**1.3a**	-1.28E+04	1.33E+06	-8.45E+06	8.56E+06	-7.61E+06	3.38E+03	-2.20E+03	**4.03E+03**	1.35

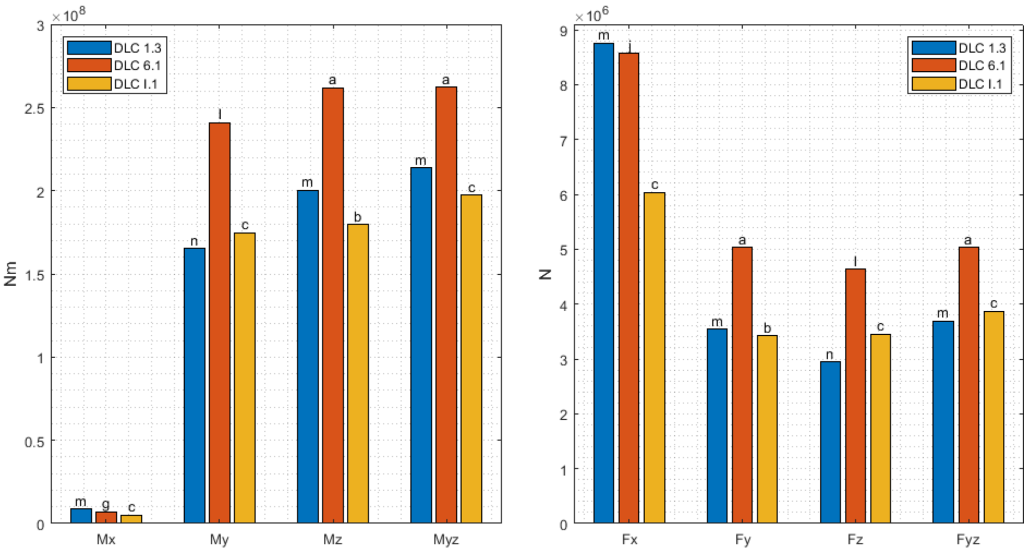

Figure 5.18: Ultimate load histogram - Tower 1

Tower 2 - Member 18 End 2 - Steel

Table 5.12: Ultimate load table - Tower 2 - Steel

		Load case	Mx Nm	My Nm	Mz Nm	Myz Nm	Fx N	Fy N	Fz N	Fyz N	Safety factor
Mx	**Max**	**1.3m**	**8.65E+06**	-8.12E+07	1.45E+08	1.66E+08	-8.27E+06	-2.29E+06	-1.10E+06	2.54E+06	1.35
Mx	**Min**	**6.1g**	**-7.05E+06**	1.46E+08	-1.94E+08	2.43E+08	-9.05E+06	3.35E+06	2.62E+06	4.25E+06	1.35
My	**Max**	**6.1l**	4.82E+06	**2.84E+08**	-4.00E+07	2.87E+08	-7.23E+06	8.05E+05	5.07E+06	5.14E+06	1.35
My	**Min**	**6.1k**	4.09E+06	**-2.79E+08**	5.96E+06	2.79E+08	-7.34E+06	-2.42E+05	-4.99E+06	4.99E+06	1.35
Mz	**Max**	**6.1a**	5.45E+06	-1.44E+07	**3.09E+08**	3.10E+08	-8.25E+06	-5.54E+06	-1.27E+05	5.54E+06	1.35
Mz	**Min**	**6.1e**	-6.29E+06	6.84E+07	**-2.50E+08**	2.59E+08	-9.01E+06	4.27E+06	1.30E+06	4.46E+06	1.35
Myz	**Max**	**6.1a**	5.45E+06	-1.44E+07	3.09E+08	**3.10E+08**	-8.25E+06	-5.54E+06	-1.27E+05	5.54E+06	1.35
Myz	**Min**	**1.3a**	9.63E+04	5.33E+04	4.84E+04	**7.20E+04**	-8.69E+06	-1.13E+05	-3.34E+04	1.17E+05	1.35
Fx	**Max**	**I.1b**	2.30E+06	8.17E+07	1.92E+08	2.08E+08	**-5.64E+06**	-3.41E+06	1.66E+06	3.79E+06	1
Fx	**Min**	**1.3m**	5.35E+06	-4.66E+07	1.70E+08	1.76E+08	**-9.95E+06**	-2.70E+06	-5.30E+05	2.75E+06	1.35
Fy	**Max**	**6.1c**	-5.63E+06	1.60E+07	-2.49E+08	2.49E+08	-9.02E+06	**4.28E+06**	4.13E+05	4.30E+06	1.35
Fy	**Min**	**6.1a**	5.45E+06	-1.44E+07	3.09E+08	3.10E+08	-8.25E+06	**-5.54E+06**	-1.27E+05	5.54E+06	1.35
Fz	**Max**	**6.1l**	5.08E+06	2.82E+08	2.81E+07	2.84E+08	-7.44E+06	-3.83E+05	**5.08E+06**	5.10E+06	1.35
Fz	**Min**	**6.1m**	5.11E+06	-2.77E+08	-1.29E+07	2.77E+08	-7.49E+06	8.10E+04	**-5.01E+06**	5.01E+06	1.35
Fyz	**Max**	**6.1a**	5.45E+06	-1.44E+07	3.09E+08	3.10E+08	-8.25E+06	-5.54E+06	-1.27E+05	**5.54E+06**	1.35
Fyz	**Min**	**1.3b**	-2.43E+04	-2.64E+05	-5.83E+06	5.83E+06	-8.70E+06	2.81E+03	-2.03E+03	**3.46E+03**	1.35

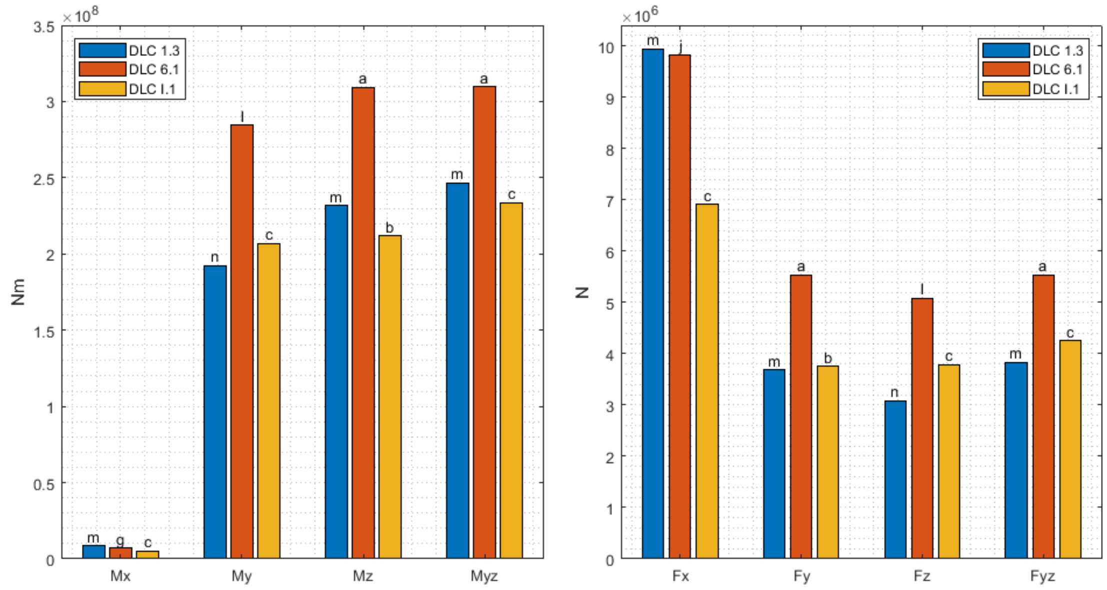

Figure 5.19: Ultimate load histogram - Tower 2 - Steel

Tower 2 - Member 19 End 1 - Concrete

Table 5.13: Ultimate load table - Tower 2 - Concrete

		Load case	Mx Nm	My Nm	Mz Nm	Myz Nm	Fx N	Fy N	Fz N	Fyz N	Safety factor
Mx	**Max**	**1.3m**	**8.65E+06**	-8.12E+07	1.45E+08	1.66E+08	-8.37E+06	-2.29E+06	-1.10E+06	2.54E+06	1.35
Mx	**Min**	**6.1g**	**-7.05E+06**	1.46E+08	-1.94E+08	2.43E+08	-9.16E+06	3.38E+06	2.64E+06	4.29E+06	1.35
My	**Max**	**6.1l**	4.82E+06	**2.84E+08**	-4.00E+07	2.87E+08	-7.31E+06	8.10E+05	5.11E+06	5.17E+06	1.35
My	**Min**	**6.1k**	4.09E+06	**-2.79E+08**	5.96E+06	2.79E+08	-7.43E+06	-2.44E+05	-5.03E+06	5.03E+06	1.35
Mz	**Max**	**6.1a**	5.45E+06	-1.44E+07	**3.09E+08**	3.10E+08	-8.35E+06	-5.58E+06	-1.28E+05	5.58E+06	1.35
Mz	**Min**	**6.1e**	-6.29E+06	6.84E+07	**-2.50E+08**	2.59E+08	-9.11E+06	4.31E+06	1.31E+06	4.50E+06	1.35
Myz	**Max**	**6.1a**	5.45E+06	-1.44E+07	3.09E+08	**3.10E+08**	-8.35E+06	-5.58E+06	-1.28E+05	5.58E+06	1.35
Myz	**Min**	**1.3a**	9.63E+04	5.33E+04	4.84E+04	**7.20E+04**	-8.79E+06	-1.13E+05	-3.37E+04	1.18E+05	1.35
Fx	**Max**	**I.1b**	2.30E+06	8.17E+07	1.92E+08	2.08E+08	**-5.70E+06**	-3.43E+06	1.67E+06	3.81E+06	1
Fx	**Min**	**1.3m**	5.35E+06	-4.66E+07	1.70E+08	1.76E+08	**-1.01E+07**	-2.70E+06	-5.28E+05	2.76E+06	1.35
Fy	**Max**	**6.1c**	-5.63E+06	1.60E+07	-2.49E+08	2.49E+08	-9.12E+06	**4.32E+06**	4.17E+05	4.34E+06	1.35
Fy	**Min**	**6.1a**	5.45E+06	-1.44E+07	3.09E+08	3.10E+08	-8.35E+06	**-5.58E+06**	-1.28E+05	5.58E+06	1.35
Fz	**Max**	**6.1l**	5.08E+06	2.82E+08	2.81E+07	2.84E+08	-7.52E+06	-3.86E+05	**5.12E+06**	5.13E+06	1.35
Fz	**Min**	**6.1m**	5.11E+06	-2.77E+08	-1.29E+07	2.77E+08	-7.58E+06	8.04E+04	**-5.05E+06**	5.05E+06	1.35
Fyz	**Max**	**6.1a**	5.45E+06	-1.44E+07	3.09E+08	3.10E+08	-8.35E+06	-5.58E+06	-1.28E+05	**5.58E+06**	1.35
Fyz	**Min**	**1.3b**	-2.43E+04	-2.64E+05	-5.83E+06	5.83E+06	-8.79E+06	4.05E+03	-1.56E+03	**4.34E+03**	1.35

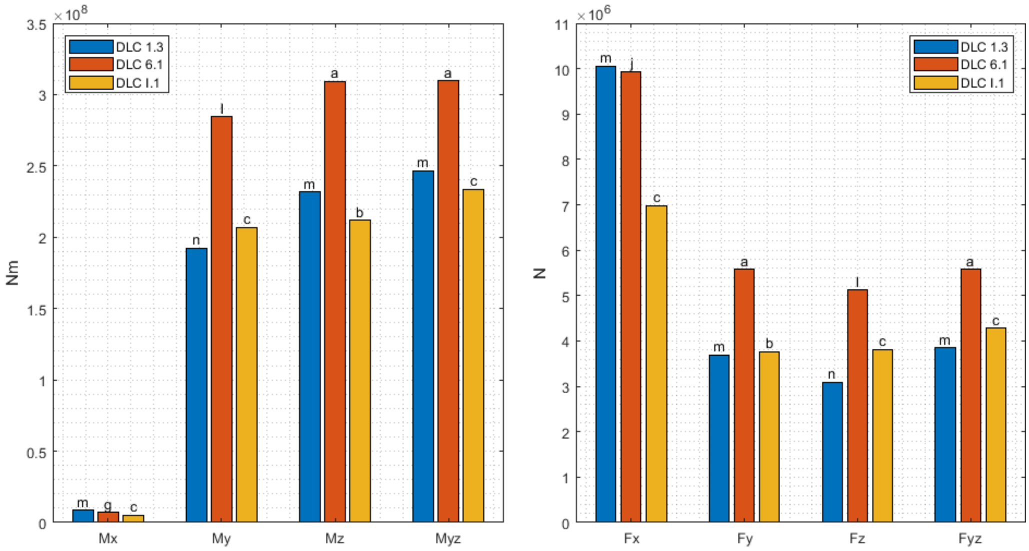

Figure 5.20: Ultimate load histogram - Tower 2 - Concrete

Tower 3 - Member 21 End 2 - Concrete

Table 5.14: Ultimate load table - Tower 3

		Load case	Mx Nm	My Nm	Mz Nm	Myz Nm	Fx N	Fy N	Fz N	Fyz N	Safety factor
Mx	**Max**	**1.3m**	**8.86E+06**	-1.13E+08	2.15E+08	2.43E+08	-2.04E+07	-3.05E+06	-1.46E+06	3.38E+06	1.35
Mx	**Min**	**6.1g**	**-6.93E+06**	2.49E+08	-3.30E+08	4.14E+08	-2.35E+07	4.83E+06	3.56E+06	6.00E+06	1.35
My	**Max**	**6.1l**	4.81E+06	**4.83E+08**	-6.98E+07	4.88E+08	-1.85E+07	1.24E+06	8.22E+06	8.31E+06	1.35
My	**Min**	**6.1k**	4.27E+06	**-4.80E+08**	1.62E+07	4.80E+08	-1.88E+07	-3.04E+05	-7.99E+06	8.00E+06	1.35
Mz	**Max**	**6.1a**	5.45E+06	-2.06E+07	**5.30E+08**	5.30E+08	-2.09E+07	-8.99E+06	-2.75E+05	9.00E+06	1.35
Mz	**Min**	**6.1c**	-5.56E+06	3.34E+07	**-4.22E+08**	4.23E+08	-2.31E+07	6.26E+06	5.55E+05	6.28E+06	1.35
Myz	**Max**	**6.1a**	5.45E+06	-2.06E+07	5.30E+08	**5.30E+08**	-2.09E+07	-8.99E+06	-2.75E+05	9.00E+06	1.35
Myz	**Min**	**6.1h**	-9.52E+05	-1.64E+04	2.90E+05	**2.90E+05**	-2.31E+07	5.38E+04	2.27E+05	2.33E+05	1.35
Fx	**Max**	**I.1a**	2.00E+06	1.90E+08	1.67E+08	2.53E+08	**-1.45E+07**	-2.94E+06	3.50E+06	4.57E+06	1
Fx	**Min**	**6.1a**	-1.82E+06	-1.66E+07	-1.38E+08	1.39E+08	**-2.54E+07**	2.07E+06	-9.20E+04	2.07E+06	1.35
Fy	**Max**	**6.1a**	-4.97E+06	-3.27E+07	-4.00E+08	4.02E+08	-2.25E+07	**7.70E+06**	-3.38E+05	7.71E+06	1.35
Fy	**Min**	**6.1a**	5.49E+06	-2.53E+07	5.15E+08	5.15E+08	-2.10E+07	**-9.19E+06**	-2.80E+05	9.19E+06	1.35
Fz	**Max**	**6.1j**	4.92E+06	4.55E+08	1.71E+08	4.86E+08	-2.06E+07	-3.43E+06	**8.98E+06**	9.61E+06	1.35
Fz	**Min**	**6.1k**	5.34E+06	-4.47E+08	1.57E+08	4.74E+08	-2.06E+07	-3.32E+06	**-8.92E+06**	9.51E+06	1.35
Fyz	**Max**	**6.1h**	4.75E+06	4.22E+08	2.69E+08	5.00E+08	-2.02E+07	-5.30E+06	8.51E+06	**1.00E+07**	1.35
Fyz	**Min**	**1.3b**	7.30E+05	-1.07E+05	-3.77E+05	3.92E+05	-2.20E+07	-2.37E+03	9.90E+02	**2.57E+03**	1.35

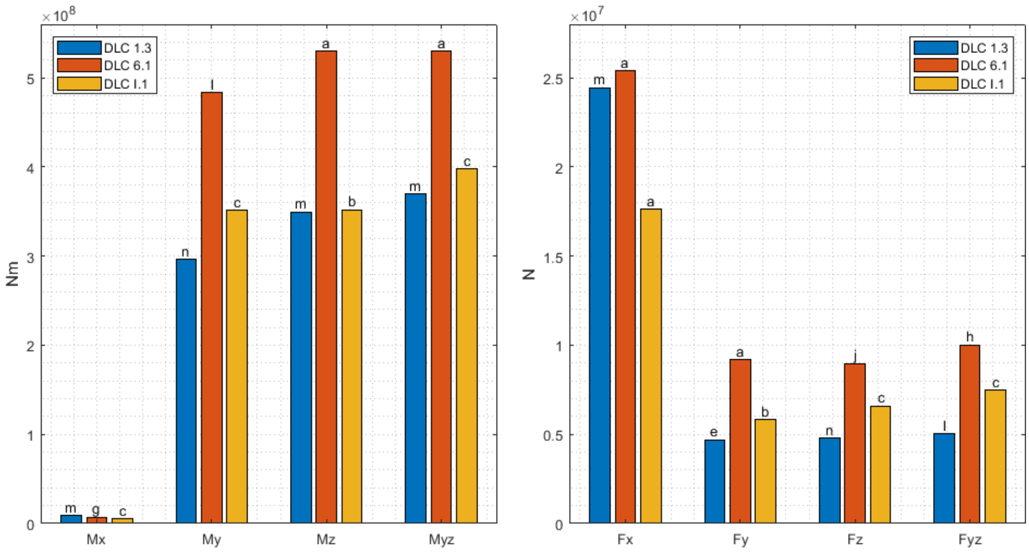

Figure 5.21: Ultimate load histogram - Tower 3

Tower 4 - Member 25 End 2 - Concrete

Table 5.15: Ultimate load table - Tower 4

		Load case	Mx Nm	My Nm	Mz Nm	Myz Nm	Fx N	Fy N	Fz N	Fyz N	Safety factor
Mx	Max	1.3m	**9.04E+06**	-1.42E+08	2.60E+08	2.96E+08	-2.98E+07	-3.58E+06	-2.69E+06	4.48E+06	1.35
Mx	Min	6.1g	**-6.83E+06**	2.76E+08	-3.84E+08	4.73E+08	-3.80E+07	2.09E+06	1.35E+06	2.49E+06	1.35
My	Max	6.1l	5.41E+06	**5.79E+08**	5.30E+07	5.81E+08	-2.89E+07	-3.99E+05	5.87E+06	5.88E+06	1.35
My	Min	6.1m	4.89E+06	**-5.67E+08**	-1.42E+07	5.67E+08	-2.93E+07	2.29E+04	-5.24E+06	5.24E+06	1.35
Mz	Max	6.1a	5.48E+06	-2.38E+07	**6.19E+08**	6.20E+08	-3.18E+07	-4.90E+06	-1.17E+05	4.91E+06	1.35
Mz	Min	6.1a	-4.97E+06	-3.42E+07	**-4.95E+08**	4.96E+08	-3.46E+07	6.22E+06	-1.41E+05	6.22E+06	1.35
Myz	Max	6.1a	5.48E+06	-2.38E+07	6.19E+08	**6.20E+08**	-3.18E+07	-4.90E+06	-1.17E+05	4.91E+06	1.35
Myz	Min	1.3a	-4.71E+05	-1.25E+05	-2.48E+05	**2.78E+05**	-3.37E+07	-3.65E+05	1.68E+04	3.65E+05	1.35
Fx	Max	I.1a	3.26E+06	2.96E+08	2.47E+08	3.85E+08	**-2.11E+07**	-1.45E+06	1.86E+06	2.36E+06	1
Fx	Min	6.1d	-2.64E+06	-5.47E+07	1.11E+08	1.24E+08	**-4.27E+07**	-5.07E+06	2.47E+06	5.65E+06	1.35
Fy	Max	6.1a	-3.81E+06	-3.71E+07	-4.54E+08	4.56E+08	-3.75E+07	**6.63E+06**	-1.92E+05	6.63E+06	1.35
Fy	Min	6.1a	2.56E+06	-8.30E+06	3.90E+08	3.90E+08	-3.14E+07	**-9.20E+06**	2.11E+04	9.20E+06	1.35
Fz	Max	6.1h	4.19E+06	4.39E+08	2.37E+08	4.99E+08	-3.05E+07	-3.92E+06	**7.67E+06**	8.61E+06	1.35
Fz	Min	6.1i	3.79E+06	-4.49E+08	2.12E+08	4.97E+08	-3.05E+07	-3.82E+06	**-7.67E+06**	8.57E+06	1.35
Fyz	Max	6.1a	2.56E+06	-8.30E+06	3.90E+08	3.90E+08	-3.14E+07	-9.20E+06	2.11E+04	**9.20E+06**	1.35
Fyz	Min	6.1h	-1.08E+06	-4.94E+07	-1.37E+07	5.13E+07	-3.26E+07	-1.20E+03	7.40E+02	**1.41E+03**	1.35

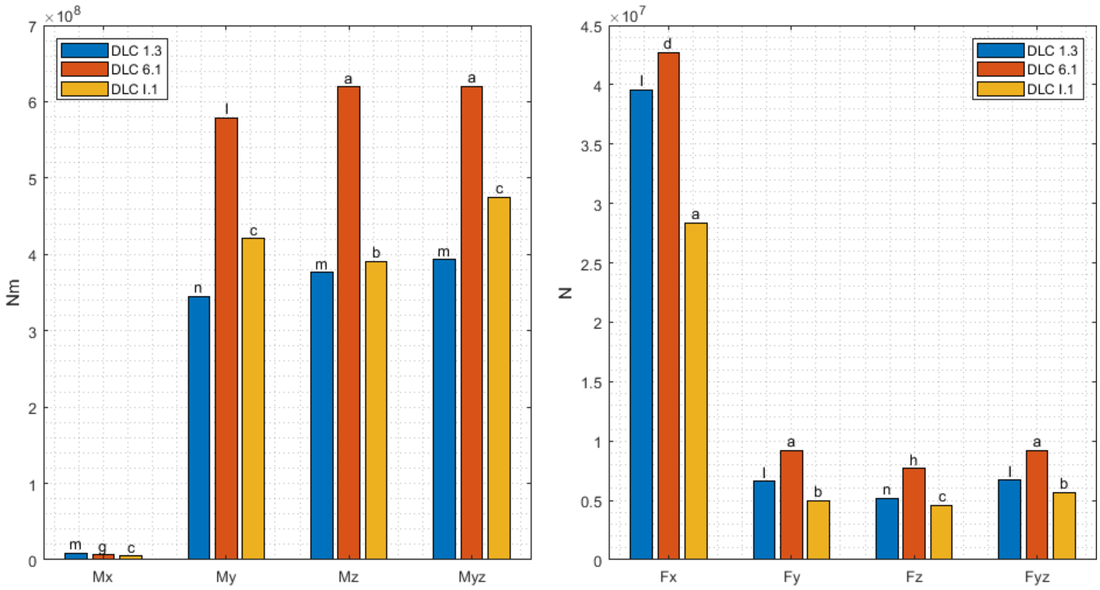

Figure 5.22: Ultimate load histogram - Tower 4

Platform Arm - Member 74 End 2 - Concrete

Table 5.16: Ultimate load table - Platform arm

		Load case	Mx Nm	My Nm	Mz Nm	Myz Nm	Fx N	Fy N	Fz N	Fyz N	Safety factor
Mx	Max	6.1e	**2.75E+07**	-1.10E+07	2.62E+06	1.13E+07	-3.78E+04	6.32E+05	-7.60E+05	9.89E+05	1.35
Mx	Min	6.1j	**-7.24E+07**	1.75E+08	7.63E+06	1.75E+08	-1.38E+07	-5.48E+06	1.88E+06	5.80E+06	1.35
My	Max	6.1l	-6.36E+07	**2.17E+08**	2.42E+06	2.17E+08	-1.65E+07	-5.10E+06	4.66E+06	6.90E+06	1.35
My	Min	6.1l	1.30E+07	**-5.65E+07**	1.89E+06	5.65E+07	6.90E+06	2.79E+06	3.58E+06	4.54E+06	1.35
Mz	Max	6.1h	-6.48E+07	1.27E+08	**1.05E+07**	1.27E+08	-1.11E+07	-5.23E+06	1.48E+06	5.43E+06	1.35
Mz	Min	6.1a	8.42E+06	6.52E+07	**-1.18E+07**	6.62E+07	-2.49E+06	2.85E+06	1.35E+07	1.38E+07	1.35
Myz	Max	6.1l	-6.36E+07	2.17E+08	2.42E+06	**2.17E+08**	-1.65E+07	-5.10E+06	4.66E+06	6.90E+06	1.35
Myz	Min	6.1j	-1.88E+06	-1.65E+04	1.55E+04	**2.26E+04**	8.52E+05	1.15E+06	1.05E+06	1.56E+06	1.35
Fx	Max	6.1l	1.32E+07	-4.23E+07	1.36E+05	4.23E+07	**7.67E+06**	3.69E+06	2.59E+06	4.51E+06	1.35
Fx	Min	6.1l	-6.20E+07	2.13E+08	2.42E+06	2.13E+08	**-1.66E+07**	-5.16E+06	4.99E+06	7.18E+06	1.35
Fy	Max	6.1h	7.46E+06	-1.33E+07	-7.26E+06	1.51E+07	5.15E+06	**4.42E+06**	3.43E+06	5.59E+06	1.35
Fy	Min	6.1j	-6.98E+07	1.75E+08	7.72E+06	1.75E+08	-1.44E+07	**-5.78E+06**	2.36E+06	6.25E+06	1.35
Fz	Max	6.1g	-1.00E+07	5.56E+07	-2.12E+06	5.56E+07	2.48E+06	2.56E+06	**1.65E+07**	1.67E+07	1.35
Fz	Min	6.1l	-7.39E+06	2.09E+07	3.23E+06	2.11E+07	-3.36E+05	-2.54E+04	**-8.28E+06**	8.28E+06	1.35
Fyz	Max	6.1g	-1.00E+07	5.56E+07	-2.12E+06	5.56E+07	2.48E+06	2.56E+06	1.65E+07	**1.67E+07**	1.35
Fyz	Min	6.1e	1.66E+07	-1.59E+07	5.02E+06	1.67E+07	8.67E+05	1.91E+04	-3.69E+03	**1.95E+04**	1.35

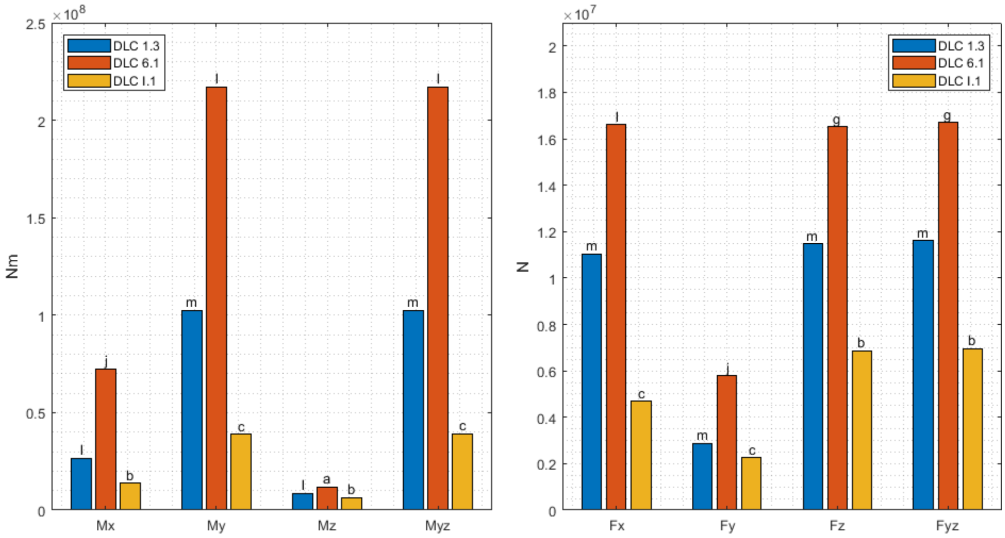

Figure 5.23: Ultimate load histogram - Platform arm

Mooring Lines and Anchors

Table 5.17: Ultimate load table - Mooring Lines Tension and Gravity Anchors Horizontal Loads

		Load case	ML1 N	ML2 N	ML3 N	ML4 N	ML5 N	ML6 N	A13 N	A24 N	A56 N	Safety factor
ML1	**Max**	**6.1m**	**2.73E+06**	4.71E+05	2.12E+06	4.50E+05	9.60E+05	1.20E+06	4.08E+06	2.27E+05	1.41E+06	1.35
ML1	**Min**	**I.1c**	**3.49E+05**	7.17E+05	4.10E+05	6.97E+05	4.73E+05	5.39E+05	2.56E+05	9.38E+05	5.12E+05	1
ML2	**Max**	**6.1l**	4.74E+05	**2.75E+06**	4.49E+05	2.14E+06	1.18E+06	9.44E+05	2.29E+05	4.11E+06	1.37E+06	1.35
ML2	**Min**	**6.1m**	1.13E+06	**4.28E+05**	8.96E+05	4.90E+05	9.21E+05	8.18E+05	1.40E+06	2.31E+05	1.09E+06	1.35
ML3	**Max**	**6.1e**	2.21E+06	1.11E+06	**2.89E+06**	9.47E+05	4.51E+05	5.00E+05	4.33E+06	1.32E+06	2.54E+05	1.35
ML3	**Min**	**I.1c**	3.91E+05	1.25E+06	**3.05E+05**	1.12E+06	5.06E+05	4.07E+05	1.94E+05	1.83E+06	4.19E+05	1
ML4	**Max**	**6.1d**	1.13E+06	2.21E+06	9.65E+05	**2.88E+06**	4.98E+05	4.51E+05	1.35E+06	4.32E+06	2.52E+05	1.35
ML4	**Min**	**6.1m**	1.43E+06	4.78E+05	1.44E+06	**4.03E+05**	9.93E+05	1.07E+06	2.13E+06	1.92E+05	1.36E+06	1.35
ML5	**Max**	**6.1l**	5.33E+05	1.00E+06	6.46E+05	8.89E+05	**1.28E+06**	8.57E+05	4.79E+05	1.15E+06	1.38E+06	1.35
ML5	**Min**	**I.1b**	8.42E+05	1.03E+06	8.60E+05	1.16E+06	**2.65E+05**	2.41E+05	1.22E+06	1.68E+06	5.23E+03	1
ML6	**Max**	**6.1m**	9.70E+05	5.45E+05	8.53E+05	6.64E+05	8.57E+05	**1.26E+06**	1.09E+06	5.08E+05	1.37E+06	1.35
ML6	**Min**	**I.1b**	8.38E+05	1.01E+06	8.52E+05	1.14E+06	2.66E+05	**2.41E+05**	1.21E+06	1.66E+06	4.84E+03	1
A13	**Max**	**6.1e**	2.21E+06	1.11E+06	2.89E+06	9.47E+05	4.51E+05	5.00E+05	**4.33E+06**	1.32E+06	2.54E+05	1.35
A13	**Min**	**6.1l**	4.70E+05	1.46E+06	4.00E+05	1.42E+06	1.11E+06	9.89E+05	**1.82E+05**	2.13E+06	1.39E+06	1.35
A24	**Max**	**6.1d**	1.13E+06	2.21E+06	9.65E+05	2.88E+06	4.98E+05	4.51E+05	1.35E+06	**4.32E+06**	2.52E+05	1.35
A24	**Min**	**6.1m**	1.43E+06	4.78E+05	1.44E+06	4.03E+05	9.93E+05	1.07E+06	2.13E+06	**1.92E+05**	1.36E+06	1.35
A56	**Max**	**1.3n**	4.71E+05	9.29E+05	4.59E+05	9.11E+05	-2.97E+04	1.08E+06	2.43E+05	1.16E+06	**1.62E+06**	1.35
A56	**Min**	**I.1b**	8.40E+05	1.02E+06	8.56E+05	1.15E+06	2.65E+05	2.41E+05	1.21E+06	1.67E+06	**5.03E+03**	1

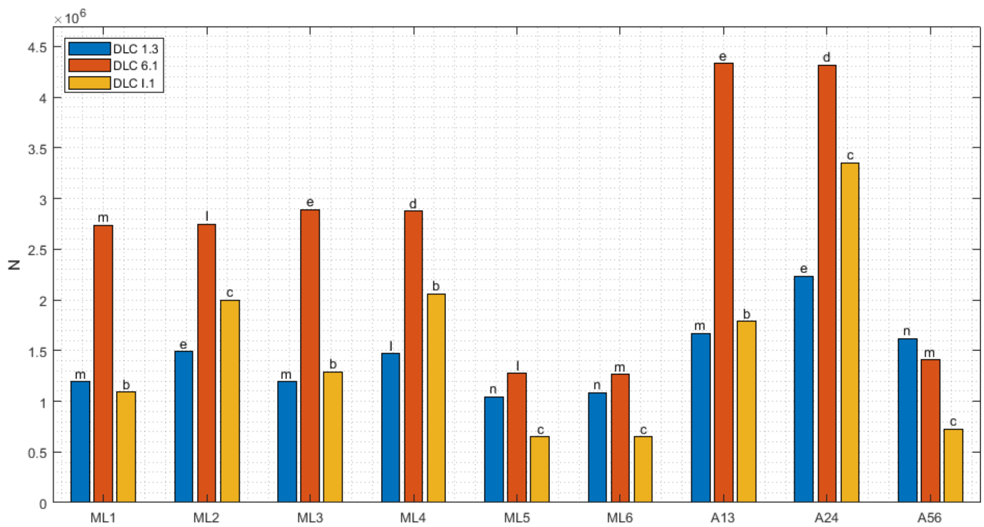

Figure 5.24: Ultimate load histogram - Mooring Lines Tension and Gravity Anchors Horizontal Loads

5.3.2. Ultimate Load Analysis

Based on the data presented in Subsection 5.3.1, it was possible to calculate the ultimate stress experienced by each turbine component during simulation. The process of calculating these ultimate stresses is described in this section, on a component-by-component basis. The maximum bending stress (σ_{max}) for each component is calculated using Equation 5.7 [23].

$$\sigma_{max} = \frac{M_{max} \cdot y}{I_{circ./rect.}} \tag{5.7}$$

where M_{max} is the maximum experienced bending moment, y is the distance from the neutral axis, and $I_{circ./rect.}$ is the moment of inertia of the circular or rectangular, hollow cross-section of the component. These are calculated using Equation 5.8 and Equation 5.9, respectively, below [23].

$$I_{circ} = \frac{\pi \cdot (d_{outer}^4 - d_{inner}^4)}{64} = \frac{\pi \cdot (d_{outer}^4 - (d_{outer} - 2t)^4)}{64} \tag{5.8}$$

$$I_{rect,yy} = \frac{h_{outer} w_{outer}^3}{12} - \frac{(h_{outer} - 2t)(w_{outer} - 2t)^3}{12} \tag{5.9}$$

where, for Equation 5.8, d_{outer} is the outer cross-sectional diameter and t is the thickness of the annulus for circular components, including the hub, yaw bearing, and turbine tower. For Equation 5.9, h_{outer} is the outer height, w_{outer} is the outer width, and t is the thickness of the hollow rectangular turbine components, including the blade roots and platform arms. A comparison was then made between the respective maximum allowable stresses, based on Seawind 6 prospective manufacturer's specifications, to determine if the turbine is likely to survive in operation. This was the first time that the current Seawind 6 model, with improved platform dynamics and mooring line configuration, in combination with the new Sowento controller has undergone a loading analysis. An overview of the key findings from this ultimate loads analysis is provided in Table 5.18.

Table 5.18: Ultimate loads analysis overview

Component	DLC	Max. Load	Max. Stress	Capacity
Blade 1 Root	1.3m	52.2 MNm	9.51 MPa	390 MPa
Blade 2 Root	1.3m	49.3 MNm	8.98 MPa	390 MPa
Rotating Hub	1.3m	10.3 MNm	1.70 MPa	450 MPa
Stationary Hub	1.3m	10.3 MNm	1.70 MPa	450 MPa
Yaw Bearing	6.1h	18.4 MNm	7.54 MPa	450 MPa
Tower 1 - Steel	6.1a	262 MNm	44.86 MPa	450 MPa
Tower 2 - Steel	6.1a	310 MNm	21.45 MPa	200 MPa
Tower 2 - Concrete	6.1a	310 MNm	26.05 MPa	200 MPa
Tower 3 - Concrete	6.1a	530 MNm	24.64 MPa	200 MPa
Tower 4 - Concrete	6.1a	620 MNm	28.82 MPa	200 MPa
Platform Arm	6.1l	217 MNm	9.72 MPa	200 MPa
Mooring Lines	6.1d	2.88 MN	N/A	18.16 MN
Gravity Anchor	6.1d	4.32 MN	N/A	22.5 MN

Blade 1 and 2 Roots

The maximum and minimum values for the four bending moments and forces experienced at the root of Blade 1 are tabulated in Table 5.6. These are selected from all the simulated ultimate DLC runs, with the corresponding safety factors already applied. The maximum absolute value for each load component for the three ultimate DLCs is then displayed as a histogram in Figure 5.13. Selecting the largest moment value from the histogram and correlating it to the table, the exact absolute maximum load was obtained. This same procedure was carried out for the root of Blade 2, with Table 5.7 and Figure 5.14

being considered. The maximum root loads for Blade 1 were a resultant Mxy bending moment of 52.2 MNm experienced during DLC 1.3m, and an axial Fz force of 47.9 MN, also experienced during DLC 1.3m. For Blade root 2, the maximum bending moment was a flatwise My of 49.3 MNm during DLC 1.3m, and the maximum axial force was an Fz of 47.9 MN, again during DLC 1.3m. Examining Figure 5.13 and Figure 5.14, all the moments and forces were largest for DLC 1.3. This investigation focused on the turbine's design driving loads and so, for the blades, just the bending moments were considered.

The Seawind 6's blade root has a rectangular shape with two curved sides, as per image Figure 3.10, with the glass fiber shell skin (% GLASS 3AX 0/-45/45 1250) making up 70% of the root thickness and the glass fibre root reinforcement (% GLASS UD 1200) making up the remainder [9]. These have minimum ultimate bending stresses of 300 MPa and 600 MPa, respectively, so for a conservative approach, the maximum stress allowable ($\sigma_{ultimate}$) in the material is approximately 390 MPa (0.7 · 300 MPa + 0.3 · 600 MPa) before failure may occur [9]. The maximum bending stresses (σ_{max}) in both the blade roots were then calculated using Equation 5.7, where M_{max} is 52.2 MNm for Blade 1 and 49.3 MNm for Blade 2, y is 2.281 m, and $I_{rect,yy}$ was found to equal 12.52 m^4 using Equation 5.9. Here, h_{outer} was 4.562 m, w_{outer} was 3.74 m, and t was 0.43 m. This results in a maximum bending stress ($\sigma_{max,1}$) of 9.51 MPa for Blade 1 and 8.98 MPa for Blade 2 ($\sigma_{max,2}$), both of which are substantially less than the maximum allowable stress ($\sigma_{ultimate}$) of 390 MPa. Therefore, the blade roots are expected to survive and have been adequately engineered for safety. These final values are included in Table 5.18 for the benefit of the reader.

Rotating and Stationary Hub

Looking at Figure 5.15 and Figure 5.16, both variations of the hub experienced the same maximum loads. The largest bending moment and axial force experienced by these components were an Myz of 10.3 MNm and an Fx of 2.96 MN, respectively, both during DLC 1.3m. All the moments and forces were again shown to be largest for DLC 1.3, due to the increased turbulence and power production rotor orientation.

As shown in Figure 5.10, the origin for the hub loads is at the hub centre where the blade and shaft axes intersect. The hub is constructed from a rectangular S355J2+N steel frame, with an ultimate bending stress between 450 and 600 MPa, and is displayed in Figure 3.14 [10]. Again, for a conservative approach, the lower value was used. Using Equation 5.7 and Equation 5.9, with an M_{max} of 10.3 MNm, y of 1.75 m, h_{outer} of 4.562 m, w_{outer} of 3.5 m, and t of 0.43 m, the maximum bending stress experienced was calculated to be 1.70 MPa for both variations of the hub. This means the hub is expected to survive any extreme loading and it passes the ultimate load analysis.

Yaw Bearing

A maximum yaw bearing bending moment of 18.4 MNm (Mxy) was experienced during DLC 6.1h, as per Figure 5.17. A maximum axial force of magnitude 5.46 MN (Fz) was shown to occur during DLC 1.3m. The spread between the three DLCs for the various loads is not too large. The yaw bearing is constantly having to change angle to remain -90° out of the wind, as well as withstand aerodynamic loading. From previous in-house analyses, the maximum yaw drive torque is generally shown to be about 1.50 MNm, with peaks of 2.00 MNm. This is against a yaw capability of 4.57 MNm at 350 bar and 5.00 MNm at 400 bar. In case of emergency shutdown, with high yaw rate, the yaw torque can reach 3.20 MNm [8]. Here, the effect of operational loading is also included, so the bending moments are greater than just the pure yaw torque scenario. Using this bending moment, a maximum stress (σ_{max}) of 7.54 MPa was calculated for the yaw bearing using Equation 5.7 and Equation 5.8 for a circular cross-section, with an M_{max} of 18.4 MNm, y of 2.5 m, d_{outer} of 5 m and t of 0.135 m, as per Figure 3.17 in Subsection 3.2.2. The yaw bearing is again manufactured from S355J2+N steel, with a minimum ultimate stress of 450 MPa. Based on these figures, the yaw bearing is expected to withstand any significant experienced loading.

Steel Tower and Concrete Shaft

Various sections of interest along the turbine's support structure, displayed in Figure 5.25, have also been investigated. The focus here is confined only to the tower and central shaft. The maximum bending stresses for each section are again calculated using Equation 5.7 and Equation 5.8. Section

1 (Member 18 End 2) is at the base of the uniform-diameter steel tower segment, 60 m from where the nacelle is situated at Section 0. It is of hollow, circular construction with a d_{outer} of 5 m and t of 0.75 m. The maximum bending moment experienced at Section 1 was 262 MNm (Myz) during DLC 6.1a, as per Figure 5.18. This results in a maximum bending stress of 44.86 MPa. The particular type of steel used (S355J2+N) has an ultimate bending stress of 450 MPa, meaning the tower survives [8]. Section 2 is at the interface of the steel tower and concrete shaft, 69 m from the tower top. The steel section experienced a maximum bending moment of 310 MNm (Myz) during DLC 6.1a, as per Figure 5.19. With a d_{outer} of 8 m and t of 0.65 m, the maximum bending stress is calculated to be 21.45 MPa. Compared to the ultimate bending stress of 450 MPa, this tower section is shown to survive. The concrete section results, shown in Figure 5.20, also displays the same maximum bending moment of 310 MNm (Myz). With a d_{outer} of 9 m and t of 0.40 m, the maximum bending stress is calculated to be 26.05 MPa. The shaft is constructed from reinforced and post-tensioned concrete with an ultimate bending stress of 200 MPa, meaning it will survive [15]. Section 3 is found 95.5 m below the tower top, where the concrete shaft diameter becomes uniform, just below sea level. At this point a maximum bending moment of 530 MNm (Myz) was experienced during DLC 6.1a, as per Figure 5.21. With a d_{outer} of 12 m and t of 0.40 m, this resulted in a maximum bending stress of 24.64 MPa. Again, this was less than the maximum allowable stress of 200 MPa, so the tower survives. The final location investigated was Section 4, composed of concrete with a 12 m d_{outer} and t of 0.40 m, located 108.25 m below the tower top. The maximum bending moment of 620 MNm (Myz), observed in Figure 5.22, resulted in a maximum bending stress of 28.82 MPa which meant the shaft survived. The magnitudes of moments and forces increases with distance down the tower towards the platform base, with the section diameters and widths altered to maintain the maximum bending stress below 50 MPa.

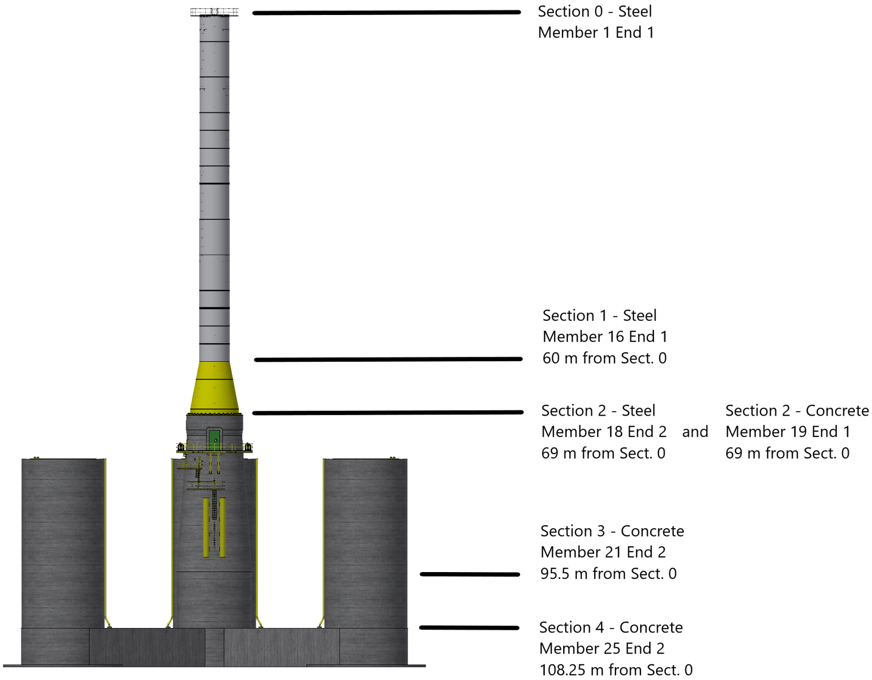

Figure 5.25: Steel tower and concrete shaft sections

Platform Arm

From previous in-house testing carried out by Seawind with Bladed on the concrete platform structure, it was deduced that the most stressed sections were the two arms at the angled base of the arrow head platform and connected to the central shaft. These arms are rectangular in cross-section and are again constructed from reinforced and post-tensioned concrete with an ultimate bending stress of 200 MPa. A suitable section of the platform (Member 74 End 2) was selected for this analysis. As per Figure 5.23, the maximum bending moment experienced was 217 MNm (My) during DLC 6.1l. The bending stress was then calculated to be 9.72 MPa using Equation 5.7 and Equation 5.9, where h_{outer} was 6.5 m, w_{outer} was 8 m, and t was 0.35 m. This is less than the assumed ultimate bending stress, meaning the arm section survives.

Mooring Lines and Gravity Anchors

Table 5.17 is a slightly altered compared to previous tables. Here, maximum and minimum loads of the six mooring line and three gravity anchors are tabulated. Both sets of maximum absolute loads are also joined in the same histogram, in Figure 5.24, as they all have the same units (N) and are similar in magnitude. The maximum mooring line tension of 2.88 MN (ML4) and resultant gravity anchor horizontal force of 4.32 MN (A24), from Figure 5.24, was compared to the chain MBL (Minimum Breaking Load) of 18.16 MN and gravity anchor horizontal capacity of 22.5 MN, respectively [22]. This MBL is conditioned on the chain being studless link R4S, with diameter of 134 mm and mass of 359 kg/m. The anchor capacity was calculated based on a wet weight of 5000 t and assuming a friction of 0.45 for the seabed. Both simulated forces are lower than the maximum allowable ultimate loads, so they pass this analysis. Of course, over the 25 year lifetime of the Seawind 6, corrosion will have reduced this mooring line MBL. With an approximate corrosion rate of 0.2 mm/y, an MBL of 16.83 MN would be expected after this time period. This is still greater than the maximum experienced mooring line tension, so this should not be an issue.

From previous in-house analyses using Bladed it was discovered that, due to the arrow shape of the platform, the maximum tension of the mooring lines caused by high waves (like those of DLC 6.1 and I.1) depends on the wave direction and is the lowest for the prevailing direction (0°). For smaller waves, like those of DLC 1.2, the response of the platform is the same irrespective of the wave direction and results in a maximum value 1.2 MN for all angles [22]. As such, Figure 5.26 has been plotted in Matlab to visualise the variation in mooring line tensions for different prevailing wave directions. Looking at the mooring configuration in Figure 3.20, the expected behaviour can be estimated. With wind incoming at -90°, the forcing on the side of the nacelle (with rotor facing -180°) would be expected to be greatest at ML2 and ML4, with minimum values at ML1 and ML3. The opposite behaviour should be true when there is a prevailing direction of 90° (with rotor facing 0°). As such, there should be an intersection of these four mooring line tensions at 0° and maximum values experienced between these. As the prevailing direction remains between -90° and 90°, the tensions in ML5 and ML6 will remain minimal with small peaks at both these extremes. These predictions have been verified by examining Figure 5.26, with maximum tensions of 2.18 MN occurring at -30° and 30° for ML4 and ML3, respectively. Perhaps the control system could be optimised to avoid these instances if the mooring lines were ever to be re-designed with lighter chains. It is also slightly unusual that there is variation between the mooring line pairs of ML1 and ML3, and ML2 and ML4.

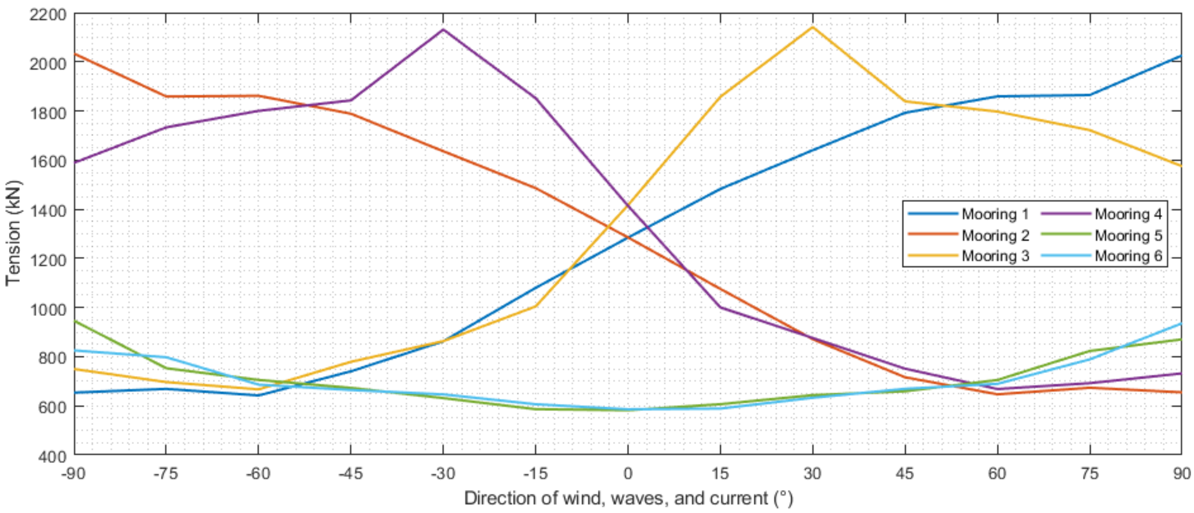

Figure 5.26: Seawind 6 DLC 6.1 Mooring line max. tension

5.4. Fatigue Loads

The objective of this fatigue load analysis is to determine whether or not the various Seawind 6 components are capable of sustaining the full spectrum of loads they will experience during their lifetime. The process for calculating the fatigue loads is as follows. First, for all load components of the investigated turbine components, lifetime cumulative rainflow cycle distributions have been generated using Bladed. These distributions are presented in Subsection 5.4.1 for the yaw bearing only (so the reader can understand the graphs without being inundated with too many), with the output of this computation being a counting matrix of the number of cycles for each range and mean load value of the component. Damage Equivalent Loads (DELs) are used to equate the fatigue damage represented by rain flow cycle counted data to that caused by a single stress range repeating at a single frequency. The method is based on the Miner's rule [71]. The Damage Equivalent Load (DEL) could then be calculated using Equation 5.10 below.

$$DEL = \sqrt[m]{\frac{\sum L_i^m n_i}{N}} \tag{5.10}$$

where L_i is the load range bin i, n_i is the number of rain flow cycles at stress range bin i, m is the negative inverse of the slope on the material's Wöhler curve, and N is the number of cycle repetitions in the turbine lifetime. It is worth noting that m is also referred to as the S-N curve slope, which relates applied stress to allowable cycles to failure. The equivalent loads (in Nm and N) are presented in Subsection 5.4.2 for each investigated turbine component assuming 10^7 cycles over the Seawind 6's expected lifetime of 25 years. A partial safety factor for fatigue loads of 1.0 has been applied, as per IEC 61400-1 [30]. The values are given for different slopes of the S-N curve (m = 3 to 10), accounting for different materials, with all the load cases integrated together for total fatigue load values for each component.

5.4.1. Rainflow Cycle Distributions

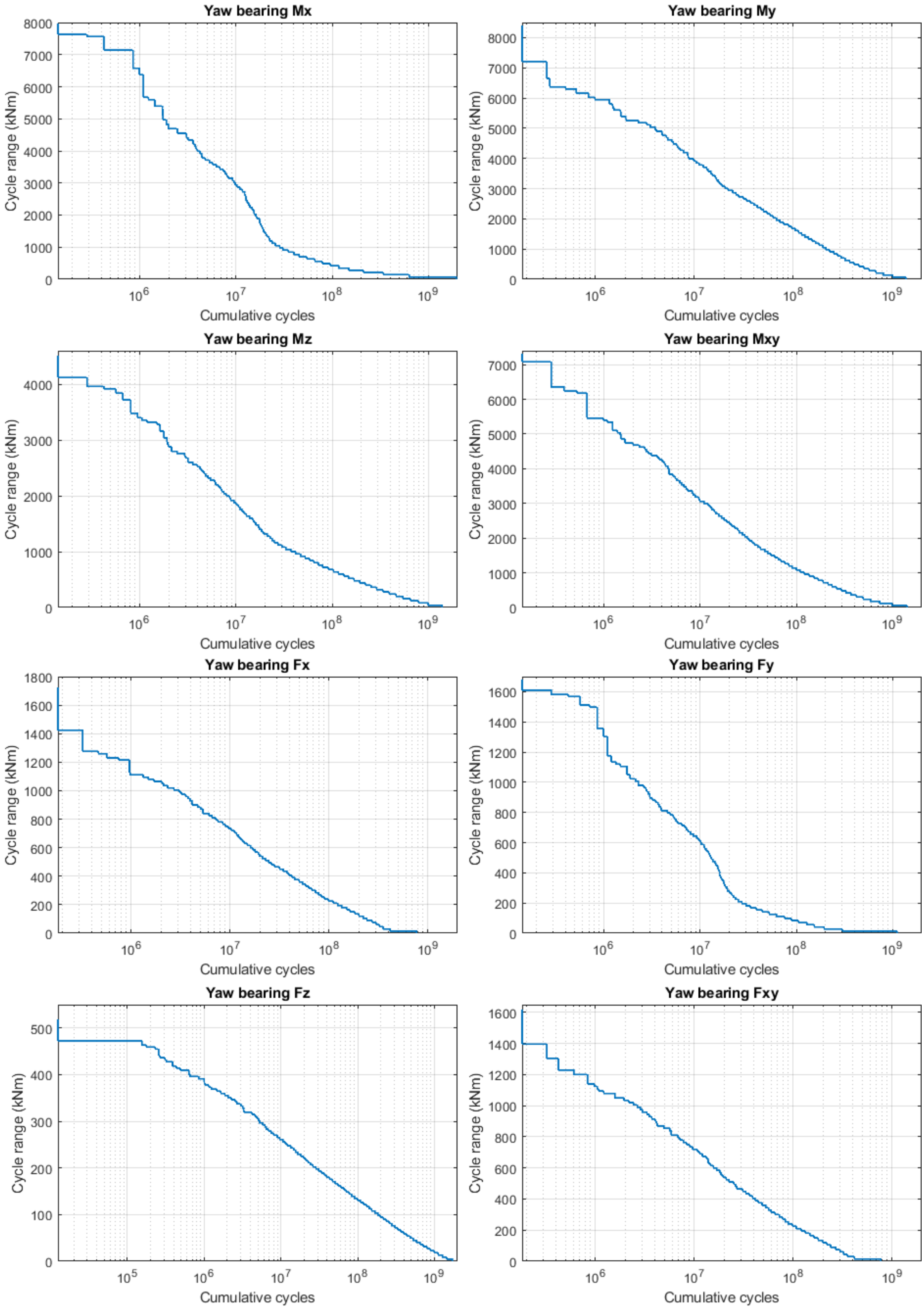

Figure 5.27: Rainflow cycle plots - Yaw bearing

5.4.2. Damage Equivalent Load Tables

Table 5.19: Damage Equivalent Loads - Blade Root 1

	Blade Root 1							
m	Mx	My	Mxy	Mz	Fx	Fy	Fxy	Fz
-	Nm	Nm	Nm	Nm	N	N	N	N
3	2.01E+07	1.17E+07	1.22E+07	7.02E+05	3.88E+05	1.10E+06	4.47E+05	1.35E+06
4	1.57E+07	1.04E+07	1.07E+07	6.09E+05	3.42E+05	8.58E+05	3.73E+05	1.30E+06
5	1.37E+07	1.03E+07	1.05E+07	5.73E+05	3.35E+05	7.41E+05	3.53E+05	1.36E+06
6	1.25E+07	1.05E+07	1.06E+07	5.58E+05	3.38E+05	6.73E+05	3.52E+05	1.44E+06
7	1.18E+07	1.07E+07	1.08E+07	5.54E+05	3.45E+05	6.29E+05	3.57E+05	1.51E+06
8	1.13E+07	1.10E+07	1.11E+07	5.55E+05	3.52E+05	5.98E+05	3.64E+05	1.57E+06
9	1.10E+07	1.13E+07	1.13E+07	5.59E+05	3.59E+05	5.75E+05	3.72E+05	1.62E+06
10	1.08E+07	1.15E+07	1.16E+07	5.65E+05	3.66E+05	5.58E+05	3.79E+05	1.66E+06

Table 5.20: Damage Equivalent Loads - Blade Root 2

	Blade Root 2							
m	Mx	My	Mxy	Mz	Fx	Fy	Fxy	Fz
-	Nm	Nm	Nm	Nm	N	N	N	N
3	2.02E+07	1.16E+07	1.18E+07	6.93E+05	3.69E+05	1.11E+06	4.38E+05	1.32E+06
4	1.59E+07	1.03E+07	1.04E+07	6.00E+05	3.26E+05	8.65E+05	3.63E+05	1.28E+06
5	1.38E+07	1.02E+07	1.03E+07	5.63E+05	3.22E+05	7.47E+05	3.44E+05	1.34E+06
6	1.26E+07	1.04E+07	1.05E+07	5.48E+05	3.29E+05	6.78E+05	3.43E+05	1.42E+06
7	1.19E+07	1.07E+07	1.08E+07	5.43E+05	3.38E+05	6.34E+05	3.48E+05	1.49E+06
8	1.14E+07	1.10E+07	1.11E+07	5.43E+05	3.48E+05	6.03E+05	3.56E+05	1.55E+06
9	1.11E+07	1.13E+07	1.14E+07	5.46E+05	3.57E+05	5.80E+05	3.64E+05	1.60E+06
10	1.09E+07	1.16E+07	1.17E+07	5.52E+05	3.66E+05	5.63E+05	3.72E+05	1.65E+06

Table 5.21: Damage Equivalent Loads - Rotating Hub

	Rotating Hub							
m	Mx	My	Mz	Myz	Fx	Fy	Fz	Fyz
-	Nm	Nm	Nm	Nm	N	N	N	N
3	1.01E+06	1.36E+06	1.34E+06	1.01E+06	6.65E+05	3.56E+06	3.43E+06	4.40E+05
4	1.01E+06	1.22E+06	1.13E+06	8.43E+05	6.08E+05	2.78E+06	2.68E+06	3.50E+05
5	1.08E+06	1.22E+06	1.04E+06	7.91E+05	6.10E+05	2.40E+06	2.31E+06	3.17E+05
6	1.16E+06	1.26E+06	9.93E+05	7.91E+05	6.27E+05	2.17E+06	2.10E+06	3.05E+05
7	1.23E+06	1.31E+06	9.73E+05	8.15E+05	6.48E+05	2.03E+06	1.95E+06	3.03E+05
8	1.28E+06	1.37E+06	9.65E+05	8.49E+05	6.68E+05	1.92E+06	1.85E+06	3.06E+05
9	1.33E+06	1.42E+06	9.64E+05	8.83E+05	6.88E+05	1.85E+06	1.78E+06	3.12E+05
10	1.38E+06	1.47E+06	9.66E+05	9.16E+05	7.06E+05	1.79E+06	1.72E+06	3.19E+05

Table 5.22: Damage Equivalent Loads - Stationary Hub

	Stationary Hub							
m	Mx	My	Mz	Myz	Fx	Fy	Fz	Fyz
-	Nm	Nm	Nm	Nm	N	N	N	N
3	1.01E+06	1.46E+06	1.43E+06	1.01E+06	6.65E+05	3.16E+05	4.40E+05	4.40E+05
4	1.01E+06	1.23E+06	1.20E+06	8.43E+05	6.08E+05	2.93E+05	3.50E+05	3.50E+05
5	1.08E+06	1.16E+06	1.13E+06	7.91E+05	6.10E+05	2.92E+05	3.17E+05	3.17E+05
6	1.16E+06	1.16E+06	1.11E+06	7.91E+05	6.27E+05	2.97E+05	3.04E+05	3.05E+05
7	1.23E+06	1.18E+06	1.13E+06	8.15E+05	6.48E+05	3.04E+05	3.02E+05	3.03E+05
8	1.28E+06	1.21E+06	1.16E+06	8.49E+05	6.68E+05	3.11E+05	3.05E+05	3.06E+05
9	1.33E+06	1.25E+06	1.20E+06	8.83E+05	6.88E+05	3.17E+05	3.11E+05	3.12E+05
10	1.38E+06	1.28E+06	1.23E+06	9.16E+05	7.06E+05	3.24E+05	3.18E+05	3.19E+05

Table 5.23: Damage Equivalent Loads - Yaw Bearing

	Yaw bearing							
m	Mx	My	Mxy	Mz	Fx	Fy	Fxy	Fz
-	Nm	Nm	Nm	Nm	N	N	N	N
3	4.80E+06	6.64E+06	5.24E+06	3.14E+06	1.16E+06	9.95E+05	1.15E+06	4.78E+05
4	4.87E+06	5.75E+06	4.77E+06	2.90E+06	1.06E+06	1.02E+06	1.04E+06	3.91E+05
5	5.05E+06	5.50E+06	4.71E+06	2.89E+06	1.05E+06	1.06E+06	1.02E+06	3.61E+05
6	5.25E+06	5.47E+06	4.78E+06	2.95E+06	1.06E+06	1.10E+06	1.03E+06	3.50E+05
7	5.44E+06	5.53E+06	4.89E+06	3.02E+06	1.09E+06	1.15E+06	1.05E+06	3.48E+05
8	5.61E+06	5.64E+06	5.02E+06	3.10E+06	1.12E+06	1.18E+06	1.08E+06	3.49E+05
9	5.77E+06	5.76E+06	5.14E+06	3.17E+06	1.15E+06	1.22E+06	1.10E+06	3.52E+05
10	5.90E+06	5.89E+06	5.26E+06	3.24E+06	1.19E+06	1.25E+06	1.13E+06	3.57E+05

Table 5.24: Damage Equivalent Loads - Tower 1

	Tower 1 - Member 16 End 1 - Steel							
m	Mx	My	Mz	Myz	Fx	Fy	Fz	Fyz
-	Nm	Nm	Nm	Nm	N	N	N	N
3	3.14E+06	7.22E+07	8.68E+07	8.15E+07	5.26E+05	1.48E+06	1.33E+06	1.37E+06
4	2.90E+06	7.67E+07	7.98E+07	7.42E+07	4.47E+05	1.38E+06	1.42E+06	1.26E+06
5	2.89E+06	8.22E+07	7.84E+07	7.27E+07	4.24E+05	1.36E+06	1.53E+06	1.24E+06
6	2.95E+06	8.73E+07	7.90E+07	7.31E+07	4.20E+05	1.38E+06	1.62E+06	1.25E+06
7	3.02E+06	9.17E+07	8.05E+07	7.42E+07	4.24E+05	1.40E+06	1.70E+06	1.27E+06
8	3.10E+06	9.55E+07	8.22E+07	7.57E+07	4.30E+05	1.43E+06	1.77E+06	1.30E+06
9	3.17E+06	9.89E+07	8.42E+07	7.73E+07	4.38E+05	1.46E+06	1.83E+06	1.32E+06
10	3.24E+06	1.02E+08	8.62E+07	7.89E+07	4.46E+05	1.49E+06	1.89E+06	1.35E+06

Table 5.25: Damage Equivalent Loads - Tower 2 - Steel

	Tower 2 - Member 18 End 2 - Steel							
m	Mx	My	Mz	Myz	Fx	Fy	Fz	Fyz
-	Nm	Nm	Nm	Nm	N	N	N	N
3	3.14E+06	8.44E+07	1.00E+08	9.38E+07	5.49E+05	1.55E+06	1.44E+06	1.41E+06
4	2.90E+06	8.98E+07	9.22E+07	8.55E+07	4.72E+05	1.45E+06	1.55E+06	1.31E+06
5	2.90E+06	9.62E+07	9.07E+07	8.38E+07	4.53E+05	1.44E+06	1.67E+06	1.30E+06
6	2.96E+06	1.02E+08	9.14E+07	8.43E+07	4.51E+05	1.46E+06	1.77E+06	1.31E+06
7	3.03E+06	1.07E+08	9.31E+07	8.57E+07	4.57E+05	1.48E+06	1.86E+06	1.33E+06
8	3.11E+06	1.12E+08	9.51E+07	8.74E+07	4.65E+05	1.51E+06	1.94E+06	1.36E+06
9	3.18E+06	1.16E+08	9.73E+07	8.92E+07	4.75E+05	1.54E+06	2.00E+06	1.39E+06
10	3.25E+06	1.19E+08	9.95E+07	9.11E+07	4.85E+05	1.57E+06	2.06E+06	1.41E+06

Table 5.26: Damage Equivalent Loads - Tower 2 - Concrete

	Tower 2 - Member 19 End 1 - Concrete							
m	Mx	My	Mz	Myz	Fx	Fy	Fz	Fyz
-	Nm	Nm	Nm	Nm	N	N	N	N
3	3.14E+06	8.44E+07	1.00E+08	9.38E+07	5.51E+05	1.55E+06	1.45E+06	1.42E+06
4	2.90E+06	8.98E+07	9.22E+07	8.55E+07	4.74E+05	1.45E+06	1.56E+06	1.32E+06
5	2.90E+06	9.62E+07	9.07E+07	8.38E+07	4.55E+05	1.44E+06	1.68E+06	1.30E+06
6	2.96E+06	1.02E+08	9.14E+07	8.43E+07	4.54E+05	1.46E+06	1.78E+06	1.32E+06
7	3.03E+06	1.07E+08	9.31E+07	8.57E+07	4.60E+05	1.49E+06	1.87E+06	1.34E+06
8	3.11E+06	1.12E+08	9.51E+07	8.74E+07	4.68E+05	1.51E+06	1.95E+06	1.37E+06
9	3.18E+06	1.16E+08	9.73E+07	8.92E+07	4.78E+05	1.54E+06	2.01E+06	1.40E+06
10	3.25E+06	1.19E+08	9.95E+07	9.11E+07	4.88E+05	1.57E+06	2.07E+06	1.43E+06

Table 5.27: Damage Equivalent Loads - Tower 3

	Tower 3 - Member 21 End 2 - Concrete							
m	Mx	My	Mz	Myz	Fx	Fy	Fz	Fyz
-	Nm	Nm	Nm	Nm	N	N	N	N
3	3.15E+06	1.40E+08	1.50E+08	1.38E+08	8.80E+05	2.56E+06	2.42E+06	2.19E+06
4	2.91E+06	1.50E+08	1.41E+08	1.28E+08	8.42E+05	2.42E+06	2.61E+06	2.06E+06
5	2.90E+06	1.62E+08	1.40E+08	1.27E+08	8.63E+05	2.41E+06	2.81E+06	2.05E+06
6	2.95E+06	1.72E+08	1.41E+08	1.28E+08	9.01E+05	2.43E+06	2.98E+06	2.08E+06
7	3.03E+06	1.80E+08	1.44E+08	1.31E+08	9.45E+05	2.46E+06	3.13E+06	2.13E+06
8	3.10E+06	1.88E+08	1.46E+08	1.34E+08	9.89E+05	2.50E+06	3.25E+06	2.17E+06
9	3.18E+06	1.94E+08	1.49E+08	1.36E+08	1.03E+06	2.54E+06	3.36E+06	2.22E+06
10	3.25E+06	2.00E+08	1.52E+08	1.39E+08	1.07E+06	2.58E+06	3.45E+06	2.26E+06

Table 5.28: Damage Equivalent Loads - Tower 4

	Tower 4 - Member 25 End 2 - Concrete							
m	Mx	My	Mz	Myz	Fx	Fy	Fz	Fyz
-	Nm	Nm	Nm	Nm	N	N	N	N
3	3.17E+06	1.65E+08	1.82E+08	1.64E+08	2.06E+06	4.91E+06	1.49E+06	3.42E+06
4	2.91E+06	1.77E+08	1.70E+08	1.52E+08	2.13E+06	4.38E+06	1.50E+06	2.97E+06
5	2.90E+06	1.90E+08	1.69E+08	1.51E+08	2.28E+06	4.20E+06	1.58E+06	2.80E+06
6	2.96E+06	2.02E+08	1.70E+08	1.53E+08	2.43E+06	4.14E+06	1.66E+06	2.72E+06
7	3.03E+06	2.12E+08	1.73E+08	1.56E+08	2.57E+06	4.15E+06	1.73E+06	2.70E+06
8	3.11E+06	2.21E+08	1.76E+08	1.59E+08	2.70E+06	4.18E+06	1.80E+06	2.69E+06
9	3.18E+06	2.28E+08	1.80E+08	1.62E+08	2.81E+06	4.23E+06	1.85E+06	2.71E+06
10	3.26E+06	2.34E+08	1.83E+08	1.66E+08	2.92E+06	4.29E+06	1.90E+06	2.72E+06

Table 5.29: Damage Equivalent Loads - Platform Arm

	Platform Arm - Member 74 End 2 - Concrete							
m	Mx	My	Mz	Myz	Fx	Fy	Fz	Fyz
-	Nm	Nm	Nm	Nm	N	N	N	N
3	1.59E+07	2.34E+07	6.13E+06	2.32E+07	1.49E+06	1.66E+06	3.94E+06	3.96E+06
4	1.46E+07	2.30E+07	5.53E+06	2.28E+07	1.48E+06	1.52E+06	3.97E+06	3.98E+06
5	1.44E+07	2.38E+07	5.34E+06	2.35E+07	1.55E+06	1.49E+06	4.10E+06	4.11E+06
6	1.45E+07	2.48E+07	5.29E+06	2.45E+07	1.63E+06	1.49E+06	4.26E+06	4.27E+06
7	1.47E+07	2.58E+07	5.32E+06	2.55E+07	1.70E+06	1.51E+06	4.42E+06	4.42E+06
8	1.50E+07	2.67E+07	5.38E+06	2.64E+07	1.77E+06	1.54E+06	4.56E+06	4.56E+06
9	1.53E+07	2.76E+07	5.46E+06	2.72E+07	1.83E+06	1.57E+06	4.69E+06	4.69E+06
10	1.56E+07	2.84E+07	5.55E+06	2.79E+07	1.89E+06	1.60E+06	4.80E+06	4.80E+06

Table 5.30: Damage Equivalent Loads - Mooring Lines Tension and Gravity Anchors Horizontal Loads

	Mooring Lines						**Anchors**		
m	ML1	ML2	ML3	ML4	ML5	ML6	A13	A24	A56
-	N	N	N	N	N	N	N	N	N
3	1.52E+05	2.47E+05	1.83E+05	2.70E+05	7.26E+04	6.79E+04	3.28E+05	5.12E+05	1.37E+05
4	1.76E+05	2.91E+05	2.11E+05	3.13E+05	7.81E+04	7.46E+04	3.81E+05	6.00E+05	1.50E+05
5	1.98E+05	3.25E+05	2.35E+05	3.48E+05	8.29E+04	8.00E+04	4.27E+05	6.69E+05	1.60E+05
6	2.17E+05	3.52E+05	2.56E+05	3.76E+05	8.70E+04	8.42E+04	4.66E+05	7.24E+05	1.69E+05
7	2.33E+05	3.74E+05	2.73E+05	3.99E+05	9.04E+04	8.76E+04	4.99E+05	7.70E+05	1.76E+05
8	2.47E+05	3.92E+05	2.87E+05	4.18E+05	9.32E+04	9.03E+04	5.27E+05	8.07E+05	1.81E+05
9	2.58E+05	4.08E+05	2.99E+05	4.34E+05	9.57E+04	9.26E+04	5.51E+05	8.40E+05	1.86E+05
10	2.68E+05	4.22E+05	3.09E+05	4.48E+05	9.78E+04	9.46E+04	5.71E+05	8.68E+05	1.90E+05

5.4.3. Fatigue Load Analysis

Subsection 5.4.1 presents a typical example of the lifetime rainflow cycle counts from which the DELs have been derived. Here, only the yaw bearing distributions in Figure 5.27 have been included as it would have taken up too much space to include them all. These are representative of what the others would look like, however. The cumulative cycles is shown on the x-axis with logarithmic scaling, accompanied by the cycle range in kNm on the y-axis. Each of the plots shows the cycle range to decrease with increasing cumulative cycles. The DEL tables are then examined one-by-one to determine the greatest fatigue load and its corresponding values of m. Blade 1 and 2 roots experienced largest DELs of 2.01E+07 Nm and 2.02E+07 Nm, respectively, both for Mx with an m of 3. The largest DEL experienced at the rotating hub was 3.56E+06 N for Fy with an m of 3, while the largest at the stationary hub was 1.46E+06 Nm for My with an m of 3. My produced the largest DEL for the yaw bearing, with a value of 6.64E+06 Nm at an m of 3. For these tower top components, each of the maximum DELs corresponds to an m of 3. This is a result of x. The largest DEL experienced at the first tower section was 1.02E+08 Nm for My with an m of 10. Both tower 2 sections, steel and concrete, share the same largest DEL value of 1.19E+08 Nm for My with an m of 10. Again, both Tower sections 3 and 4 experienced their largest DELs of 2.00E+08 Nm and 2.34E+08 Nm, respectively, for My at an m of 10. The largest DELs were shown to occur for My with an m of 10 for all the tower sections, with the values increasing with distance from the hub. The largest DEL experienced at the platform arm was 2.84E+07 Nm for My with an m of 10, again following the trend of the tower sections. The maximum mooring line DEL was 4.48E+05 N for ML4 with an m of 10, and the maximum anchor DEL was 8.68E+05 N for A24 with an m of 10. It is interesting to examine these results in Table 5.30 as you can see ML2 and ML4, as well as A24, are greater than rest due to the turbine rotor yawing during power control. Ideally, these DELs would be compared to results from an actual fatigue loading test of each investigated component. However, until the Seawind 6 demonstrator is constructed, this will not be possible. As such, for the purposes of this project, the best form of analysis is to compare these fatigue loads to those of a comparable three-blader. This is covered later in Section 7.2.

6

Seawind 6 - Aerodynamic Teeter Damping Investigation

In this chapter, the fundamental areas of the Seawind 6 operating envelope are explored in steady, uniform winds to gain a better appreciation of the turbine's operation. In particular, the Seawind engineers were keen to investigate the effect of aerodynamic damping on the turbine's teeter motion as a consequence of yawing. This misalignment between the rotor and oncoming wind causes the angles of attack to differ between the two blades when in a vertical orientation. This is explained further in Section 6.3 and displayed in Figure 6.5. To investigate this, multiple wind speeds were simulated, with zero wind shear and zero turbulence, recording the angle of attack across the rotor and net aerodynamic moment when the blades were vertical. The general effect was expected to be a negative moment (i.e. bottom blade being pushed downwind) which is beneficial in terms of opposing the effect of wind shear, a positive moment where the top blade is pushed downwind. It was also of interest to determine whether the sign of the moment would change at any wind speed below cut-out. To test the effect of this misalignment, only wind speeds above rated would be of interest due to yaw-regulation. It was decided that a 12 m/s simulation would also be investigated to verify the effect, and blades horizontal would also be examined to prove the extent of the phenomenon.

Section 6.1 presents time series of the most interesting variables for two of these uniform wind simulations, 14 m/s and 22 m/s. 14 m/s is of particular interest as it is just above the rated speed of 12.5 m/s for the Seawind 6 and 22 m/s provides nice insight into wind speeds close to cut-out. Each simulation lasted 100 s, with just the final 20 s being analysed for the purposes of this investigation (ease of reading plots and lack of unwanted transient behaviour). Section 6.2 looks more closely at how the angle of attack changes across the length of both blades in the horizontal and vertical positions at the same two uniform wind speeds as above. Section 6.3 is the culmination of this investigation, with all the simulation data tabulated and a thorough analysis presented.

6.1. Time Series

14 m/s

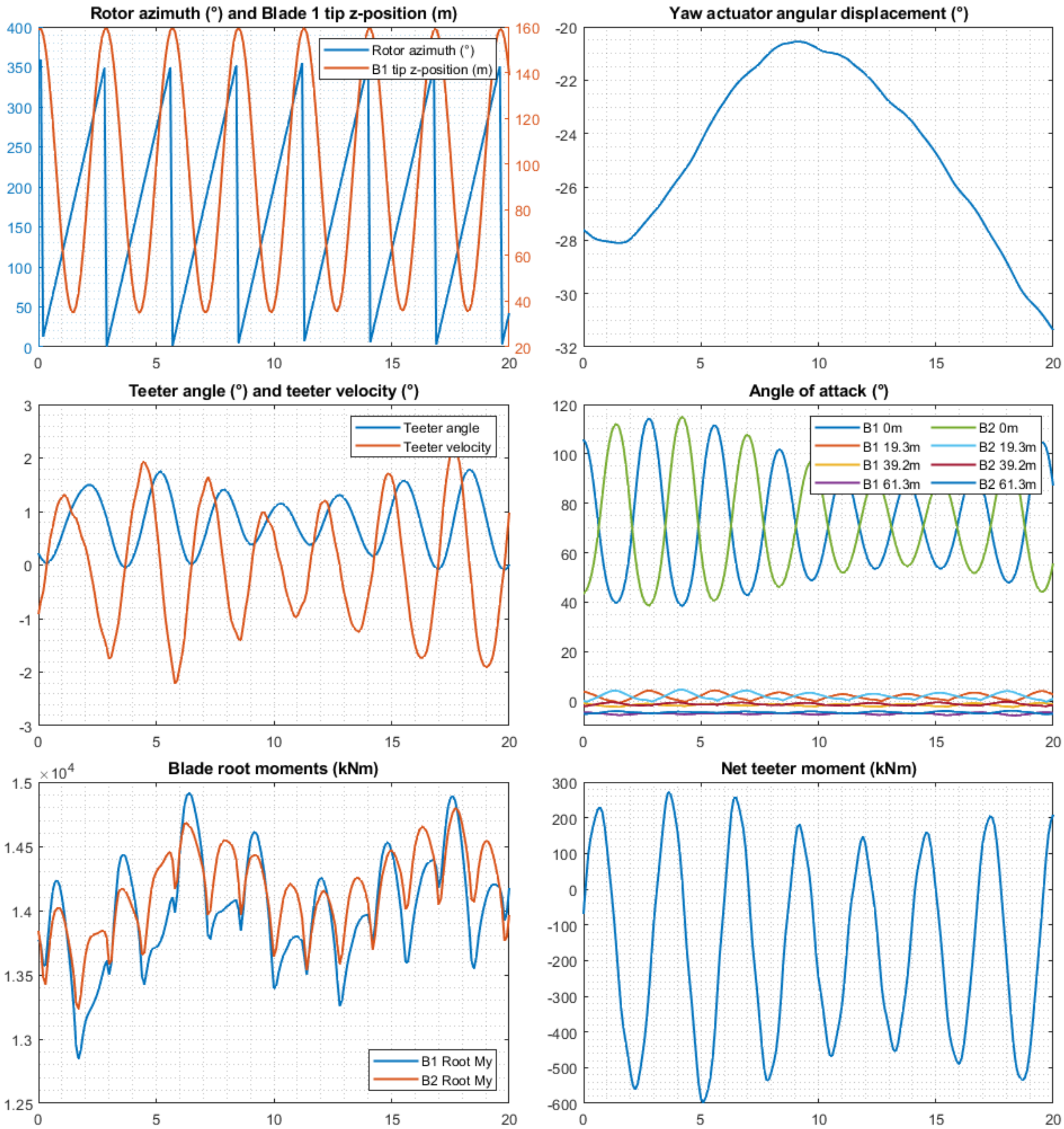

Figure 6.1: Seawind 6 - 14 m/s uniform wind time series plots

The first time series graph shows the rotor azimuth angle and the Blade 1 tip position in the z-plane. These are used to determine what orientation the blades have. As the hub height of the turbine is 95 m and the blade is 61.2 m in length, when Blade 1 is vertical its tip will be at 158 m (including hub) and when horizontal it will be at 95 m. The rotor azimuth confirms this, outputting 0° when vertical and 90° when horizontal. For compiling Table 6.1 it is important to select data from the same rotation to reduce variability when comparing between different wind speeds. For this investigation, the first rotation was selected for all wind speeds as it typically had the most accurate yaw angle and rotor speed. Above rated wind speeds this was possible as the turbine had the same rated speed, and so had completed the same number of rotations in total. For wind speeds below rated, the lower rotor speed meant a later rotation was selected. The yaw angle is shown to vary about -27.5° as per the active yaw control schedule. The teeter angle and velocity vary sinusoidally with each rotor rotation up to 1.8° and 2.2°/s, respectively. The angle of attack varies sinusoidally again, half a period behind each other, with the largest angles present at the blade roots and reaching 115°. When completing Table 6.1 the angle of attack corresponding to when the blades were horizontal and vertical would be recorded. The flatwise bending moment experienced at the root of each blade is then displayed, followed by the net of the moments. When vertical, Blade 2 moments are slightly larger than those from Blade 1 meaning a negative net aerodynamic moment exists which reduces the teeter motion resulting from wind shear as hoped. When horizontal, the effect does not exist due to a lack in variation of the angles of attack.

22 m/s

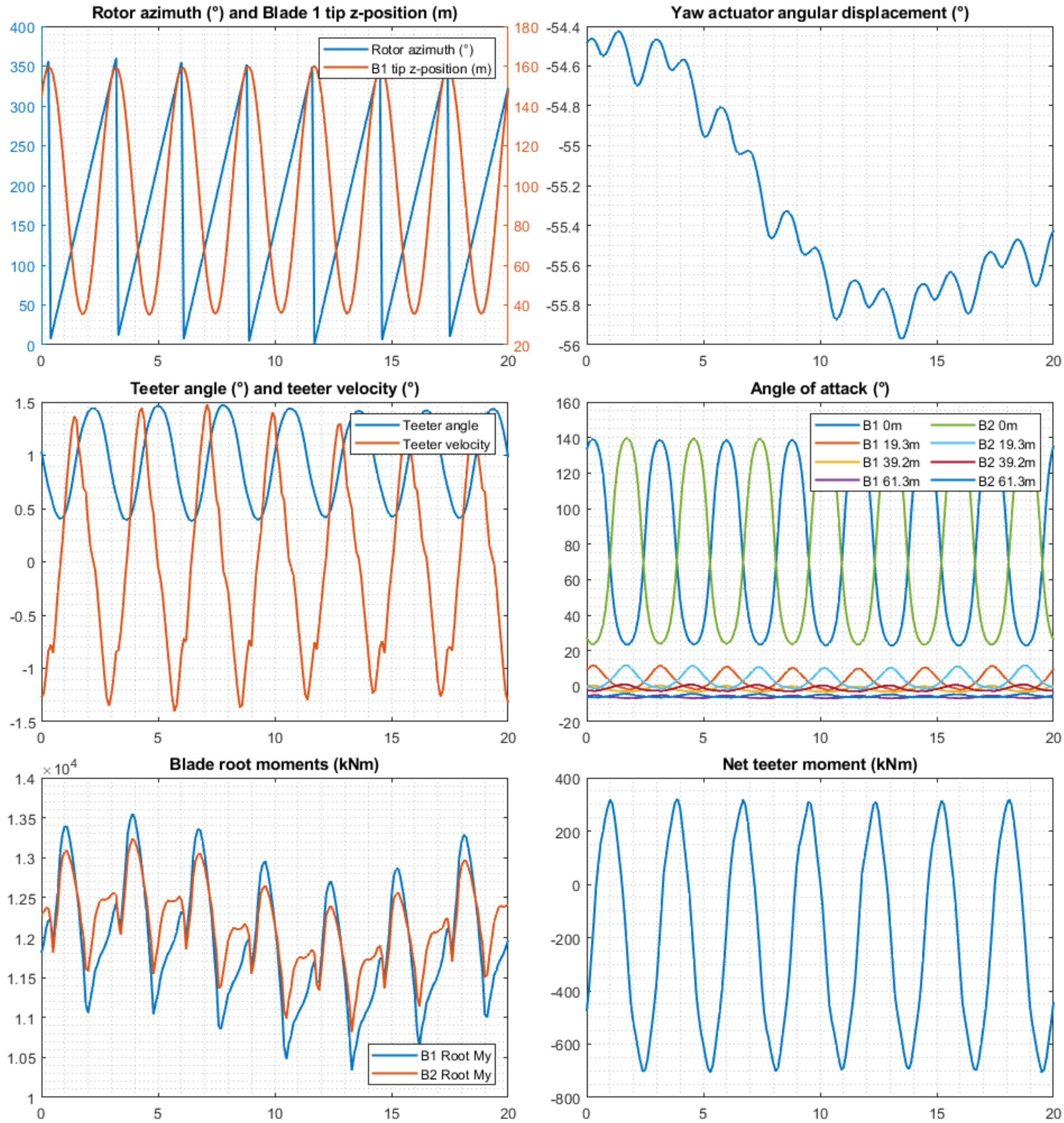

Figure 6.2: Seawind 6 - 22 m/s uniform wind time series plots

When compared to the 14 m/s data in Figure 6.1, the same values are shown for the rotor azimuth angle and the Blade 1 tip position in the z-plane, as expected. Due to the increase in wind speed, the yaw angle now varies about 55° to maintain rated power output. The maximum teeter angle and velocity have both decreased slightly to 1.5° and 1.5°/s, respectively. The angles of attack on both blades have increased in amplitude and magnitude, reaching 140° at the blade roots. The amplitude of the net teeter moments have increased slightly reaching a maximum of approximately 300 kNm and minimum of -700 kNm. The beneficial aerodynamic damping due to yaw misalignment also still exists.

6.2. Angle of Attack Across Blade Length

14 m/s

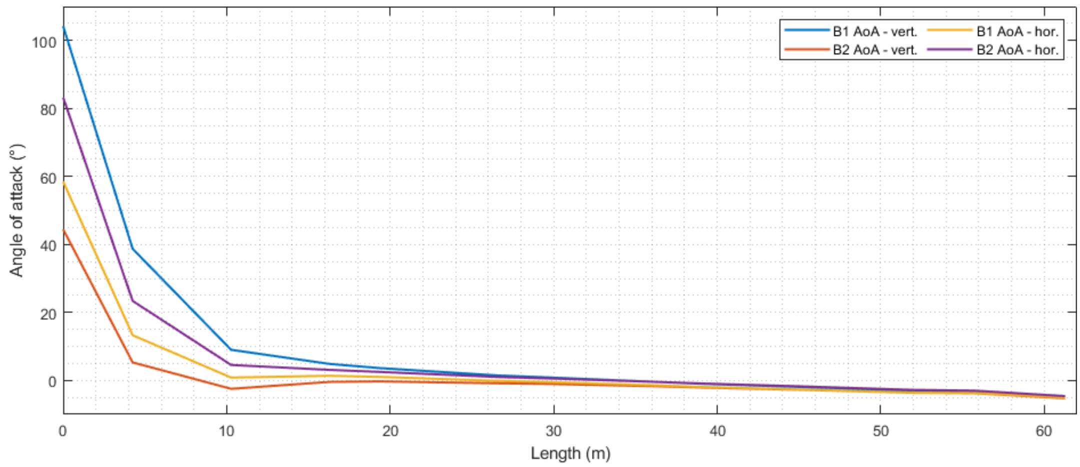

Figure 6.3: Seawind 6 - 14 m/s uniform wind angle of attack vs. length plots

22 m/s

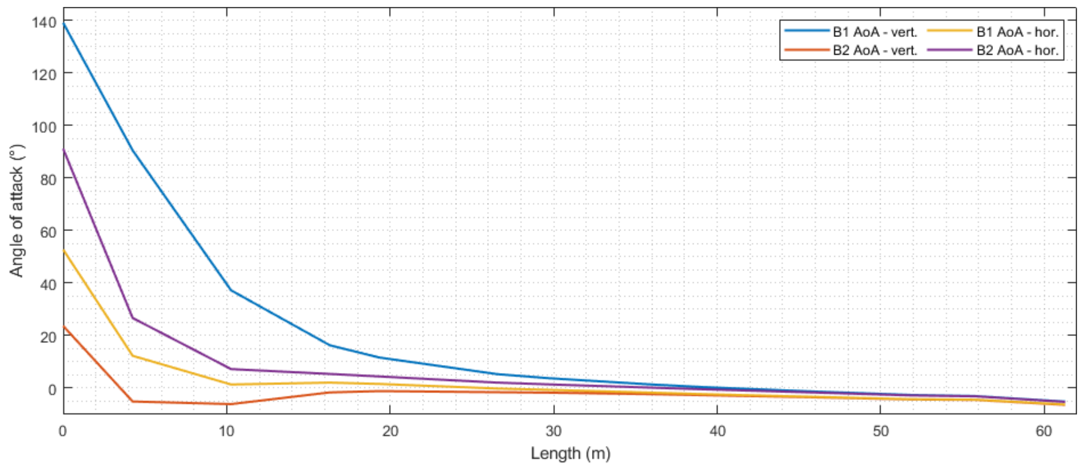

Figure 6.4: Seawind 6 - 22 m/s uniform wind angle of attack vs. length plots

Above, the variation in angle of attack across the length of the two 61.2 m blades are displayed for the first rotation of each series. Both plots show a decrease in angle of attack from the blade root towards the tip. This decrease is rather steep for the first 20 m before plateauing at approximately 0° for the remainder of each blade's span. The same sequence is present in both plots, with Blade 1 in the vertical position being the greatest initially, followed by horizontal Blade 2, horizontal Blade 1, and vertical Blade 2. This is what was expected, with a much larger difference in angles of attack when the blades are vertical compared to horizontal. The spread of angles of attack are also shown to be greater for the 22 m/s data set than for 14 m/s. This is most likely a result of larger blade deformations at higher speeds.

6.3. Overview Table

Table 6.1 below starts with the yaw misalignment angles and rotor speeds associated with each of the seven investigated wind speeds tabulated by row. The 0° heading and lack of turbulence means these values stay constant throughout each simulation. Each row is then divided into vertical and horizontal blade orientations, 0° and 90° rotor azimuth angles respectively. The elapsed simulation time when the first rotation values were selected is recorded next, followed by the corresponding teeter angles and velocities. The rows are then further divided into Blade 1 and 2, with the angle of attack across the length of each of these blades in vertical and horizontal orientation tabulated. Second from the end the flatwise root moments are presented, before the net of these is recorded with particular interest being paid to whether it is positive or negative.

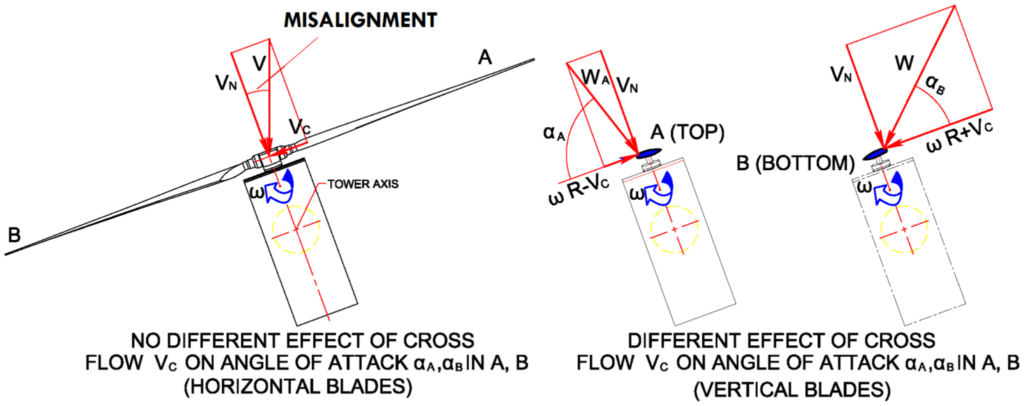

Figure 6.5: Seawind 6 - Effect of misalignment on vertical blades angle of attack [22]

Examining Table 6.1, the most important result is that there is typically a negative net teeter moment when the blades are vertical above the rated wind speed of 12.5 m/s. This is a result of a differential change in angles of attack between the advancing and retreating blades when the rotor is misaligned with the incoming wind. This provides aerodynamic damping which, in the absence of aerodynamic forcing, progressively eliminates the teeter and causes the rotor to realign with the shaft. The difference in angles of attack are also shown to be much greater when the blades are vertical compared to horizontal above rated. This is the desired outcome, proving that yaw misalignment does indeed increase the disparity between angles of attack when blades are vertical, resulting in 1P teeter forcing in two-bladed yaw controlled turbines that opposes forcing due to wind shear. This effect is visualised in Figure 6.5 above, where the misalignment is shown to alter the angle of attack in an opposing manner for the top and bottom blades when vertical. This effect was detailed in Subsection 2.4.1 and is a result of the addition and subtraction of the cross component of the incoming wind in relation to the rotors running direction. Strangely, the first rotation of the 14 m/s shows a positive net teeter moment with the blades vertical. However, all the following rotations at this speed result in negative net moments when vertical. This is rather unexpected and inexplicable and certainly deserves further analysis in subsequent studies. Below rated, at 12 m/s, there is barely any difference between angles of attack in the vertical position, while the horizontal difference is comparable to those seen above rated. Both orientations result in negative net teeter moments, which is surprising as this would indicate that, even without the effect of yaw misalignment, negative aerodynamic forcing is still generated to counteract the undesirable positive moment generated by wind shear forcing and reduce teeter amplitudes. Again, further study of this topic would be recommended to verify that this is indeed a reliably positive effect for the turbine's dynamic operation. For example, one variation of interest would be to investigate the effect of yawing in the opposite direction on the net teeter moment.

Table 6.1: Seawind 6 - uniform wind - angles of attack and aerodynamic moments overview

Wind Speed (m/s)	Yaw Angle (°)	Rotor Speed (rpm)	Azimuth Angle (°)	Sim. Time (s)	Teeter Angle (°)	Teeter Velocity (°/s)	Blade	Angle of Attack (°) at blade length (m)													Root My Moment (kNm)	Net Teeter Moment (kNm)
								0	4.3	10.3	16.3	19.3	26.5	29.7	36.0	39.2	45.5	51.8	55.8	61.3		
12	0	17.6	0	0.9	0.88	-1.17	1	75.15	24.38	5.42	4.47	3.77	2.30	1.88	0.83	0.26	-0.58	-1.44	-1.63	-2.26	14778.50	-168.97
							2	73.34	21.70	3.75	3.62	3.25	2.25	1.94	1.09	0.58	-0.20	-1.07	-1.29	-2.05	14947.47	
			90	1.8	0.05	-0.02	1	65.31	18.87	3.61	3.70	3.24	2.03	1.66	0.71	0.17	-0.65	-1.51	-1.70	-2.47	15008.07	-9.36
							2	84.02	29.21	7.30	5.41	4.57	3.02	2.58	1.54	0.96	0.13	-0.73	-0.93	-1.49	15017.43	
14	-27.5	20.8	0	0.1	0.14	-0.68	1	104.23	38.71	8.99	4.84	3.62	1.46	0.86	-0.40	-1.02	-1.99	-2.96	-3.18	-4.64	13739.24	17.86
							2	44.45	5.29	-2.48	-0.45	-0.29	-0.86	-1.05	-1.70	-2.11	-2.81	-3.62	-3.80	-5.28	13721.38	
			90	0.8	0.32	1.11	1	58.47	13.28	0.83	1.36	1.03	-0.14	-0.50	-1.43	-1.95	-2.75	-3.58	-3.73	-5.09	14234.65	215.12
							2	83.26	23.37	4.54	3.09	2.49	1.00	0.57	-0.40	-0.93	-1.81	-2.78	-3.03	-4.63	14019.52	
16	-39	20.8	0	0.3	0.58	-1.17	1	119.67	56.59	16.19	8.12	6.00	2.62	1.72	0.09	-0.66	-1.85	-2.99	-3.29	-5.06	13035.96	-131.02
							2	35.45	1.36	-3.42	-0.45	-0.19	-0.80	-1.02	-1.70	-2.13	-2.89	-3.78	-3.97	-5.67	13166.98	
			90	1.1	0.28	0.81	1	54.42	12.22	0.94	1.75	1.38	-0.02	-0.46	-1.45	-2.00	-2.88	-3.79	-3.97	-5.56	13840.67	292.75
							2	89.17	27.16	6.59	4.53	3.68	1.67	1.09	-0.06	-0.65	-1.67	-2.76	-3.07	-4.92	13547.92	
18	-46	20.8	0	0.2	0.60	-1.12	1	127.04	68.50	22.00	10.50	7.67	3.41	2.30	0.42	-0.42	-1.74	-2.97	-3.31	-5.22	12614.83	-99.89
							2	30.92	-1.09	-4.46	-0.98	-0.64	-1.20	-1.41	-2.04	-2.44	-3.19	-4.05	-4.24	-6.04	12714.72	
			90	0.9	0.29	0.63	1	60.59	15.70	2.38	2.49	1.86	0.16	-0.36	-1.47	-2.05	-3.00	-3.94	-4.14	-5.84	13520.47	330.75
							2	80.81	22.17	5.23	4.13	3.43	1.50	0.94	-0.19	-0.76	-1.81	-2.92	-3.23	-5.22	13189.72	
20	-52	20.8	0	0.3	0.65	-0.95	1	134.08	80.66	29.10	13.22	9.54	4.35	3.03	0.91	0.00	-1.43	-2.74	-3.12	-5.12	12490.74	-109.27
							2	26.77	-3.38	-5.39	-1.40	-0.97	-1.46	-1.64	-2.23	-2.62	-3.35	-4.21	-4.38	-6.23	12600.02	
			90	1.0	0.41	0.62	1	62.19	16.83	2.96	2.76	2.09	0.23	-0.32	-1.48	-2.07	-3.05	-4.01	-4.20	-5.95	13542.61	310.05
							2	78.67	20.39	4.83	4.13	3.47	1.55	0.99	-0.13	-0.70	-1.75	-2.89	-3.21	-5.27	13232.56	
22	-56	20.8	0	0.3	0.71	-0.84	1	139.00	90.45	37.21	16.33	11.64	5.33	3.78	1.38	0.38	-1.18	-2.59	-3.01	-5.11	12220.29	-145.79
							2	23.67	-5.09	-6.07	-1.64	-1.13	-1.55	-1.72	-2.30	-2.69	-3.43	-4.30	-4.47	-6.37	12366.08	
			90	1.1	0.51	0.79	1	52.71	12.30	1.38	2.10	1.59	-0.15	-0.65	-1.72	-2.29	-3.24	-4.20	-4.39	-6.21	13389.24	301.50
							2	91.07	26.69	7.24	5.40	4.44	2.10	1.42	0.17	-0.45	-1.58	-2.77	-3.11	-5.23	13087.74	
24	-59	20.8	0	0.4	0.67	-0.73	1	141.62	97.06	45.30	19.40	13.60	6.18	4.40	1.73	0.65	-1.04	-2.54	-3.00	-5.17	11984.05	-47.22
							2	21.77	-6.44	-6.91	-2.26	-1.70	-2.05	-2.18	-2.67	-3.01	-3.68	-4.48	-4.63	-6.54	12031.27	
			90	1.1	0.50	0.68	1	57.43	15.15	2.59	2.70	2.01	0.01	-0.56	-1.71	-2.30	-3.29	-4.28	-4.47	-6.34	13254.89	333.32
							2	84.37	22.56	5.98	4.93	4.11	1.90	1.26	0.05	-0.56	-1.68	-2.87	-3.21	-5.38	12921.57	

7

Seawind 6 - Conventional Three Bladed Comparison

In order to better understand the advantages of a teetering rotor, a comparison between the Seawind 6 and a state-of-the-art three-bladed wind turbine with rigid hub and pitch regulation should be performed. Ultimate and fatigue loads from Bladed simulations are first compared for the onshore variation of the Seawind 6 and the onshore NREL 5-MW reference wind turbine. This is a reference turbine developed by the National Renewable Energy Laboratory, with a 5 MW power rating, three blades, rigid hub, and 125 m diameter [53]. An offshore variation of the NREL 5-MW turbine was not readily available and, due to time constraints for this project, it was unfortunately not possible to create a floating model for a better comparison to the Seawind 6. With only a slightly lower rated power, but almost equal rotor diameters, an interesting comparison could be made between the two turbines. Previously acquired in-house simulation data for both turbines was used for this high level comparison. Verified against the data acquired during simulations for this project, these in-house simulations concluded that main loads are 15% to 20% higher for the offshore floating Seawind 6 than the onshore version [21]. This is in comparison to the rumoured 30% to 40% increase for a state-of-the-art three-blader when transferred from onshore to floating offshore. A brief ultimate load comparison is made between the two onshore turbines in Section 7.1 and a similarly brief fatigue load comparison is made in Section 7.2. Following this, the Seawind 6 was compared against one of the current state-of-the-art three-bladed rigid hub turbines, the offshore Siemens Gamesa SWT-6.0-154 [41]. Five of these turbines are used in the Hywind project off Scotland, the first of only three large scale floating offshore projects currently operational worldwide [57]. These are conventional three-bladed turbines with a rated power of 6 MW, direct drive Permanent Magnet synchronous Generator (PMG), with rigid hub, and sit atop a floating spar-buoy platform. With similar rated power and rotor diameter, a good comparison can be made to the Seawind 6 turbines. Section 7.3 investigates the times and costs associated with developing and deploying Seawind 6 turbines versus Siemens turbines in the Hywind project. While Section 7.4, compares the expected operational availability of turbines for calculating Annual Energy Production (AEP) and expected lifetimes. Below in Table 7.1 is an overview of both comparable turbines. The Seawind 6 values have been well established and defined in previous chapters, in particular Table 3.2 in Section 3.2.

Table 7.1: Competitor overview - NREL 5-MW and Siemens Gamesa SWT-6.0-154 [53] [41]

Parameter	NREL 5-MW	SWT-6.0-154
Rated power (MW)	5	6
Number of blades	3	3
Power regulation	Collective pitch, variable speed	Collective pitch, variable speed
Drivetrain	Gearbox	Direct drive
Hub type	Rigid	Rigid
Rotor diameter (m)	126	154
Blade mass (t)	17.7	25
Hub type	Rigid	Rigid
Hub height (m)	90	98
Cut-in wind speed (m/s)	3	4
Rated wind speed (m/s)	11.4	13
Cut-out wind speed (m/s)	25	25
Survival rotor speed (m/s)	50	70
Rated rotor speed (rpm)	12.1	11
Rated tip speed (m/s)	80	89
Setting	Onshore	Floating offshore
Certified wind class	N/A	IEC 1S

7.1. Ultimate Loads

The in-house ultimate load analysis investigated DLCs 1.3 and 6.1. Examining Table 7.2 below, the majority of the 126 m diameter Seawind loads are shown to be significantly lower than those of the 125 m diameter three-blader. These Bladed results confirm the first principle benefits of teetering outlined at the start of this report in Section 2.3. Again, it is important to note that these findings relate to the onshore versions of both turbines. First, the blade root Mxy moments are actually shown to be 27% larger for the Seawind machine than the NREL counterpart. This is a result of the Seawind 6 having two larger blades, rather than three smaller ones, meaning greater blade masses and rated tip speeds. As the teetering hinge decouples the rotor from the drivetrain, the shaft torque is shown to decrease by 50% for the Seawind 6. The thrusts experienced on both hubs are very similar, which is expected with almost identical rotor swept areas. Again, the My and Mz moments are both reduced to 6% and 10%, respectively, of the NREL machine. This is another positive effect of the teetering hinge, which negates any aerodynamic imbalances of the blades caused, for example, by wind shear. The maximum yaw bearing Mz and Mxy moments experienced by the Seawind 6 were 17% and 50%, respectively, of those experienced by the NREL 5-MW. These were experienced when exposed to tropical cyclone winds with the two-bladed turbine parked. Aerodynamic asymmetry on a fixed hub causes imbalanced blade root flap moments, which are the dominant cause of yaw moments for fixed hub turbine. Teetering removes this imbalance as well as preventing the motion from building up by aerodynamically damping it [18]. It should be noted that an unknown fraction of these ultimate load variations is also due to the different power rating, the different control system, and other characteristics of the two machines [7]. However, in any case, the Seawind 6 design is proven to be superior for reducing ultimate loads.

Table 7.2: Ultimate loads comparison - Onshore Seawind 6 and NREL 5-MW [22]

Parameter	Seawind 6	NREL 5-MW	Ratio
Blade Root:			
Mxy (kNm)	27000	21200	127%
Shaft:			
Mz (kNm)	5000	10200	50%
Hub:			
Thrust (kN)	1500	1600	94%
My (kNm)	1090	18900	6%
Mz (kNm)	1960	18600	10%
Yaw Bearing:			
Mz (kNm)	3200	18000	17%
Mxy (kNm)	13000	26000	50%

At this juncture it would have been great to compare the offshore Seawind 6 loads to a comparable state-of-the-art three-bladed floating offshore turbine. However, as this is such a new and competitive industry, this data has not yet been made publicly available. Industry talk is that conventional three-blader main loads increase by 30% to 40% when going from onshore to floating offshore. This ratio has been verified by Robertson et al. in a loads analysis study of the NREL 5-MW turbine, investigated for various floating offshore platform concepts [59]. This is in comparison to the 15% to 20% increase for the offshore floating Seawind 6 than the onshore version. This ratio is validated again from the findings of this thesis project, where the ultimate loads of the floating Seawind 6 from Section 5.3 have been compared to those from Table 7.2 relating to the onshore version. Table 7.2 has already proven that the main ultimate loads of the onshore Seawind 6 two-bladed turbine are substantially reduced in relation to those of an onshore three-bladed turbine alternative. As such, even the most conservative comparison, assuming an increase of 20% and 30% respectively to the Seawind 6 and NREL 5-MW loads, concludes that floating offshore ultimate loads of the Seawind 6 two-blader are expected to be reduced by approximately 30% to 40% compared to those of an analogous three-blader.

7.2. Fatigue Loads

Again, much like Section 5.4, the in-house fatigue load analysis was based on DLC 1.2. Table 7.3 below displays the key DELs computed at the blade roots, hub, and yaw bearing of both turbines for turbine lifetimes of 25 years and at 10^7 cycles. Here, the maximum value is taken for the Seawind 6 and compared to that of the NREL 5-MW for the same S-N curve slope. As one can see, the DELs related to the blade root bending moments are highly reduced on the Seawind 6. A ratio of 90%, 54%, and 66% were found for the Mx, My, and Mxy moments, respectively. Even though greater ultimate loads were shown to occur for the Seawind 6 in Section 7.1, over its lifetime, the teeter hinge is shown to reduce them. This reduction is more evident for the hub where the Mx moment is 52% of that experienced by the rigid NREL hub and, even more significantly, 52% of the Mz moment. The teetering hinge removes the inertial and gyroscopic effects of yawing experienced by the rigid hub turbine. The My and Mxy DEL moments are reduced by 83% and 82%, respectively, as a result. The DEL of the torsional Mz on the yaw bearing is also much lower for the Seawind 6 wind turbine, with a reduction of 88%. Again, it is unknown what fraction of these DEL variations is due to the power down-rating, but they are certainly conclusive that the Seawind 6 design is superior [7]. Again, the study by Roberton et al. showed that, in general, the fatigue load ratios of the NREL-5MW onshore and floating offshore configurations show similar trends to those of the ultimate load ratios as discussed in Section 7.1 [59]. This is verified by the findings discussed previously in Subsection 5.4.3. As such, it can be concluded that the fatigue loads of the Seawind 6 will also be considerably reduced compared to those of the state-of-the-art floating three-blader.

To maintain the highest reliability against fatigue loading, general turbine inspections and grease changes are to be carried out every year for the operational Seawind 6. The yaw drive should have an expected lifetime of twenty-five years, however Seawind's maintenance plan considers the possibility to restore the hydraulic motor every four years. The Nacelle UPS Batteries are changed and blade coatings restored every six years, while it is planned to change the teetering hinge pieces subjected to wear and fatigue every twelve years. At the same time, the pads of brake calipers and generator bearings are also changed. Additionally, Seawind engineers can accept to change the gearbox once every 25 years [22].

Table 7.3: Fatigue DEL comparison - Onshore Seawind 6 and NREL 5-MW [22]

Parameter	Seawind 6	NREL 5-MW	Ratio
Blade Root:			
Mx (kNm)	14400	15922	90%
My (kNm)	14200	26102	54%
Mxy (kNm)	20224	30575	66%
Hub:			
Mx (kNm)	1296	2484	52%
Mz (kNm)	1222	16631	7%
Yaw Bearing:			
My (kNm)	8640	50107	17%
Mxy (kNm)	9088	50151	18%
Mz (kNm)	2050	17139	12%

7.3. Development

Unlike the Hywind turbines, the Seawind 6 has a fully integrated, second generation, design. This allows it to be optimised for floating offshore wind, in terms of ease of deployment, load bearing management, and economic optimisation [18]. Economics is the driving force behind any commercial venture, especially in such a competitive sector as renewables. Weight is the key to minimising the cost of wind energy, with wind turbine manufacturers needing to design machines that sweep the greatest area with the smallest amount of material. This is a fundamental principle which has driven wind turbine development for the last 40 years [69]. Weight affects the capital cost of manufacturing the entire turbine system, as well as the installation and maintenance fees particularly regarding craneage. Figure 7.1 below displays the various competitor's towerhead masses against their rated power. The 6 MW Seawind machine is shown to be most economical at this power, with the advantage only improving with increasing power to the 12 MW and 16 MW versions. The weight advantage of the Seawind 6 will allow competitive pricing from early days. In addition to the lighter turbine head, replacing the pitch mechanisms and costly PMG with simple and reliable solutions for offshore deployment ensures lower CAPEX and OPEX [22].

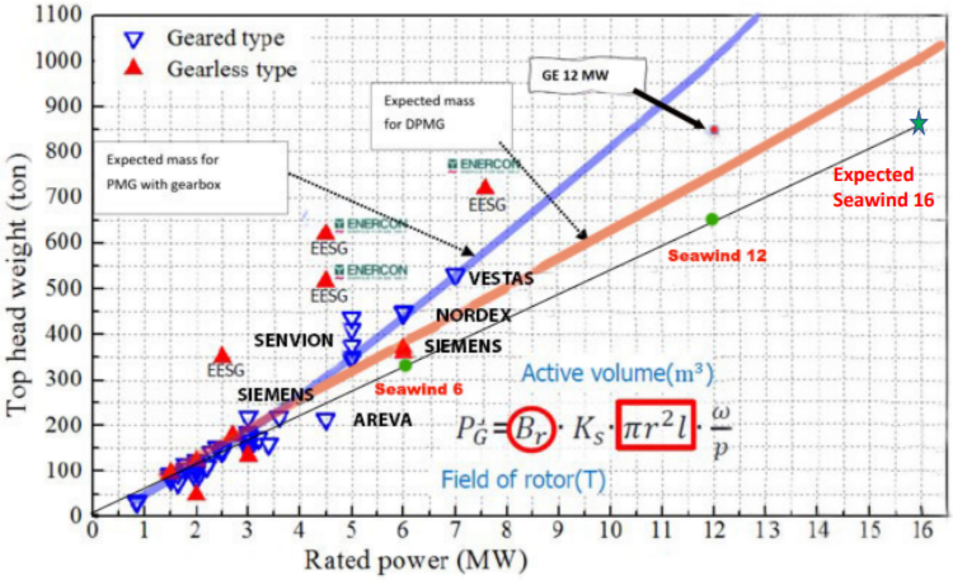

Figure 7.1: Seawind turbine head weight versus competitors [22]

An overview of both turbine's dimensions and masses are provided in Table 7.4 below. The SWT-6.0-154 turbine uses Siemen's B75 blades which, at the time of deployment, were the longest turbine blades in the world at 75 m. They are manufactured in one piece without glue joints to save weight from glass fibre-reinforced epoxy resin and balsa wood [41]. The Seawind 6 blades are slightly smaller in length and mass at 61.2 m and 25 t. This results in the SWT-6.0-154 having a larger swept area of 18600 m^2 compared to 12462 m^2. However, due to the extra blade of the Siemens machine, its towerhead mass is slightly higher at 360 t compared to the 340 t of the Seawind 6. Both values can be shown in Figure 7.1. Considering this difference in swept area, in order for both turbines to generate 6 MW of power, the Seawind 6 must rotate much faster. The SWT-6.0-154 has a rated rotor speed of 11 rpm and tip speed of 89 m/s. These are both far smaller than the 20.8 rpm and 137 m/s of the Seawind 6. Both towers are constructed from tubular steel, with the three-blader being 14 m taller to ensure a sufficient blade-water clearance. This also means the tower of the Seawind 6 is roughly 190 t lighter than its conventional counterpart. Both turbines also sit on different types of floating substructures. The SWT-6.0-154 sits atop a spar-buoy type structure specially developed for Hywind, while the Seawind 6 is fully integrated with its concrete semi-submersible Tension Leg Platform (TLP) type floater. The Seawind 6, without water in platform arms and concrete ballast in floaters, has a mass of 12806.41 t. With the water in arms and concrete ballast (total of 649 t), the total turbine mass is 18797.51 t [5]. The SWT-6.0-154 has a mass of roughly 12000 t, however when the substructure is upended and ballasted for stability it has a total mass in excess of 19200 t [39]. Below, an artists impression of the Seawind 6 is shown in in Figure 7.2a beside the image of the operational Hywind turbine in Figure 7.2b.

Table 7.4: Dimensions and mass comparison - Siemens Gamesa SWT-6.0-154 and Seawind 6 [39] [8]

Parameter	**SWT-6.0-154**	**Seawind 6**
Blade length (m)	75	61.2
Blade material	FG, Epoxy, Balsa	CF, FG
Blade mass (t)	25	20
Rotor mass (t)	75	40
Rotor diameter (m)	154	126
Swept area (m^2)	18600	12462
Hub type	Rigid	Teeter
Nacelle material	Steel	Steel
Towerhead mass (t)	360	340
Tower height (m)	83	69
Tower mass (t)	670	480
Tower material	Steel	Steel
Floater type	Spar-buoy	Semi-sub TLP
Floater material	Steel	Concrete
Total mass (t)	12000	12806.41

(a) Seawind 6

(b) Siemens Gamesa 6 MW - Hywind [40]

Figure 7.2: Seawind 6 - Three bladed competitor comparison

Based on the simple, fully integrated design of the Seawind 6, in combination with its thoroughly planned supply chain and logistics, its expected preparation, procurement, and integration times are all reduced compared to its conventional counterpart, as shown in Table 7.5. The Seawind 6 is integrated together on a mobile drydock and simply tugged out to its offshore location. The Hywind turbines, on the other hand, required specialty jack-up and crane vessels during installation. These vessels are typically either not rated or prohibitively expensive when installing and operating FOW turbines in deep waters (>50 m) or far offshore (>25 km). These rapidly drive up site-dependent costs [18]. With a long system design lifetime of 25 years for the RNA and 50 years for the platform, accompanied by less maintenance, the lifetime costs are dramatically reduced. Competitive against nuclear, fossil fuels and other renewable energy technologies with a LCOE of €0.076/kWh for the Seawind 6 at average wind speeds of 10.5 m/s [22]. The Seawind 6 also is expected to have a 60% lower life-cycle energy footprint compared to the industry standard, with an embedded carbon footprint of 4.43 kt/TWh [18]. This is in part a result of not using any costly rare earths in its generator, using a concrete platform, no sacrificial anodes, substantial recovery of energy and materials at lifetime end through circular design, and low decommissioning costs [17]. Based on data published for the Hywind project and estimated Seawind 6 values, the total CAPEX and OPEX costs for the Seawind machine is expected to be almost half that of the conventional system. The end of lifetime expenses is also due to be slightly lower at €1.3 M compared to between €1.75 M and €2.3 M.

Table 7.5: Deployment time and cost comparison - Siemens Gamesa SWT-6.0-154 and Seawind 6 [18]

Parameter	SWT-6.0-154	Seawind 6
Preparation time (months)	2.3	1
Procurement time (months)	16 - 17	7
Integration time (months)	3.3 - 3.5	0.5
Integration infrastructure	Jack-up vessel	Mobile drydock
Installation time (months)	3 - 3.25	0.25
Installation infrastructure	Crane vessel	Tugs only
Total CAPEX and OPEX (€M)	18.5 - 19.5	10.4
End of lifetime costs (€M)	1.75 - 2.3	1.3

7.4. Operation

Although the maximum system efficiency of the two-bladed design is slightly less than that of the three-bladed design, as per Section 2.2, the less complex, more robust, reliable, and fully integrated Seawind 6 design leads to an almost identical Annual Energy Productions (AEP). The SWT-6.0-154 turbines in the Hywind farm generate an individual average AEP of 26.5 GWh with an annual availability of 68.5%, which is just over the expected 26.2 GWh of the Seawind turbines with an annual availability of 85.9% at anticipated sites [39] [22]. This increase in availability is a result of a higher percentage of rated output power being generated over a greater range of sea conditions, with less downtime due to Operations, Maintenance, and Service (OMS) procedures, as per Table 7.6 below. OMS for the Seawind 6 adds to 8 hrs/yr, 16 hrs/yr and 92 hrs/yr, respectively [22]. Additionally, in a wind farm setting, the rotors of the two-bladed turbines will be misaligned from the prevailing wind direction at high wind speeds in order to regulate power output. As such, the wake losses in a wind farm are expected to be lower than using three bladed turbines [8].

Table 7.6: Operational availability comparison - Siemens Gamesa SWT-6.0-154 and Seawind 6 [18]

Parameter	SWT-6.0-154	Seawind 6
Wind alignment error (°)	7	1
Wind alignment factor (no units)	0.99	0.999
Cut out sea state (Wave height Hs, in m)	5	7
Availability from Windspeed (% year)	87.5	87.5
Availability from Sea State (% year)	85	99.5
Weather Availability (% year)	74.5	87.1
OMS Availability (% year)	92.0	98.7
Total Availability (% year)	**68.5**	**85.9**

8 Conclusion and Recommendations

8.1. Conclusion of Results

At the start of this report, in Section 1.3, six key research questions were formulated by the author. It was then the aim of this project to answer these over the course of the subsequent chapters. They were as follows:

- **Research Question 1:** What design and control features of two-bladed turbine technology makes it ideal for floating offshore installations? In particular, with respect to the Gamma 60 and Seawind 6.
- **Research Question 2:** To what extent does the Gamma 60 Bladed simulation results match those of the operational data, and how can this model be calibration to improve the real-world accuracy of its performance?
- **Research Question 3:** What improvements to the accuracy of the Seawind 6 models can be achieved as a result of these calibrations?
- **Research Question 4:** What are the key ultimate and fatigue loads of the Seawind 6 with its updated model and controller?
- **Research Question 5:** Can the theory that yaw misalignment of the rotor to the prevailing wind will aerodynamically damp the two-bladed turbine's teeter motion be validated?
- **Research Question 6:** How will the Seawind 6's predicted performance compare to that of a state-of-the-art three-bladed competitor turbine?

Following from the fundamentals shared in Chapter 2, the design and control features discussed in Chapter 3 helped to address Research Question 1. In particular, the addition of the teetering hinge proved to be particularly important for reducing turbine loads and expenses, enabling its competitiveness for the floating offshore market. The simplicity of design and installation, redundancy of components, low fatigue, maintainability, and optimised integrated floating structure make the Seawind 6 ideal for floating offshore applications. Following this, Research Question 2 was covered in Chapter 4. The general and in-depth validation investigations concluded that the Gamma 60's Bladed model and controller produced simulation results to a high level of accuracy compared to the available operational data. The key calibrations suggested to improve its real-world accuracy involved minor adjustments to the torque and speed control loops of the external controller, as well as modifying the tower and blade's structural properties. As the model and controller used for the Seawind 6 was so heavily based on those of the Gamma 60, these aforementioned calibrations could also be applied for the Seawind 6 model to improve its own performance. This fulfilled the requirements of Research Question 3. Chapter 5 considered the ultimate and fatigue loading analyses for the updated Seawind 6 for a variety of DLCs using Bladed 4.12. Both analyses provided positive results for the Seawind 6 in terms of verifying the structural design and material selection. However, it was unfortunately noted that these results were slightly inaccurate due to the external controller's incorrect yaw velocity schedule and lack of supervisory control. One other peculiarity was that lower loads than expected were obtained for DLCI.1, simulating tropical cyclones. The theory posed in Research Question 5 was proven to be true following the investigation detailed in Chapter 6. A negative teeter moment was generated when the blades of the Seawind 6 were vertically oriented and misaligned from the prevailing wind direction. This negative moment aerodynamically damped the teeter motion caused by wind shear, reducing the chance of teeter-end impacts. The effect was not as evident for lower wind speeds above rated, especially at 14 m/s where it reversed and caused a harmful positive net moment. Finally, in Chapter 7, a detailed comparison was drawn between the performance of the two-bladed Seawind 6 and the industry standard three-blader. Unfortunately, operational loading data for state-of-the-art floating offshore three-bladed turbines was unavailable, but this was worked around. The floating offshore Seawind 6 was shown to have roughly 30% to 40% lower ultimate and fatigue loads, cost approximately 40% less, take less than 20% the time to integrate and install, and have a 25.4% higher availability rate than its conventional counterpart, all while producing the same energy output of approximately 26 GWh/year. This is a comprehensive seal of approval for the application of Seawind's two-bladed technology for the floating offshore market.

8.2. Recommendations

A great swathe of work was covered in this thesis project. However, there is still plenty of scope for further tasks to be undertaken. First, in Chapter 4, the single point history wind profile should be selected so that the actual experienced wind profile may be simulated. The calibrations from the Gamma 60 investigation should be applied to the Seawind 6 and simulations should be re-run to determine changes in its performance. Second, the Seawind 6 models could be examined in more depth, experimenting with turbine design and control parameters to optimise them, separate from the calibration exercise. Hydrodynamics should also be more thoroughly examined to determine optimal mooring configurations and platform designs. Fourth, all the selected DLCs in Chapter 5 should be tested again for the floating Seawind 6 with the updated external controller. The correct yaw rates and inclusion of the supervisory control will have a positive effect on the turbine's operation and should reduce the experienced design driving loads. Furthermore, additional DLCs should be run in order to improve the accuracy of the analyses. Following this, for the ultimate loads analysis, heightened emphasis should be placed on finding exact ultimate strength values for each of the specified materials. In this same vein, a more accurate fatigue loads analysis can only be achieved when the turbine is actually built and fatigue loading tests can be carried out. Carrying on from the work in Chapter 6, further analysis of the turbine's operating envelope in steady, uniform winds should be explored, particularly investigating the undesirable positive net teeter moment at 14 m/s. Additionally, for Chapter 7, it would be of great interest if offshore load data for a comparable three-bladed turbine could be acquired and compared against the Seawind 6 simulation results. Lastly, when the Seawind 6 demonstrator is finally constructed, there would be a brilliant opportunity to compare real world sensor measurements to these simulated data-sets and see if the all the engineer's hard work paid off in terms of modelling accuracy.

It seems that the two-bladed technology that Seawind has developed, based on the legacy of the Gamma 60, is finally about to make the big time. It has been shown to be incredibly well suited for floating offshore applications and has the potential to revolutionise the industry. It is a hugely exciting time for all those involved with the company and within the wider offshore wind community. The overwhelming feeling here is that this technology, that got its start from helicopter rotors and NASA research, is going to play a leading role in the green energy future.

Bibliography

[1] Khan Academy. *What is buoyant force?* `https://www.khanacademy.org/science/physics/fluids/buoyant-force-and-archimedes-principle`. Accessed: 3-11-2022.

[2] MB Anderson, AD Garrad, and U Hassan. "Teeter excursions of a two-bladed horizontal-axis wind-turbine rotor in a turbulent velocity field". In: *Journal of wind engineering and industrial aerodynamics* 17.1 (1984), pp. 71–88.

[3] John Arimond. "Teetering towards two-blade turbines". In: *Wind Power Engineering & Development* 4 (2012), pp. 32–35.

[4] Seawind Ocean Technologies B.V. *601126 DD 0701 Rev 7 - Prescriptions for turbine controller and yaw system simulation*. 2019.

[5] Seawind Ocean Technologies B.V. *601126 DW 0002 - Rev 9 - Seawind 6 geometrical proprieties 20211002*. 2022.

[6] Seawind Ocean Technologies B.V. *601126 FA 0005 Rev1 - Bladed Modelling Input Data*. 2015.

[7] Seawind Ocean Technologies B.V. *601126 FA 0007 Rev 2 - Prof. Bottasso Independent Analysis*. 2016.

[8] Seawind Ocean Technologies B.V. *601126 GS 0001 Rev5 - General Technical Specification with Design Data and Safety Principles*. 2018.

[9] Seawind Ocean Technologies B.V. *601126 TS 0101 Rev.6 - Blade technical specification*. 2019.

[10] Seawind Ocean Technologies B.V. *601126 TS 0102 Rev.2 - Hub Technical Specification*. 2017.

[11] Seawind Ocean Technologies B.V. *601126 TS 0103 Rev.5 - Bushes and teeters of teetering hinge Technical Specification*. 2019.

[12] Seawind Ocean Technologies B.V. *601126 TS 0201 Rev.2 - Nacelle metal structure Technical Specification*. 2017.

[13] Seawind Ocean Technologies B.V. *601126 TS 0301 Rev2 - Yaw Housing Technical Specification*. 2017.

[14] Seawind Ocean Technologies B.V. *601126 TS 0303 Rev 6 - Technical Specification Yaw Drive for DHHI*. 2020.

[15] Seawind Ocean Technologies B.V. *601126 TS 1002 Rev.1 - Specification of Concrete floating Platform*. 2020.

[16] Seawind Ocean Technologies B.V. *Fundamental advantages of the Seawind Technology*. 2022.

[17] Seawind Ocean Technologies B.V. *Introduction for Seawind Partners*. 2020.

[18] Seawind Ocean Technologies B.V. *Performance comparison of 3 bladed rigid rotor vs 2 bladed teetered rotor*. 2021.

[19] Seawind Ocean Technologies B.V. *Seawind Brochure*. 2022.

[20] Seawind Ocean Technologies B.V. *Seawind Information Memorandum*. 2022.

[21] Seawind Ocean Technologies B.V. *Seawind Technical Seminar*. 2022.

[22] Seawind Ocean Technologies B.V. *Seawind Technology Dive*. 2021.

[23] Tony Burton et al. *Wind energy handbook*. John Wiley & Sons, 2011.

[24] RJ Bussolari. "Status of the 4 MW WTS-4 wind turbine". In: *NASA. Lewis Research Center Large Horizontal-Axis Wind Turbines* (1982).

[25] Palmer W Carlin, Alan S Laxson, and Eduard B Muljadi. "The history and state of the art of variable-speed wind turbine technology". In: *Wind Energy: An International Journal for Progress and Applications in Wind Power Conversion Technology* 6.2 (2003), pp. 129–159.

[26] S Caruso. *Overview of the Gamma 60 Experience*. 2020.

[27] Silvestro Caruso, Martin Jakubowski, and Luciano Caioli. *Systems for minimizing yaw torque needed to control power output in two-bladed, teetering hinge wind turbines that control power output by yawing*. US Patent 9,719,491. Aug. 2017.

[28] Jia-hao Chen et al. “Study on Gyroscopic Effect of Floating Offshore Wind Turbines”. In: *China Ocean Engineering* 35.2 (2021), pp. 201–214.

[29] P Christianesen. “WEGA-II large wind turbine scientific evaluation project”. In: (1996).

[30] International Electrotechnical Commission. *IEC 61400-1 Ed. 4.0, Wind turbines – Part 1: Design requirements*. 2019.

[31] International Electrotechnical Commission. *IEC 61400-3-1 Ed. 1.0, Wind energy generation systems - Part 3-1: Design requirements for fixed offshore wind turbines*. 2019.

[32] International Electrotechnical Commission. *IEC 61400-3-2 Ed. 1.0, Wind energy generation systems - Part 3-2: Design requirements for floating offshore wind turbines*. 2019.

[33] University College Cork. *Renewable and Sustainable Energy Review*. `https://www.pv-magazine.com/2022/04/07/renewable-offshore-floating-hydrogen-production/`. Accessed: 3-11-2022.

[34] Ray Dackerman. *Gamma wind turbine evolution*. `https://www.linkedin.com/feed/update/urn:li:activity:6653642683719962624/`. Accessed: 20-6-2022.

[35] E De Vries. “Development of two-bladed offshore wind turbine”. In: *Wind Stats Report* 24.2 (2011).

[36] DNV. *Floating Wind: The Power to Commercialize*. 2021.

[37] GL DNV. “Bladed User Manual: Version 4.12”. In: *Gerrad Hassan & Partners Ltd.: Bristol, UK* (2021).

[38] Blue H Engineering. *Historical development*. `http://www.bluehengineering.com/historical-development.html`. Accessed: 1-11-2022.

[39] Equinor. *Hywind Brochure*. `https://www.equinor.com/content/dam/statoil/documents/newsroom-additional-documents/news-attachments/brochure-hywind-a4.pdf`. Accessed: 18-10-2022.

[40] Wind Europe. *A breakthrough for offshore wind: world’s first floating wind farm opens in Scotland*. `https://windeurope.org/newsroom/news/a-breakthrough-for-offshore-wind-worlds-first-floating-wind-farm-opens-in-scotland/`. Accessed: 17-10-2022.

[41] Siemens Gamesa. *SWT-6.0-154 Offshore wind turbine*. `https://www.siemensgamesa.com/products-and-services/offshore/wind-turbine-swt-6-0-154`. Accessed: 18-10-2022.

[42] A Garrad. “The prediction of teeter excursions on a horizontal axis wind turbine”. In: *4th BWEA Conference*. 1982.

[43] DNV GL. *Bladed technical brochure*. 2020.

[44] A.L. Gordon and C Cenedese. “Ocean currents”. In: *Encyclopedia Britannica*. Encyclopedia Britannica. 2021.

[45] GWEC. *Global Offshore Wind Report 2022*. 2022.

[46] Carsten Hansen. “Aeroelastic load simulation of a 3 MW two bladed wind turbine”. PhD thesis. Hochschule für angewandte Wissenschaften Hamburg, 2014.

[47] Erich Hau, Jens Langenbrinck, and Wolfgang Palz. *WEGA large wind turbines*. Springer Science & Business Media, 2013.

[48] G Henderson. “Teetering and gyroscopic effects”. In: (2021).

[49] GM Henderson, RS Haines, and DC Quarton. “The analysis and design implications of pitch teeter coupling”. In: *Proc. EWEC*. Vol. 89. 1989, pp. 71–88.

[50] KH Hohenemser and AHP Swift. “On the design of horizontal axis two-bladed hinged wind turbines”. In: (1984).

[51] IEA. *Offshore Wind Outlook 2019*. 2019.

[52] IEA. *Wind Electricity Report 2022*. 2022.

[53] J Jonkman et al. “Definition of a 5 MW Reference Wind Turbine”. In: *Offshore System Development.* (2009).

[54] MG Kim and PH Dalhoff. “Yaw Systems for wind turbines–Overview of concepts, current challenges and design methods”. In: *Journal of Physics: Conference Series*. Vol. 524. 1. IOP Publishing. 2014, p. 012086.

[55] Germanischer Lloyd. “Regulation for the Certification of Wind Energy Conversion Systems”. In: *Germanische Lloyd, Hamburg* (1999).

[56] WindPower Monthly. *Seawind steps up development of radical two-blade offshore turbine*. `https://www.windpowermonthly.com/article/1678312/seawind-steps-development-radical-two-blade-offshore-turbine`. Accessed: 20-6-2022.

[57] United Nations. *Floating wind turbines: a new player in cleantech*. `https://unric.org/en/floating-wind-turbines-a-new-player-in-cleantech/`. Accessed: 18-10-2022.

[58] G Olsson et al. “Operational experiences from WTS-3 wind turbine, Maglarp, Sweden”. In: *IEE Proceedings A-Physical Science, Measurement and Instrumentation, Management and Education-Reviews* 5.134 (1987), pp. 431–434.

[59] Amy N Robertson and Jason M Jonkman. “Loads analysis of several offshore floating wind turbine concepts”. In: *The twenty-first international offshore and polar engineering conference*. OnePetro. 2011.

[60] Ankit Rohatgi. *Webplotdigitizer: Version 4.6*. `https://automeris.io/WebPlotDigitizer`. Accessed: 6-9-2022.

[61] Oceanira S.r.l. *601126 FA 0042 F&IV - Hydrostar analysis - Oceanira Report TR-21-03 Rev1*. 2021.

[62] V Schorbach, P Dalhoff, and P Gust. “Taming the inevitable: significant parameters of teeter end impacts”. In: *Journal of physics: Conference series*. Vol. 524. 1. IOP Publishing. 2014, p. 012070.

[63] Vera Schorbach and Peter Dalhoff. “Two bladed wind turbines: antiquated or supposed to be resurrected?” In: *EWEA Conference; Kopenhagen*. 2012.

[64] Vera Schorbach, Peter Dalhoff, and Peter Gust. “Teeter design for lowest extreme loads during end impacts”. In: *Wind Energy* 21.1 (2018), pp. 1–14.

[65] Vera Schorbach, Peter Dalhoff, and Peter Gust. “Two bladed wind turbines: undetermined for more than 30 years”. In: *Proceedings of the PhD Wind Seminar ETH Zürich*. 2012.

[66] Crown Estate Scotland. *ScotWind*. `https://www.crownestatescotland.com/our-projects/scotwind`. Accessed: 1-11-2022.

[67] Zhuxiao Shao et al. “Extreme significant wave height of tropical cyclone waves in the South China Sea”. In: *Natural Hazards and Earth System Sciences* 19.10 (2019), pp. 2067–2077.

[68] Shikha, TS Bhatti, and DP Kothari. “New horizons for offshore wind energy: Shifting paradigms and challenges”. In: *Energy sources* 27.4 (2005), pp. 349–360.

[69] Georgios Sieros et al. “Upscaling wind turbines: theoretical and practical aspects and their impact on the cost of energy”. In: *Wind energy* 15.1 (2012), pp. 3–17.

[70] David A Spera. “Large-scale wind turbine structures”. In: *Lewis Structures Technology, 1988. Volume 3: Structural Integrity Fatigue and Fracture Wind Turbines HOST* (1988).

[71] Herbert J Sutherland. “On the fatigue analysis of wind turbines”. In: (1999).

[72] JW Twidell et al. “Recommissioning and operating the LS1 3MW, Burgar Hill, Orkney wind turbine using novel crack repair”. In: (1995).

[73] JW Wagenaar, L Machielse, and J Schepers. “Controlling wind in ECN’s scaled wind farm”. In: *Proc. Europe Premier Wind Energy Event* 1.01 (2012).

[74] CM Wang et al. “Research on floating wind turbines: a literature survey”. In: *The IES Journal Part A: Civil & Structural Engineering* 3.4 (2010), pp. 267–277.

[75] Wikipedia. *Floating wind turbine*. https://en.wikipedia.org/wiki/Floating_wind_turbine. Accessed: 1-11-2022.